

Synthesis of Bifunctional Iron Complexes Having 2-Aminophenyl-Substituted N-Heterocyclic Carbene Ligands and Their Application to Catalytic Dehydrogenation of Ammonia-Borane

著者	TAKAHASHI HIROTSUGU
学位授与機関	Tohoku University
学位授与番号	11301甲第17879号
URL	http://hdl.handle.net/10097/00123070

博士論文

**Synthesis of Bifunctional Iron Complexes Having
2-Aminophenyl-Substituted *N*-Heterocyclic Carbene Ligands
and Their Application to Catalytic Dehydrogenation of
Ammonia-Borane**

(2-アミノフェニル基をもつ *N*-ヘテロ環式カルベンが配位した二官能性鉄錯体の合成
およびアンモニア-ボランの触媒的脱水素反応への応用)

高橋 拓嗣

平成 29 年

Acknowledgements

I would like to express my deepest appreciation to Prof. Hiromi Tobita who gave me insightful comments and suggestions throughout my research. I would also like to express my gratitude to Dr. Takahito Watanabe for his technical help and valuable advices, especially on theoretical calculation. I would like to offer my thanks to Prof. Hisako Hashimoto and Dr. Takashi Komuro who gave me many constructive suggestions. I would also like to thank our laboratory secretary Mrs. Eri Suzuki and all members of the Inorganic Chemistry Laboratory for their enormous help.

I am grateful to the Comprehensive Analysis Center, the Institute of Scientific and Industrial Research, Osaka University, for the measurement of ^{11}B MQMAS NMR spectra. I am also grateful to the staff members of Tohoku University Research and Analytical Center for Giant Molecules for elemental analyses and high resolution mass spectroscopy analyses and the Tohoku University Glass Factory for preparing and repairing glassware.

Finally, I would like to show my greatest appreciation to my family for their tremendous supports and constant warm encouragements.

January 22, 2018 Hirotugu Takahashi

Abbreviations

Ac	acetyl	$-\text{COCH}_3$
AB	ammonia-borane	$\text{BH}_3 \cdot \text{NH}_3$
9-BBN	9-borabicyclo[3.3.1]nonane	$\text{C}_8\text{H}_{14}\text{BH}$
ⁿ Bu	<i>n</i> -butyl	$-\text{CH}_2\text{CH}_2\text{CH}_2\text{CH}_3$
^t Bu	<i>tert</i> -butyl	$-\text{C}(\text{CH}_3)_3$
Cy	cyclohexyl	$-\text{C}_6\text{H}_{11}$
Cp	η^5 -cyclopentadienyl	$\eta^5\text{-C}_5\text{H}_5$
Cp*	η^5 -pentamethylcyclopentadienyl	$\eta^5\text{-C}_5(\text{CH}_3)_5$
cod	(1 <i>Z</i> , 5 <i>Z</i>)-cycloocta-1,5-diene	C_8H_{12}
dcpe	1,2-bis(dicyclohexylphosphino)ethane	$\text{Cy}_2\text{PCH}_2\text{CH}_2\text{PCy}_2$
Dipp	2,6-diisopropylphenyl	2,6- ⁱ Pr ₂ -C ₆ H ₃
DME	1,2-dimethoxyethane	$\text{H}_3\text{COCH}_2\text{CH}_2\text{OCH}_3$
DMF	<i>N,N</i> -dimethylformamide	$(\text{H}_3\text{C})_2\text{NCHO}$
DMSO	dimethyl sulfoxide	$(\text{H}_3\text{C})_2\text{SO}$
Et	ethyl	$-\text{CH}_2\text{CH}_3$
ⁱ Pr	isopropyl	$-\text{CH}(\text{CH}_3)_2$
Me	methyl	$-\text{CH}_3$
Ph	phenyl	$-\text{C}_6\text{H}_5$
THF	tetrahydrofuran	$\text{C}_4\text{H}_8\text{O}$
Ts	<i>p</i> -toluenesulfonyl	$-\text{O}_2\text{S}(4\text{-Me-C}_6\text{H}_4)$
Tf	trifluoromethanesulfonyl	$-\text{O}_2\text{SCF}_3$

Contents

Chapter 1 General Introduction

1-1	Hydrogen as Energy Source	2
1-2	Ammonia-Borane	2
1-3	Transition Metal-Catalyzed Dehydrogenation of AB	4
1-4	Dehydrogenation of AB with Iron-Based Catalysts	6
1-5	Mechanisms for Dehydrogenation of AB with Transition Metal Catalysts	8
1-6	Bifunctional Complexes	9
1-7	Dehydrogenation of AB Using Bifunctional Catalyst and Their Mechanisms	10
1-8	This Work	12
1-9	References	15

Chapter 2 Synthesis of Bifunctional Iron Complexes Having 2-Aminophenyl-Substituted *N*-Heterocyclic Carbene Ligands

2-1	Introduction	18
2-2	Experimental Section	19
2-3	Results and Discussion	58
2-4	Conclusion	80
2-5	References	81

Chapter 3 Dehydrogenation of Ammonia-Borane with Bifunctional Iron Complex Having 2-Aminophenyl-Substituted *N*-Heterocyclic Carbene Ligands

3-1	Introduction	84
3-2	Experimental Section	85
3-3	Results and Discussion	87
3-4	Conclusion	99
3-5	References	100

Chapter 4 Conclusion 101

Supporting Information	109
------------------------	-----

Chapter 1

General Introduction

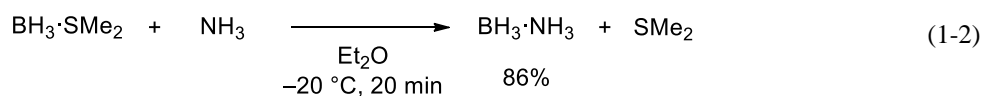
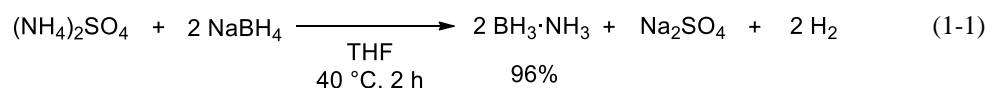
1-1. Hydrogen as Energy Source

Dihydrogen (H₂) has attracted much attention as a candidate of energy sources alternative to fossil fuels, because it emits nothing but water when it is used as fuel. The main usage of dihydrogen is a negative-electrode active material of a fuel cell, which generates electricity. Dihydrogen is regarded as a good energy carrier because its *gravimetric* density of energy is three times larger than that of petroleum.^[1] On the other hand, its *volumetric* density of energy is 3500 times smaller than that of petroleum^[1] because dihydrogen is a gas under ambient conditions and thus it is difficult to store in high density. In order to overcome these problems, many technologies have been developed.^[2] Among these technologies, the technology that exploits chemical hydrides capable of reversible dehydrogenation and hydrogenation, have received considerable research interest and have been studied extensively.^[3]

1-2. Ammonia-Borane

Ammonia-borane (AB) is a complex between borane BH₃, which is a Lewis acid, and ammonia NH₃, which is a Lewis base. It is a stable solid under ambient temperature and pressure and does not react with air and moisture. Furthermore, it has high gravimetric density of 19.6 wt% and this value is larger than that of liquid hydrogen system (5 wt%, containing weight of a gas cylinder^[4]) or metal hydrides (e.g. NaBH₄ 10.6 wt%). From these features, AB is regarded as one of the best hydrogen storage materials in chemical hydride method.

AB is easily prepared by the metathesis reaction of an ammonium salt with tetrahydroborate (eq 1-1)^[5] or Lewis base exchange of a base-stabilized borane complex such as borane-dimethylsulfide with ammonia (eq 1-2).^[6]



Since electronegativities of B and N are 2.04 and 3.04, respectively,^[7] the B–N bond in AB is strongly polarized and H atoms on adjacent B and N atoms are oppositely charged. Namely, the H atoms bound to boron are hydridic and those bound to nitrogen are protic (Figure 1-1).

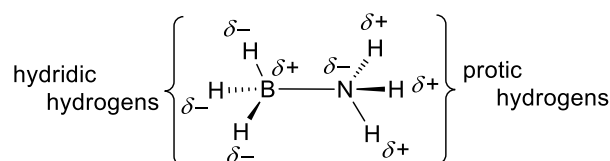
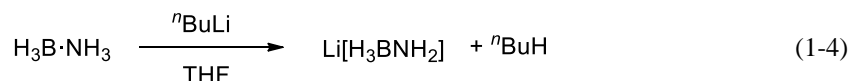
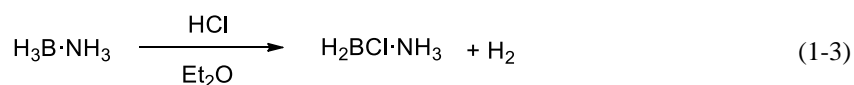
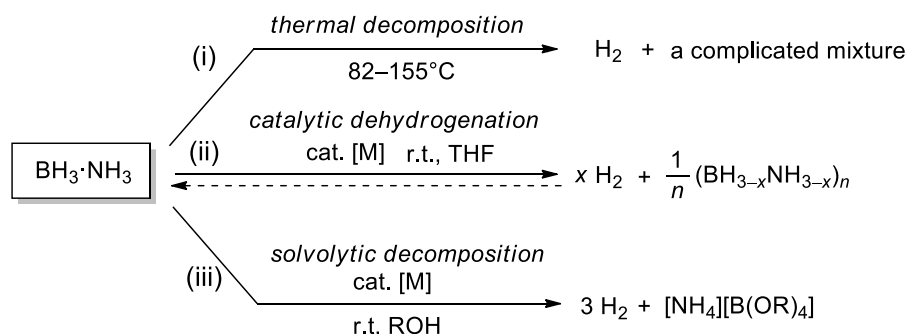


Figure 1-1. A schematic diagram of polarization of B–H and N–H bonds in AB.

The hydridic and protic characters are clearly demonstrated by the reactions with hydrochloric acid and *n*-butyllithium, which give ammonia-chloroborane^[8] (eq 1-3) and lithium amidotrihydroborate^[9] (eq 1-4), respectively.



Methods for dihydrogen release from AB are roughly classified into three categories: (i) thermal decomposition; (ii) catalytic dehydrogenation; and (iii) solvolytic decomposition (Scheme 1-1).



Scheme 1-1. Three methods for dihydrogen release from AB.

In method (i), high temperature ($> 82\text{ }^\circ\text{C}$) is required in order to release H_2 from AB and the reaction gives a mixture of wide variety of dehydrogenated products such as poly(aminoborane) (PAB), poly(iminoborane) (PIB), borazine (BZ), poly(borazylene) (PBZ), and their cross-linked materials (Figure 1-2).^[3]

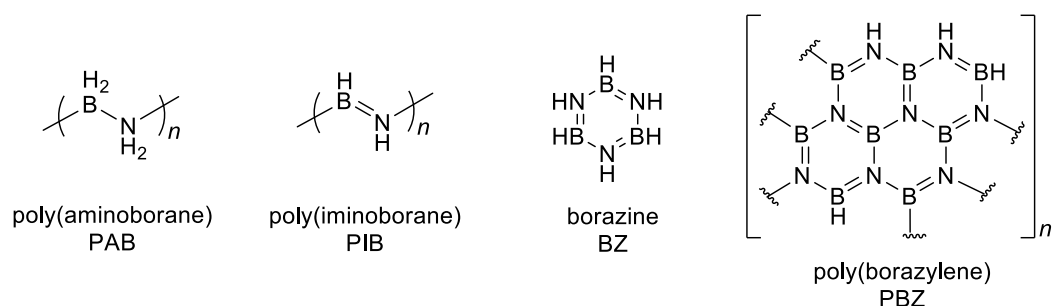


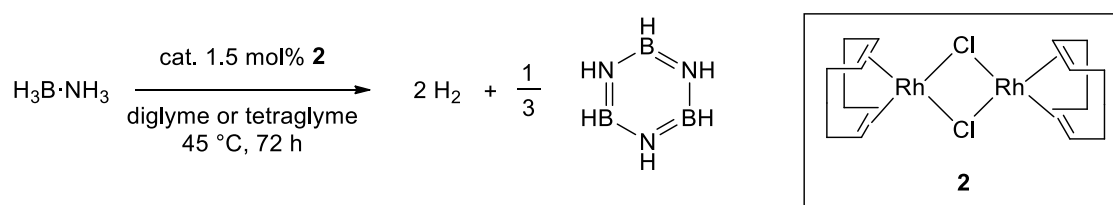
Figure 1-2. The structures of thermal decomposition product of AB.

On the other hand, the dihydrogen release occurs under even lower temperature ($< 70\text{ }^\circ\text{C}$) in method (ii) and (iii), and the products have relatively simple compositions. For example, a dehydrogenation reaction of AB catalyzed by an iridium pincer complex $(\text{POCOP})\text{Ir}(\text{H})_2$ ($\text{POCOP} =$

κ^3 -(*P,C,P*)-1,3-(OP^tBu₂)C₆H₃) (**1**) gives cyclopentaborazane (H₂BNH₂)₅ as a sole dehydrogenation product.^[10] In method (iii), methanol (R = Me) or water (R = H) is often used as a solvent and a wide variety of metal nanoparticles^[3,11] and complexes^[12] are used as catalysts. This method usually gives 3 equivalents of H₂ per AB and a dehydrogenated product [NH₄][B(OR)₄]. Although method (iii) has an advantage that H₂ can be extracted to the maximum limit for AB, method (ii) is preferable from the viewpoint of using AB for hydrogen carrier because AB can be regenerated by addition of H₂ to dehydrogenated BN-products.

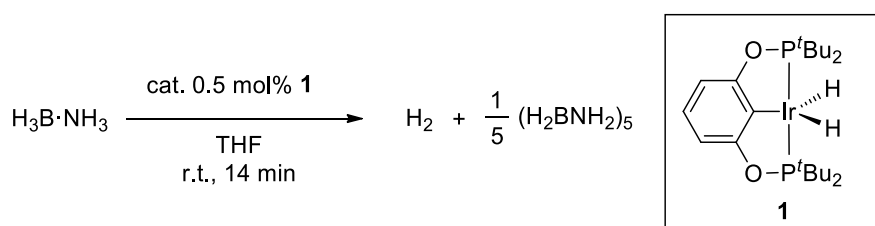
1-3. Transition Metal-Catalyzed Dehydrogenation of AB

Although several researchers briefly mentioned about the ability of some transition metal complexes as catalysts for the dehydrogenation of amine-boranes since 1989,^[13] a pioneering work on transition metal catalysts for dehydrogenation of AB was carried out in 2001 by Manners and co-workers.^[14] They found that the dehydrogenation reaction of AB in the presence of catalytic amount (1.5 mol%) of [Rh(1,5-cod)(μ-Cl)]₂ (**2**) at 45°C afforded borazine together with two molar equivalents of dihydrogen (Scheme 1-2).^[6]



Scheme 1-2. Dehydrogenation of AB using [Rh(1,5-cod)(μ-Cl)]₂ (**2**).

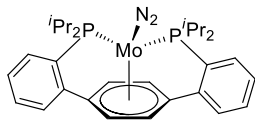
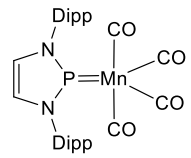
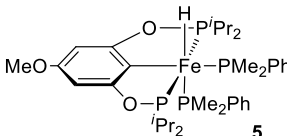
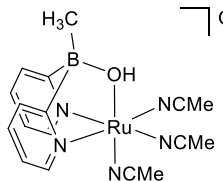
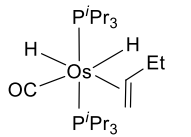
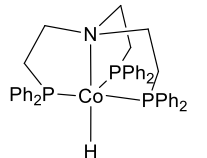
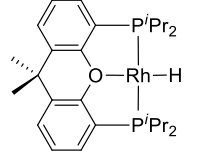
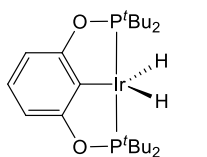
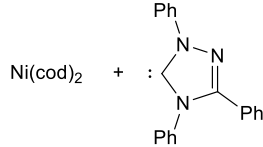
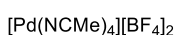
An extremely effective catalyst was reported by Goldberg and Heinekey in 2006 (Scheme 1-3).^[10] They reported that 0.5 mol% of (POCOP)Ir(H)₂ (**1**) catalyzed the dehydrogenation of AB and the reaction finished within 14 minutes under ambient temperature to afford 1 molar equivalent of H₂ and a polymerized product, which is presumed to be cyclopentaborazane (H₂BNH₂)₅ (Scheme 1-3).



Scheme 1-3. Dehydrogenation of AB using (POCOP)Ir(H)₂ (**1**).

Several active catalysts containing molybdenum,^[15] manganese,^[16] iron,^[17] ruthenium,^[18] osmium,^[19] cobalt,^[20] rhodium,^[21] iridium,^[10] nickel,^[22] and palladium^[23] as a metal center have been reported (Table 1-1).

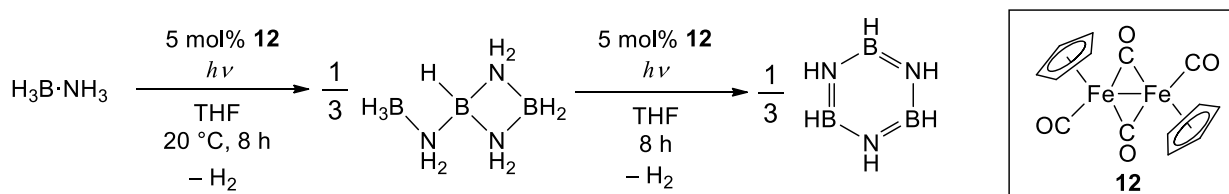
Table 1-1. Selected examples of AB dehydrogenation catalysts

catalyst	loading	solvent	temperature	time	$n(\text{H}_2)/n(\text{AB})$	ref.
 3	5 mol%	diglyme	70 °C	<15 h	2.5	15
 4	2.5 mol%	THF/toluene	50 °C	30 h	1.7	16
 5	5 mol%	THF/diglyme	60 °C	16 h	2.5	17
 6	2 mol%	benzene/diglyme	70 °C	6.5 h	2.1	18
 7	5 mol%	THF	31 °C	n/a ^a	1.0	19
 8	33 mol%	THF- <i>d</i> ₈	55 °C	24 h	2.0	20
 9	1 mol%	THF	31 °C	<8 min	1.0	21
 1	0.5 mol%	THF	r.t.	14 min	1.0	10
 10	10 mol%	C ₆ D ₆ /diglyme	60 °C	4 h	>2.5	22
 10	3 mol%	tetraglyme/MeNO ₂	25 °C	<1 min	2.0	23

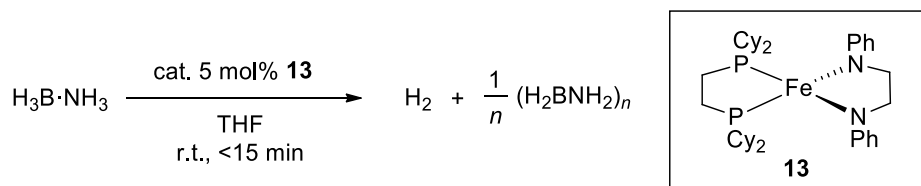
^a The data was not reported.

1-4. Dehydrogenation of AB with Iron-Based Catalysts

Although noble metal-based catalysts for dehydrogenation of AB have been well-studied over a decade and a half, iron-based catalysts are still few in number. Iron is the most abundant transition metal in Earth's crust. It is not only inexpensive but also environmentally benign. The first example of dehydrogenation of AB with iron catalyst was reported by Baker et al. in 2007. They have shown that $\text{Fe}(\text{H})(\text{CH}_2\text{PMe}_2)(\text{PMe}_3)_3$ (**11**) catalyzed dehydrogenation of AB at 20 °C.^[24] However, the reaction did not proceed to completion due to precipitation of black inactive solids and formation of phosphine-borane. In 2011, Manners et al. reported that the dinuclear iron complex $[\text{CpFe}(\text{CO})_2]_2$ (**12**) catalyzed a stepwise dehydrogenation of AB (Scheme 1-4).^[24] This reaction, however, required UV-irradiation to make the reaction progress and later it was found that the active species was not the homogeneous iron complex but heterogeneous iron nanoparticles.^[25] In 2012, Baker et al. reported that the iron complex $(\text{dcpe})\text{Fe}(\text{PhNCH}_2\text{CH}_2\text{NPh})$ (**13**) catalyzed dehydrogenation of AB.^[26] The reaction of AB with 5 mol% of **13** caused rapid generation of H_2 and the reaction was completed within 15 minutes under ambient conditions (Scheme 1-5). This reaction gave a large amount of insoluble precipitate, which was characterized as poly(aminoborane) $(\text{H}_2\text{BNH}_2)_n$ based on its IR spectrum.



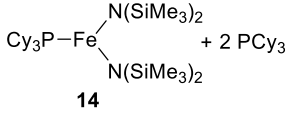
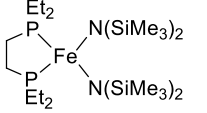
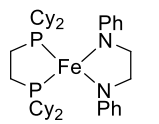
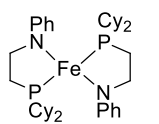
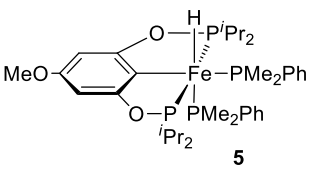
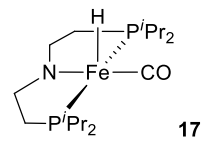
Scheme 1-4. Stepwise dehydrogenation of AB using iron complex **12** under UV-irradiation.



Scheme 1-5. Dehydrogenation of AB using iron complex **13**.

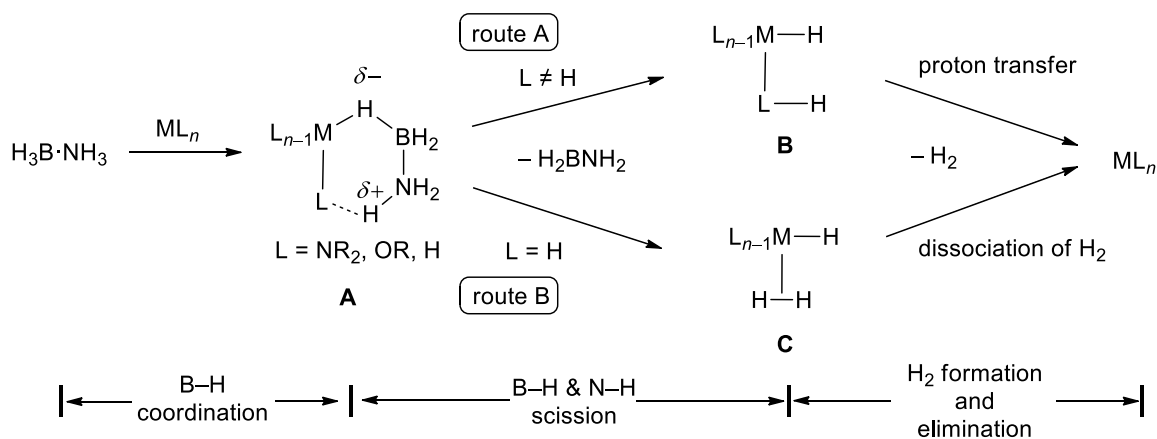
After these reports, several iron-based homogeneous dehydrogenation catalysts have been reported (Table 1-2), but most of them required elevated temperature (up to 60 °C) and/or relatively long reaction time for completion of the H_2 evolution.

Table 1-2. Reported iron-based homogeneous catalysts for dehydrogenation of AB

catalyst	loading	solvent	temperature	time	$n(\text{H}_2)/n(\text{AB})$	ref.
 14	5 mol%	diglyme	60 °C	20 h	1.7	26
 15	5 mol%	diglyme	60 °C	20 h	1.2	26
 13	5 mol%	diglyme	r.t.	15 min	1.0	26
 16	5 mol%	diglyme	60 °C	20 h	1.3	26
 5	5 mol%	THF/diglyme	60 °C	16 h	2.5	17
 17	2 mol%	THF	r.t.	5 h	1.0	27

1-5. Mechanisms for Dehydrogenation of AB with Transition Metal Catalysts

In general, elucidation of the mechanism for a certain reaction is considered to be important because it can lead to the development of more active catalysts in comparison with known ones. Considering the reaction mechanism for AB dehydrogenation by homogeneous metal catalysts (ML_n), it can be regarded to involve roughly three elemental reaction processes, namely, B–H scission, N–H scission, and H_2 formation and elimination.^[19,28] Schematic reaction mechanisms are shown in Scheme 1-6. In most cases, dehydrogenation starts from coordination of a B–H bond to a vacant site on the metal center (M) to give a σ -complex **A**. Then, heterolytic N–H bond cleavage occurs by the intramolecular attack of the basic ligand (L), such as NR_2 , OR, and H. In this stage, there are two possible routes depending on the L. In the case of $L \neq H$ (route A), the electronegative element in the L abstracts a protic H on the nitrogen atom of AB, then the coordinated B–H bond cleaves to give monohydride complex **B** together with aminoborane H_2BNH_2 . Finally, the proton on the L is transferred to the hydrido ligand on the metal center to generate H_2 and also regenerate catalyst ML_n . In the case of $L = H$ (route B), the hydrido ligand and a protic H on the nitrogen atom of AB interact with each other to give a dihydrogen complex **C** as an intermediate. Subsequent dissociation of H_2 gives ML_n . These two routes are similar in the way that the metal center acts as a Lewis acidic site and the ligand (L) acts as a Lewis basic site to activate B–H and N–H bond cooperatively.



Scheme 1-6. Schematic reaction mechanisms for dehydrogenation of AB with transition metal catalysts.

1-6. Bifunctional Complexes

On the basis of the above mentioned dehydrogenation mechanisms, if there is a catalyst which has both Lewis acidic and basic sites, AB would be smoothly activated at those sites. Catalysts having such electronic features are already known as “bifunctional catalysts” in the fields of catalytic transfer hydrogenation of unsaturated molecules such as ketones or imines typically using alcohols as a hydrogen source.^[29] Several famous bifunctional catalysts are displayed in Figure 1-3.^[30-32] Noyori et al. studied the mechanism of transfer hydrogenation of benzaldehyde catalyzed by the ethanolamine-ligated Ru complex ($\eta^6\text{-C}_6\text{H}_6$)Ru(H)(OCH₂CH₂NH₂) (**21**) using 2-propanol as a hydrogen source by theoretical calculation. They found that the mechanism involves six-membered cyclic transition states denoted as **TS**₂₂₋₂₃ and **TS**₂₅₋₂₆ at the stage where hydrogen migration occurs (Scheme 1-7).^[33] To date, many experimental and theoretical studies have revealed that not only transfer hydrogenation but also hydrogenation with H₂ using bifunctional catalyst involves such a six-membered cyclic transition state in their reaction mechanisms.^[29]

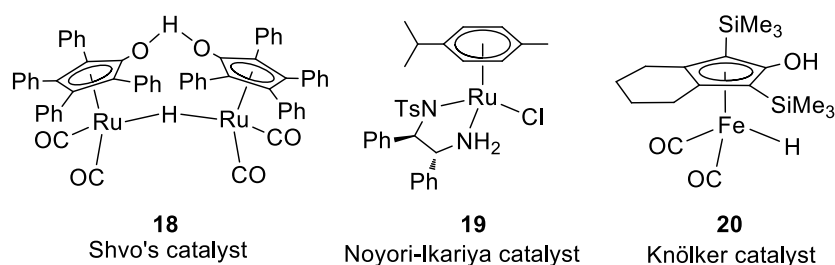
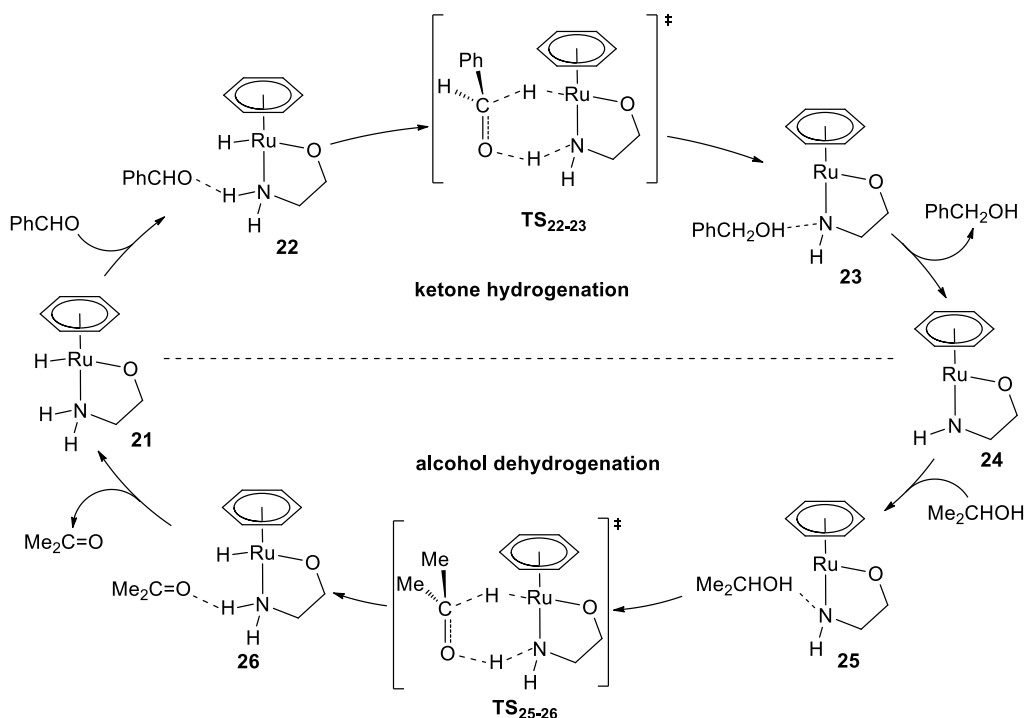


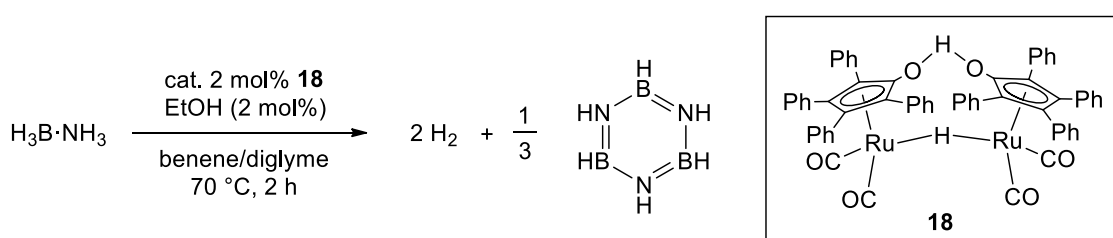
Figure 1-3. Representative bifunctional catalysts.



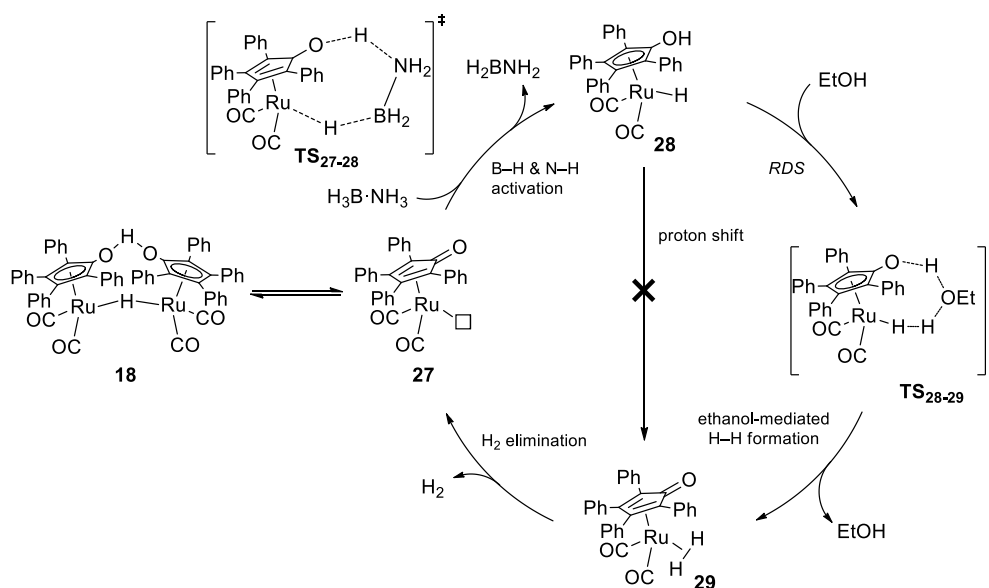
Scheme 1-7. A proposed mechanism for transfer hydrogenation with the Ru catalyst **21**.

1-7. Dehydrogenation of AB Using Bifunctional Catalysts and Their Mechanisms

The concept of bifunctional activation, i.e. metal-ligand cooperative activation, can be applied to the dehydrogenation of AB. Indeed, Williams et al. revealed that 2 mol% of Shvo's catalyst **18** released 2 equivalents of H₂ from AB at 70 °C in the presence of catalytic amount of ethanol (Scheme 1-8).^[34] They also investigated the mechanism of the reaction, which is shown in Scheme 1-9.^[34,35] They revealed that the bond activation step (**27–28**) is fast and the H–H bond formation step (**28–29**) is the rate-determining step, which involves ethanol-mediated H–H bond formation at its transition state. The direct proton transfer from the η⁵-C₅Ph₄OH ligand to RuH have been denied by a calculation on a simplified model of **28**, in which hydrogens were substituted for the aryl groups on the cyclopentadienyl ring, performed by Casey et al.^[36] because its activation energy is 43.2 kcal/mol, which is too high to proceed under the dehydrogenation reaction condition in Scheme 1-8.

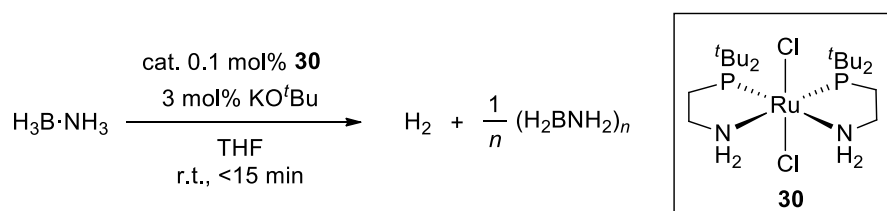


Scheme 1-8. Catalytic dehydrogenation of AB with Shvo's catalyst **18**.

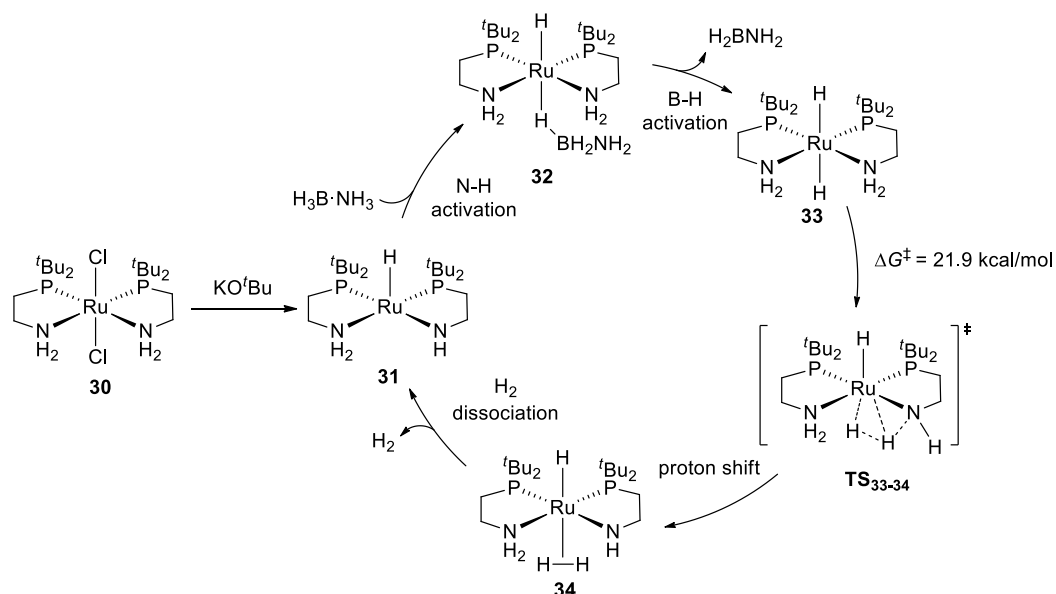


Scheme 1-9. A proposed mechanism for catalytic dehydrogenation with Shvo's catalyst **18**.

Another example of dehydrogenation of AB by bifunctional catalysts is reported by Fagnou et al.^[37] They discovered that 0.1 mol% of the Ru catalyst **30**, which had been originally developed for ketone hydrogenation catalyst,^[38] catalyzed rapid dehydrogenation of AB in the presence of 3 mol% of KO^tBu to afford 1 equivalent of H₂ and poly(aminoborane) within 15 min (Scheme 1-10). They also performed DFT calculation for the dehydrogenation pathway (Scheme 1-11) and the largest kinetic barrier of 21.9 kcal/mol was found in the process of formation of the dihydrogen complex **34** via the transition state **TS₃₃₋₃₄**, which is consistent with the experimental result.



Scheme 1-10. Catalytic dehydrogenation of AB with the Ru complex **30**.



Scheme 1-11. A proposed mechanism for dehydrogenation of AB with the Ru catalyst **30**.

1-8. This Work

The rate of H_2 release from AB is an important factor to evaluate performance of catalysts. As mentioned in Section 1-3, the rates achieved by iron catalysts are still lower than those attained by noble metal catalysts. Considering the proposed mechanisms that were introduced in Section 1-5 and 1-7, if all of the three elemental reaction steps (B–H scission, N–H scission, and H_2 formation) for the AB dehydrogenation become faster, the overall reaction will become faster. Therefore, the key requirements to develop active catalysts are the following three: (i) the iron center has a vacant site; (ii) the ligand has a Lewis basic site; and (iii) these reaction sites are adjacent to each other. Thus, we designed a bifunctional iron complex **35** illustrated in Figure 1-4. Its characteristic features are as follows:

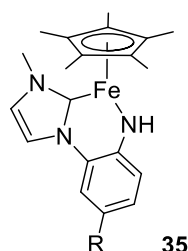
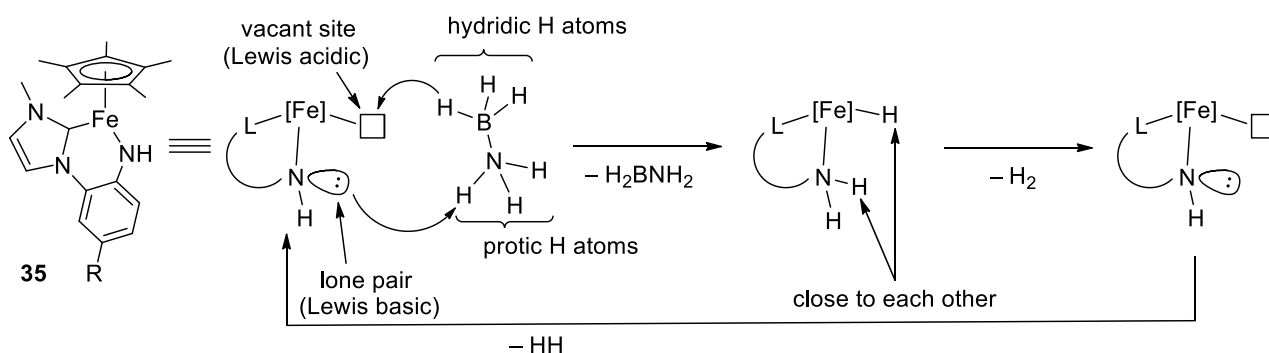


Figure 1-4. The target bifunctional iron complex **35**.

(1) The iron center of **35** can be regarded as 16e, and, therefore, the iron center has a vacant site. The hydridic H on B of AB can interact with the vacant site of the iron center of **35**, and, at the same time, the lone pair on N of the amido ligand can attack the protic H on N of AB to activate both B–H and N–H bonds synergistically (Scheme 1-12). In addition, since these two abstracted hydrogens are located close to each other, H_2 formation and dissociation will occur smoothly. The structure of this reaction site of **35** would satisfy the three requirements stated above.



Scheme 1-12. A schematic diagram for dehydrogenation of AB using the bifunctional iron complex **35**.

(2) The NHC ligand stabilizes the coordinatively unsaturated iron center. As mentioned above, a vacant site on the metal center is indispensable for the bifunctional activation. In general, coordinatively unsaturated iron complexes are so reactive that it can exist only for a short period of time. Nevertheless, NHC ligands can stabilize coordinatively unsaturated complexes by means of their strong σ -donating

ability and large steric influence.^[39] Indeed, several coordinatively unsaturated and stable iron complexes have been synthesized using NHC as its ligands (Figure 1-5).^[40-42]

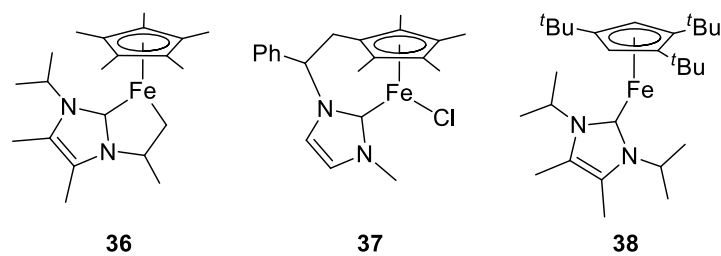
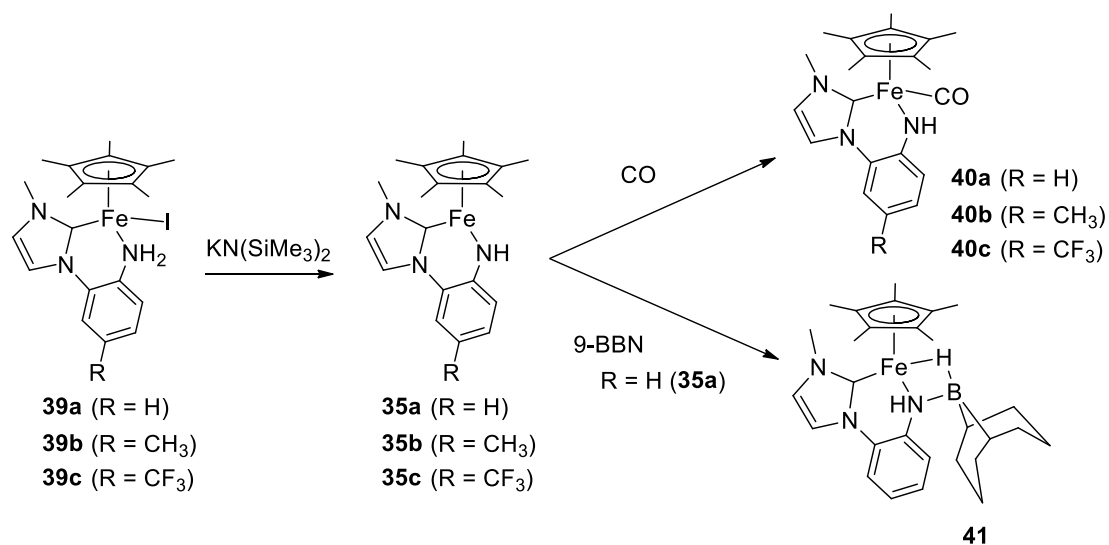


Figure 1-5. Selected examples of reported coordinatively unsaturated iron complexes having NHC ligands.

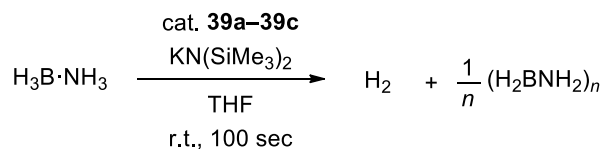
(3) The rigid phenylene backbone reduces the flexibility of the κ^2 -(C,N)-(amido)NHC chelate ligand and increases the stability of the complex **35**. It also minimizes the risk of loss of the ligand during the catalytic reaction. In addition, the substituent R on the phenylene linkage can control the basicity of the amido nitrogen through the aromatic ring.

In Chapter 2, I will describe the synthesis and structure of the precatalysts, i.e. iron complexes ligated by 2-aminophenyl-substituted NHCs **39a–39c** (Scheme 1-13). The observation and trapping of the bifunctional complex **35a**, which is considered to be an active species in the catalytic dehydrogenation of AB, will also be described (Scheme 1-13).



Scheme 1-13. Reactions of **39** with KN(SiMe₃)₂ and trapping of **35**.

In Chapter 3, I will report the dehydrogenation reaction of AB catalyzed by **35** generated from the precatalysts **39** and KN(SiMe₃)₂ (Scheme 1-14). The catalytic reaction mechanism will also be discussed on the basis of the results of DFT calculation.



Scheme 1-14. Catalytic dehydrogenation of AB using the precatalysts **39a–39c** in the presence of KN(SiMe₃)₂.

Finally, the conclusions drawn from this work will be summarized in Chapter 4.

1-9. References

- [1] J. Graetz, *Chem. Soc. Rev.* **2009**, *38*, 73.
- [2] a) D. J. Durbin, C. Malardier-Jugroot, *Int. J. Hydrogen Energy* **2013**, *38*, 14595; b) F. Zhang, P. Zhao, M. Niu, J. Maddy, *Int. J. Hydrogen Energy* **2016**, *41*, 14535.
- [3] a) B. Sakintuna, F. Lamari-Darkrim, M. Hircsher, *Int. J. Hydrogen Energy* **2007**, *32*, 1121; b) M. Yadav, Q. Xu, *Energy Environ. Sci.* **2012**, *5*, 9698; c) G. Moussa, R. Moury, U. B. Demirci, T. Şener, P. Miele, *Int. J. Energy Res.* **2013**, *37*, 825; d) N. A. A. Rusman, M. Dahari, *Int. J. Hydrogen Energy* **2016**, *41*, 12108. e) F. Alhumaidan, D. Cresswell, A. Garforth, *Energy Fuels* **2011**, *25*, 4217; f) Q.-L. Zhu, Q. Xu, *Energy Environ. Sci.* **2015**, *8*, 478.
- [4] A. Staubitz, A. P. M. Robertson, I. Manners, *Chem. Rev.* **2010**, *110*, 4079.
- [5] P. V. Ramachandran, P. D. Gagare, *Inorg. Chem.* **2007**, *46*, 7810.
- [6] C. A. Jaska, K. Temple, A. J. Lough, I. Manners, *J. Am. Chem. Soc.* **2003**, *125*, 9424.
- [7] A. L. Allred, *J. Inorg. Nucl. Chem.* **1961**, *17*, 215.
- [8] D. R. Ketchum, A. L. DeGraffenreid, P. M. Niedenzu, S. G. Shore, *J. Mater. Res.* **1999**, *14*, 1934.
- [9] A. G. Myers, B. H. Yang, D. J. Kopecky, *Tetrahedron Lett.* **1996**, *37*, 3623.
- [10] M. C. Denny, V. Pons, T. J. Hebden, D. M. Heineley, K. I. Goldberg, *J. Am. Chem. Soc.* **2006**, *128*, 12048.
- [11] W.-W. Zhan, Q.-L. Zhu, Q. Xu, *ACS Catal.* **2016**, *6*, 6892.
- [12] a) R. Ciganda, M. A. Garralda, L. Ibarlucea, E. Pinilla, M. R. Torres, *Dalton Trans.* **2010**, *39*, 7226; b) C. Boulho, J.-P. Djukic, *Dalton Trans.* **2010**, *39*, 8893; c) T. W. Graham, C. W. Tsang, X. Chen, R. Guo, W. Jia, S. M. Lu, C. Sui-Seng, C. B. Ewart, A. Lough, D. Amoroso, K. Abdur-Rashid, *Angew. Chem. Int. Ed.* **2010**, *49*, 8708; d) G. C. Fortman, A. M. Slawin, S. P. Nolan, *Organometallics* **2011**, *30*, 5487; e) D. J. Nelson, B. J. Truscott, J. D. Egbert, S. P. Nolan, *Organometallics* **2013**, *32*, 3769; f) M. A. Garralda, C. Mendicute-Fierro, A. Rodríguez-Diéguez, J. M. Seco, C. Ubide, I. Zumeta, *Dalton Trans.* **2013**, *42*, 11652; g) V. S. Nacianceno, L. Ibarlucea, C. Mendicute-Fierro, A. Rodríguez-Diéguez, J. M. Seco, I. Zumeta, C. Ubide, M. A. Garralda, *Organometallics* **2014**, *33*, 6044; h) M. Muñoz-Olasagasti, A. Telleria, J. Pérez-Miqueo, M. A. Garralda, Z. Freixa, *Dalton Trans.* **2014**, *43*, 11404; i) Z. Freixa, M. A. Garralda, *Inorg. Chim. Acta* **2015**, *431*, 184; j) V. San Nacianceno, S. Azpeitia, L. Ibarlucea, C. Mendicute-Fierro, A. Rodríguez-Diéguez, J. M. Seco, E. San Sebastian, M. A. Garralda, *Dalton Trans.* **2015**, *44*, 13141; k) A. Telleria, P. W. N. M. van Leeuwen, Z. Freixa, *Dalton Trans.* **2017**, *46*, 3569.
- [13] Y. D. Blum, R. M. Laine, U. S. Patent 4801439, **1989**.
- [14] C. A. Jaska, K. Temple, A. J. Lough, I. Manners, *Chem. Commun.* **2001**, 962.
- [15] J. A. Buss, G. A. Edouard, C. Chang, J. Shi, T. Agapie, *J. Am. Chem. Soc.* **2014**, *136*, 11272.
- [16] M. Gediga, C. M. Feil, S. H. Schlindwein, J. Bender, M. Nieger, D. Gudat, *Chem. Eur. J.* **2017**, *23*, 11560.
- [17] P. Bhattacharya, J. A. Krause, H. Guan, *J. Am. Chem. Soc.* **2014**, *136*, 11153.
- [18] B. L. Conley, D. Guess, T. J. Williams, *J. Am. Chem. Soc.* **2011**, *133*, 14212.
- [19] M. A. Esteruelas, A. M. López, M. Mora, E. Oñate, *ACS Catal.* **2015**, *5*, 187.

- [20] S. Todisco, L. Luconi, G. Giambastiani, A. Rossin, M. Peruzzini, I. E. Golub, O. A. Filippov, N. V. Belkova, E. S. Shubina, *Inorg. Chem.* **2017**, *56*, 4296.
- [21] M. A. Esteruelas, P. Nolis, M. Oliván, E. Oñate, A. Vallribera, A. Vélez, *Inorg. Chem.* **2016**, *55*, 7176.
- [22] R. J. Keaton, J. M. Blacquiere, R. T. Baker, *J. Am. Chem. Soc.* **2007**, *129*, 1844.
- [23] S.-K. Kim, W.-S. Han, T.-J. Kim, T.-Y. Kim, S. W. Nam, M. Mitoraj, Ł. Piekoś, A. Michalak, S.-J. Hwang, S. O. Kang, *J. Am. Chem. Soc.* **2010**, *132*, 9954.
- [24] J. R. Vance, A. P. M. Robertson, K. Lee, I. Manners, *Chem. Eur. J.* **2011**, *17*, 4099.
- [25] J. R. Vance, A. Schäfer, A. P. M. Robertson, K. L. J. Turner, G. R. Whittell, I. Manners, *J. Am. Chem. Soc.* **2014**, *136*, 3048.
- [26] R. T. Baker, J. C. Gordon, C. W. Hamilton, N. J. Henson, P.-H. Lin, S. Maguire, M. Murugesu, B. J. Scott, N. C. Smythe, *J. Am. Chem. Soc.* **2012**, *134*, 5598.
- [27] A. Glüer, M. Förster, V. R. Celinski, J. S. auf der Günne, M. C. 30 Holthausen, S. Schneider, *ACS Catal.* **2015**, *5*, 7214.
- [28] a) A. Rossin, M. Peruzzini, *Chem. Rev.* **2016**, *116*, 8848; b) S. Bhunya, T. Malakar, G. Ganguly, A. Paul, *ACS Catal.* **2016**, *6*, 7907.
- [29] J. R. Khusnutdinova, D. Milstein, *Angew. Chem. Int. Ed.* **2015**, *54*, 12236.
- [30] Y. Blum, D. Czarkie, Y. Rahamim, Y. Shvo, *Organometallics* **1985**, *4*, 1459.
- [31] K.-J. Haack, S. Hashiguchi, A. Fujii, T. Ikariya, R. Noyori, *Angew. Chem. Int. Ed. Engl.* **1997**, *36*, 285.
- [32] H.-J. Knölker, E. Baum, H. Goesmann, R. Klauss, *Angew. Chem. Int. Ed.* **1999**, *38*, 2064.
- [33] R. Noyori, M. Yamashita, S. Hashiguchi, *J. Org. Chem.* **2001**, *66*, 7931.
- [34] B. L. Conley, T. J. Williams, *Chem. Commun.* **2010**, *46*, 4815.
- [35] Z. Lu, B. L. Conley, T. J. Williams, *Organometallics* **2012**, *31*, 6705.
- [36] C. P. Casey, J. B. Johnson, S. W. Singer, Q. Cui, *J. Am. Chem. Soc.* **2005**, *127*, 3100.
- [37] N. Blaquiere, S. Diallo-Garcia, S. I. Gorelsky, D. A. Black, K. Fagnou, *J. Am. Chem. Soc.* **2008**, *130*, 14034.
- [38] W. Jia, X. Chen, R. Guo, C. Sui-Seng, D. Amoroso, A. J. Lough, K. Abdur-Rashid, *Dalton Trans.* **2009**, 8301.
- [39] M. N. Hopkinson, C. Richter, M. Schedler, F. Glorius, *Nature*, **2014**, *510*, 485.
- [40] Y. Ohki, T. Hatanaka, K. Tatsumi, *J. Am. Chem. Soc.* **2008**, *130*, 17174.
- [41] V. V. K. M. Kandepi, J. M. S. Cardoso, E. Peris, B. Royo, *Organometallics* **2010**, *29*, 2777.
- [42] M. Reiners, D. Baabe, M.-K. Zaretske, M. Freytag, M. D. Walter, *Chem. Commun.* **2017**, *53*, 7274.

Chapter 2

Synthesis of Bifunctional Iron Complexes Having 2-Aminophenyl-Substituted *N*-Heterocyclic Carbene Ligands

2-1. Introduction

As mentioned in Chapter 1, transition metal catalyzed dehydrogenation of ammonia-borane (AB) was extensively studied in terms of development of hydrogen storage techniques. Although many homogeneous dehydrogenation catalysts have been reported to date, iron-based catalysts are still few in number and their catalytic activities are still lower than those of noble metal-based catalysts. Considering a general dehydrogenation mechanism of AB by transition metal catalysts, bifunctional activation, i.e. metal-ligand cooperative activation, has been considered to be one of the most effective methods for the dehydrogenation of AB (Figure 2-1). Therefore, I have designed the bifunctional complexes having a 2-aminophenyl-substituted NHC ligand, which can serve as the catalysts for the dehydrogenation of AB.

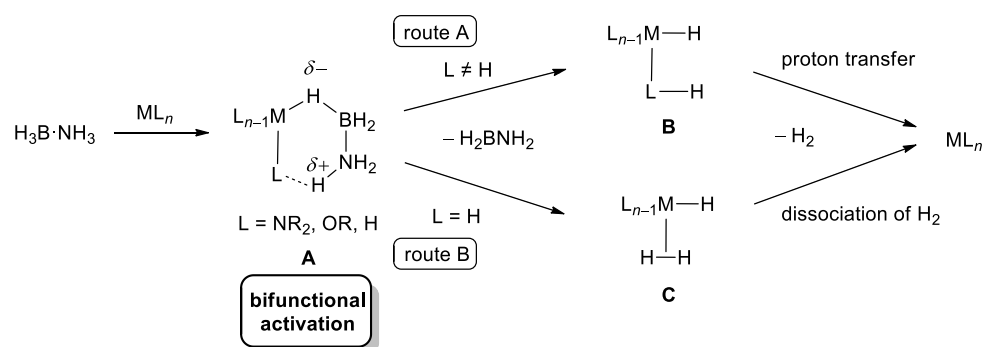


Figure 2-1. A Schematic diagram for bifunctional dehydrogenation of AB with transition metal catalysts (ML_n).

In this chapter, I will describe the synthesis and structure of iron complexes **1** and the generation of bifunctional complexes **2** by the reaction of **1** with $KN(SiMe_3)_2$. Trapping of **2** using CO and 9-BBN will also be mentioned in this chapter (Figure 2-2).

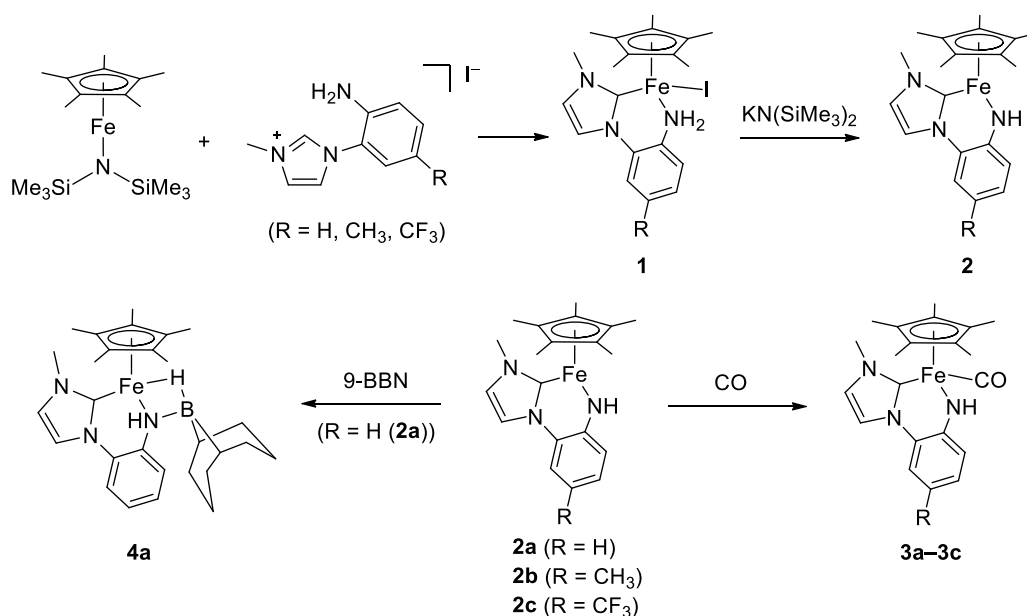
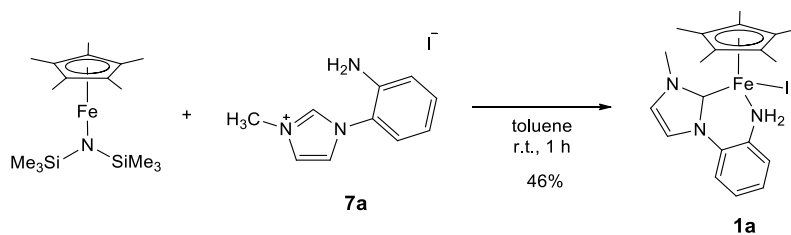


Figure 2-2. Synthesis and trapping of **2**.

2-2. Experimental Section

General Procedures and Materials All reactions were carried out under an argon atmosphere in a glove box or under nitrogen atmosphere using Schlenk techniques. Dry *n*-hexane, acetonitrile, THF, and diethyl ether were obtained using an Ultimate Solvent System (NIKKO HANSEN&CO., LTD). Dry toluene was obtained using an MB SPS Compact (M. Braun Inertgas-Systeme GmbH) or purchased from Wako Chemicals. Dry methanol was obtained by distillation from CaH₂. DMSO and DMF were dried over MS4A for more than 24 h. Benzene-*d*₆ and THF-*d*₈ were dried over CaH₂, degassed, and vacuum-transferred prior to use. CO gas was dried by a column of SICAPENT® with indicator (purchased from Merck) prior to use. 9-BBN was purchased from Sigma-Aldrich and recrystallized from DME prior to use. Other solvents and chemicals were purchased from chemical suppliers and used as received unless otherwise noted. Cp*FeN(SiMe₃)₂,^[1] CuMeSal (Copper (I) 3-methylsalicylate),^[2] 3-methyl-1-(2-aminophenyl)imidazolium iodide **7a**,^[3] 2-bromo-4-methyl-1-nitrobenzene,^[4] and 2-bromo-4-(trifluoromethyl)aniline^[5] were prepared according to literature methods. All NMR spectra were recorded on a Bruker AVANCE III 400 Fourier transform spectrometer at room temperature unless otherwise noted. The residual proton (CHCl₃, 7.26 ppm, CDHCl₂, 5.32 ppm, C₆D₅H, 7.15 ppm, THF-*d*₇, 1.73 ppm, and DMSO-*d*₅, 2.50 ppm) and the carbon resonances (CDCl₃, 77.0 ppm, C₆D₆, 128.06 ppm, THF-*d*₈ 25.3 ppm, and DMSO-*d*₆ 39.5 ppm) of deuterated solvents were used as internal standards for ¹H and ¹³C resonances, respectively. The other NMR spectra were referenced to external standards (BF₃·OEt₂ 0.0 ppm for ¹¹B, C₆H₅CF₃ -62.1 ppm for ¹⁹F). IR spectra were recorded on a HORIBA FT-720 spectrometer. High resolution mass spectrometry and elemental analyses were performed on a Bruker Daltonics solari-X 9.4T and a J-SCIENCE LAB JM-11 analyzer, respectively, at the Research and Analytical Center for Giant Molecules, Graduate School of Science, Tohoku University.

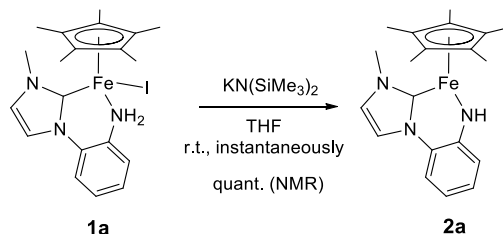
2-2-1. Synthesis of **1a**



A 30 mL Schlenk tube was charged with Cp*FeN(SiMe₃)₂ (0.317 g, 0.902 mmol) and dry toluene (15 mL). To this solution was added 1-(2-aminophenyl)-3-methylimidazolium iodide (0.272 g, 0.903 mmol) in one portion. The color of solution immediately became dark. After stirring the solution for 1 h, it was filtered to remove insoluble materials and the filtrate was evaporated to dryness. The resulting black residue was recrystallized from THF piled with hexane to give the title compound **1a** as black crystals (0.204 g, 0.415 mmol, 46%). ¹H NMR (400 MHz, C₆D₆, δ), 1.50 (s, 15H, Cp*), 2.47 (br, 2H, NH₂), 4.09 (s, NCH₃, 3H), 6.28 (d, ³J_{HH} = 6.8 Hz, ArH, 1H), 6.55 (s, ImH, 1H), 6.63 (t, ³J_{HH} = 6.8 Hz, 1H, ImH), 6.70-6.80 (m, 2H, ArH), 6.84 (s, 1H, ImH). ¹H NMR (400 MHz, THF-*d*₈, δ), 1.46 (s, 15H, Cp*), 4.31 (s, 3H, NCH₃), 7.12 (t, ³J_{HH} = 7.2 Hz, 1H, ArH), 7.17 (t, ³J_{HH} = 7.0 Hz, 1H, ArH), 7.25 (d, ³J_{HH} = 7.2 Hz, 1H, ArH), 7.55 (d, ³J_{HH} = 7.6 Hz, 1H, ArH), 7.58 (d, *J* = 1.6 Hz, 1H, ImH), 7.90 (d, *J* = 1.6 Hz, 1H, ImH). ¹³C{¹H} NMR (101

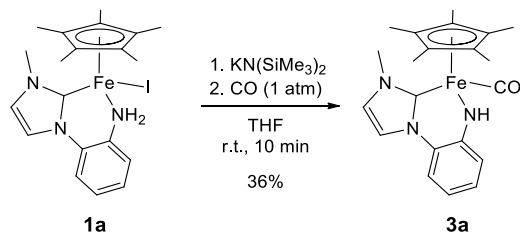
MHz, THF-*d*₈, δ), 10.7 (*C*₅*Me*₅), 42.0 (NCH₃), 74.8 (*C*₅*Me*₅), 120.2 (ImC), 121.3 (ArC), 121.7 (ArC), 125.4 (ArC), 125.8 (ArC), 126.2 (ImC), 135.7 (ArC), 138.7 (ArC), 220.8 (carbene). IR (KBr pellet, cm⁻¹), 3263, 3203, 3168, 3130, 2887, 2848, 1506, 1456, 1433, 1344, 1257, 1211, 1065, 1024, 945, 758, 714, 683, 629, 567, 511, 409. HRMS (APCI, *m/z*), Calcd. for ¹²C₂₀¹H₂₆⁵⁶Fe¹⁴N₃¹²⁷I: 491.0515, Found: 491.0516. Elemental Analysis, Calcd. for C₂₀H₂₆FeN₃I: C, 48.90; H, 5.34; N, 8.55. Found: C, 49.03; H, 5.36; N, 8.51.

2-2-2. Generation and Characterization of 2a



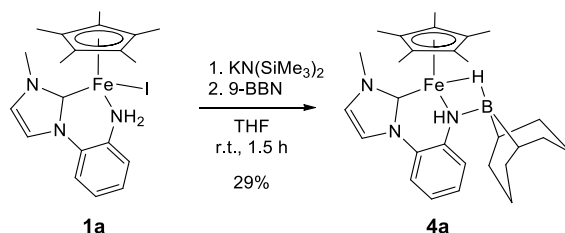
An NMR tube equipped with a J. Young Teflon valve was charged with **1a** (8.3 mg, 0.017 mmol) and THF-*d*₈ (0.4 mL). To this solution was added 1 equivalent of KN(SiMe₃)₂ (3.4 mg, 0.017 mmol). The reaction was completed immediately. The product **2a** was too reactive to be isolated, and was thus characterized by ¹H NMR and HRMS. ¹H NMR (400 MHz, THF-*d*₈, δ), 1.28 (s, 15H, Cp*), 3.39 (s, 3H, NCH₃), 6.53 (t, ³*J*_{HH} = 7.6 Hz, 1H, ArH), 6.65 (t, ³*J*_{HH} = 7.2 Hz, 1H, ArH), .02 (d, ³*J*_{HH} = 7.8 Hz, 1H, ArH), 7.06 (d, ³*J*_{HH} = 1.8 Hz, 1H, ImH), 7.09 (d, ³*J*_{HH} = 7.8 Hz, 1H, ArH), 7.58 (d, ³*J*_{HH} = 1.5 Hz, 1H, ImH), 10.32 (1H, NH). HRMS (ESI, positive, *m/z*), Calcd. for ¹²C₂₀¹H₂₅⁵⁶Fe¹⁴N₃: 363.1392, Found: 363.1392.

2-2-3. Synthesis of 3a



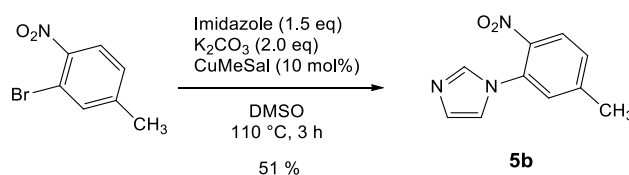
A glass vessel equipped with a J. Young Teflon valve was charged with **1a** (21.8 mg, 0.0444 mmol) and THF (3 mL). To this solution was added 1 equivalent of KN(SiMe₃)₂ (8.9 mg, 0.045 mmol) to generate **2a**, and the reaction mixture was exposed to CO (1 atm) with vigorous stirring. The color of the solution changed from brown to reddish brown. Volatiles were evaporated to dryness from the resulting mixture and the residue was extracted with a minimum amount of dry toluene. Crystallization from the extract at -30°C afforded **3a** as red crystals (6.2 mg, 0.016 mmol, 36%). ¹H NMR (400 MHz, C₆D₆, δ), -0.10 (br s, 1H, NH), 1.38 (s, 15H, Cp*), 3.15 (s, 3H, NCH₃), 6.08 (d, ³*J*_{HH} = 2.1 Hz, 1H, ImH), 6.39 (td, ³*J*_{HH} = 7.4, ⁴*J*_{HH} = 1.4 Hz, 1H, ArH), 6.68 (dd, ³*J*_{HH} = 8.5, ⁴*J*_{HH} = 1.3 Hz, 1H, ArH), 6.88 (d, ³*J*_{HH} = 2.0 Hz, 1H, ImH), 6.92–6.96 (m, 2H, ArH). ¹³C{¹H} NMR (101 MHz, C₆D₆, δ), 9.5 (*C*₅*Me*₅), 37.0 (NCH₃), 90.3 (*C*₅*Me*₅), 108.8 (ArC), 118.6 (ArC), 119.0 (ImC), 122.2 (ArC), 122.9 (ImC), 126.6 (ArC), 126.9 (ArC), 154.7 (ArC), 189.6 (carbene), 225.5 (CO). IR (KBr pellet, cm⁻¹), 1894 (s, ν_{CO}). HRMS (ESI, positive, *m/z*), Calcd. for ¹²C₂₁¹H₂₆⁵⁶Fe¹⁴N₃¹⁶O ([M+H]⁺): 392.1420, Found: 392.1420. Elemental Analysis, Calcd. for C₂₁H₂₅FeN₃O: C, 64.46; H, 6.44; N, 10.74. Found: C, 64.64, H, 6.55; N, 10.49.

2-2-4. Synthesis of 4a



A 15 mL Schlenk tube was charged with **1a** (90.7 mg, 0.185 mmol) and THF (6.5 mL). To this solution was added $\text{KN}(\text{SiMe}_3)_2$ (38.6 mg, 0.194 mmol) to generate **2a**. To the reaction mixture was added 9-BBN (22.5 mg, 0.185 mmol) with vigorous stirring. After stirring for 1.5 h, volatiles were evaporated to dryness from the resulting mixture and the residue was extracted with dry toluene (6 mL). The solvent was evaporated to dryness from the extract and the resulting residue was recrystallized from THF/hexane (1:2) mixture at -30°C to give **4a** as brown crystals (25.8 mg, 0.0532 mmol, 29%). ^1H NMR (400 MHz, $\text{THF-}d_8$, δ), -15.13 (br, 1H, Fe–H–B), -2.14 (s, 1H, CH, BBN), 0.47 (s, 1H, CH, BBN), 0.74–0.78 (m, 1H, CH_2 , BBN), 0.90–1.05 (m, 1H, CH_2 , BBN), 1.10–1.25 (m, 2H, CH_2 , BBN), 1.27–1.38 (m, 1H, CH_2 , BBN), 1.47–1.90 (m, 7H, CH_2 , BBN), 1.55 (s, 15H, Cp^*), 2.15 (s, 1H, NH), 2.25–2.40 (m, 1H, CH_2 , BBN), 4.09 (s, 3H, NCH_3), 6.97–7.05 (m, 2H, ArH), 7.18 (s, 1H, ImH), 7.27 (d, $^3J_{\text{HH}} = 7.6$ Hz, 1H, ArH), 7.36 (d, $^3J_{\text{HH}} = 7.6$ Hz, 1H, ArH), 7.55 (s, 1H, ImH). ^{11}B NMR (128 MHz, $\text{THF-}d_8$, δ), -9.0 (br). $^{13}\text{C}\{^1\text{H}\}$ NMR (101 MHz, $\text{THF-}d_8$, δ), 10.8 (C_5Me_5), 23.4 (br, CH, BBN), 26.3 (CH_2 , BBN), 28.6 (br, CH, BBN), 32.5 (CH_2 , BBN), 33.1 (CH_2 , BBN), 34.9 (CH_2 , BBN), 35.2 (CH_2 , BBN), 35.6 (CH_2 , BBN), 40.0 (NCH_3), 79.3 (C_5Me_5), 118.5 (ImC), 120.6 (ArC), 122.8 (ArC), 124.0 (ImC), 124.6 (ArC), 125.8 (ArC), 132.5 (ArC), 143.7 (ArC), 211.9 (carbene). IR (KBr pellet, cm^{-1}), 3329, 3134, 2902, 2871, 2825, 1603, 1512, 1429, 1338, 1279, 1242, 1207, 1065, 962, 904, 829, 744, 698, 675, 501. HRMS (ESI, positive, m/z), Calcd. for $^{12}\text{C}_{28}^{1}\text{H}_{40}^{11}\text{B}^{56}\text{Fe}^{14}\text{N}_3$: 485.2659, Found: 485.2659. Elemental Analysis, Calcd. for $\text{C}_{21}\text{H}_{40}\text{BFeN}_3$: C, 69.30; H, 8.31; N, 8.66. Found: C, 68.97, H, 8.50; N, 8.52.

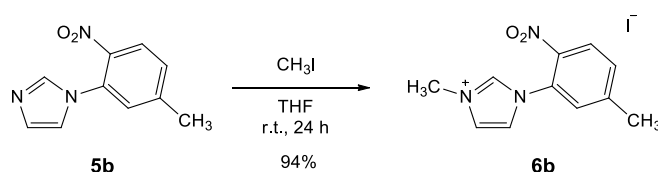
2-2-5. Synthesis of 1-(5-methyl-2-nitrophenyl)imidazole 5b



This compound was synthesized by a modified literature procedure.^[6] A dry 300 mL three-necked round bottom flask was charged with imidazole (2.37 g, 34.7 mmol), 2-bromo-4-methyl-1-nitrobenzene (4.88 g, 22.6 mmol), potassium carbonate (6.41 g, 46.4 mmol), CuMeSal (0.508 g, 2.37 mmol, 10 mol%), and DMSO (150 mL). The mixture was heated at 110°C for 3 h. The color of the mixture changed from pale green to dark brown. After cooling the resulting mixture to room temperature in air, it was filtered through Celite pad. The filtrate was poured into water (300 mL) and precipitate formed was filtered out to give a yellow solution. This solution was extracted by ethyl acetate (300 mL x 3 and 200 mL x 3) and a combined organic phase was washed by water (400 mL x 2) and brine (400 mL x 1). The organic phase was dried over MgSO_4 and concentrated to afford a brown oil. This crude product was purified by flash

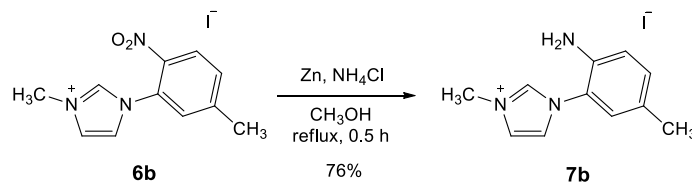
chromatography (75% EtOAc/hexane) to give **5b** as yellow crystals (2.32 g, 1.14 mmol, 51%). ¹H NMR (400 MHz, CDCl₃, δ), 2.50 (s, 3H, CH₃), 7.05 (t, ³J_{HH} = 1.3 Hz, 1H, ImH), 7.20 (t, ³J_{HH} = 1.2 Hz, 1H, ImH), 7.25 (d, ⁴J_{HH} = 1.7 Hz, 1H, ArH), 7.39 (ddd, ³J_{HH} = 8.3, ⁴J_{HH} = 1.8, ⁴J_{HH} = 0.7 Hz, 1H, ArH), 7.62 (t, ³J_{HH} = 1.4 Hz, 1H, ImH), 7.94 (d, ³J_{HH} = 8.3 Hz, 1H, ArH). ¹³C{¹H} NMR (101 MHz, CDCl₃, δ), 21.4 (CH₃), 120.3 (ImC), 125.5 (ArC), 129.2 (ArC), 130.0 (ImC), 130.2 (ArC), 130.7 (ArC), 137.2 (ImC), 142.9 (ArC), 145.5 (ArC). IR (KBr pellet, cm⁻¹), 3130, 3114, 3016, 1614, 1591, 1522, 1516, 1344, 1263, 1207, 1109, 1086, 1055, 821, 766, 652, 445. MS (EI, 70 eV, *m/z*), 203 (M⁺). Elemental Analysis, Calcd. for C₁₀H₉N₃O₂: C, 59.11; H, 4.46; N, 20.68. Found: C, 58.93; H, 4.38; N, 20.42.

2-2-6. Synthesis of 3-methyl-1-(5-methyl-2-nitrophenyl)imidazolium iodide **6b**



This compound was synthesized by a modified literature procedure.^[3] A 50 mL Schlenk flask was charged with **5b** (1.08 g, 5.31 mmol) and THF (10 mL). Iodomethane (4.12 g, 29.0 mmol, 5.5 eq) was added dropwise to this solution at room temperature. After the addition was completed, the reaction vessel was wrapped with an aluminum foil to shield it from light. After 24 h, a large amount of yellow precipitate was formed, which was collected by filtration. The precipitate was washed with diethyl ether and dried to give **6b** as a yellow powder (1.72 g, 4.98 mmol, 94%). ¹H NMR (400 MHz, DMSO-*d*₆, δ), 2.51 (s, 3H, ArCH₃), 3.99 (s, 3H, NCH₃), 7.75–7.77 (m, 2H, ArH), 7.95 (t, ³J_{HH} = 1.7 Hz, 1H, ImH), 8.10 (t, ³J_{HH} = 1.8 Hz, 1H, ImH), 8.32 (d, ³J_{HH} = 8.8 Hz, 1H, ArH), 9.56 (s, 1H, ImH). ¹³C{¹H} NMR (101 MHz, DMSO-*d*₆, δ), 20.8 (ArCH₃), 36.3 (NCH₃), 123.8 (ImC), 124.2 (ImC), 126.4 (ArC), 128.0 (ArC), 130.3 (ArC), 132.5 (ArC), 138.0 (ImC), 141.2 (ArC), 147.0 (ArC). IR (KBr pellet, cm⁻¹), 3163, 3130, 3087, 2995, 1599, 1525, 1340, 1232, 1194, 1113, 1084, 1061, 847, 822, 744, 644, 611, 445. HRMS (ESI, positive, *m/z*), Calcd. for ¹²C_{11¹H₁₂¹⁴N₃¹⁶O₂: 218.0924; Found: 218.0924 ([M–I]⁺). Elemental Analysis, Calcd. for C₁₁H₁₂N₃O₂I: C, 38.28; H, 3.50; N, 12.18. Found: C, 38.27; H, 3.55; N, 12.05.}

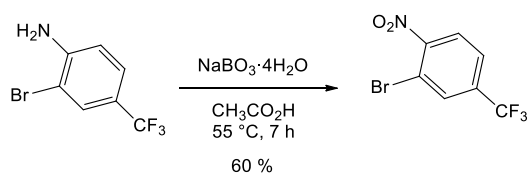
2-2-7. Synthesis of 3-methyl-1-(2-amino-5-methylphenyl)imidazolium iodide **7b**



This compound was synthesized by a modified literature procedure.^[3] A 100 mL Schlenk flask was charged with **6b** (1.70 g, 4.93 mmol) and dry methanol (50 mL). To this suspension was added zinc powder (6.45 g, 0.0987 mol, 20.0 eq) and ammonium chloride (1.63 g, 0.0305 mmol, 6.2 eq) and heated to reflux for 0.5 h. After cooling to room temperature, insoluble materials were filtered off. The obtained colorless filtrate was evaporated to dryness to afford pale yellow solids. The solids were washed with a minimum amount of acetonitrile followed by a large amount (> 50 mL) of diethyl ether and dried to give **7b** as a

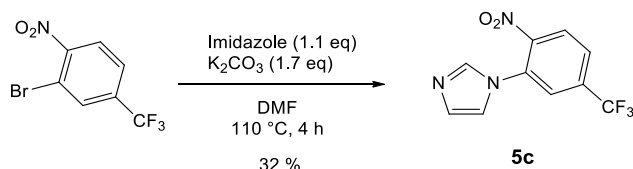
colorless powder (1.18 g, 3.74 mmol, 76%). ^1H NMR (400 MHz, $\text{DMSO-}d_6$, δ), 2.19 (s, 1H, ArCH_3), 3.90 (s, 1H, NCH_3), 5.28 (s, 2H, NH_2), 6.81 (d, $^3J_{\text{HH}} = 8.3$ Hz, 1H, ArH), 7.02 (d, $^4J_{\text{HH}} = 1.4$ Hz, 1H, ArH), 7.09 (dd, $^3J_{\text{HH}} = 8.3$, $^4J_{\text{HH}} = 1.6$ Hz, 1H, ArH), 7.83 (d, $^3J_{\text{HH}} = 1.8$ Hz, 1H, ImH), 7.88 (d, $^3J_{\text{HH}} = 1.7$ Hz, 1H, ImH), 9.34 (s, 1H, ImH). $^{13}\text{C}\{^1\text{H}\}$ NMR (101 MHz, $\text{DMSO-}d_6$, δ), 19.5 (ArCH_3), 35.9 (NCH_3), 116.6 (ArC), 119.6 (ArC), 123.5 (ImC), 123.8 (ImC), 125.1 (ArC), 127.0 (ArC), 131.8 (ArC), 137.8 (ImC), 141.1 (ArC). IR (KBr pellet, cm^{-1}), 3344, 3294, 3203, 3060, 1635, 1558, 1514, 1275, 1234, 1180, 1072, 972, 835, 742, 640, 613, 478. HRMS (ESI, positive, m/z) Calcd. for $^{12}\text{C}_{11}\text{H}_{14}\text{N}_3$: 188.1182; Found: 188.1183 ($[\text{M-I}]^+$). Elemental Analysis, Calcd. for $\text{C}_{11}\text{H}_{14}\text{N}_3\text{I}$: C, 41.92; H, 4.48; N, 13.33. Found: C, 40.51; H, 4.41; N, 13.44.

2-2-8. Preparation of 2-bromo-1-nitro-4-(trifluoromethyl)benzene



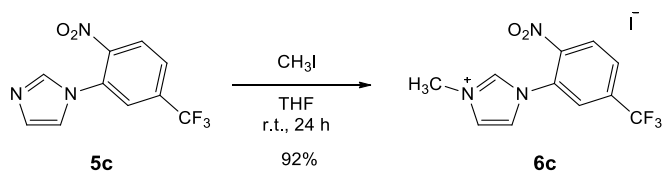
This compound was prepared by application of the procedure for oxidation of 4-(trifluoromethyl)aniline.^[7] A 300 mL three-necked round-bottom flask equipped with a reflux condenser and a dropping funnel was charged with sodium perborate tetrahydrate (40.69 g, 0.264 mol) and glacial acetic acid (50 mL). The dropping funnel was charged with 2-bromo-4-(trifluoromethyl)aniline (6.31 g, 26.8 mmol) and glacial acetic acid (50 mL). The suspension in the flask was heated to 55°C and the content of the funnel was added dropwise to it. After 3 h, an additional sodium perborate tetrahydrate (20.00 g, 0.130 mol) was added to the reaction mixture and stirred at 55°C for 4 h. The resulting yellow suspension was cooled to room temperature and filtered through a Celite pad. To the filtrate was added diethyl ether (200 mL) and water (100 mL). The organic phase was separated from the mixture and aqueous phase was extracted with diethyl ether (150 mL x 2). Combined organic phase was neutralized by aqueous sodium hydroxide solution (3 M) and separated. The separated organic phase was dried over sodium sulfate and concentrated to afford a brown liquid. This crude product was purified by flash column chromatography (12% EtOAc/hexane) to give the title compound as a yellow liquid (4.22 g, 15.6 mmol, 60 %). ^1H NMR (400 MHz, CDCl_3 , δ), 7.74 (ddd, $^3J_{\text{HH}} = 8.4$, $^4J_{\text{HH}} = 1.8$, 1H, ArH), 7.93 (d, $^3J_{\text{HH}} = 8.4$ Hz, 1H, ArH), 8.02 (br, 1H, ArH). $^{13}\text{C}\{^1\text{H}\}$ NMR (101 MHz, CDCl_3 , δ), 115.1 (ArC), 122.1 (q, $^1J_{\text{CF}} = 274$ Hz, CF_3), 125.5 (q, $^3J_{\text{CF}} = 3.3$ Hz, ArC), 125.9 (ArC), 132.3 (q, $^3J_{\text{CF}} = 3.7$ Hz, ArC), 134.9 (q, $^2J_{\text{CF}} = 34$ Hz, CCF_3), 152.0 (ArC). $^{19}\text{F}\{^1\text{H}\}$ NMR (376 MHz, CDCl_3 , δ), -63.2. IR (film, cm^{-1}), 3107, 3051, 1539, 1319, 1178, 1136, 1080, 895, 864, 841, 798, 710, 492. MS (EI, 70 eV, m/z), 271 ($\text{M}^{(81}\text{Br})^+$, 40), 269 ($\text{M}^{(79}\text{Br})^+$, 40). Elemental Analysis, Calcd. for $\text{C}_7\text{H}_3\text{NO}_2\text{BrF}_3$: C, 31.14; H, 1.12; N, 5.19. Found: C, 31.17; H, 1.17; N, 5.13.

2-2-9. Synthesis of 1-[2-nitro-5-(trifluoromethyl)phenyl]imidazole **5c**



This compound was synthesized by a modified literature procedure.^[8] A glass vessel equipped with a J. Young Teflon valve was charged with imidazole (0.964 g, 14.2 mmol, 1.1 eq), 2-bromo-1-nitro-4-(trifluoromethyl)benzene (3.45 g, 12.8 mmol), and DMF (1.8 mL). This vessel was heated to 100°C, potassium carbonate (3.01 g, 21.8 mmol, 1.7 eq) was added to it, and the mixture was stirred for 4 h at 110°C. After cooling the mixture to room temperature, water (30 mL) was added to it and the mixture was extracted with ethyl acetate (40 mL x 3). The combined organic layer was washed with water (50 mL x 2) and brine (50 mL x 1). The organic layer was dried over sodium sulfate and concentrated to afford a brown liquid. This crude product was purified by flash column chromatography (75% EtOAc/hexane) to give **5c** as a yellow solid (1.06 g, 4.12 mmol, 32%). ¹H NMR (400 MHz, CDCl₃, δ), 7.11 (t, ³J_{HH} = 1.2 Hz, 1H, ImH), 7.27 (m, 1H, ImH), 7.68 (s, 1H, ImH), 7.76 (d, ⁴J_{HH} = 2.0 Hz, 1H, ArH), 7.89 (ddd, ³J_{HH} = 8.5, ⁴J_{HH} = 1.9, 1H, ArH), 8.10 (d, ³J_{HH} = 8.4 Hz, 1H, ArH). ¹H NMR (400 MHz, CD₂Cl₂, δ), 7.13 (t, ³J_{HH} = 1.4 Hz, 1H, ImH), 7.21 (t, ³J_{HH} = 1.0 Hz, 1H, ImH), 7.65 (s, 1H, ImH), 7.79 (d, ⁴J_{HH} = 1.6 Hz, 1H, ArH), 7.91 (ddd, ³J_{HH} = 8.5, ⁴J_{HH} = 1.9, 1H, ArH), 8.12 (d, ³J_{HH} = 8.4 Hz, 1H, ArH). ¹³C{¹H} NMR (101 MHz, CDCl₃, δ), 120.0 (ImC), 122.1 (q, ¹J_{CF} = 274 Hz, CF₃), 125.9 (q, ³J_{CF} = 3.5 Hz, ArC), 126.0 (ArC), 126.6 (q, ³J_{CF} = 3.5 Hz, ArC), 131.0 (ImC), 131.1 (ArC), 135.5 (q, ²J_{CF} = 34 Hz, CCF₃), 137.1 (ImC), 147.2 (ArC). ¹⁹F{¹H} NMR (376 MHz, CDCl₃, δ), -63.1. IR (KBr pellet, cm⁻¹), 3103, 3026, 2983, 2910, 1604, 1537, 1508, 1439, 1329, 1288, 1248, 1184, 1133, 1055, 904, 860, 839, 737, 656, 623, 509, 455, 422. MS (EI, 70 eV, *m/z*), 257 (M⁺). Elemental Analysis, Calcd. for C₁₀H₆N₃O₂F₃: C, 46.70; H, 2.35; N, 16.34. Found: C, 46.77; H, 2.39; N, 16.34.

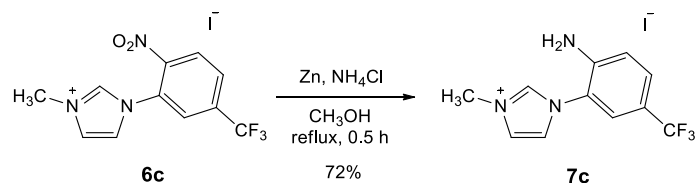
2-2-10. Synthesis of 1-[2-nitro-5-(trifluoromethyl)phenyl]-3-methylimidazolium iodide **6c**



This compound was synthesized by the same method as that for synthesis of **6b** using **5c** (1.05 g, 4.08 mmol). A yellow powder. Yield 1.50 g (3.76 mmol, 92%). ¹H NMR (400 MHz, DMSO-*d*₆, δ), 4.00 (s, 3H, NCH₃), 7.95 (t, ³J_{HH} = 1.8 Hz, 1H, ImH), 8.12 (t, ³J_{HH} = 1.8 Hz, 1H, ImH), 8.38 (dd, ³J_{HH} = 8.3, ⁴J_{HH} = 1.8 Hz, 1H, ArH), 8.47 (d, ⁴J_{HH} = 1.9 Hz, 1H, ArH), 8.61 (d, ³J_{HH} = 8.6 Hz, 1H, ArH), 9.57 (s, 1H, ImH). ¹³C{¹H} NMR (101 MHz, DMSO-*d*₆, δ), 36.3 (NCH₃), 122.4 (q, ¹J_{CF} = 274 Hz, CF₃), 123.8 (ImC), 124.3 (ImC), 127.7 (ArC), 127.8 (³J_{CF} = 3.6 Hz, ArC), 128.9 (ArC), 129.5 (q, ³J_{CF} = 3.4 Hz, ArC), 133.9 (q, ²J_{CF} = 34 Hz, CCF₃), 138.5 (ImC), 146.1 (ArC). ¹⁹F{¹H} NMR (376 MHz, CDCl₃, δ), -61.7. IR (KBr pellet, cm⁻¹), 3169, 3138, 3053, 1539, 1442, 1336, 1315, 1174, 1138, 1130, 1109, 1074, 856, 744, 615, 509. HRMS (ESI, positive, *m/z*), Calcd. for ¹²C₁₁¹H₉¹⁴N₃¹⁶O₂¹⁹F₃: 272.0641; Found: 272.0641 ([M-I]⁺).

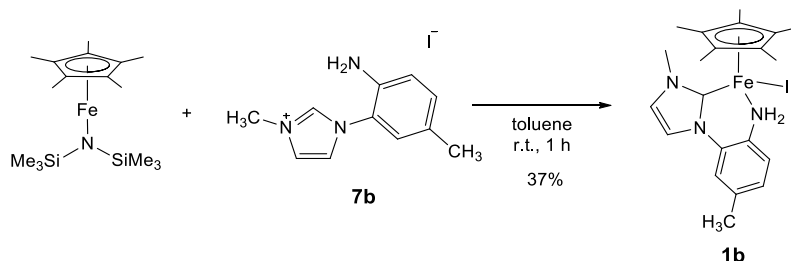
Elemental Analysis, Calcd. for $C_{11}H_9N_3O_2IF_3$: C, 33.10; H, 2.27; N, 10.53. Found: C, 33.21; H, 2.48; N, 10.48.

2-2-11. Synthesis of 1-[2-amino-5-(trifluoromethyl)phenyl]-3-methylimidazolium iodide **7c**



This compound was synthesized by the same method as that for synthesis of **7b** using **6c** (1.48g, 3.71 mmol). A colorless powder. Yield 0.980 g (2.65 mmol, 72%). ^1H NMR (400 MHz, $\text{DMSO-}d_6$, δ), 3.90 (s, 3H, NCH_3), 6.24 (s, 2H, NH_2), 7.00 (d, $^3J_{\text{HH}} = 8.4$ Hz, 1H, ArH), 7.58 (dd, $^3J_{\text{HH}} = 8.8$, $^4J_{\text{HH}} = 1.8$ Hz, 1H, ArH), 7.65 (d, $^4J_{\text{HH}} = 1.6$ Hz, 1H, ArH), 7.88 (t, $^3J_{\text{HH}} = 1.6$ Hz, 1H, ImH), 7.89 (t, $^3J_{\text{HH}} = 1.6$ Hz, 1H, ImH), 9.40 (s, 1H, ImH). $^{13}\text{C}\{^1\text{H}\}$ NMR (101 MHz, $\text{DMSO-}d_6$, δ), 36.0 (NCH_3), 115.5 (q, $^2J_{\text{CF}} = 33$ Hz, CCF_3), 116.2 (ArC), 118.5 (ArC), 123.7 (ImC), 124.1 (ImC), 124.4 (q, $^1J_{\text{CF}} = 270$ Hz, CF_3), 125.4 (q, $^3J_{\text{CF}} = 4.0$ Hz, ArC), 128.1 (q, $^3J_{\text{CF}} = 3.3$ Hz, ArC), 138.4 (ImC), 147.5 (ArC). $^{19}\text{F}\{^1\text{H}\}$ NMR (376 MHz, CDCl_3 , δ), -59.3 . IR (KBr pellet, cm^{-1}), 3379, 3303, 3207, 3089, 3055, 1641, 1556, 1523, 1450, 1340, 1325, 1311, 1176, 1159, 1130, 1099, 1076, 897, 843, 744, 615, 482. HRMS (ESI, positive, m/z), Calcd. for $^{12}\text{C}_{11}^{14}\text{H}_{14}^{14}\text{N}_3^{19}\text{F}_3$: 242.0900; Found: 242.0900 ($[\text{M}-\text{I}]^+$). Elemental Analysis, Calcd. for $C_{11}H_{11}N_3IF_3$: C, 35.79; H, 3.00; N, 11.38. Found: C, 34.68; H, 3.14; N, 11.58.

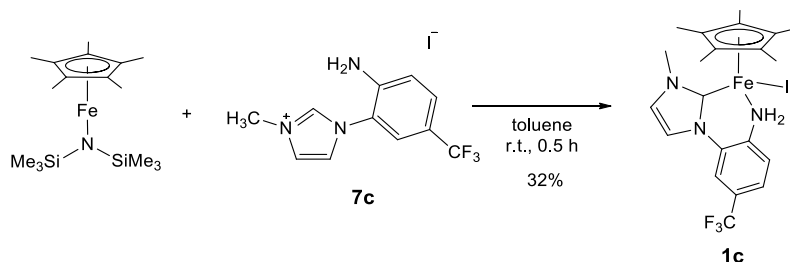
2-2-12. Synthesis of **1b**



This complex was synthesized by a procedure similar to that for the synthesis of **1a** using $\text{Cp}^*\text{FeN}(\text{SiMe}_3)_2$ (0.107 g, 0.304 mmol), 3-methyl-1-(2-amino-5-methylphenyl)imidazolium iodide **7b** (0.0967 g, 0.307 mmol), dry toluene (7 mL) to give **1b** as black crystals containing one equivalent of THF molecule as solvent of crystallization (65.6 mg, 0.114 mmol, 37% as **1b**·THF). ^1H NMR (400 MHz, C_6D_6 , δ), 1.50 (s, 15H, Cp^*), 2.00 (s, 3H, ArCH_3), 2.56 (br, 2H, NH_2), 4.12 (s, NCH_3 , 3H), 6.27, 6.47, 6.56, 6.72, 6.83 (ImH, ArH). ^1H NMR (400 MHz, $\text{THF-}d_8$, δ), 1.42 (s, 15H, Cp^*), 2.35 (s, 3H, ArCH_3), 4.32 (s, 3H, NCH_3), 6.92 (d, $^3J_{\text{HH}} = 7.6$ Hz, 1H, ArH), 7.10 (d, $^3J_{\text{HH}} = 7.6$ Hz, 1H, ArH), 7.39 (s, 1H, ArH), 7.56 (s, 1H, ImH), 7.86 (s, 1H, ImH). $^{13}\text{C}\{^1\text{H}\}$ NMR (101 MHz, $\text{THF-}d_8$, δ), 10.7 (C_5Me_5), 20.9 (ArCH_3), 42.0 (NCH_3), 74.7 (C_5Me_5), 120.1 (ImC), 121.6 (ArC), 121.9 (ArC), 126.0 (ImC), 126.1 (ArC), 135.2 (ArC), 135.4 (ArC), 135.9 (ArC), 220.6 (carbene). IR (KBr pellet, cm^{-1}), 3249, 3199, 3124, 2968, 2941, 2895, 2852, 1518, 1448, 1340, 1263, 1215, 1065, 1053, 1026, 823, 714, 681, 625. HRMS (ESI, positive, m/z), Calcd. for $^{12}\text{C}_{21}^{14}\text{H}_{28}^{56}\text{Fe}^{14}\text{N}_3^{127}\text{I}$: 505.0672, Found: 505.0672. Elemental Analysis, Calcd. for $\text{C}_{21}\text{H}_{28}\text{FeN}_3\text{I} + \text{C}_4\text{H}_8\text{O}$:

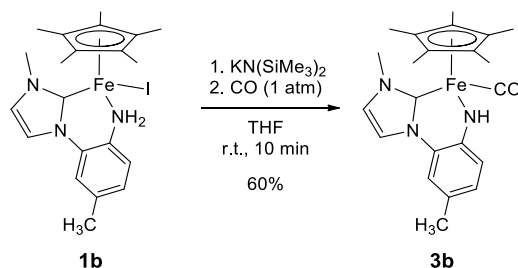
C, 52.01; H, 6.29; N, 7.28. Found: C, 51.90; H, 6.26; N, 7.50.

2-2-13. Synthesis of **1c**



This complex was synthesized by a procedure similar to that for the synthesis of **1a** using Cp*FeN(SiMe₃)₂ (0.144 g, 0.410 mmol), 1-[2-amino-5-(trifluoromethyl)phenyl]-3-methylimidazolium iodide **7c** (0.151 g, 0.409 mmol), and dry toluene (9 mL) to afford **1c** as black crystals (73.3 mg, 0.131 mmol, 32%). ¹H NMR (400 MHz, C₆D₆, δ), 1.43 (s, 15H, Cp*), 2.41 (br, 2H, NH₂), 3.94 (s, NCH₃, 3H), 6.11, 6.43, 6.54, 6.89 (ImH, ArH). ¹H NMR (400 MHz, THF-*d*₈, δ), 1.47 (s, 15H, Cp*), 4.29 (s, NCH₃, 3H), 7.35 (d, ³J_{HH} = 7.6 Hz, 1H, ArH), 7.46 (d, ³J_{HH} = 7.6 Hz, 1H, ArH), 7.62 (s, 1H, ImH), 7.89 (s, 1H, ArH), 8.07 (s, 1H, ImH). ¹³C{¹H} NMR (101 MHz, THF-*d*₈, δ), 9.5, 41.4, 74.6, 117.5, 119.4, 120.8, 122.0, 123.0, 125.6, 135.1, 141.6, 215.9. ¹⁹F{¹H} NMR (377 MHz, THF-*d*₈, δ), -62.6. IR (KBr pellet, cm⁻¹), 3248, 3199, 3159, 3086, 2900, 2854, 1608, 1512, 1448, 1321, 1292, 1271, 1171, 1130, 1082, 1059, 1018, 877, 825, 773, 723, 681, 648, 609, 515. HRMS (ESI, positive, *m/z*), Calcd. for ¹²C₂₁¹H₂₅⁵⁶Fe¹⁴N₃¹²⁷I¹⁹F₃: 559.0388, Found: 505.0389. Elemental Analysis, Calcd. for C₂₁H₂₅FeN₃IF₃: C, 45.11; H, 4.51; N, 7.51. Found: C, 45.19; H, 4.57; N, 7.53.

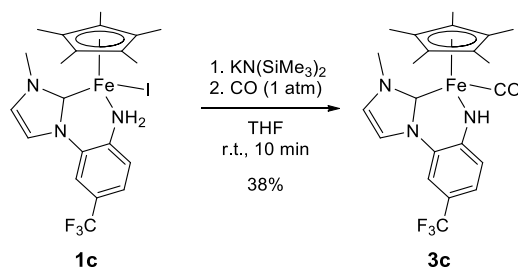
2-2-14. Synthesis of **3b**



This complex was synthesized by a procedure similar to that for the synthesis of **3a** using **1b**·THF (28.0 mg, 0.0485 mmol), KN(SiMe₃)₂ (9.7 mg, 0.049 mmol), THF (3 mL), and CO (1 atm). Crystallization from toluene/hexane (1:1) at -30°C afforded **3b** as orange crystals (11.7 mg, 0.0289 mmol, 60%). ¹H NMR (400 MHz, C₆D₆, δ), -0.30 (br s, 1H, NH), 1.40 (s, 15H, Cp*), 2.33 (s, 3H, ArCH₃), 3.18 (s, 3H, NCH₃), 6.10 (d, ³J_{HH} = 1.6 Hz, 1H, ImH), 6.65 (d, ³J_{HH} = 8.0 Hz, 1H, ArH), 6.75 (dd, ³J_{HH} = 8.0, ⁴J_{HH} = 1.6 Hz, 1H, ArH), 6.81 (br, 1H, ArH), 6.89 (d, ³J_{HH} = 2.0 Hz, 1H, ImH). ¹³C{¹H} NMR (101 MHz, C₆D₆, δ), 9.5 (C₅Me₅), 20.8 (ArCH₃), 37.0 (NCH₃), 90.2 (C₅Me₅), 117.1 (ArC), 118.9 (ImC), 119.2 (ArC), 122.0 (ArC), 122.9 (ImC), 126.6 (ArC), 127.3 (ArC), 152.3 (ArC), 189.8 (carbene), 225.5 (CO). IR (KBr pellet, cm⁻¹), 1884 (s, ν_{CO}). HRMS (ESI, positive, *m/z*), Calcd. for ¹²C₂₂¹H₂₈⁵⁶Fe¹⁴N₃¹⁶O ([M+H]⁺): 406.1578, Found: 406.1576. Elemental Analysis, Calcd. for C₂₂H₂₇FeN₃O: C, 65.19; H, 6.71; N, 10.37. Found: C, 65.15; H,

6.78; N, 10.26.

2-2-15. Synthesis of 3c



This complex was synthesized by a procedure similar to that for the synthesis of **3a** using **1c** (34.5 mg, 0.0617 mmol), $\text{KN}(\text{SiMe}_3)_2$ (12.3 mg, 0.062 mmol), THF (3 mL), and CO (1 atm). Crystallization from toluene/hexane (1:1) at -30°C afforded **3c** as orange crystals (10.7 mg, 0.0233 mmol, 38%). ^1H NMR (400 MHz, C_6D_6 , δ), 0.53 (br s, 1H, NH), 1.26 (s, 15H, Cp*), 3.05 (s, 3H, NCH₃), 5.95 (d, $^3J_{\text{HH}} = 2.1$ Hz, 1H, ImH), 6.35 (d, $^3J_{\text{HH}} = 8.5$ Hz, 1H, ArH), 6.58 (d, $^3J_{\text{HH}} = 2.1$ Hz, 1H, ImH), 7.11 (dd, $^3J_{\text{HH}} = 8.6$, $^4J_{\text{HH}} = 1.9$ Hz, 1H, ArH), 7.28 (d, $^3J_{\text{HH}} = 1.8$ Hz, 1H, ArH). $^{13}\text{C}\{^1\text{H}\}$ NMR (101 MHz, C_6D_6 , δ), 9.3 (C_5Me_5), 37.0 (NCH₃), 90.5 (C_5Me_5), 108.8 (q, $^2J_{\text{CF}} = 32.8$ Hz, ArC), 116.0 (q, $^3J_{\text{CF}} = 3.7$ Hz, ArC), 119.2 (ImC), 121.2 (ArC), 123.2 (ImC), 123.4 (q, $^3J_{\text{CF}} = 3.3$ Hz, ArC), 125.4 (ArC), 127.2 (q, $^1J_{\text{CF}} = 268.5$ Hz, CF₃), 157.5 (ArC), 189.8 (carbene), 224.8 (CO). $^{19}\text{F}\{^1\text{H}\}$ NMR (376 MHz, C_6D_6 , δ), -58.4 . IR (KBr pellet, cm^{-1}), 1896 (s, ν_{CO}). HRMS (ESI, positive, m/z), Calcd. for $^{12}\text{C}_{22}^{1}\text{H}_{25}^{56}\text{Fe}^{14}\text{N}_3^{16}\text{O}^{19}\text{F}_3$ ($[\text{M}+\text{H}]^+$): 460.1294, Found: 460.1294. Elemental Analysis, Calcd. for $\text{C}_{22}\text{H}_{24}\text{FeN}_3\text{OF}_3$: C, 57.53; H, 5.27; N, 9.15. Found: C, 57.88, H, 5.34; N, 9.37.

2-2-16. X-ray Crystallography Single crystals of **1a–1c**, **3a–3c**, and **4a** were immersed in liquid paraffin and were mounted on a glass fiber. Diffraction measurements were made on a Rigaku RAXIS-RAPID imaging plate diffractometer with graphite-monochromated Mo K α radiation ($\lambda = 0.71073$ Å) under cold nitrogen stream ($T = 150$ K). Numerical absorption corrections were made using the NUMABS. The structures were solved by either direct or Patterson methods using the program SHELXS-97^[9] and refined by full matrix least-squares techniques on all F^2 data using the program SHELXL-97.^[10] Yadokari-XG 2009 software^[11] was used as a graphical user interface for SHELXS-97 and SHELXL-97. Conditions of the measurement of reflection intensity, handlings of anisotropic displacement parameters and hydrogen atoms, and locations of crystallographic data are listed in Table 2-1.

2-2-17. DFT Calculations Gaussian 09 (G09) program package (revision D.01)^[12] was used for all computations. Geometry optimizations of **1a–1c** in gas phase were performed at the B3PW91 level using 6-31G(d) basis sets for H, C, N, and F atoms and LanL2DZ basis sets for Fe and I atoms. Frequency analysis calculations were performed to characterize the structures to be the minima (no imaginary frequency). These functional and basis sets were used as implemented in G09. The optimized atomic coordinates of **1a–1c** are listed in Supporting Information (Tables S1-S3).

Table 2-1. Conditions of the measurement of reflection intensity, handlings of anisotropic displacement parameters and hydrogen atoms, and locations of crystallographic data

Complexes	1a	1b·THF	1c
Images	58	69	57
Oscillation angles /deg	290.0	345.0	285.0
Goniometer setting	3	3	3
Exposure time (min/deg)	1.00	1.00	0.80
Camera radius (mm)	127.40	127.40	127.40
Readout	0.100 mm pixel mode	0.100 mm pixel mode	0.100 mm pixel mode
Anisotropic displacement parameters	Anisotropic displacement parameters were applied to all non-hydrogen atoms.	Anisotropic displacement parameters were applied to all non-hydrogen atoms except for a THF molecule.	Anisotropic displacement parameters were applied to all non-hydrogen atoms.
Hydrogen atoms	All the hydrogen atoms were placed at their geometrically calculated positions except for amino protons.	All the hydrogen atoms were placed at their geometrically calculated positions except for amino protons.	All the hydrogen atoms were placed at their geometrically calculated positions.
Crystallographic data	Table 2-2	Table 2-6	Table 2-10
Atomic coordinates and equivalent isotropic displacement parameters	Table 2-3	Table 2-7	Table 2-11
Anisotropic displacement parameters	Table 2-4	Table 2-8	Table 2-12
Hydrogen coordinates	Table 2-5	Table 2-9	Table 2-13

(continued) **Table 2-1.**

Complexes	3a	3b	3c	4a
Images	44	56	58	60
Oscillation angles (°)	220.0	280.0	290.0	300.0
Goniometer setting	2	3	3	3
Exposure time (min/°)	1.70	1.00	1.00	4.50
Camera radius (mm)	127.40	127.40	127.40	127.40
Readout	0.100 mm pixel mode	0.100 mm pixel mode	0.100 mm pixel mode	0.100 mm pixel mode
Anisotropic displacement parameters	Anisotropic displacement parameters were applied to all non-hydrogen atoms.	Anisotropic displacement parameters were applied to all non-hydrogen atoms.	Anisotropic displacement parameters were applied to all non-hydrogen atoms.	Anisotropic displacement parameters were applied to all non-hydrogen atoms.
Hydrogen atoms	All the hydrogen atoms were placed at their geometrically calculated positions except for an amido proton.	All the hydrogen atoms were placed at their geometrically calculated positions except for an amido proton.	All the hydrogen atoms were placed at their geometrically calculated positions except for an amido proton.	All the hydrogen atoms were placed at their geometrically calculated positions except for an amido proton and bridged hydrogen of Fe–H–B.
Crystallographic data	Table 2-14	Table 2-18	Table 2-22	Table 2-26
Atomic coordinates and equivalent isotropic displacement parameters	Table 2-15	Table 2-19	Table 2-23	Table 2-27
Anisotropic displacement parameters	Table 2-16	Table 2-20	Table 2-24	Table 2-28
Hydrogen coordinates	Table 2-17	Table 2-21	Table 2-25	Table 2-29

Table 2-2. Crystal data and structure refinement for **1a**

Empirical formula	$C_{20}H_{26}FeIN_3$	
Formula weight	491.19	
Temperature	150(2) K	
Wavelength	0.71073 Å	
Crystal system	Monoclinic	
Space group	$P2_1/n$	
Unit cell dimensions	$a = 10.4328(3)$ Å	$\alpha = 90^\circ$
	$b = 13.7120(4)$ Å	$\beta = 106.3483(7)^\circ$
	$c = 14.7125(3)$ Å	$\gamma = 90^\circ$
Volume	2019.59(9) Å ³	
<i>Z</i>	4	
Density (calculated)	1.615 g/cm ³	
Absorption coefficient	2.283 mm ⁻¹	
<i>F</i> (000)	984	
Crystal size	0.45 x 0.42 x 0.34 mm ³	
Theta range for data collection	2.07 to 27.48°	
Index ranges	$-13 \leq h \leq 13, -17 \leq k \leq 16, -19 \leq l \leq 17$	
Reflections collected	24573	
Independent reflections	4632 [<i>R</i> (int) = 0.0313]	
Reflections with $I > 2\sigma(I)$	4475	
Completeness to $\theta = 27.48^\circ$	100.0 %	
Max. and min. transmission	0.5108 and 0.4265	
Refinement method	Full-matrix least-squares on F^2	
Data / restraints / parameters	4632 / 0 / 240	
Goodness-of-fit on F^2	1.369	
Final <i>R</i> indices [$I > 2\sigma(I)$]	$R1 = 0.0204, wR2 = 0.0630$	
<i>R</i> indices (all data)	$R1 = 0.0223, wR2 = 0.0706$	
Largest diff. peak and hole	0.716 and -0.822 e Å ⁻³	

$$R1 = \Sigma||F_o| - |F_c|| / \Sigma|F_o|.$$

$$wR2 = [\Sigma[w(F_o^2 - F_c^2)^2] / \Sigma[w(F_o^2)^2]]^{0.5},$$

$$\text{calc } w = 1/[\sigma^2(F_o^2) + (0.0376P)^2 + 0.6532P] \text{ where } P = (F_o^2 + 2F_c^2)/3.$$

Table 2-3. Atomic coordinates ($\times 10^4$) and equivalent isotropic displacement parameters ($\text{\AA}^2 \times 10^3$)
for **1a**

	<i>x</i>	<i>y</i>	<i>z</i>	<i>U</i> (eq)
I(1)	1435(1)	3676(1)	9366(1)	19(1)
Fe(1)	745(1)	5132(1)	8077(1)	13(1)
N(1)	-1072(2)	5129(1)	8387(1)	16(1)
N(2)	-1490(2)	4285(1)	6598(1)	17(1)
N(3)	291(2)	3474(1)	6672(1)	19(1)
C(1)	-144(2)	4247(1)	7077(1)	15(1)
C(2)	-1849(2)	3549(2)	5921(2)	22(1)
C(3)	-733(2)	3042(2)	5973(1)	23(1)
C(4)	1647(2)	3091(2)	6951(2)	27(1)
C(5)	-2353(2)	5042(1)	6719(1)	18(1)
C(6)	-2160(2)	5462(2)	7615(1)	17(1)
C(7)	-2989(2)	6221(2)	7731(2)	23(1)
C(8)	-3982(2)	6575(2)	6962(2)	29(1)
C(9)	-4170(2)	6155(2)	6074(2)	29(1)
C(10)	-3364(2)	5389(2)	5953(2)	24(1)
C(11)	2112(2)	6143(2)	8880(1)	20(1)
C(12)	992(2)	6636(2)	8283(1)	19(1)
C(13)	868(2)	6373(1)	7318(2)	19(1)
C(14)	1964(2)	5734(2)	7323(1)	19(1)
C(15)	2719(2)	5581(2)	8278(1)	20(1)
C(16)	2655(3)	6259(2)	9932(2)	31(1)
C(17)	134(2)	7364(2)	8603(2)	30(1)
C(18)	-90(2)	6799(2)	6456(2)	30(1)
C(19)	2312(2)	5401(2)	6454(2)	29(1)
C(20)	4017(2)	5034(2)	8610(2)	30(1)

U(eq) is defined as one third of the trace of the orthogonalized U_{ij} tensor.

Table 2-4. Anisotropic displacement parameters ($\text{\AA}^2 \times 10^3$) for **1a**

	U_{11}	U_{22}	U_{33}	U_{23}	U_{13}	U_{12}
I(1)	22(1)	16(1)	17(1)	4(1)	3(1)	1(1)
Fe(1)	13(1)	12(1)	13(1)	1(1)	3(1)	0(1)
N(1)	17(1)	16(1)	14(1)	-1(1)	4(1)	0(1)
N(2)	17(1)	18(1)	14(1)	-2(1)	2(1)	0(1)
N(3)	24(1)	16(1)	19(1)	-2(1)	7(1)	3(1)
C(1)	17(1)	14(1)	16(1)	2(1)	6(1)	1(1)
C(2)	29(1)	20(1)	16(1)	-4(1)	3(1)	-5(1)
C(3)	33(1)	19(1)	18(1)	-4(1)	7(1)	-3(1)
C(4)	25(1)	25(1)	32(1)	-3(1)	9(1)	10(1)
C(5)	15(1)	18(1)	20(1)	0(1)	3(1)	0(1)
C(6)	14(1)	18(1)	17(1)	1(1)	4(1)	0(1)
C(7)	20(1)	25(1)	24(1)	-1(1)	6(1)	4(1)
C(8)	23(1)	30(1)	34(1)	1(1)	6(1)	11(1)
C(9)	20(1)	34(1)	27(1)	6(1)	-2(1)	7(1)
C(10)	20(1)	30(1)	19(1)	0(1)	-1(1)	1(1)
C(11)	21(1)	17(1)	19(1)	0(1)	3(1)	-7(1)
C(12)	22(1)	14(1)	23(1)	1(1)	8(1)	-4(1)
C(13)	21(1)	15(1)	21(1)	5(1)	5(1)	-2(1)
C(14)	20(1)	18(1)	20(1)	2(1)	8(1)	-3(1)
C(15)	15(1)	20(1)	23(1)	4(1)	3(1)	-4(1)
C(16)	37(1)	31(1)	22(1)	-4(1)	2(1)	-15(1)
C(17)	36(1)	16(1)	42(1)	-2(1)	19(1)	-1(1)
C(18)	29(1)	30(1)	29(1)	14(1)	4(1)	3(1)
C(19)	34(1)	33(1)	24(1)	2(1)	15(1)	-1(1)
C(20)	17(1)	34(1)	38(1)	7(1)	4(1)	1(1)

The anisotropic displacement factor exponent takes the form: $-2\pi^2[h^2a^{*2}U_{11} + k^2b^{*2}U_{22} + l^2c^{*2}U_{33} + 2klb^{*c^{*}}U_{23} + 2hla^{*b^{*}}U_{13} + 2hka^{*b^{*}}U_{12}]$.

Table 2-5. Hydrogen coordinates ($\times 10^4$) and isotropic displacement parameters ($\text{\AA}^2 \times 10^3$) for **1a**

	<i>x</i>	<i>y</i>	<i>z</i>	<i>U</i> (eq)
H(1)	-1060(30)	5430(20)	8880(20)	23(6)
H(2)	-1180(20)	4550(20)	8486(17)	17(6)
H(3)	-2713	3429	5506	27
H(4)	-655	2491	5602	28
H(5)	2208	3501	7452	40
H(6)	2005	3091	6403	40
H(7)	1639	2423	7186	40
H(8)	-2874	6498	8340	28
H(9)	-4530	7102	7043	35
H(10)	-4853	6393	5548	35
H(11)	-3502	5101	5346	29
H(12)	1950	6505	10192	47
H(13)	3401	6721	10072	47
H(14)	2968	5626	10218	47
H(15)	547	8011	8649	44
H(16)	47	7172	9224	44
H(17)	-753	7385	8144	44
H(18)	310	7378	6255	45
H(19)	-917	6983	6604	45
H(20)	-290	6315	5945	45
H(21)	2993	4889	6624	43
H(22)	2660	5953	6172	43
H(23)	1511	5143	5996	43
H(24)	4762	5498	8759	45
H(25)	4107	4590	8109	45
H(26)	4029	4657	9178	45

Table 2-6. Crystal data and structure refinement for **1b·THF**

Empirical formula	C ₂₅ H ₃₆ Fe I N ₃ O	
Formula weight	577.32	
Temperature	150(2) K	
Wavelength	0.71073 Å	
Crystal system	Monoclinic	
Space group	<i>P</i> 2 ₁ / <i>a</i>	
Unit cell dimensions	<i>a</i> = 10.6689(4) Å	$\alpha = 90^\circ$
	<i>b</i> = 18.3209(5) Å	$\beta = 103.4358(12)^\circ$
	<i>c</i> = 13.4716(5) Å	$\gamma = 90^\circ$
Volume	2561.14(15) Å ³	
<i>Z</i>	4	
Density (calculated)	1.497 g/cm ³	
Absorption coefficient	1.815 mm ⁻¹	
<i>F</i> (000)	1176	
Crystal size	0.41 x 0.27 x 0.25 mm ³	
Theta range for data collection	1.55 to 27.48°	
Index ranges	-13 ≤ <i>h</i> ≤ 13, -23 ≤ <i>k</i> ≤ 23, -17 ≤ <i>l</i> ≤ 17	
Reflections collected	36538	
Independent reflections	5876 [<i>R</i> (int) = 0.0620]	
Reflections with <i>I</i> > 2σ(<i>I</i>)	5517	
Completeness to $\theta = 27.48^\circ$	100.0 %	
Absorption correction	Numerical	
Max. and min. transmission	0.6597 and 0.5232	
Refinement method	Full-matrix least-squares on <i>F</i> ²	
Data / restraints / parameters	5876 / 0 / 270	
Goodness-of-fit on <i>F</i> ²	1.194	
Final <i>R</i> indices [<i>I</i> > 2σ(<i>I</i>)]	<i>R</i> 1 = 0.0408, <i>wR</i> 2 = 0.1185	
<i>R</i> indices (all data)	<i>R</i> 1 = 0.0455, <i>wR</i> 2 = 0.1283	
Largest diff. peak and hole	1.631 and -0.976 e Å ⁻³	

$$R1 = \Sigma||F_o| - |F_c|| / \Sigma|F_o|.$$

$$wR2 = [\Sigma[w(F_o^2 - F_c^2)^2] / \Sigma[w(F_o^2)^2]]^{0.5},$$

$$\text{calc } w = 1/[\sigma^2(F_o^2) + (0.0676P)^2 + 4.5937P] \text{ where } P = (F_o^2 + 2 F_c^2)/3.$$

Table 2-7. Atomic coordinates ($\times 10^4$) and equivalent isotropic displacement parameters ($\text{\AA}^2 \times 10^3$) for **1b**

	<i>x</i>	<i>y</i>	<i>z</i>	<i>U</i> (eq)
I(1)	69(1)	6311(1)	4247(1)	26(1)
Fe(1)	817(1)	5392(1)	2914(1)	19(1)
N(1)	1649(3)	4793(2)	4184(2)	22(1)
N(2)	3650(3)	5493(2)	3518(2)	22(1)
N(3)	2872(3)	6539(2)	2977(2)	24(1)
C(1)	2490(3)	5847(2)	3139(3)	20(1)
C(2)	4692(3)	5960(2)	3574(3)	27(1)
C(3)	4201(4)	6612(2)	3243(3)	28(1)
C(4)	2015(4)	7144(2)	2600(3)	30(1)
C(5)	3758(3)	4737(2)	3765(3)	21(1)
C(6)	2758(3)	4385(2)	4081(3)	22(1)
C(7)	2853(4)	3641(2)	4269(3)	27(1)
C(8)	3931(4)	3249(2)	4162(3)	31(1)
C(9)	4962(4)	3605(2)	3899(3)	30(1)
C(10)	4850(3)	4348(2)	3682(3)	27(1)
C(11)	6171(4)	3192(3)	3862(4)	44(1)
C(12)	-1073(3)	5115(2)	2153(3)	27(1)
C(13)	-250(4)	4504(2)	2184(3)	28(1)
C(14)	767(4)	4707(2)	1705(3)	27(1)
C(15)	524(4)	5440(2)	1345(3)	26(1)
C(16)	-589(3)	5696(2)	1630(3)	26(1)
C(17)	-2284(4)	5134(3)	2542(4)	43(1)
C(18)	-415(5)	3767(2)	2617(4)	42(1)
C(19)	1787(4)	4208(3)	1476(3)	41(1)
C(20)	1294(4)	5832(3)	711(3)	38(1)
C(21)	-1247(5)	6423(2)	1373(4)	39(1)
O(1)	5253(19)	3651(10)	1064(16)	285(9)
C(22)	5338(15)	3976(9)	66(13)	158(5)
C(23)	5270(12)	3375(8)	-594(9)	129(4)
C(24)	4535(6)	2847(4)	-272(5)	60(1)
C(25)	4632(12)	2941(7)	748(9)	120(4)

U(eq) is defined as one third of the trace of the orthogonalized U_{ij} tensor.

Table 2-8. Anisotropic displacement parameters ($\text{\AA}^2 \times 10^3$) for **1b**

	U_{11}	U_{22}	U_{33}	U_{23}	U_{13}	U_{12}
I(1)	34(1)	19(1)	27(1)	-2(1)	13(1)	0(1)
Fe(1)	19(1)	18(1)	20(1)	-2(1)	5(1)	-1(1)
N(1)	25(1)	18(1)	25(1)	2(1)	7(1)	-2(1)
N(2)	21(1)	18(1)	25(1)	-1(1)	4(1)	-2(1)
N(3)	28(2)	19(1)	27(2)	2(1)	8(1)	-3(1)
C(1)	23(2)	17(2)	20(2)	-1(1)	5(1)	-1(1)
C(2)	22(2)	27(2)	32(2)	-2(2)	6(1)	-6(1)
C(3)	26(2)	23(2)	36(2)	1(2)	7(2)	-6(1)
C(4)	33(2)	19(2)	38(2)	7(2)	9(2)	2(1)
C(5)	22(2)	18(2)	22(2)	0(1)	3(1)	0(1)
C(6)	22(2)	19(2)	22(2)	-1(1)	2(1)	-1(1)
C(7)	29(2)	20(2)	30(2)	4(1)	4(2)	-3(1)
C(8)	33(2)	19(2)	38(2)	-1(2)	2(2)	2(1)
C(9)	28(2)	25(2)	35(2)	-3(2)	2(2)	6(1)
C(10)	23(2)	25(2)	32(2)	-2(2)	6(1)	0(1)
C(11)	34(2)	32(2)	66(3)	-3(2)	12(2)	10(2)
C(12)	21(2)	35(2)	26(2)	-6(2)	4(1)	-5(1)
C(13)	31(2)	26(2)	24(2)	-7(1)	1(1)	-6(1)
C(14)	26(2)	31(2)	23(2)	-9(1)	2(1)	2(1)
C(15)	25(2)	34(2)	20(2)	-5(1)	3(1)	-1(1)
C(16)	24(2)	30(2)	23(2)	-1(1)	1(1)	3(1)
C(17)	24(2)	61(3)	47(3)	-8(2)	11(2)	-10(2)
C(18)	51(3)	26(2)	43(2)	-5(2)	1(2)	-12(2)
C(19)	40(2)	47(3)	34(2)	-15(2)	4(2)	14(2)
C(20)	39(2)	53(3)	24(2)	-1(2)	11(2)	-8(2)
C(21)	39(2)	38(2)	36(2)	0(2)	0(2)	12(2)

The anisotropic displacement factor exponent takes the form: $-2\pi^2[h^2a^{*2}U_{11} + k^2b^{*2}U_{22} + l^2c^{*2}U_{33} + 2klb^{*c^{*}}U_{23} + 2hla^{*b^{*}}U_{13} + 2hka^{*b^{*}}U_{12}]$.

Table 2-9. Hydrogen coordinates ($\times 10^4$) and isotropic displacement parameters ($\text{\AA}^2 \times 10^3$) for **1b**

	<i>x</i>	<i>y</i>	<i>z</i>	<i>U</i> (eq)
H(1)	1100(50)	4520(30)	4420(40)	32(12)
H(2)	1860(50)	5140(30)	4630(40)	34(12)
H(3)	5579	5840	3801	32
H(4)	4675	7045	3199	34
H(5)	2098	7278	1914	45
H(6)	2245	7564	3058	45
H(7)	1124	7000	2575	45
H(8)	2171	3394	4473	32
H(9)	3964	2736	4270	37
H(10)	5531	4594	3475	32
H(11)	6635	3066	4557	66
H(12)	6722	3497	3542	66
H(13)	5944	2744	3462	66
H(14)	-3022	5003	1989	65
H(15)	-2407	5626	2787	65
H(16)	-2211	4785	3104	65
H(17)	-790	3821	3211	63
H(18)	427	3527	2825	63
H(19)	-988	3470	2098	63
H(20)	2025	3844	2021	61
H(21)	2548	4496	1436	61
H(22)	1451	3961	824	61
H(23)	1128	5612	30	57
H(24)	2213	5792	1038	57
H(25)	1044	6348	652	57
H(26)	-682	6751	1102	58
H(27)	-1433	6637	1990	58
H(28)	-2055	6354	859	58
H(29)	4614	4317	-186	189
H(30)	6160	4242	130	189
H(31)	4870	3521	-1304	155
H(32)	6145	3185	-570	155
H(33)	3624	2893	-650	72
H(34)	4847	2356	-402	72
H(35)	5152	2542	1136	144
H(36)	3764	2929	893	144

Table 2-10. Crystal data and structure refinement for **1c**

Empirical formula	C ₂₁ H ₂₅ F ₃ Fe I N ₃	
Formula weight	559.19	
Temperature	150(2) K	
Wavelength	0.71073 Å	
Crystal system	Triclinic	
Space group	<i>P</i> -1	
Unit cell dimensions	<i>a</i> = 9.9338(19) Å	<i>α</i> = 99.024(8)°
	<i>b</i> = 10.635(2) Å	<i>β</i> = 103.649(3)°
	<i>c</i> = 10.9075(17) Å	<i>γ</i> = 98.830(6)°
Volume	1083.9(3) Å ³	
<i>Z</i>	2	
Density (calculated)	1.713 g/cm ³	
Absorption coefficient	2.157 mm ⁻¹	
<i>F</i> (000)	556	
Crystal size	0.48 x 0.38 x 0.27 mm ³	
Theta range for data collection	1.96 to 27.47°	
Index ranges	-12 ≤ <i>h</i> ≤ 12, -12 ≤ <i>k</i> ≤ 13, -14 ≤ <i>l</i> ≤ 14	
Reflections collected	11220	
Independent reflections	4802 [<i>R</i> (int) = 0.0741]	
Reflections with <i>I</i> > 2σ(<i>I</i>)	4572	
Completeness to θ = 27.47°	96.6 %	
Max. and min. transmission	0.5935 and 0.4241	
Refinement method	Full-matrix least-squares on <i>F</i> ²	
Data / restraints / parameters	4802 / 0 / 296	
Goodness-of-fit on <i>F</i> ²	1.226	
Final <i>R</i> indices [<i>I</i> > 2σ(<i>I</i>)]	<i>R</i> 1 = 0.0688, <i>wR</i> 2 = 0.1930	
<i>R</i> indices (all data)	<i>R</i> 1 = 0.0723, <i>wR</i> 2 = 0.1984	
Largest diff. peak and hole	2.984 and -1.257 e Å ⁻³	

$$R1 = \Sigma||F_o| - |F_c|| / \Sigma|F_o|.$$

$$wR2 = [\Sigma[w(F_o^2 - F_c^2)^2] / \Sigma[w(F_o^2)^2]]^{0.5},$$

$$\text{calc } w = 1/[\sigma^2(F_o^2) + (0.0856P)^2 + 6.4310P] \text{ where } P = (F_o^2 + 2 F_c^2)/3.$$

Table 2-11. Atomic coordinates ($\times 10^4$) and equivalent isotropic displacement parameters ($\text{\AA}^2 \times 10^3$) for **1c**

	<i>x</i>	<i>y</i>	<i>z</i>	<i>U</i> (eq)
Fe(1)	6797(1)	3586(1)	1977(1)	24(1)
I(1)	4126(1)	3544(1)	1991(1)	37(1)
F(1A)	9790(20)	731(17)	-3500(30)	83(7)
F(2A)	9500(40)	-660(30)	-2390(30)	110(12)
F(3A)	7950(20)	-630(30)	-4040(30)	99(9)
F(1B)	9190(60)	650(40)	-3860(40)	140(20)
F(2B)	10050(30)	-130(40)	-2290(40)	111(16)
F(3B)	8130(30)	-1100(30)	-3430(50)	86(11)
N(1)	6423(7)	3359(5)	124(5)	30(1)
N(2)	6839(6)	932(5)	707(5)	28(1)
N(3)	6167(6)	868(5)	2440(5)	30(1)
C(1)	6577(7)	1713(6)	1714(6)	26(1)
C(2)	6584(9)	-375(7)	810(7)	37(2)
C(3)	6171(9)	-406(7)	1899(7)	37(2)
C(4)	5735(9)	1199(7)	3627(7)	39(2)
C(5)	7226(7)	1359(6)	-361(6)	28(1)
C(6)	7846(8)	565(7)	-1111(7)	33(1)
C(7)	8167(8)	945(8)	-2189(7)	38(2)
C(8)	7816(9)	2072(8)	-2553(7)	38(2)
C(9)	7236(8)	2869(7)	-1785(7)	32(1)
C(10)	6942(7)	2548(6)	-668(6)	26(1)
C(11)	8847(11)	97(10)	-2992(9)	53(2)
C(12)	8975(7)	4250(7)	2451(6)	31(1)
C(13)	8627(7)	3880(7)	3571(6)	29(1)
C(14)	7705(7)	4669(6)	3937(6)	31(1)
C(15)	7506(8)	5547(7)	3073(7)	38(2)
C(16)	8312(8)	5326(7)	2193(7)	37(2)
C(17)	9964(8)	3694(9)	1780(7)	41(2)
C(18)	9228(8)	2891(7)	4263(7)	35(1)
C(19)	7115(9)	4686(8)	5084(7)	41(2)
C(20)	6692(13)	6631(8)	3180(10)	62(3)
C(21)	8504(12)	6053(9)	1159(9)	61(3)

U(eq) is defined as one third of the trace of the orthogonalized U_{ij} tensor.

Table 2-12. Anisotropic displacement parameters ($\text{\AA}^2 \times 10^3$) for **1c**

	U_{11}	U_{22}	U_{33}	U_{23}	U_{13}	U_{12}
Fe(1)	32(1)	21(1)	21(1)	3(1)	8(1)	7(1)
I(1)	34(1)	41(1)	34(1)	-2(1)	9(1)	13(1)
F(1A)	90(12)	52(8)	141(17)	20(9)	80(11)	37(9)
F(2A)	200(30)	94(16)	114(19)	66(15)	110(20)	117(19)
F(3A)	101(11)	97(17)	75(12)	-54(11)	32(10)	10(12)
F(1B)	240(40)	170(30)	140(20)	130(20)	170(30)	180(30)
F(2B)	56(13)	140(30)	110(20)	-70(20)	-11(12)	60(14)
F(3B)	78(16)	63(13)	120(30)	-31(14)	64(19)	4(10)
N(1)	46(3)	26(3)	23(2)	7(2)	14(2)	11(2)
N(2)	39(3)	19(2)	26(3)	5(2)	9(2)	8(2)
N(3)	40(3)	23(3)	29(3)	6(2)	11(2)	5(2)
C(1)	29(3)	25(3)	25(3)	6(2)	8(2)	4(2)
C(2)	49(4)	24(3)	37(4)	5(3)	10(3)	8(3)
C(3)	50(4)	27(3)	32(3)	11(3)	6(3)	9(3)
C(4)	52(4)	36(4)	30(3)	11(3)	14(3)	3(3)
C(5)	35(3)	27(3)	24(3)	4(2)	10(2)	8(3)
C(6)	40(4)	27(3)	33(3)	4(3)	12(3)	11(3)
C(7)	42(4)	41(4)	33(3)	2(3)	17(3)	12(3)
C(8)	48(4)	41(4)	29(3)	8(3)	19(3)	10(3)
C(9)	44(4)	25(3)	30(3)	7(2)	13(3)	9(3)
C(10)	33(3)	24(3)	20(3)	4(2)	8(2)	7(2)
C(11)	66(6)	53(5)	53(5)	11(4)	36(5)	24(4)
C(12)	34(3)	33(3)	24(3)	7(2)	6(3)	-1(3)
C(13)	34(3)	30(3)	24(3)	5(2)	9(3)	3(3)
C(14)	36(3)	24(3)	28(3)	-1(2)	4(3)	6(3)
C(15)	44(4)	25(3)	35(4)	0(3)	-1(3)	4(3)
C(16)	44(4)	27(3)	29(3)	6(3)	-2(3)	-3(3)
C(17)	38(4)	54(5)	32(3)	9(3)	14(3)	5(3)
C(18)	40(4)	40(4)	27(3)	9(3)	6(3)	14(3)
C(19)	47(4)	49(4)	27(3)	-4(3)	13(3)	16(4)
C(20)	83(7)	24(4)	64(6)	-6(4)	-9(5)	23(4)
C(21)	78(7)	41(5)	50(5)	24(4)	-4(5)	-18(4)

The anisotropic displacement factor exponent takes the form: $-2\pi^2[h^2a^{*2}U_{11} + k^2b^{*2}U_{22} + l^2c^{*2}U_{33} + 2klb^{*c^{*}}U_{23} + 2hla^{*b^{*}}U_{13} + 2hka^{*b^{*}}U_{12}]$.

Table 2-13. Hydrogen coordinates ($\times 10^4$) and isotropic displacement parameters ($\text{\AA}^2 \times 10^3$) for **1c**

	<i>x</i>	<i>y</i>	<i>z</i>	<i>U</i> (eq)
H(1)	5456	3134	-189	36
H(2)	6680	4175	-34	36
H(3)	6684	-1097	227	44
H(4)	5928	-1157	2234	44
H(5)	5808	2141	3846	58
H(6)	6354	918	4330	58
H(7)	4756	760	3499	58
H(8)	8047	-228	-888	39
H(9)	7974	2293	-3325	45
H(10)	7031	3655	-2022	39
H(11)	9557	3537	846	61
H(12)	10114	2873	2037	61
H(13)	10871	4308	2015	61
H(14)	10099	3319	4927	53
H(15)	9437	2224	3647	53
H(16)	8539	2485	4668	53
H(17)	7345	3963	5497	62
H(18)	6086	4597	4805	62
H(19)	7527	5509	5700	62
H(20)	7336	7431	3694	93
H(21)	5945	6396	3599	93
H(22)	6267	6770	2318	93
H(23)	7624	6330	795	92
H(24)	8749	5488	479	92
H(25)	9266	6818	1525	92

Table 2-14. Crystal data and structure refinement for **3a**

Empirical formula	C ₂₁ H ₂₅ Fe N ₃ O	
Formula weight	391.29	
Temperature	150(2) K	
Wavelength	0.71073 Å	
Crystal system	Monoclinic	
Space group	P2 ₁ /n	
Unit cell dimensions	<i>a</i> = 8.2406(8) Å	$\alpha = 90^\circ$
	<i>b</i> = 13.3458(10) Å	$\beta = 96.124(3)^\circ$
	<i>c</i> = 16.7742(14) Å	$\gamma = 90^\circ$
Volume	1834.3(3) Å ³	
<i>Z</i>	4	
Density (calculated)	1.417 g/cm ³	
Absorption coefficient	0.837 mm ⁻¹	
<i>F</i> (000)	824	
Crystal size	0.41 x 0.38 x 0.27 mm ³	
Theta range for data collection	1.95 to 27.36°	
Index ranges	-10 ≤ <i>h</i> ≤ 10, -17 ≤ <i>k</i> ≤ 17, -21 ≤ <i>l</i> ≤ 21	
Reflections collected	14207	
Independent reflections	4146 [<i>R</i> (int) = 0.0643]	
Reflections with <i>I</i> > 2σ(<i>I</i>)	3560	
Completeness to $\theta = 27.36^\circ$	99.7 %	
Absorption correction	Numerical	
Max. and min. transmission	0.8056 and 0.7253	
Refinement method	Full-matrix least-squares on <i>F</i> ²	
Data / restraints / parameters	4146 / 0 / 245	
Goodness-of-fit on <i>F</i> ²	1.067	
Final <i>R</i> indices [<i>I</i> > 2σ(<i>I</i>)]	<i>R</i> 1 = 0.0471, <i>wR</i> 2 = 0.1151	
<i>R</i> indices (all data)	<i>R</i> 1 = 0.0568, <i>wR</i> 2 = 0.1216	
Largest diff. peak and hole	0.702 and -0.422 e Å ⁻³	

$$R1 = \frac{\sum ||F_o| - |F_c||}{\sum |F_o|}$$

$$wR2 = \left[\frac{\sum [w(F_o^2 - F_c^2)^2]}{\sum [w(F_o^2)^2]} \right]^{0.5}$$

$$\text{calc } w = 1 / [\sigma^2(F_o^2) + (0.0582P)^2 + 1.6829P] \text{ where } P = (F_o^2 + 2F_c^2) / 3.$$

Table 2-15. Atomic coordinates ($\times 10^4$) and equivalent isotropic displacement parameters ($\text{\AA}^2 \times 10^3$) for **3a**

	<i>x</i>	<i>y</i>	<i>z</i>	<i>U</i> (eq)
Fe(1)	1314(1)	7335(1)	3933(1)	21(1)
O(1)	-64(3)	7995(2)	5360(1)	46(1)
N(1)	-860(3)	7028(2)	3373(1)	28(1)
N(2)	698(2)	5186(2)	3697(1)	24(1)
N(3)	2092(2)	5419(2)	4835(1)	28(1)
C(1)	1389(3)	5926(2)	4184(1)	24(1)
C(2)	1830(3)	4401(2)	4760(2)	32(1)
C(3)	965(3)	4251(2)	4048(2)	31(1)
C(4)	2958(3)	5873(2)	5547(2)	33(1)
C(5)	-317(3)	5342(2)	2960(1)	25(1)
C(6)	-525(3)	4565(2)	2409(2)	33(1)
C(7)	-1617(4)	4663(3)	1724(2)	40(1)
C(8)	-2479(3)	5551(3)	1604(2)	40(1)
C(9)	-2241(3)	6334(2)	2136(2)	33(1)
C(10)	-1114(3)	6274(2)	2839(1)	26(1)
C(11)	475(3)	7707(2)	4796(2)	29(1)
C(12)	2632(3)	7440(2)	2919(1)	25(1)
C(13)	1814(3)	8362(2)	3034(1)	26(1)
C(14)	2397(3)	8747(2)	3798(2)	27(1)
C(15)	3590(3)	8062(2)	4162(1)	26(1)
C(16)	3740(3)	7269(2)	3613(2)	26(1)
C(17)	2485(3)	6815(2)	2169(2)	31(1)
C(18)	608(3)	8846(2)	2424(2)	34(1)
C(19)	1982(4)	9736(2)	4145(2)	36(1)
C(20)	4646(3)	8239(2)	4937(2)	37(1)
C(21)	4924(3)	6417(2)	3727(2)	34(1)

U(eq) is defined as one third of the trace of the orthogonalized U_{ij} tensor.

Table 2-16. Anisotropic displacement parameters ($\text{\AA}^2 \times 10^3$) for **3a**

	U_{11}	U_{22}	U_{33}	U_{23}	U_{13}	U_{12}
Fe(1)	18(1)	23(1)	23(1)	0(1)	2(1)	0(1)
O(1)	63(1)	36(1)	44(1)	-7(1)	28(1)	-2(1)
N(1)	19(1)	28(1)	36(1)	2(1)	-2(1)	2(1)
N(2)	20(1)	24(1)	28(1)	0(1)	2(1)	0(1)
N(3)	22(1)	29(1)	30(1)	4(1)	-1(1)	0(1)
C(1)	19(1)	26(1)	26(1)	2(1)	3(1)	0(1)
C(2)	25(1)	29(1)	42(1)	11(1)	1(1)	1(1)
C(3)	27(1)	24(1)	40(1)	2(1)	4(1)	0(1)
C(4)	27(1)	40(2)	30(1)	5(1)	-5(1)	-1(1)
C(5)	19(1)	33(1)	24(1)	1(1)	3(1)	-5(1)
C(6)	26(1)	39(2)	35(1)	-6(1)	9(1)	-5(1)
C(7)	36(2)	54(2)	32(1)	-13(1)	9(1)	-14(1)
C(8)	29(1)	63(2)	26(1)	1(1)	-1(1)	-13(1)
C(9)	23(1)	48(2)	28(1)	8(1)	-1(1)	-3(1)
C(10)	18(1)	34(1)	25(1)	4(1)	4(1)	-4(1)
C(11)	28(1)	24(1)	34(1)	1(1)	5(1)	-3(1)
C(12)	23(1)	28(1)	25(1)	1(1)	5(1)	-3(1)
C(13)	24(1)	25(1)	29(1)	1(1)	5(1)	-1(1)
C(14)	27(1)	24(1)	31(1)	0(1)	7(1)	-5(1)
C(15)	22(1)	30(1)	27(1)	0(1)	4(1)	-7(1)
C(16)	20(1)	30(1)	28(1)	2(1)	4(1)	-3(1)
C(17)	31(1)	36(1)	29(1)	-5(1)	8(1)	-3(1)
C(18)	35(1)	37(2)	31(1)	10(1)	3(1)	5(1)
C(19)	47(2)	26(1)	36(1)	-2(1)	7(1)	-1(1)
C(20)	31(1)	46(2)	32(1)	-6(1)	-1(1)	-11(1)
C(21)	22(1)	40(2)	41(1)	0(1)	5(1)	5(1)

The anisotropic displacement factor exponent takes the form: $-2\pi^2[h^2a^{*2}U_{11} + k^2b^{*2}U_{22} + l^2c^{*2}U_{33} + 2klb^{*c^{*}}U_{23} + 2hla^{*b^{*}}U_{13} + 2hka^{*b^{*}}U_{12}]$.

Table 2-17. Hydrogen coordinates ($\times 10^4$) and isotropic displacement parameters ($\text{\AA}^2 \times 10^3$) for **3a**

	<i>x</i>	<i>y</i>	<i>z</i>	<i>U</i> (eq)
H(1)	-1430(50)	7520(30)	3240(20)	49(11)
H(2)	2193	3901	5141	38
H(3)	605	3624	3825	37
H(4)	2710	6591	5555	49
H(5)	4135	5779	5537	49
H(6)	2611	5555	6027	49
H(7)	83	3964	2500	39
H(8)	-1770	4133	1345	48
H(9)	-3251	5620	1145	47
H(10)	-2848	6933	2031	40
H(11)	2624	6106	2313	47
H(12)	3330	7015	1832	47
H(13)	1406	6916	1874	47
H(14)	1190	9213	2036	51
H(15)	-77	9312	2691	51
H(16)	-81	8330	2143	51
H(17)	926	9966	3886	54
H(18)	2827	10227	4054	54
H(19)	1921	9662	4722	54
H(20)	5455	8757	4858	55
H(21)	5206	7615	5109	55
H(22)	3964	8458	5348	55
H(23)	5008	6191	4286	52
H(24)	5998	6640	3597	52
H(25)	4543	5862	3372	52

Table 2-18. Crystal data and structure refinement for **3b**

Empirical formula	C ₂₂ H ₂₇ Fe N ₃ O	
Formula weight	405.32	
Temperature	150(2) K	
Wavelength	0.71073 Å	
Crystal system	Triclinic	
Space group	<i>P</i> -1	
Unit cell dimensions	<i>a</i> = 8.2738(5) Å	<i>α</i> = 86.7749(19)°
	<i>b</i> = 8.8148(5) Å	<i>β</i> = 77.730(2)°
	<i>c</i> = 14.3034(7) Å	<i>γ</i> = 75.5156(18)°
Volume	986.94(9) Å ³	
<i>Z</i>	2	
Density (calculated)	1.364 g/cm ³	
Absorption coefficient	0.780 mm ⁻¹	
<i>F</i> (000)	428	
Crystal size	0.32 x 0.23 x 0.21 mm ³	
Theta range for data collection	1.46 to 27.40°	
Index ranges	-10 ≤ <i>h</i> ≤ 10, -11 ≤ <i>k</i> ≤ 11, -18 ≤ <i>l</i> ≤ 18	
Reflections collected	11491	
Independent reflections	4440 [<i>R</i> (int) = 0.0346]	
Reflections with <i>I</i> > 2σ(<i>I</i>)	3993	
Completeness to θ = 27.40°	98.5 %	
Max. and min. transmission	0.8533 and 0.7883	
Refinement method	Full-matrix least-squares on <i>F</i> ²	
Data / restraints / parameters	4440 / 0 / 255	
Goodness-of-fit on <i>F</i> ²	1.166	
Final <i>R</i> indices [<i>I</i> > 2σ(<i>I</i>)]	<i>R</i> 1 = 0.0392, <i>wR</i> 2 = 0.1031	
<i>R</i> indices (all data)	<i>R</i> 1 = 0.0457, <i>wR</i> 2 = 0.1060	
Largest diff. peak and hole	0.455 and -0.256 e Å ⁻³	

$$R1 = \Sigma||F_o| - |F_c|| / \Sigma|F_o|.$$

$$wR2 = [\Sigma[w(F_o^2 - F_c^2)^2] / \Sigma[w(F_o^2)^2]]^{0.5},$$

$$\text{calc } w=1/[\sigma^2(F_o^2)+(0.0549P)^2+0.5112P] \text{ where } P=(F_o^2 + 2 F_c^2)/3.$$

Table 2-19. Atomic coordinates ($\times 10^4$) and equivalent isotropic displacement parameters ($\text{\AA}^2 \times 10^3$) for **3b**

	<i>x</i>	<i>y</i>	<i>z</i>	<i>U</i> (eq)
Fe(1)	6325(1)	7685(1)	7131(1)	17(1)
O(1)	5810(3)	5494(2)	5856(1)	47(1)
N(1)	3857(2)	8642(2)	7602(1)	22(1)
N(2)	5218(2)	10926(2)	6501(1)	18(1)
N(3)	7043(2)	9603(2)	5355(1)	21(1)
C(1)	6215(2)	9451(2)	6273(1)	18(1)
C(2)	6555(3)	11123(2)	5021(2)	24(1)
C(3)	5430(3)	11956(2)	5736(2)	23(1)
C(4)	8261(3)	8356(3)	4768(2)	28(1)
C(5)	3997(2)	11346(2)	7375(1)	19(1)
C(6)	3490(3)	12898(2)	7673(2)	23(1)
C(7)	2218(3)	13384(3)	8482(2)	28(1)
C(8)	1469(3)	12248(3)	8979(2)	30(1)
C(9)	1978(3)	10694(3)	8696(2)	26(1)
C(10)	3295(3)	10156(2)	7892(1)	20(1)
C(11)	1683(3)	15078(3)	8795(2)	38(1)
C(12)	5962(3)	6419(2)	6356(2)	27(1)
C(13)	7335(3)	8388(2)	8236(1)	21(1)
C(14)	6686(3)	7039(2)	8538(2)	25(1)
C(15)	7574(3)	5805(2)	7896(2)	31(1)
C(16)	8800(3)	6384(3)	7183(2)	31(1)
C(17)	8652(3)	7968(3)	7408(2)	25(1)
C(18)	6840(3)	9913(3)	8766(2)	30(1)
C(19)	5322(3)	6980(3)	9407(2)	36(1)
C(20)	7419(4)	4137(3)	7978(2)	49(1)
C(21)	10124(4)	5407(4)	6422(2)	52(1)
C(22)	9712(3)	9035(4)	6907(2)	38(1)

U(eq) is defined as one third of the trace of the orthogonalized U_{ij} tensor.

Table 2-20. Anisotropic displacement parameters ($\text{\AA}^2 \times 10^3$) for **3b**

	U_{11}	U_{22}	U_{33}	U_{23}	U_{13}	U_{12}
Fe(1)	20(1)	14(1)	19(1)	1(1)	-7(1)	-3(1)
O(1)	92(2)	25(1)	39(1)	3(1)	-33(1)	-25(1)
N(1)	21(1)	20(1)	26(1)	4(1)	-4(1)	-8(1)
N(2)	20(1)	16(1)	19(1)	2(1)	-5(1)	-5(1)
N(3)	22(1)	20(1)	21(1)	0(1)	-2(1)	-3(1)
C(1)	18(1)	17(1)	20(1)	0(1)	-5(1)	-5(1)
C(2)	26(1)	23(1)	23(1)	6(1)	-4(1)	-8(1)
C(3)	25(1)	18(1)	26(1)	6(1)	-5(1)	-7(1)
C(4)	28(1)	27(1)	24(1)	-4(1)	1(1)	-3(1)
C(5)	17(1)	20(1)	20(1)	0(1)	-6(1)	-3(1)
C(6)	24(1)	21(1)	25(1)	-1(1)	-9(1)	-3(1)
C(7)	26(1)	26(1)	28(1)	-7(1)	-10(1)	2(1)
C(8)	23(1)	38(1)	25(1)	-5(1)	-3(1)	1(1)
C(9)	23(1)	32(1)	24(1)	3(1)	-4(1)	-7(1)
C(10)	17(1)	23(1)	20(1)	2(1)	-7(1)	-4(1)
C(11)	40(1)	31(1)	38(1)	-14(1)	-9(1)	4(1)
C(12)	38(1)	18(1)	29(1)	7(1)	-14(1)	-7(1)
C(13)	23(1)	22(1)	21(1)	2(1)	-8(1)	-6(1)
C(14)	28(1)	25(1)	25(1)	8(1)	-14(1)	-8(1)
C(15)	38(1)	19(1)	39(1)	3(1)	-25(1)	-2(1)
C(16)	26(1)	34(1)	31(1)	-7(1)	-13(1)	7(1)
C(17)	19(1)	33(1)	24(1)	2(1)	-10(1)	-5(1)
C(18)	38(1)	27(1)	28(1)	-4(1)	-14(1)	-7(1)
C(19)	41(1)	46(1)	26(1)	13(1)	-11(1)	-21(1)
C(20)	69(2)	20(1)	70(2)	9(1)	-46(2)	-6(1)
C(21)	39(2)	57(2)	46(2)	-20(1)	-16(1)	24(1)
C(22)	27(1)	63(2)	31(1)	6(1)	-7(1)	-23(1)

The anisotropic displacement factor exponent takes the form: $-2\pi^2[h^2a^{*2}U_{11} + k^2b^{*2}U_{22} + l^2c^{*2}U_{33} + 2klb^{*c^{*}}U_{23} + 2hla^{*b^{*}}U_{13} + 2hka^{*b^{*}}U_{12}]$.

Table 2-21. Hydrogen coordinates ($\times 10^4$) and isotropic displacement parameters ($\text{\AA}^2 \times 10^3$) for **3b**

	<i>x</i>	<i>y</i>	<i>z</i>	<i>U</i> (eq)
H(1)	3320(30)	8110(30)	7983(19)	25(6)
H(2)	6948	11501	4401	29
H(3)	4881	13040	5723	27
H(4)	8120	7338	5036	42
H(5)	9423	8439	4759	42
H(6)	8059	8450	4114	42
H(7)	4024	13646	7317	28
H(8)	584	12546	9527	36
H(9)	1422	9962	9056	32
H(10)	1918	15151	9433	57
H(11)	460	15487	8817	57
H(12)	2325	15695	8339	57
H(13)	7076	10753	8319	45
H(14)	7501	9831	9267	45
H(15)	5621	10151	9056	45
H(16)	5807	6892	9982	53
H(17)	4860	6069	9367	53
H(18)	4405	7939	9441	53
H(19)	6262	4109	8312	74
H(20)	8245	3523	8339	74
H(21)	7648	3691	7337	74
H(22)	11009	4718	6715	78
H(23)	10639	6094	5953	78
H(24)	9588	4771	6101	78
H(25)	10704	8933	7199	57
H(26)	9029	10120	6964	57
H(27)	10099	8750	6229	57

Table 2-22. Crystal data and structure refinement for **3c**

Empirical formula	C ₂₂ H ₂₄ F ₃ Fe N ₃ O	
Formula weight	459.29	
Temperature	150(2) K	
Wavelength	0.71073 Å	
Crystal system	Triclinic	
Space group	P-1	
Unit cell dimensions	$a = 8.6589(2)$ Å	$\alpha = 110.668(4)^\circ$
	$b = 10.6459(5)$ Å	$\beta = 97.275(5)^\circ$
	$c = 12.1551(6)$ Å	$\gamma = 91.477(3)^\circ$
Volume	1036.93(7) Å ³	
<i>Z</i>	2	
Density (calculated)	1.471 g/cm ³	
Absorption coefficient	0.772 mm ⁻¹	
<i>F</i> (000)	476	
Crystal size	0.59 x 0.45 x 0.39 mm ³	
Theta range for data collection	1.81 to 27.48°	
Index ranges	-10 ≤ <i>h</i> ≤ 11, -13 ≤ <i>k</i> ≤ 13, -15 ≤ <i>l</i> ≤ 15	
Reflections collected	9245	
Independent reflections	4476 [<i>R</i> (int) = 0.0611]	
Reflections with <i>I</i> > 2σ(<i>I</i>)	3999	
Completeness to θ = 27.48°	94.1 %	
Max. and min. transmission	0.7527 and 0.6586	
Refinement method	Full-matrix least-squares on <i>F</i> ²	
Data / restraints / parameters	4476 / 0 / 309	
Goodness-of-fit on <i>F</i> ²	1.046	
Final <i>R</i> indices [<i>I</i> > 2σ(<i>I</i>)]	<i>R</i> 1 = 0.0547, <i>wR</i> 2 = 0.1527	
<i>R</i> indices (all data)	<i>R</i> 1 = 0.0609, <i>wR</i> 2 = 0.1593	
Largest diff. peak and hole	0.825 and -0.682 e Å ⁻³	

$$R1 = \frac{\sum ||F_o| - |F_c||}{\sum |F_o|}$$

$$wR2 = \left[\frac{\sum [w(F_o^2 - F_c^2)^2]}{\sum [w(F_o^2)^2]} \right]^{0.5}$$

$$\text{calc } w = 1/[\sigma^2(F_o^2) + (0.0983P)^2 + 1.0508P] \text{ where } P = (F_o^2 + 2 F_c^2)/3.$$

Table 2-23. Atomic coordinates ($\times 10^4$) and equivalent isotropic displacement parameters ($\text{\AA}^2 \times 10^3$) for **3c**

	<i>x</i>	<i>y</i>	<i>z</i>	<i>U</i> (eq)
Fe(1)	6850(1)	8505(1)	6994(1)	22(1)
F(1)	8950(30)	6678(19)	680(20)	87(6)
F(2)	7930(20)	4825(19)	580(20)	99(7)
F(3)	10061(12)	5521(15)	1562(12)	61(3)
O(1)	3902(3)	8432(3)	7868(2)	48(1)
N(1)	5958(3)	8536(2)	5431(2)	27(1)
N(2)	7092(3)	5990(2)	5019(2)	25(1)
N(3)	6692(3)	5532(2)	6555(2)	28(1)
C(1)	6864(3)	6582(3)	6187(2)	24(1)
C(2)	6805(4)	4309(3)	5658(3)	34(1)
C(3)	7054(4)	4586(3)	4702(3)	32(1)
C(4)	6359(4)	5625(3)	7728(3)	38(1)
C(5)	7207(3)	6662(3)	4210(2)	24(1)
C(6)	7900(4)	6055(3)	3210(2)	29(1)
C(7)	7927(4)	6651(3)	2356(2)	33(1)
C(8)	7249(4)	7861(3)	2512(3)	33(1)
C(9)	6594(4)	8476(3)	3522(2)	30(1)
C(10)	6565(3)	7926(3)	4428(2)	24(1)
C(11)	8639(5)	5960(4)	1266(3)	48(1)
C(12)	5062(3)	8428(3)	7480(2)	30(1)
C(13)	9197(3)	9155(3)	7038(2)	28(1)
C(14)	9096(3)	8573(3)	7929(2)	26(1)
C(15)	8099(3)	9332(3)	8718(2)	26(1)
C(16)	7603(3)	10411(3)	8323(2)	27(1)
C(17)	8279(3)	10292(3)	7299(3)	28(1)
C(18)	10202(4)	8706(4)	6080(3)	38(1)
C(19)	9994(4)	7438(3)	8052(3)	35(1)
C(20)	7758(4)	9164(3)	9837(3)	36(1)
C(21)	6663(4)	11524(3)	8973(3)	39(1)
C(22)	8092(4)	11214(3)	6611(3)	39(1)
F(4)	9330(20)	6850(16)	877(17)	61(3)
F(5)	9550(40)	5090(30)	1313(19)	117(8)
F(6)	7450(20)	5370(30)	312(8)	109(5)

U(eq) is defined as one third of the trace of the orthogonalized U_{ij} tensor.

Table 2-24. Anisotropic displacement parameters ($\text{\AA}^2 \times 10^3$) for **3c**

	U_{11}	U_{22}	U_{33}	U_{23}	U_{13}	U_{12}
Fe(1)	22(1)	24(1)	19(1)	4(1)	5(1)	2(1)
F(1)	162(14)	81(9)	58(7)	50(7)	75(9)	85(10)
F(2)	79(7)	86(8)	71(8)	-55(6)	35(6)	-20(5)
F(3)	62(6)	69(6)	60(4)	22(4)	35(4)	39(4)
O(1)	35(1)	59(2)	43(1)	5(1)	18(1)	-2(1)
N(1)	30(1)	29(1)	21(1)	6(1)	6(1)	11(1)
N(2)	27(1)	20(1)	24(1)	5(1)	3(1)	2(1)
N(3)	29(1)	26(1)	29(1)	11(1)	4(1)	-2(1)
C(1)	22(1)	28(1)	22(1)	8(1)	3(1)	-1(1)
C(2)	38(2)	25(1)	38(2)	12(1)	3(1)	0(1)
C(3)	37(2)	21(1)	35(2)	6(1)	6(1)	3(1)
C(4)	43(2)	40(2)	32(2)	16(1)	8(1)	-3(1)
C(5)	27(1)	23(1)	20(1)	4(1)	4(1)	2(1)
C(6)	37(2)	24(1)	24(1)	3(1)	9(1)	8(1)
C(7)	41(2)	33(2)	22(1)	6(1)	12(1)	9(1)
C(8)	42(2)	35(2)	24(1)	11(1)	10(1)	10(1)
C(9)	37(2)	28(1)	25(1)	10(1)	8(1)	13(1)
C(10)	23(1)	25(1)	21(1)	5(1)	3(1)	3(1)
C(11)	72(3)	42(2)	31(2)	8(1)	25(2)	17(2)
C(12)	30(1)	33(2)	22(1)	3(1)	3(1)	-1(1)
C(13)	25(1)	28(1)	29(1)	7(1)	5(1)	-3(1)
C(14)	20(1)	27(1)	28(1)	7(1)	-1(1)	0(1)
C(15)	24(1)	26(1)	24(1)	4(1)	0(1)	-1(1)
C(16)	28(1)	25(1)	25(1)	4(1)	3(1)	-1(1)
C(17)	29(1)	25(1)	30(1)	10(1)	2(1)	-6(1)
C(18)	27(1)	49(2)	37(2)	11(1)	13(1)	0(1)
C(19)	26(1)	32(2)	48(2)	14(1)	4(1)	6(1)
C(20)	42(2)	41(2)	22(1)	8(1)	4(1)	-4(1)
C(21)	43(2)	31(2)	33(2)	-1(1)	4(1)	10(1)
C(22)	41(2)	37(2)	45(2)	20(1)	7(1)	-2(1)
F(4)	85(6)	57(4)	49(5)	15(4)	47(4)	5(5)
F(5)	245(19)	89(11)	80(9)	67(9)	122(12)	127(13)
F(6)	112(8)	148(12)	27(3)	-22(5)	19(4)	4(9)

The anisotropic displacement factor exponent takes the form: $-2\pi^2[h^2a^{*2}U_{11} + k^2b^{*2}U_{22} + l^2c^{*2}U_{33} + 2klb^{*c^{*}}U_{23} + 2hla^{*b^{*}}U_{13} + 2hka^{*b^{*}}U_{12}]$.

Table 2-25. Hydrogen coordinates ($\times 10^4$) and isotropic displacement parameters ($\text{\AA}^2 \times 10^3$) for **3c**

	<i>x</i>	<i>y</i>	<i>z</i>	<i>U</i> (eq)
H(1)	5630(50)	9290(40)	5450(30)	41(10)
H(2)	6722	3442	5713	40
H(3)	7182	3950	3948	38
H(4)	6147	6552	8178	56
H(5)	7262	5370	8153	56
H(6)	5445	5017	7640	56
H(7)	8361	5228	3102	35
H(8)	7239	8259	1924	40
H(9)	6142	9305	3619	36
H(10)	9752	8941	5403	58
H(11)	10259	7728	5825	58
H(12)	11253	9154	6383	58
H(13)	11106	7739	8289	53
H(14)	9849	6683	7290	53
H(15)	9617	7149	8659	53
H(16)	7748	8210	9737	54
H(17)	6737	9494	10010	54
H(18)	8566	9680	10496	54
H(19)	7362	12244	9579	58
H(20)	5914	11176	9355	58
H(21)	6100	11882	8410	58
H(22)	7148	11694	6775	59
H(23)	8003	10686	5759	59
H(24)	9004	11866	6849	59

Table 2-26. Crystal data and structure refinement for **4a**

Empirical formula	C ₂₈ H ₄₀ B Fe N ₃	
Formula weight	485.29	
Temperature	150(2) K	
Wavelength	0.71073 Å	
Crystal system	Triclinic	
Space group	<i>P</i> -1	
Unit cell dimensions	<i>a</i> = 8.8912(12) Å	<i>α</i> = 85.826(2)°
	<i>b</i> = 9.8538(12) Å	<i>β</i> = 81.2012(16)°
	<i>c</i> = 15.3598(14) Å	<i>γ</i> = 72.3334(18)°
Volume	1266.7(3) Å ³	
<i>Z</i>	2	
Density (calculated)	1.272 g/cm ³	
Absorption coefficient	0.616 mm ⁻¹	
<i>F</i> (000)	520	
Crystal size	0.200 x 0.190 x 0.130 mm ³	
Theta range for data collection	2.170 to 27.483°	
Index ranges	-10 ≤ <i>h</i> ≤ 11, -12 ≤ <i>k</i> ≤ 12, -18 ≤ <i>l</i> ≤ 19	
Reflections collected	14236	
Independent reflections	5691 [<i>R</i> (int) = 0.0740]	
Reflections with <i>I</i> > 2σ(<i>I</i>)	4569	
Completeness to <i>θ</i> = 25.240°	98.0 %	
Absorption correction	Numerical	
Max. and min. transmission	0.9727 and 0.9097	
Refinement method	Full-matrix least-squares on <i>F</i> ²	
Data / restraints / parameters	5691 / 0 / 312	
Goodness-of-fit on <i>F</i> ²	1.062	
Final <i>R</i> indices [<i>I</i> > 2σ(<i>I</i>)]	<i>R</i> 1 = 0.0584, <i>wR</i> 2 = 0.1247	
<i>R</i> indices (all data)	<i>R</i> 1 = 0.0780, <i>wR</i> 2 = 0.1340	
Largest diff. peak and hole	0.500 and -0.399 e Å ⁻³	

$$R1 = \frac{\sum||F_o| - |F_c||}{\sum|F_o|}$$

$$wR2 = [\frac{\sum[w(F_o^2 - F_c^2)^2]}{\sum[w(F_o^2)^2]}]^{0.5},$$

$$\text{calc } w = 1/[\sigma^2(F_o^2) + (0.0484P)^2 + 1.6181P] \text{ where } P = (F_o^2 + 2 F_c^2)/3.$$

Table 2-27. Atomic coordinates ($\times 10^4$) and equivalent isotropic displacement parameters ($\text{\AA}^2 \times 10^3$) for **4a**

	<i>x</i>	<i>y</i>	<i>z</i>	<i>U</i> (eq)
Fe(1)	5053(1)	6729(1)	7210(1)	22(1)
N(1)	6058(3)	6049(2)	8298(2)	23(1)
N(2)	7804(3)	7801(2)	7234(2)	24(1)
N(3)	7591(3)	7420(3)	5907(2)	27(1)
C(1)	6852(3)	7364(3)	6749(2)	24(1)
C(2)	8940(4)	7869(3)	5866(2)	33(1)
C(3)	9080(4)	8104(3)	6692(2)	31(1)
C(4)	7220(4)	6814(4)	5160(2)	36(1)
C(5)	7601(3)	7799(3)	8168(2)	24(1)
C(6)	8216(4)	8678(3)	8586(2)	31(1)
C(7)	8063(4)	8702(3)	9493(2)	39(1)
C(8)	7266(4)	7847(4)	9999(2)	39(1)
C(9)	6641(4)	6972(3)	9595(2)	32(1)
C(10)	6794(3)	6923(3)	8671(2)	24(1)
C(11)	6324(3)	3337(3)	8053(2)	26(1)
C(12)	7088(4)	2770(3)	8896(2)	30(1)
C(13)	8905(4)	2449(3)	8769(2)	32(1)
C(14)	9521(4)	3619(3)	8252(2)	32(1)
C(15)	8720(3)	4255(3)	7425(2)	27(1)
C(16)	9154(4)	3211(3)	6666(2)	34(1)
C(17)	8521(4)	1905(3)	6855(2)	34(1)
C(18)	6783(4)	2259(3)	7305(2)	33(1)
C(19)	2995(3)	6317(4)	6966(2)	33(1)
C(20)	2751(3)	6845(3)	7819(2)	28(1)
C(21)	3023(4)	8223(3)	7745(2)	36(1)
C(22)	3380(4)	8539(4)	6833(3)	43(1)
C(23)	3370(4)	7362(4)	6338(2)	39(1)
C(24)	2822(4)	4928(4)	6726(3)	50(1)
C(25)	2238(4)	6124(4)	8657(2)	43(1)
C(26)	2874(5)	9155(4)	8502(3)	62(1)
C(27)	3659(5)	9914(5)	6445(4)	84(2)
C(28)	3379(5)	7332(7)	5359(3)	76(2)
B(1)	6820(4)	4743(3)	7692(2)	23(1)

U(eq) is defined as one third of the trace of the orthogonalized U_{ij} tensor.

Table 2-28. Anisotropic displacement parameters ($\text{\AA}^2 \times 10^3$) for **4a**

	U_{11}	U_{22}	U_{33}	U_{23}	U_{13}	U_{12}
Fe(1)	20(1)	24(1)	23(1)	2(1)	-6(1)	-7(1)
N(1)	21(1)	25(1)	22(1)	-1(1)	-3(1)	-8(1)
N(2)	24(1)	22(1)	28(1)	2(1)	-6(1)	-9(1)
N(3)	28(1)	31(1)	25(1)	2(1)	-2(1)	-13(1)
C(1)	24(1)	22(1)	27(1)	0(1)	-7(1)	-6(1)
C(2)	28(2)	37(2)	35(2)	3(1)	0(1)	-15(1)
C(3)	26(1)	30(2)	40(2)	2(1)	-5(1)	-14(1)
C(4)	38(2)	48(2)	26(2)	-4(1)	-2(1)	-19(2)
C(5)	23(1)	21(1)	28(1)	-2(1)	-9(1)	-4(1)
C(6)	34(2)	22(1)	39(2)	1(1)	-15(1)	-8(1)
C(7)	48(2)	28(2)	44(2)	-6(1)	-23(2)	-8(1)
C(8)	47(2)	41(2)	29(2)	-4(1)	-13(1)	-10(2)
C(9)	35(2)	33(2)	26(1)	-1(1)	-6(1)	-8(1)
C(10)	21(1)	23(1)	28(1)	-1(1)	-9(1)	-2(1)
C(11)	23(1)	25(1)	30(2)	4(1)	-6(1)	-8(1)
C(12)	31(2)	28(1)	30(2)	5(1)	-6(1)	-9(1)
C(13)	31(2)	30(2)	35(2)	5(1)	-11(1)	-6(1)
C(14)	23(1)	30(2)	44(2)	4(1)	-10(1)	-7(1)
C(15)	24(1)	22(1)	34(2)	2(1)	-1(1)	-7(1)
C(16)	34(2)	26(1)	36(2)	2(1)	3(1)	-5(1)
C(17)	43(2)	25(1)	34(2)	-4(1)	-5(1)	-7(1)
C(18)	41(2)	26(1)	36(2)	2(1)	-12(1)	-15(1)
C(19)	18(1)	46(2)	35(2)	-5(1)	-5(1)	-9(1)
C(20)	17(1)	36(2)	30(2)	0(1)	-3(1)	-4(1)
C(21)	24(2)	30(2)	50(2)	-7(1)	-13(1)	3(1)
C(22)	21(2)	41(2)	63(2)	23(2)	-13(1)	-5(1)
C(23)	23(2)	64(2)	29(2)	7(2)	-10(1)	-10(2)
C(24)	32(2)	65(2)	61(2)	-25(2)	-5(2)	-20(2)
C(25)	30(2)	56(2)	34(2)	9(2)	1(1)	-6(2)
C(26)	41(2)	51(2)	88(3)	-39(2)	-14(2)	5(2)
C(27)	45(2)	48(2)	148(5)	52(3)	-22(3)	-8(2)
C(28)	35(2)	160(5)	33(2)	18(2)	-15(2)	-26(3)
B(1)	23(2)	22(1)	24(2)	0(1)	-6(1)	-7(1)

The anisotropic displacement factor exponent takes the form: $-2\pi^2[h^2a^{*2}U_{11} + k^2b^{*2}U_{22} + l^2c^{*2}U_{33} + 2klb^{*c^{*}}U_{23} + 2hla^{*b^{*}}U_{13} + 2hka^{*b^{*}}U_{12}]$.

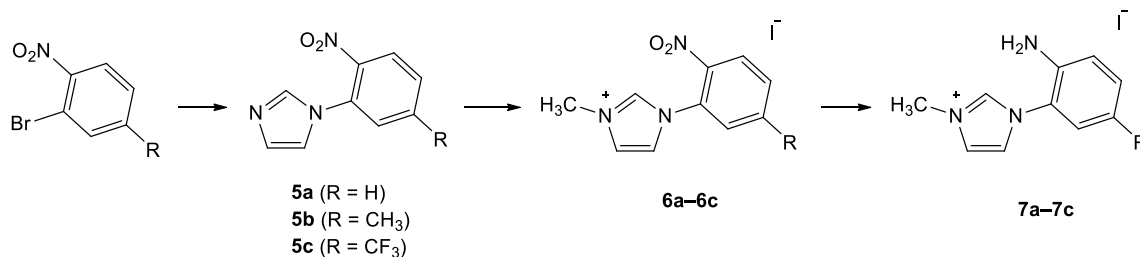
Table 2-29. Hydrogen coordinates ($\times 10^4$) and isotropic displacement parameters ($\text{\AA}^2 \times 10^3$) for **4a**

	<i>x</i>	<i>y</i>	<i>z</i>	<i>U</i> (eq)
H(1)	5370(40)	5910(30)	8700(20)	26(8)
H(2)	9632	7986	5349	39
H(3)	9890	8417	6875	37
H(4)	6525	6221	5372	54
H(5)	8209	6230	4830	54
H(6)	6677	7585	4774	54
H(7)	8753	9274	8240	37
H(8)	8500	9300	9767	46
H(9)	7149	7861	10624	46
H(10)	6096	6389	9949	38
H(11)	5139	3620	8215	31
H(12)	6619	3483	9360	36
H(13)	6818	1888	9105	36
H(14)	9390	1544	8455	39
H(15)	9267	2310	9356	39
H(16)	10681	3217	8066	39
H(17)	9370	4402	8655	39
H(18)	9059	5115	7212	32
H(19)	10329	2868	6524	41
H(20)	8729	3734	6138	41
H(21)	8609	1440	6292	41
H(22)	9209	1211	7236	41
H(23)	6581	1363	7549	39
H(24)	6073	2642	6851	39
H(25)	2951	4262	7234	75
H(26)	3638	4525	6232	75
H(27)	1762	5089	6555	75
H(28)	1073	6442	8788	64
H(29)	2699	6369	9142	64
H(30)	2608	5089	8587	64
H(31)	3552	9780	8341	93
H(32)	3211	8559	9018	93
H(33)	1762	9735	8641	93
H(34)	2647	10583	6314	125
H(35)	4415	9716	5901	125
H(36)	4096	10333	6870	125
H(37)	2284	7529	5232	115
H(38)	4017	6389	5144	115
H(39)	3841	8057	5062	115
H(40)	6080(40)	5200(30)	6970(20)	31(8)

2-3. Results and Discussion

2-3-1. Synthesis of Ligand Precursors 7a–7c

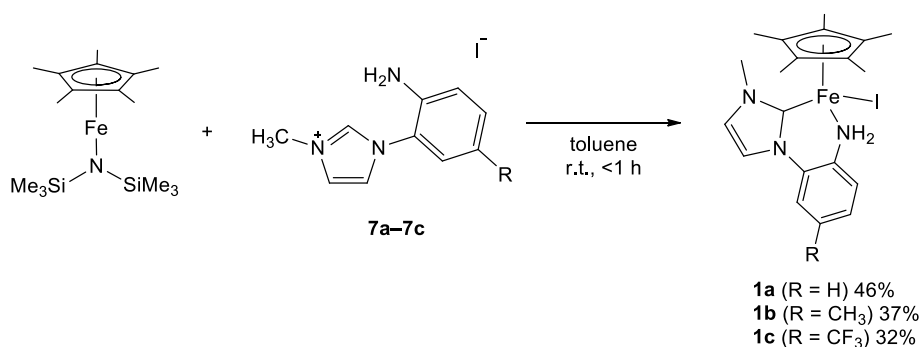
The ligand precursors **7a–7c** were synthesized by the following synthetic route (Scheme 2-1) and obtained in relatively high yields (72–76%). Each reaction was performed according to the literature or modified literature procedures.^[3,6,8] The NMR spectra of **5b**, **5c**, **6b**, **6c**, **7b**, and **7c**, which were newly synthesized in this work, were summarized in Supporting Information (Figures S1–S16).



Scheme 2-1. The synthetic route of **7a–7c**.

2-3-2. Synthesis of 1a–1c

Amino(iodido)iron complexes **1a–1c** were synthesized by the reactions of Cp*FeN(SiMe₃)₂ with the corresponding imidazolium salts **7a–7c** in toluene at room temperature. The reactions were completed within 1 h to give complexes **1a–1c** in moderate isolated yields (Scheme 2-2).



Scheme 2-2. Synthesis of **1a–1c**.

2-3-3. Characterization of 1a–1c

The structures of **1a–1c** were determined by X-ray crystallography and the ORTEP drawings of **1a–1c** were shown in Figure 2-3. All complexes adopted three-legged piano stool geometries where each of the iron centers was coordinated by a Cp* ligand, a carbene carbon, an amino nitrogen, and an iodido ligand. The selected bond lengths and angles in **1a–1c** are summarized in Table 2-30. The Fe–N lengths of **1a** and **1b** are 2.070(2) and 2.053(3) Å, respectively, which are in the range of reported Fe–N dative bond lengths (2.01–2.32 Å).^[13] However, the Fe–N length in **1c** is 1.936(5) Å, which is significantly shorter than those of **1a** and **1b**. This is probably due to bad refinement attributable to disordered F atoms because the Fe–I and N–C_{Ar} bond lengths are also significantly shorter than those of **1a** and **1b**. The optimized geometries of **1a–1c** obtained by DFT calculation (B3PW91/6-31G(d),LanL2DZ) show that the Fe–N bond lengths of them are comparable (Table 2-30).

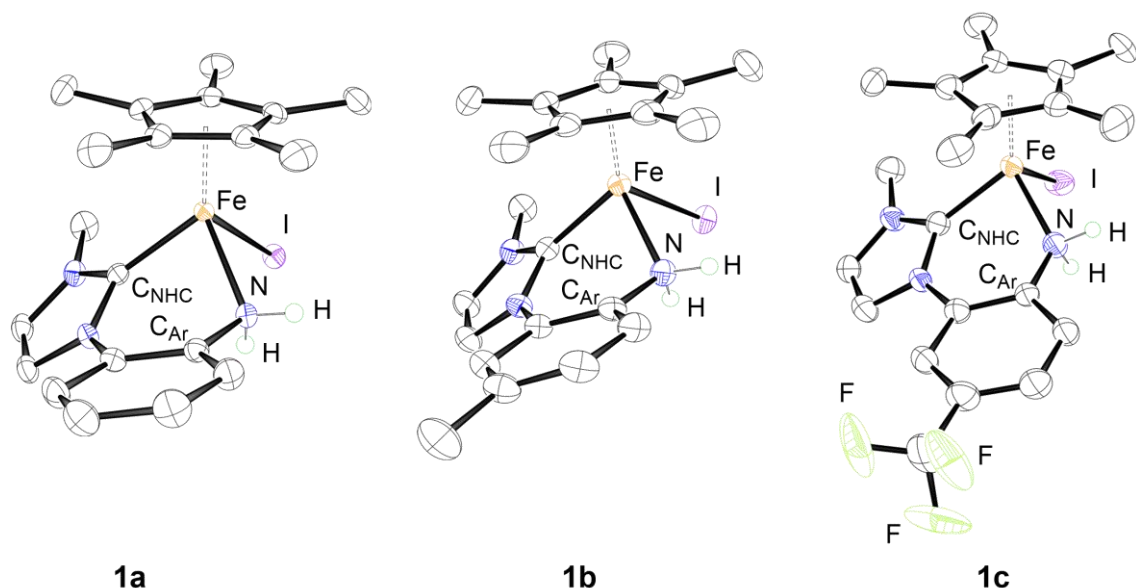


Figure 2-3. ORTEP drawings of **1a**, **1b**·THF, and **1c**. Hydrogens except for NH₂ moiety are omitted for clarity. A THF molecule of **1b**·THF was also omitted for clarity. The structure of **1c** with an occupancy factor of 58% is illustrated.

Table 2-30. Selected bond lengths and angles of **1a**, **1b**, and **1c**^a

	1a	1b	1c
Fe–C _{NHC}	1.931(2) [1.915]	1.928(3) [1.915]	1.938(6) [1.915]
Fe–I	2.7072(3) [2.762]	2.7137(5) [2.762]	2.6508(11) [2.758]
Fe–N	2.070(2) [2.046]	2.053(3) [2.045]	1.936(5) [2.050]
N–C _{Ar}	1.435(2) [1.426]	1.434(4) [1.427]	1.366(8) [1.421]
N–H (average)	0.83(3) [1.022]	0.87(7) [1.022]	n.d. ^b [1.022]
C _{NHC} –Fe–I	92.66(6) [90.84]	91.85(10) [90.95]	93.60(19) [90.70]
C _{NHC} –Fe–N	83.89(7) [85.02]	83.96(13) [85.07]	86.2(2) [85.03]
N–Fe–I	85.63(5) [83.84]	85.23(9) [83.92]	94.62(19) [83.70]

^a) DFT optimized results are shown in brackets. ^b) not determined

The ¹H NMR spectrum of **1a** in C₆D₆ is shown in Figure 2-4. The methyl protons of the Cp* ligand and N–Me are observed at 1.50 and 4.09 ppm, respectively. Protons on the aromatic ring (ArH) and the imidazole ring (ImH) appear at 6.28, 6.55, 6.63, 6.70–6.80, and 6.84 ppm. The signals of the two of six protons are overlapped accidentally at 6.70–6.80 ppm. The NH₂ protons are observed at 2.47 ppm as a broad signal with the intensity of 2H. When THF-*d*₈ is used as a solvent, protons of ArH and ImH are observed independently (Figure 2-5). However, the signal of the NH₂ protons is not observed at 300 K because of severe broadening of the signal (Figure 2-5). This broadening is caused by the dynamic behavior of the NH₂ group shown in Figure 2-6, which involves (1) dissociation of NH₂ from the iron center; (2) rotation around the N–C bond; (3) inversion at N center; and (4) coordination of NH₂ to the iron center. This was clearly demonstrated by variable temperature NMR (VT NMR) experiments (Figure 2-7). The broadened signal of NH₂ protons at 300 K started to decoalesce into two signals and became sharper as the

temperature went down. Finally, NH₂ protons were observed inequivalently at 2.17 ppm and 5.26 ppm having the intensity of 1H each at 250 K. The ¹³C{¹H} NMR of **1a** shows 12 peaks (Figure 2-8), which is consistent with its molecular structure. The signals of methyl and ring carbons of the Cp* ligand are observed at 10.7 and 74.8 ppm, respectively. The methyl carbon on nitrogen of the NHC ligand is observed at 42.0 ppm. The signals of carbons in the aromatic ring (ArC) and imidazole ring (ImC) appear at 120.2 (ImC), 121.3 (ArC), 121.7 (ArC), 125.4 (ArC), 125.8 (ArC), 126.2 (ImC), 135.7 (ArC), and 138.7 (ArC) ppm. The carbene carbon of the NHC ligand is observed at 220.8 ppm.

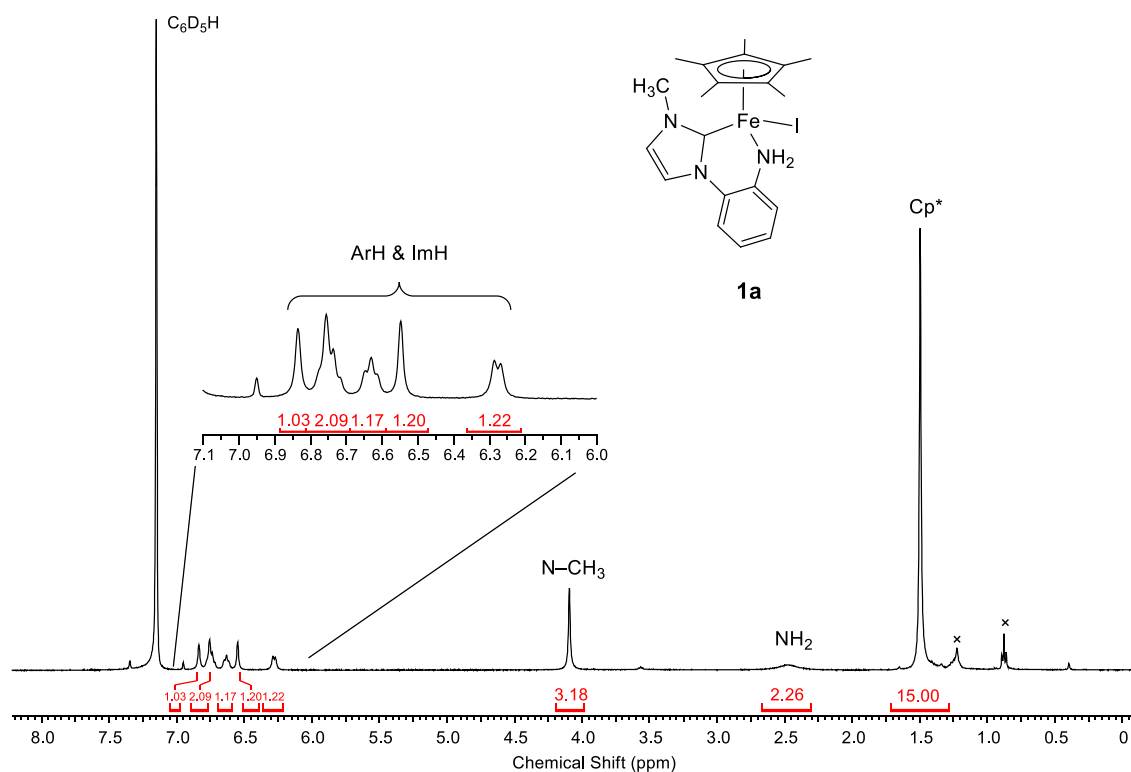


Figure 2-4. ¹H NMR spectrum of **1a** (400MHz, C₆D₆). ×-marks represent signals of hexane.

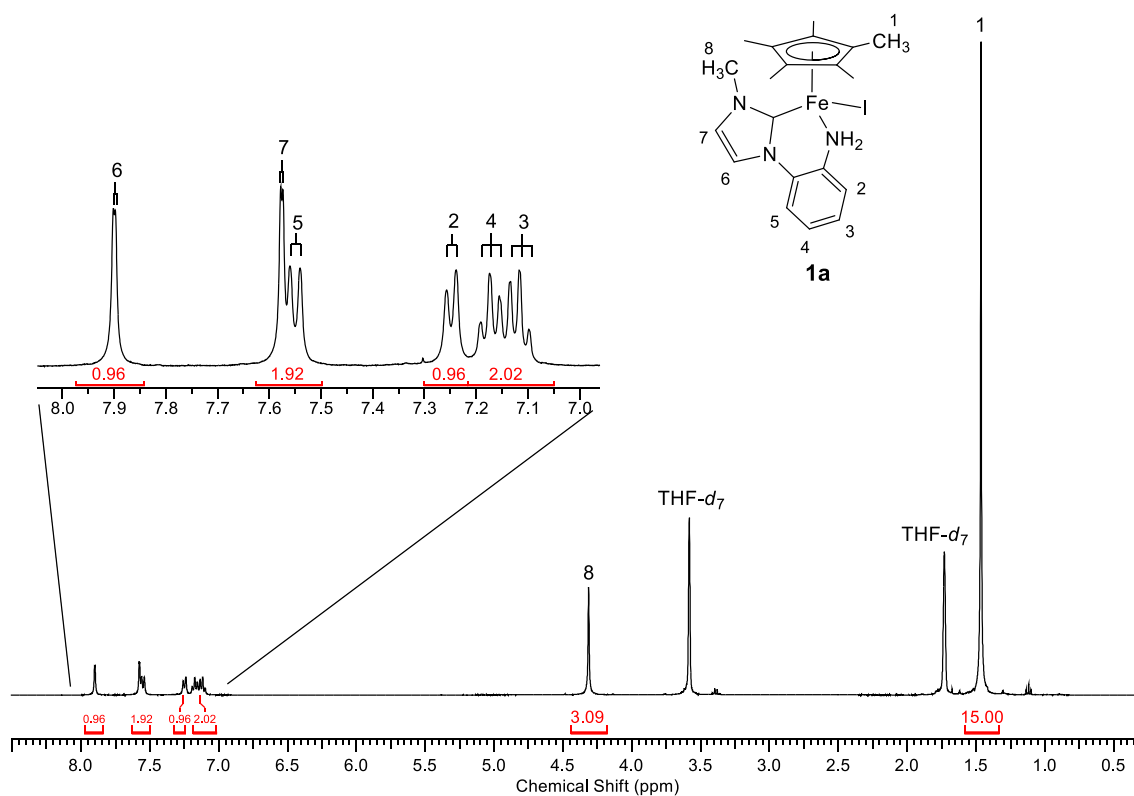


Figure 2-5. ^1H NMR spectrum of **1a** (400MHz, THF- d_8).

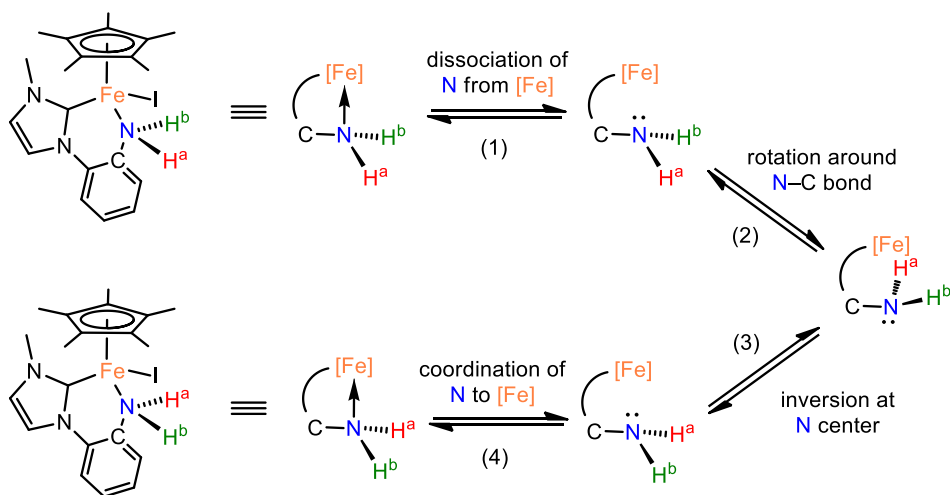


Figure 2-6. A schematic diagram of dynamic behavior of NH_2 group in **1a**.

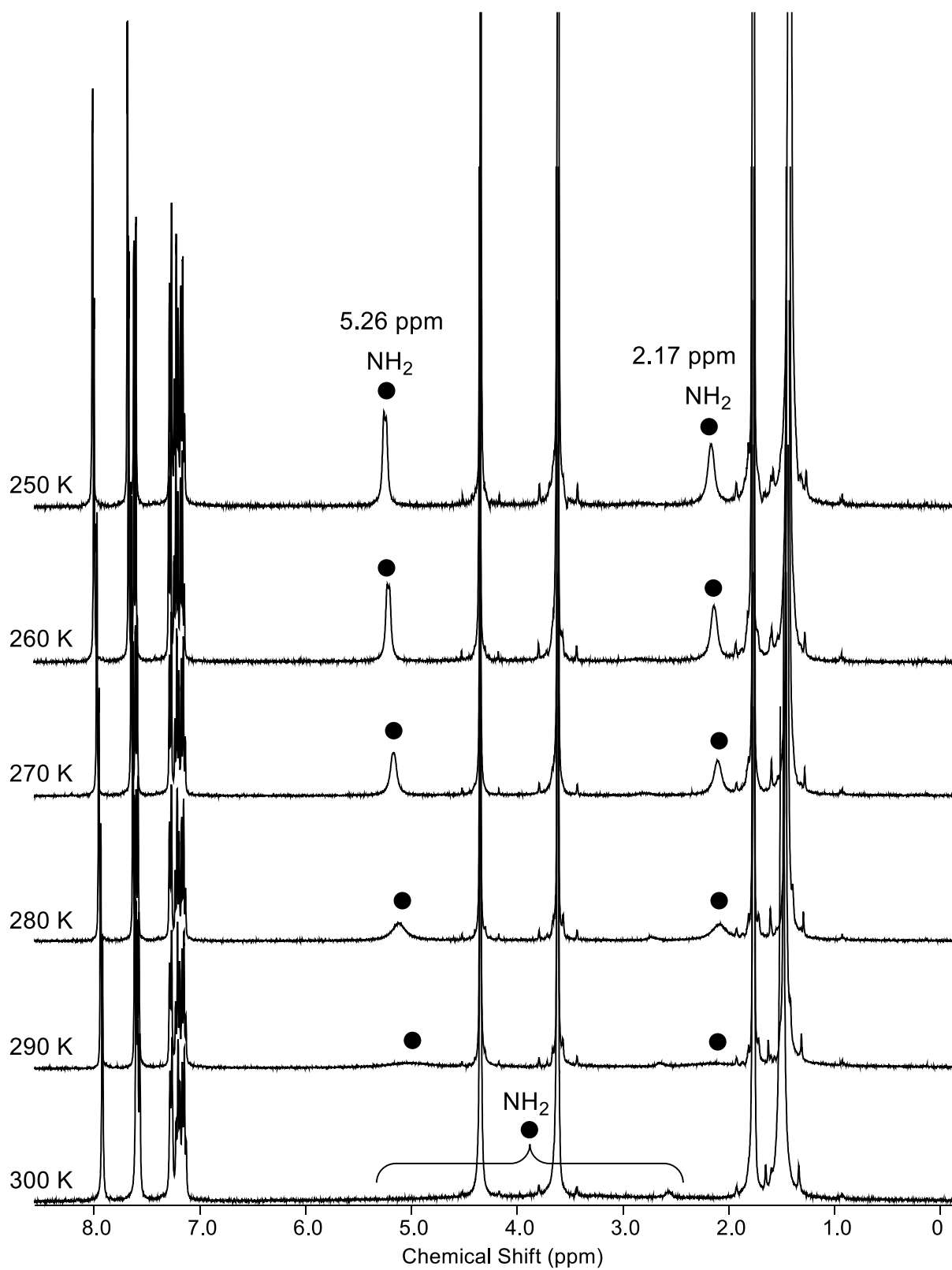


Figure 2-7. VT ¹H NMR spectra of **1a** (400 MHz, THF-*d*₈, 250–300 K).

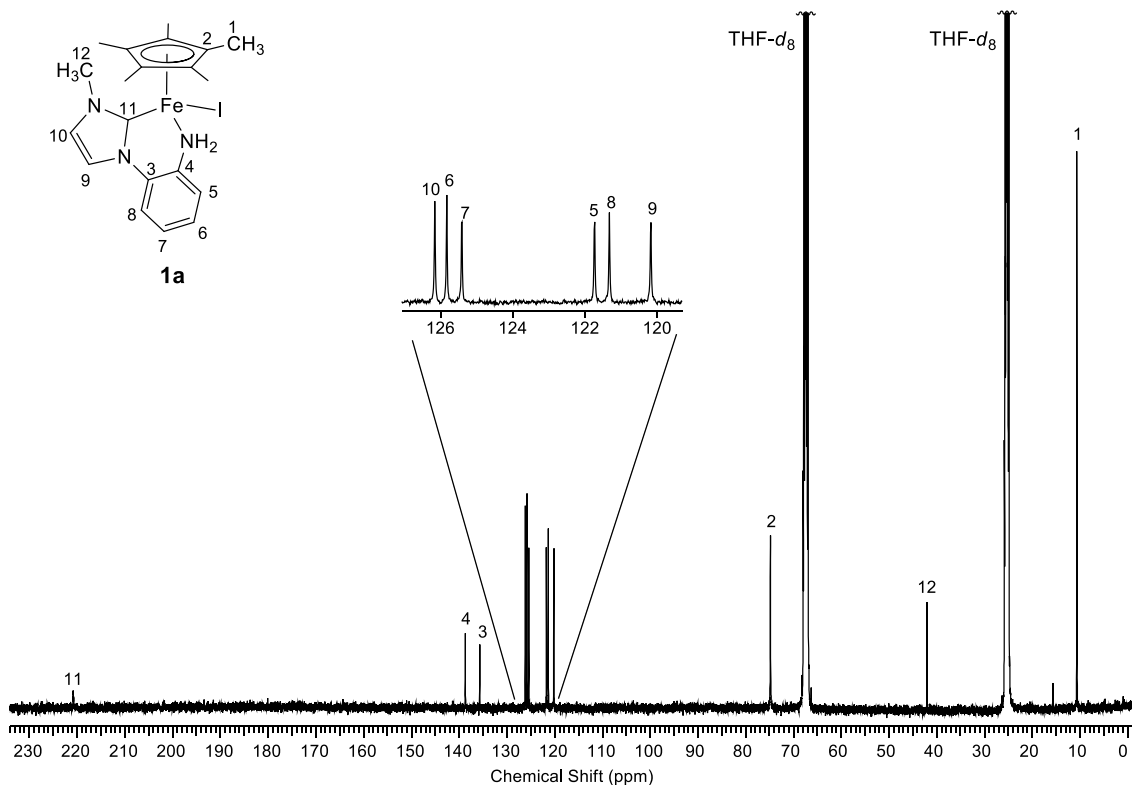


Figure 2-8. $^{13}\text{C}\{^1\text{H}\}$ NMR spectrum of **1a** (101 MHz, $\text{THF-}d_8$).

The ^1H NMR spectrum of **1b** follows the same trends as that of **1a** except for the signal of the methyl protons on the aromatic ring (2.35 ppm) (Figure 2-9). The $^{13}\text{C}\{^1\text{H}\}$ NMR spectrum of **1b** shows 13 signals which also follows the same trends as that of **1a** except for the signal of the methyl carbon on the aromatic ring (20.9 ppm) (Figure 2-10). The ^1H NMR spectrum of **1c** shows 7 resonances at ordinary chemical shifts for all protons (Figure 2-11). A clear $^{13}\text{C}\{^1\text{H}\}$ NMR spectrum of **1c** was not obtained due to severe broadening of signals (Figure 2-12). This is probably because of paramagnetic or ferromagnetic impurities, which produced during the course of acquisition. The $^{19}\text{F}\{^1\text{H}\}$ NMR spectrum of **1c** shows a single peak at -62.6 ppm, whose chemical shift is comparable with that of the CF_3 group of $\text{C}_6\text{H}_5\text{CF}_3$ (-62.1 ppm) (Figure 2-13). The molecular formulas of **1a–1c** are confirmed by high-resolution mass spectrometry (HRMS) and elemental analysis.

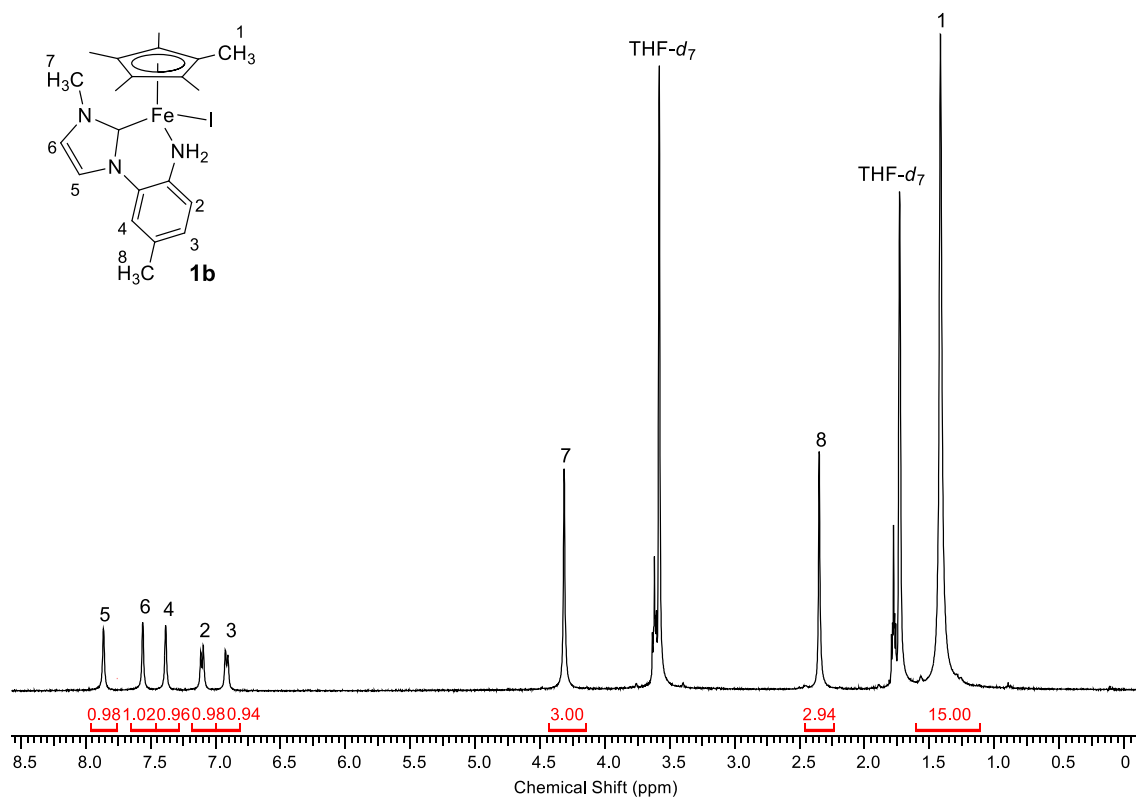


Figure 2-9. ^1H NMR spectrum of **1b** (400MHz, $\text{THF-}d_8$).

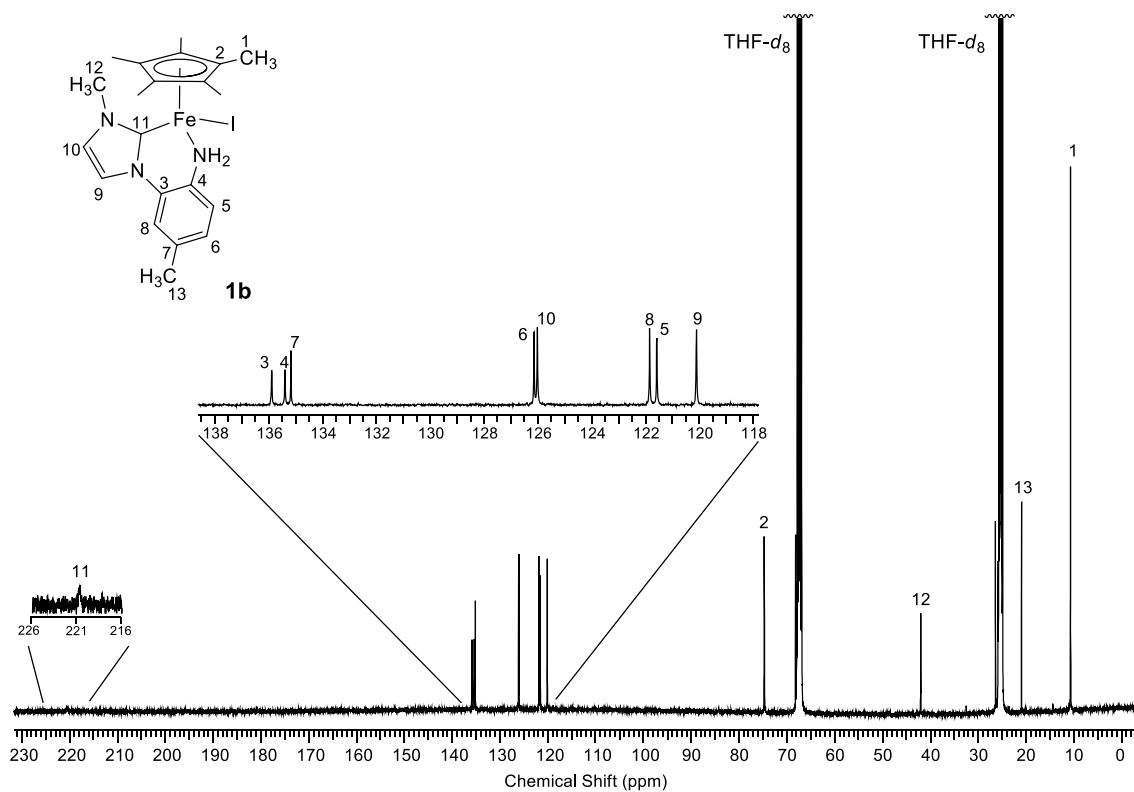


Figure 2-10. $^{13}\text{C}\{^1\text{H}\}$ NMR spectrum of **1b** (101 MHz, $\text{THF-}d_8$).

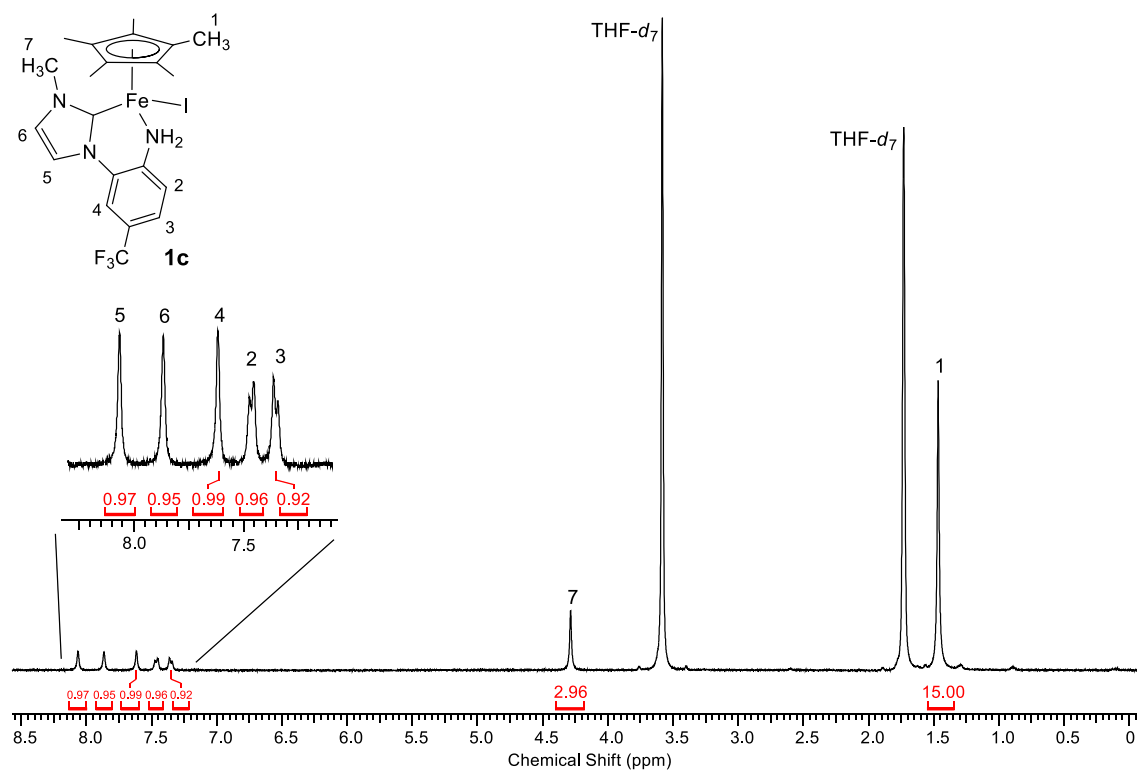


Figure 2-11. ^1H NMR spectrum of **1c** (400MHz, $\text{THF-}d_8$).

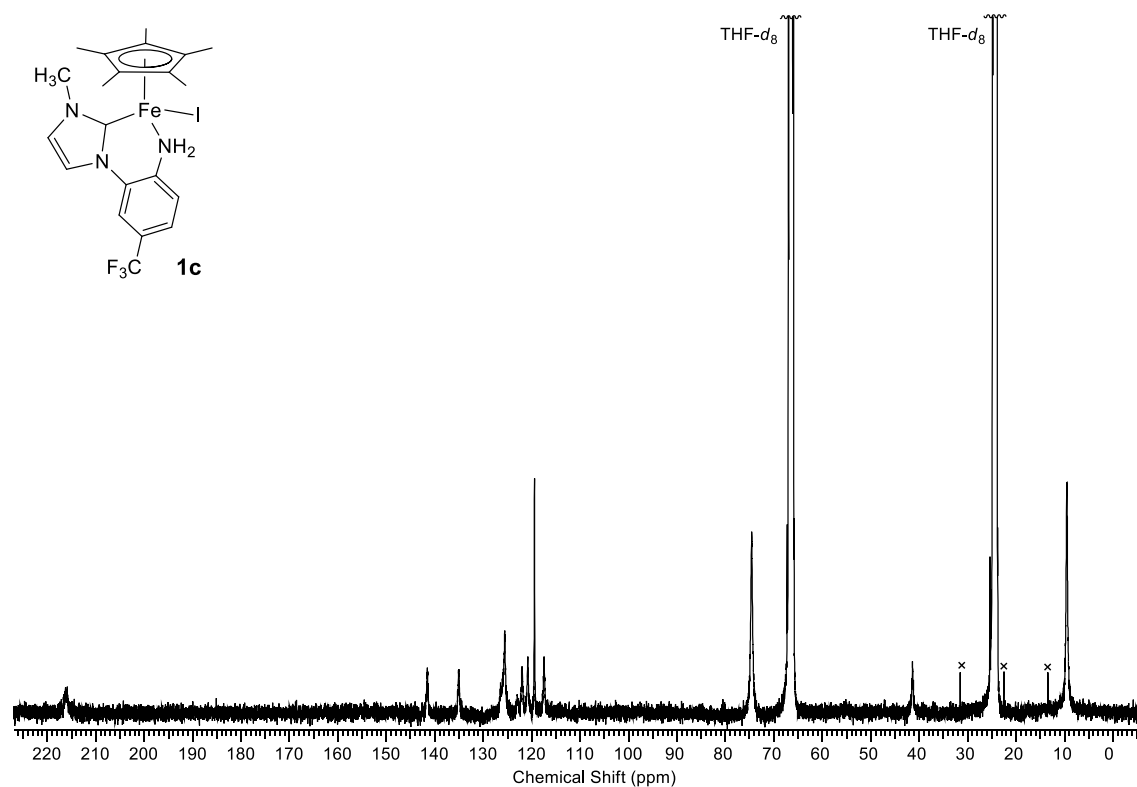


Figure 2-12. $^{13}\text{C}\{^1\text{H}\}$ NMR spectrum of **1c** (101 MHz, $\text{THF-}d_8$). \times -marks represent signals of hexane.

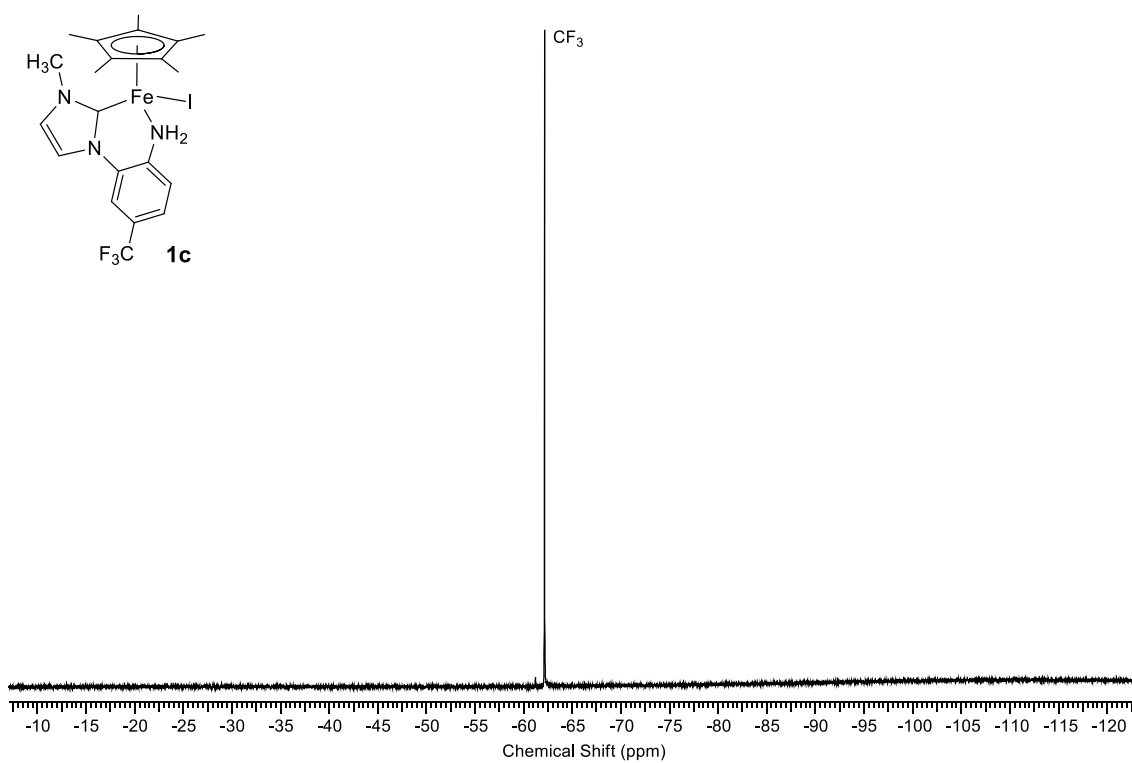
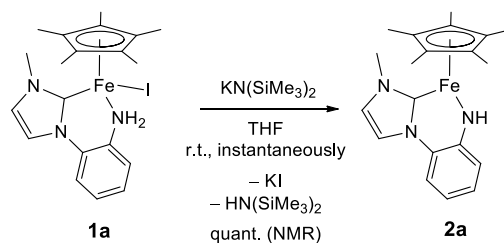


Figure 2-13. $^{19}\text{F}\{^1\text{H}\}$ NMR spectrum of **1c** (376 MHz, $\text{THF-}d_8$).

2-3-4. The Reaction of **1a** with $\text{KN}(\text{SiMe}_3)_2$



Scheme 2-3. Reaction of **1a** with $\text{KN}(\text{SiMe}_3)_2$.

Complex **1a** reacted with $\text{KN}(\text{SiMe}_3)_2$ immediately in THF to generate coordinatively unsaturated (amido)iron complex **2a** with concomitant formation of white precipitation of potassium iodide. The ^1H NMR spectrum of the reaction mixture is shown in Figure 2-14. The methyl protons of the Cp^* ligand is observed at 1.28 ppm with the intensity of 15H. The $\text{N}-\text{CH}_3$ is observed at 3.39 ppm. The signal of the proton on the amido group appears at 10.32 ppm having the intensity of 1H. Protons on the aromatic ring and the imidazole ring show their peaks at 6.53, 6.65, 7.02, 7.06, 7.09, and 7.58 ppm. Along with **2a**, hexamethyldisilazane $\text{HN}(\text{SiMe}_3)_2$ is observed at 0.07 ppm (s, SiMe_3) with the intensity of 18H, which indicates that abstraction of a proton of NH_2 occurs in the reaction almost quantitatively. The HRMS analysis shows the molecular ion peak at m/z 363.1392, which is assigned to **2a** (formula: $^{12}\text{C}_{20}^1\text{H}_{25}^{56}\text{Fe}^{14}\text{N}_3$; 363.1392). These data support the generation of **2a** via abstraction of a proton from the NH_2 group and the iodido ligand of **1a**.

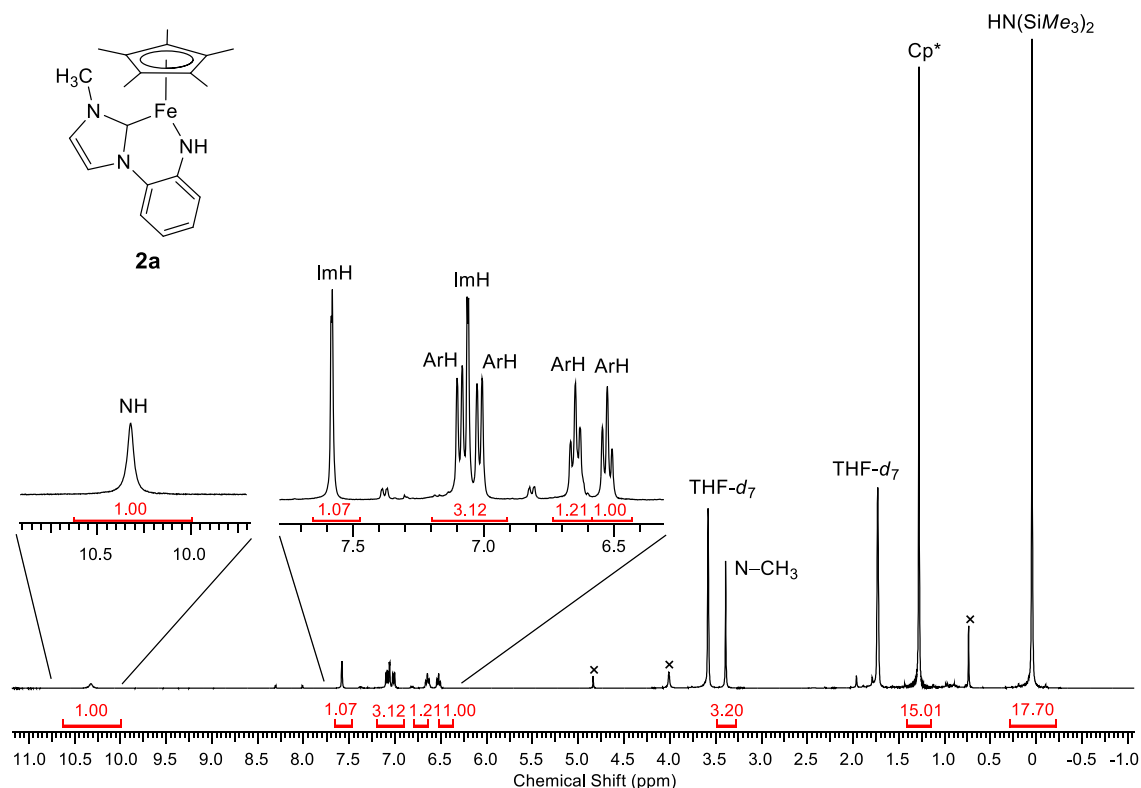
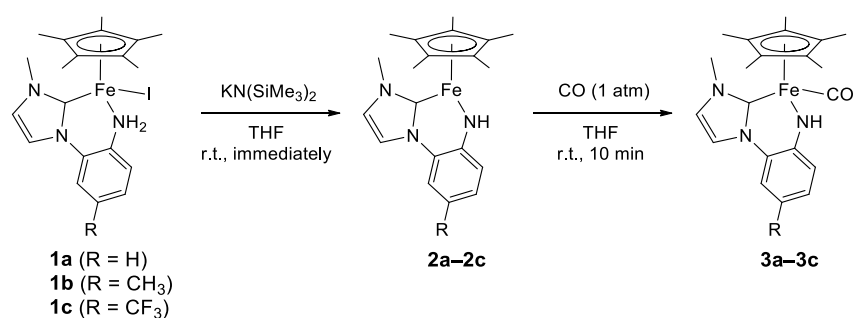


Figure 2-14. ^1H NMR spectrum of the reaction mixture of **1a** with $\text{KN}(\text{SiMe}_3)_2$ (400 MHz, $\text{THF}-d_8$). The \times -marks represent unidentified byproducts.

2-3-5. Reactions of **2** with Carbon Monoxide

Unfortunately, all attempts to crystallize **2a** were unsuccessful probably due to its high reactivity toward air and/or moisture. Therefore, I tried to trap the freshly prepared **2a** by exposing it to 1 atm CO gas, which led to formation of carbonyl adduct **3a**. Complex **3a** was isolated as red crystals in 36% yield (Scheme 2-4). Similarly, the synthesis of **3b** and **3c** were also achieved in the same way as that of **3a**. These results of trapping reactions clearly demonstrated that the reactions of **1a–1c** with $\text{KN}(\text{SiMe}_3)_2$ generated coordinatively unsaturated complexes **2a–2c**.



Scheme 2-4. Synthesis of carbonyl adducts **3a–3c**.

Molecular structures of **3a–3c** were determined by X-ray crystallography (Figure 2-15). Since there were no significant structural differences (Table 2-31), I will only describe the structural features of **3a** hereafter. The length of the Fe–N bond is 1.976(2) Å, which is ca. 0.1 Å shorter than that of **1a** (2.07 Å). This length is within the range of known Fe–N(amido) lengths (1.85–2.02 Å).^[13] The sum of angles around N is 350(4)°, which shows that the N takes a nearly planar geometry. The length of the N–C_{Ar} bond is 1.348(3) Å and is ca. 0.09 Å shorter than that of **1a** (1.435(2) Å).

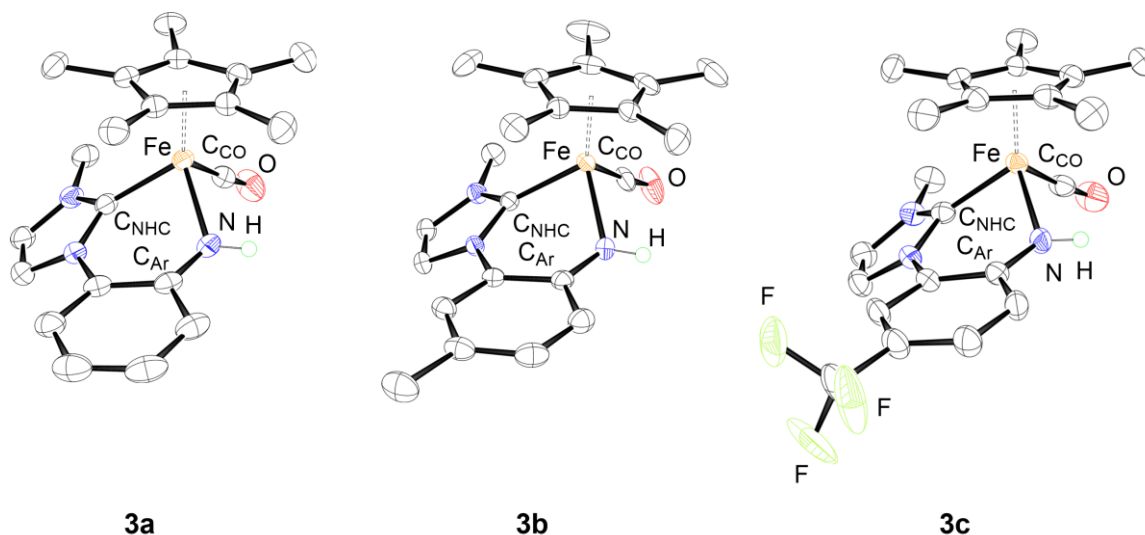


Figure 2-15. ORTEP drawings of **3a–3c**. The structure of **3c** with an occupancy factor of 50% is illustrated.

Table 2-31. Selected bond lengths (Å) and angles (°) of **3a–3c**

	3a	3b	3c
Fe–C _{NHC}	1.926(2)	1.924(2)	1.933(3)
Fe–C _{CO}	1.742(3)	1.735(2)	1.735(3)
Fe–N	1.976(2)	1.988(2)	1.970(2)
N–C _{Ar}	1.348(3)	1.356(3)	1.343(3)
N–H	0.83(4)	0.83(3)	0.86(4)
C _{NHC} –Fe–C _{CO}	95.89(11)	96.21(9)	95.27(13)
C _{NHC} –Fe–N	84.71(10)	84.34(8)	85.61(11)
N–Fe–C _{CO}	91.96(11)	93.77(10)	95.16(12)
ΣN ^a	350(4)	345.9(3)	349(4)

^a) The sum of the angles around N

This shortening of the N–C_{Ar} bond length in **3a** is caused by delocalization of the π-symmetric lone pair of the amido nitrogen to the aromatic ring. According to resonance theory, the anilido moiety in **3a** has 5 major canonical forms (Figure 2-16). If I assume that these canonical forms were comparably contributed to the structure of the moiety, bond orders of each C–C and a C–N bond would be calculated by averaging the bond orders in each canonical form. For example, C–N bond order is calculated as follows: (1+1+2+2+2)/5 = 1.6. The expected values of the bond order and X-ray determined bond lengths of **1a** and **3a** are listed in Table 2-32. As mentioned above, the N–C¹ length of **3a** is significantly shorter than that of **1a**. Both C¹–C² and C⁶–C¹ lengths of **3a** are slightly longer than those of **1a** and both C²–C³ and C⁵–C⁶ lengths are slightly shorter than those of **1a**. These trends appear to be consistent with the calculated values of the bond order. Although the above assumption for the contributions of canonical forms is rough, the results listed in Table 2-32 at least supported the delocalization of the lone pair to the aromatic ring.

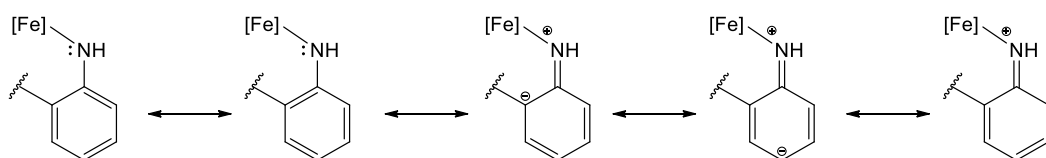
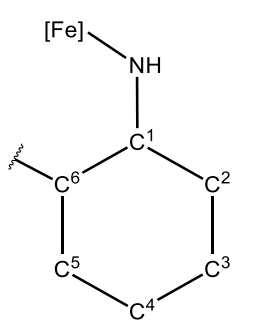
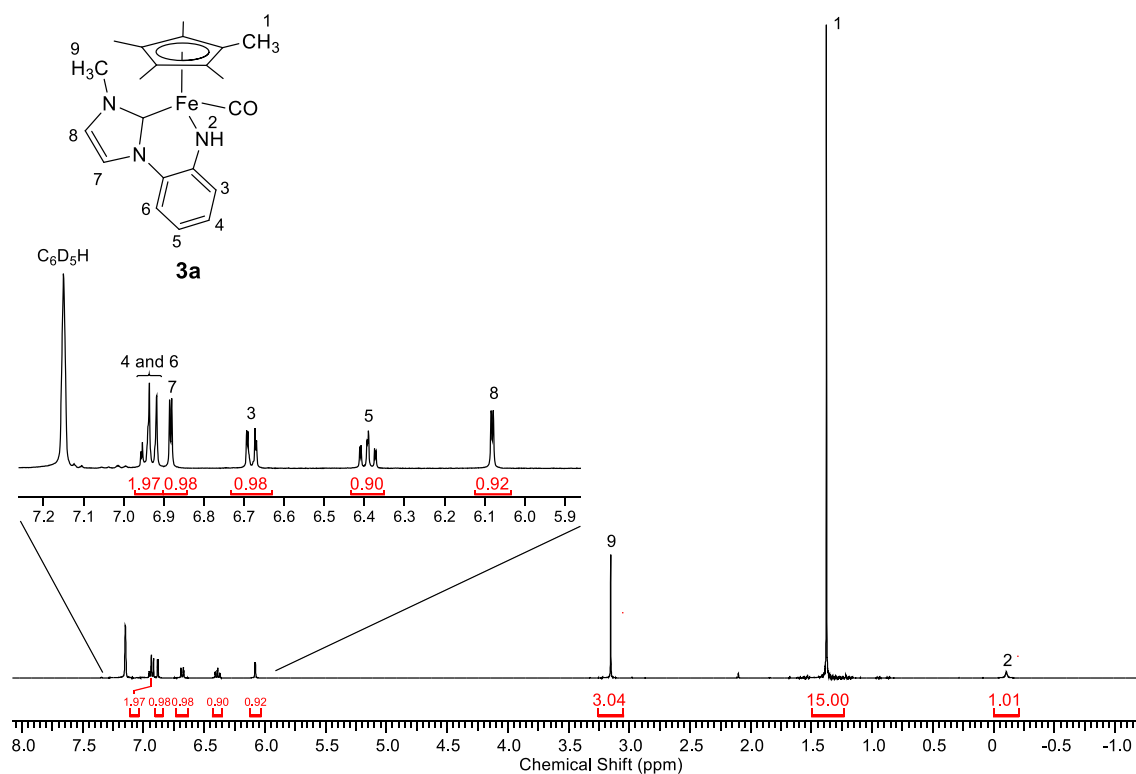
**Figure 2-16.** Five major canonical forms of the anilido moiety in **3a**.

Table 2-32. Selected bond lengths of the aromatic ring in **1a** and **3a**^a

Numbering of the ring	Bond	1a	3a
	N–C ¹	1.435(2) [1.0]	1.348(3) [1.6]
	C ¹ –C ²	1.393(3) [1.5]	1.422(3) [1.2]
	C ² –C ³	1.389(3) [1.5]	1.374(4) [1.6]
	C ³ –C ⁴	1.390(4) [1.5]	1.385(5) [1.4]
	C ⁴ –C ⁵	1.388(3) [1.5]	1.388(4) [1.4]
	C ⁵ –C ⁶	1.393(3) [1.5]	1.387(4) [1.6]
	C ⁶ –C ¹	1.401(3) [1.5]	1.412(4) [1.2]

a) The expected values of the bond order are shown in brackets.

The ¹H NMR spectrum of **3a** (Figure 2-17) shows a signal of NH at –0.10 ppm with the intensity of only 1H. The methyl protons of the Cp* ligand and N–CH₃ are observed at 1.38 and 3.15 ppm, respectively. Protons bound to the aromatic ring and the imidazole ring are observed as five signals with the total intensity of 6H in the range of 6.08–6.96 ppm. The ¹³C{¹H} NMR spectrum of **3a** shows 13 peaks, which is consistent with its molecular structure (Figure 2-18). The signals of methyl and ring carbons of the Cp* ligand are observed at 9.5 and 90.3 ppm, respectively. The methyl carbon on nitrogen of the NHC ligand is observed at 37.0 ppm. The signals of carbons in the aromatic ring (ArC) and the imidazole ring (ImC) appear at 108.8 (ArC), 118.6 (ArC), 119.0 (ImC), 122.2 (ArC), 122.9 (ImC), 126.6 (ArC), 126.9 (ArC), and 154.7 (ArC) ppm. Carbene carbon and carbonyl carbon are observed at 189.6 and 225.5 ppm, respectively.

**Figure 2-17.** ¹H NMR spectrum of **3a** (400 MHz, C₆D₆).

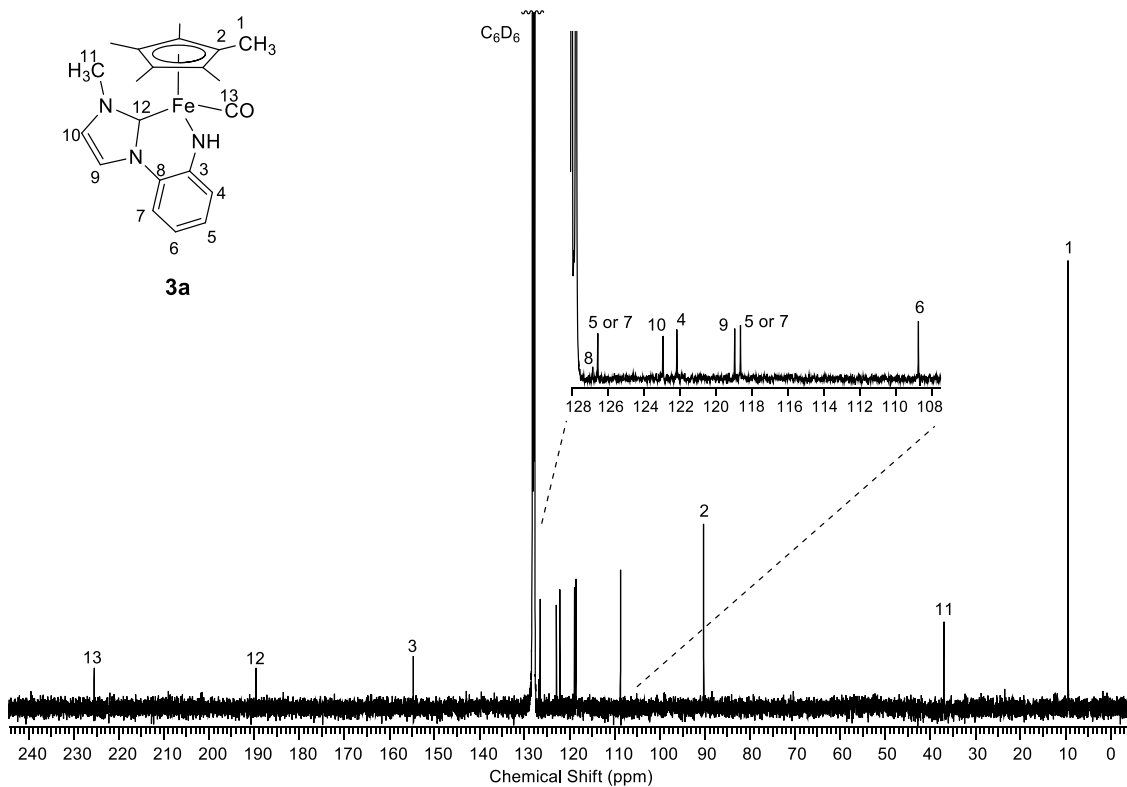


Figure 2-18. $^{13}\text{C}\{^1\text{H}\}$ NMR spectrum of **3a** (101 MHz, C_6D_6).

The ^1H and $^{13}\text{C}\{^1\text{H}\}$ NMR spectra of **3b** follow the same trends as those of **3a** (Figures 2-19 and 2-20). The methyl group on the aromatic ring is observed at 2.33 ppm in ^1H NMR and 20.8 ppm in $^{13}\text{C}\{^1\text{H}\}$ NMR. The ^1H NMR spectrum of **3c** also follows the same trends as that of **3a** (Figure 2-21). In the $^{13}\text{C}\{^1\text{H}\}$ NMR spectrum of **3c**, four carbons, which are the carbon of CF_3 group and *ipso*- and *ortho*-aromatic carbons with respect to the CF_3 group, are observed as quartet signals due to the coupling with three ^{19}F nuclei (Figure 2-22). The $^{19}\text{F}\{^1\text{H}\}$ NMR spectrum shows a single peak at -58.4 ppm, which is comparable with the chemical shift of the CF_3 group of $\text{C}_6\text{H}_5\text{CF}_3$ (Figure 2-23).

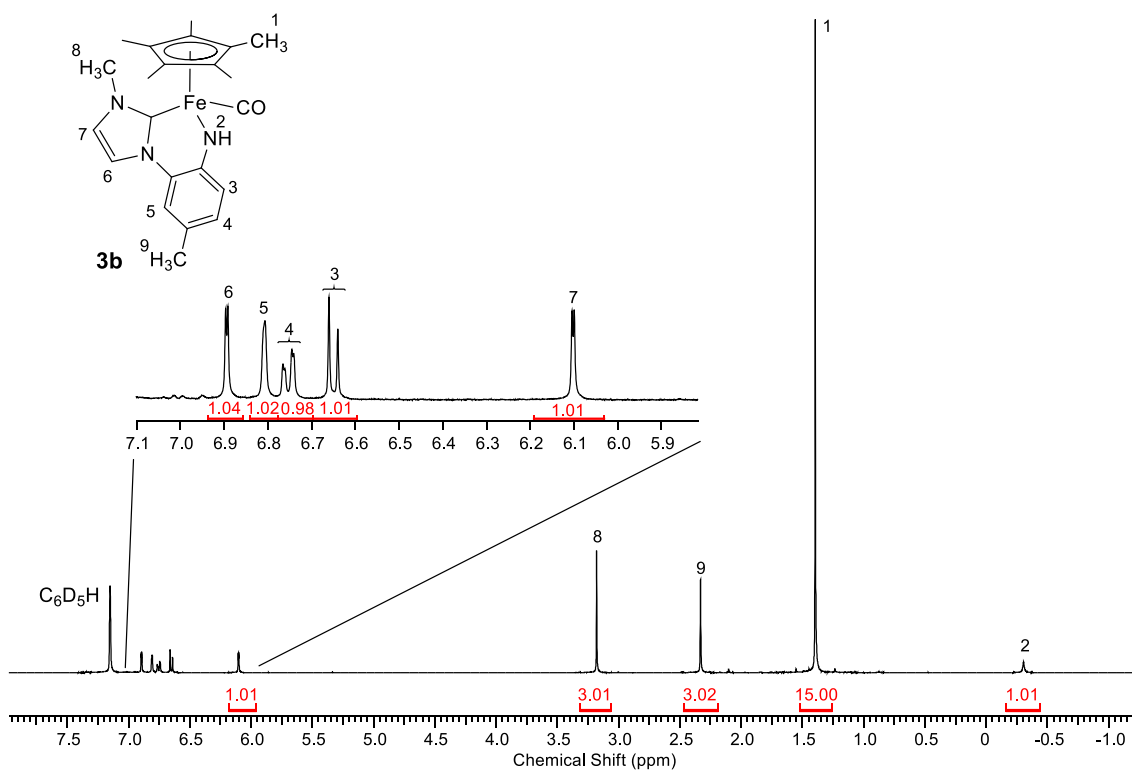


Figure 2-19. ^1H NMR spectrum of **3b** (400 MHz, C_6D_6).

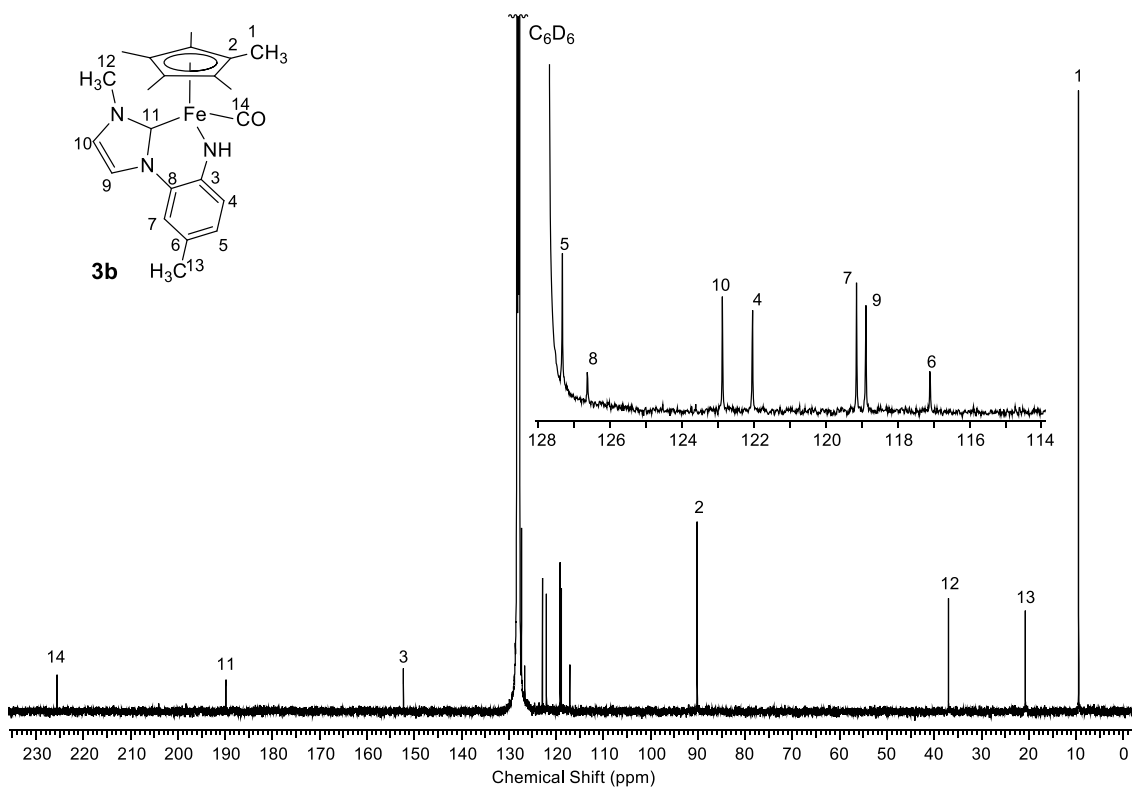
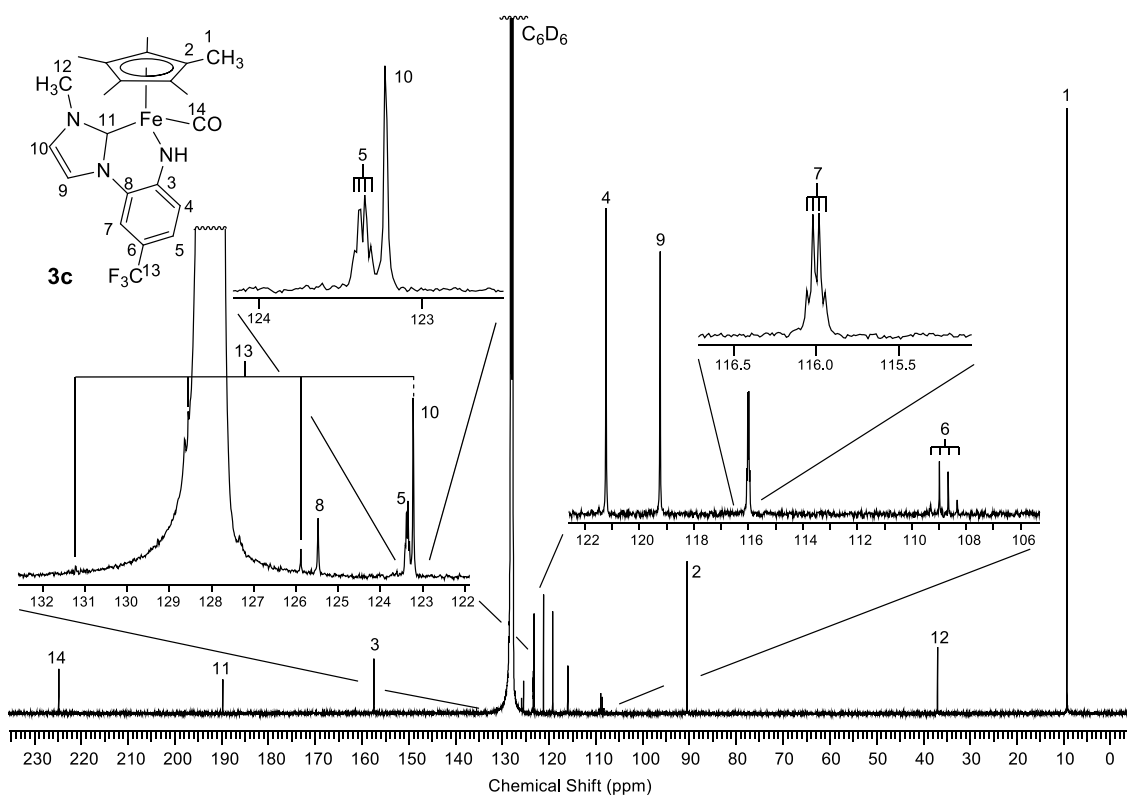
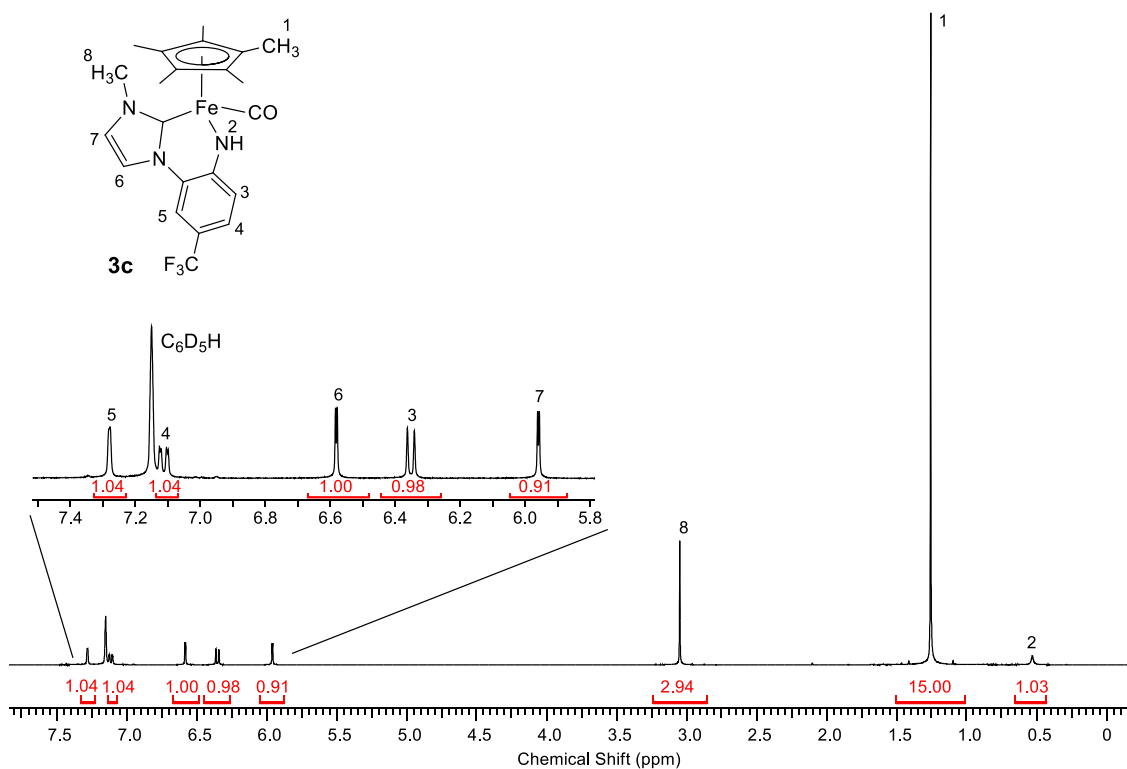


Figure 2-20. $^{13}\text{C}\{^1\text{H}\}$ NMR spectrum of **3b** (101 MHz, C_6D_6).



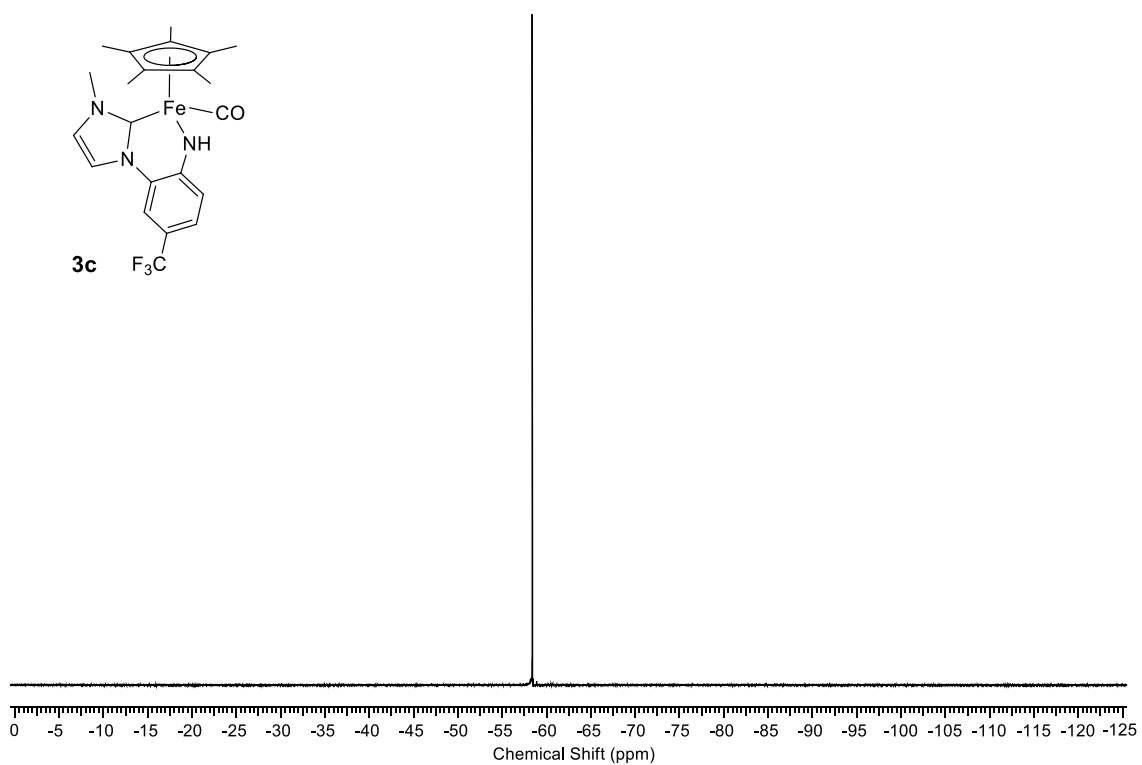
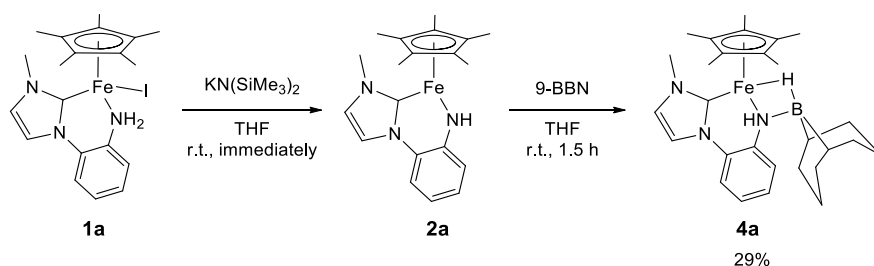


Figure 2-23. $^{19}\text{F}\{^1\text{H}\}$ NMR of **3c** (376 MHz, C_6D_6).

2-3-6. Reaction of **2a** with 9-Borabicyclo[3.3.1]nonane (9-BBN)

In order to confirm the existence of the lone pair on the amido nitrogen of **2a**, I tried the reaction of **2a** with 9-BBN. This reaction afforded borane adduct **4a** as a sole boron-containing product, which was isolated as brown crystals in 29% yield.



Scheme 2-5. Reaction of **2a** with 9-BBN.

The structure of **4a** was determined by X-ray crystallography and the ORTEP drawing was shown in Figure 2-24. The boron center of 9-BBN is coordinated by the amido nitrogen and a B–H of 9-BBN is coordinated to the iron center to form a Fe–N–B–H four-membered ring structure. The selected bond lengths and angles of **4a** are listed in Table 2-33. The length of the Fe–N bond is 1.992 Å. Although this value is slightly larger than that of **3a** (1.976(2) Å), it is still within the range of Fe–N single bond lengths of known terminal iron amido complexes (1.85–2.02 Å).^[13] Therefore, it can be regarded as a long Fe–N single bond. The reason for the elongation of the Fe–N length is probably the significant contribution of the zwitterionic form **B** (Figure 2-25). The length of the N–C_{Ar} bond is 1.425(4) Å, which is closer to that of **1a** (1.435(2) Å) than to that of **3a** (1.348(3) Å). This indicates that the delocalization of the lone pair of amido nitrogen to the aromatic ring, which existed in **3a**, does not exist anymore due to the coordination of the lone pair of the amido nitrogen of **2a** to the boron center of 9-BBN.

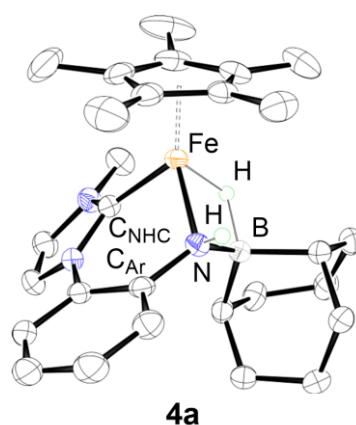
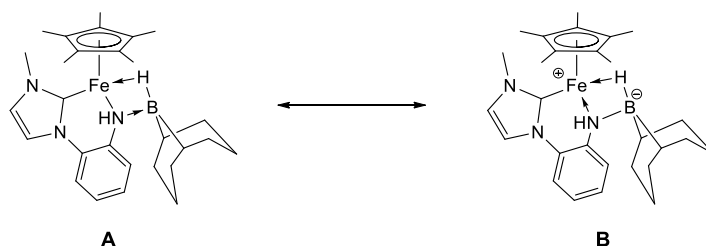


Figure 2-24. ORTEP drawing of **4a**.

Table 2-33. Selected bond lengths (Å) and angles (°) of **4a**

Fe–C _{NHC}	1.909(3)	N–C _{Ar}	1.425(4)
Fe–N	1.992(2)	N–H	0.84(3)
Fe–HB	1.54(3)	C _{NHC} –Fe–N	88.59(11)
H–B	1.35(3)	N–Fe–HB	78.0(12)
B–N	1.560(4)	C _{NHC} –Fe–HB	88.3(12)

**Figure 2-25.** Possible canonical forms of **4a**.

The ¹H NMR spectrum of **4a** was shown in Figure 2-26. The methyl protons of the Cp* ligand and N–Me are observed at 1.55 and 4.09 ppm, respectively. Protons on the aromatic ring (ArH) and the imidazole ring (ImH) are observed at 6.97–7.05 (2 ArH), 7.18 (ImH), 7.27 (ArH), 7.36 (ArH), and 7.55 (ImH) ppm. The signals of methylene protons on the 9-BBN moiety appear in the range from 0.7 to 2.4 ppm with the total intensity of 12H. The signal of NH is observed at 2.15 ppm with the intensity of 1H. The hydrido ligand, which bridges the iron center and the boron of 9-BBN moiety, is observed at –15.1 ppm as a broadened signal due to the quadrupolar relaxation and coupling caused by the boron atom. Since this signal is observed as a sharp signal in ¹H{¹¹B} NMR spectrum (Figure 2-26), it is strongly supported that complex **4a** is a B–H agostic complex. Two methyne protons on the 9-BBN moiety are inequivalently observed at 0.47 ppm and –2.14 ppm with the intensity of 1H each.

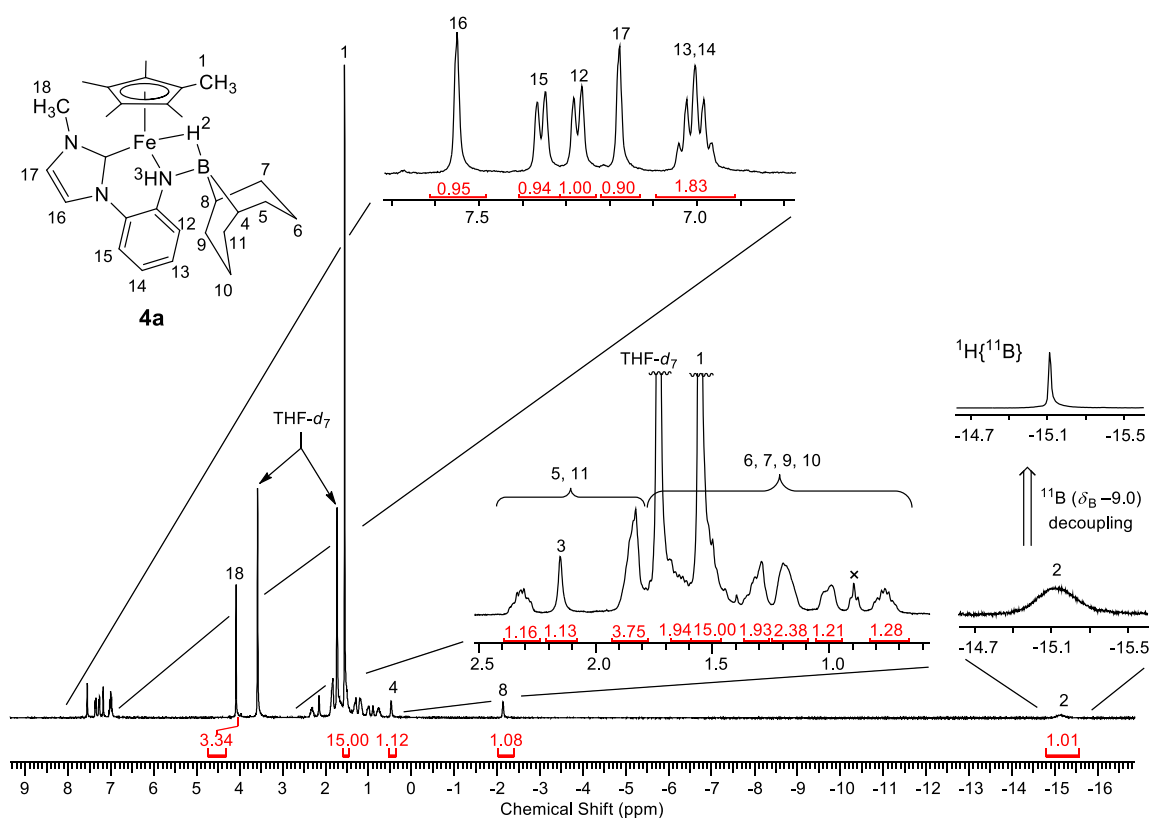


Figure 2-26. ^1H NMR and partial $^1\text{H}\{^{11}\text{B}\}$ NMR spectra of **4a** (400 MHz, $\text{THF-}d_8$). \times -mark represents a signal of hexane.

The reason why one of the two methyne protons of the 9-BBN moiety of **4a** is observed at such a remarkable high field, -2.14 ppm, is the upfield shift caused by the ring current effect of the imidazol-2-ylidene moiety. The molecular geometry of **4a**, which is obtained by X-ray crystallography, is shown in Figure 2-27. One methyne proton is located above the imidazol-2-ylidene (NHC) ring and the distance between the proton and the center of the ring is 2.660 Å. According to the literature,^[14] imidazol-2-ylidene is considered to have aromaticity. In addition, it has also been reported that the magnetic shielding due to the ring current effect extends to 5–10 Bohr radius (2.6 – 5.2 Å) when magnetic field of 4 T is applied perpendicular to the molecular plane of general aromatic compounds such as benzene, pyrrole, furan, and thiophene.^[15] Since the NMR spectrometer I used applies 9.4 T to the sample, the methyne proton would lie entirely in the shielding zone of the NHC ring. Therefore, the methyne proton is strongly shielded and the chemical shift indicates that **4a** mainly adopts the geometry shown in Figure 2-27 in solution.

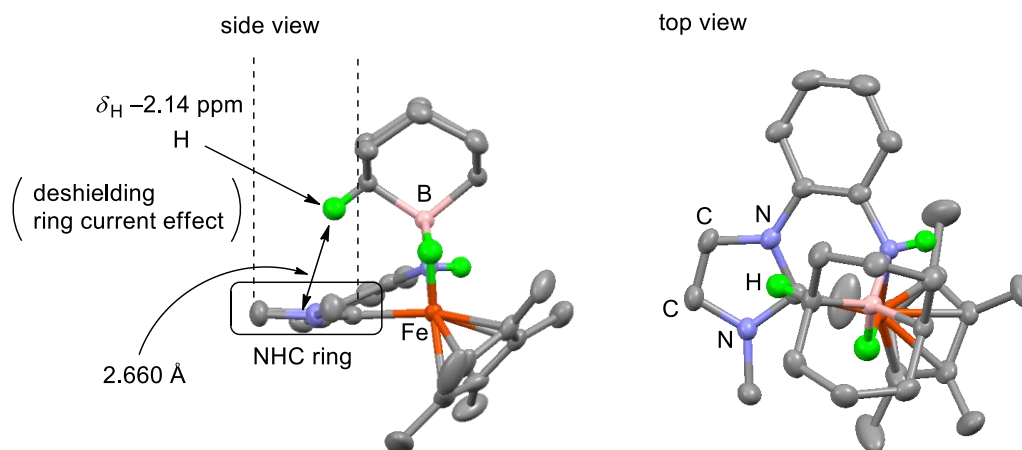


Figure 2-27. The molecular geometry of **4a** obtained by X-ray crystallography.

The $^{13}\text{C}\{^1\text{H}\}$ NMR spectrum of **4a** shows 20 peaks which is consistent with its molecular structure (Figure 2-28). The signals of methyl and ring carbons of the Cp* ligand are observed at 10.8 and 79.3 ppm, respectively. The methyl carbon on the nitrogen of the NHC ligand is observed at 40.0 ppm. Two methyne carbons of 9-BBN moiety are observed at 23.4 and 28.6 ppm as broadened signals due to the effect of the quadrupolar ^{11}B nucleus. Methylene carbons of 9-BBN moiety show six signals in the range between 25–40 ppm. The signals of carbons in the aromatic ring (ArC) and the imidazole ring (ImC) appear at 118.5 (ImC), 120.6 (ArC), 122.8 (ArC), 124.0 (ImC), 124.6 (ArC), 125.8 (ArC), 132.5 (ArC), and 143.7 (ArC) ppm. Carbene carbon is observed at 211.9 ppm. The ^{11}B NMR spectrum of **4a** show a single broad peak at -8.9 ppm, which is comparable with the chemical shifts of normal tetra-coordinated boron centers^[16] (Figure 2-29).

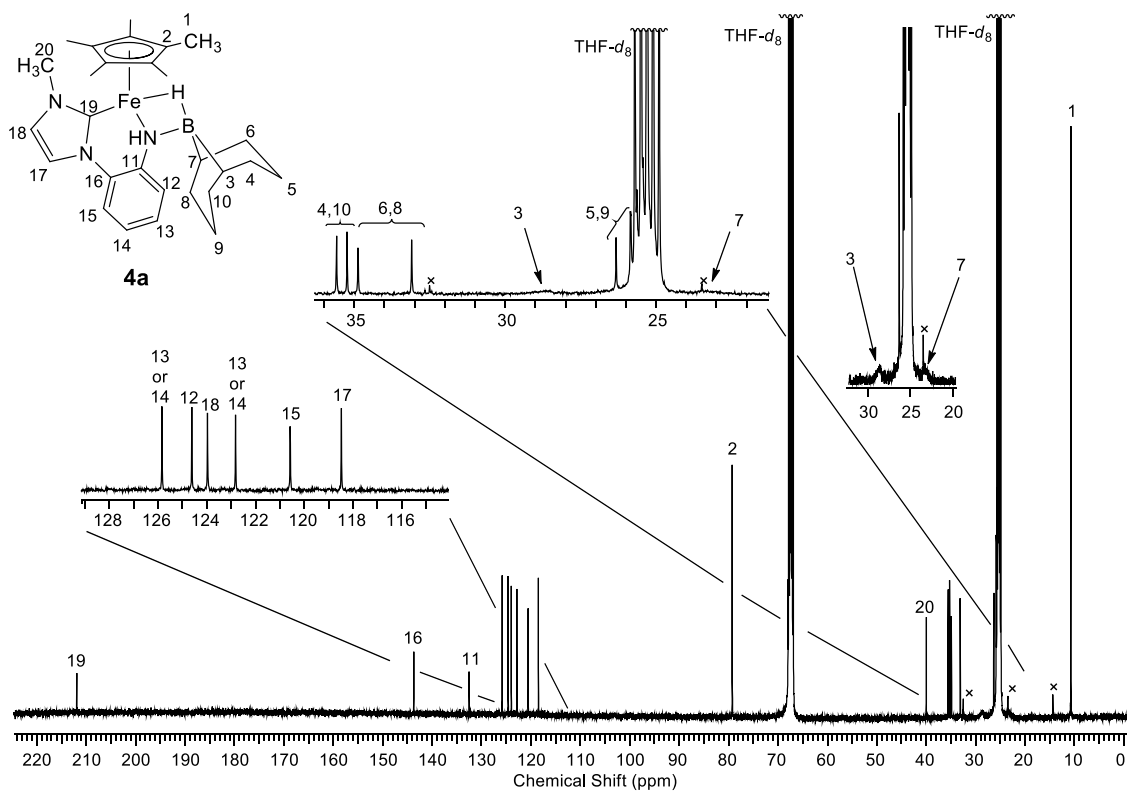


Figure 2-28. $^{13}\text{C}\{^1\text{H}\}$ NMR spectrum of **4a** (101 MHz, $\text{THF-}d_8$). The \times -marks represent signals of hexane.

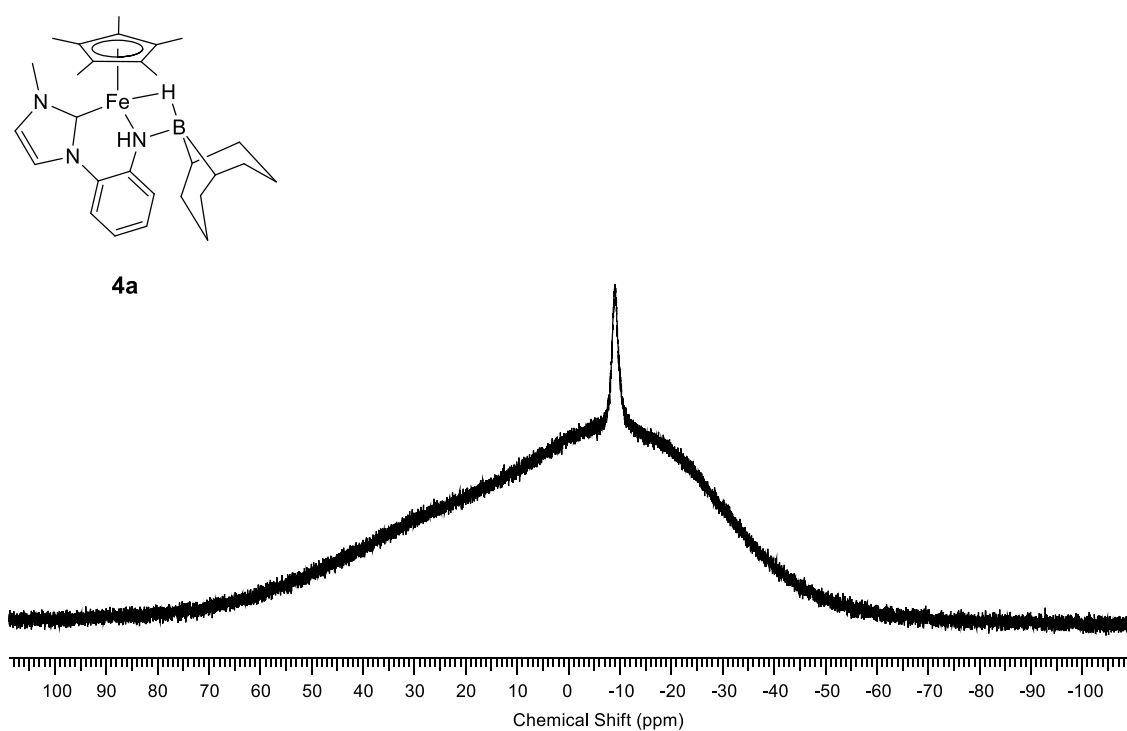
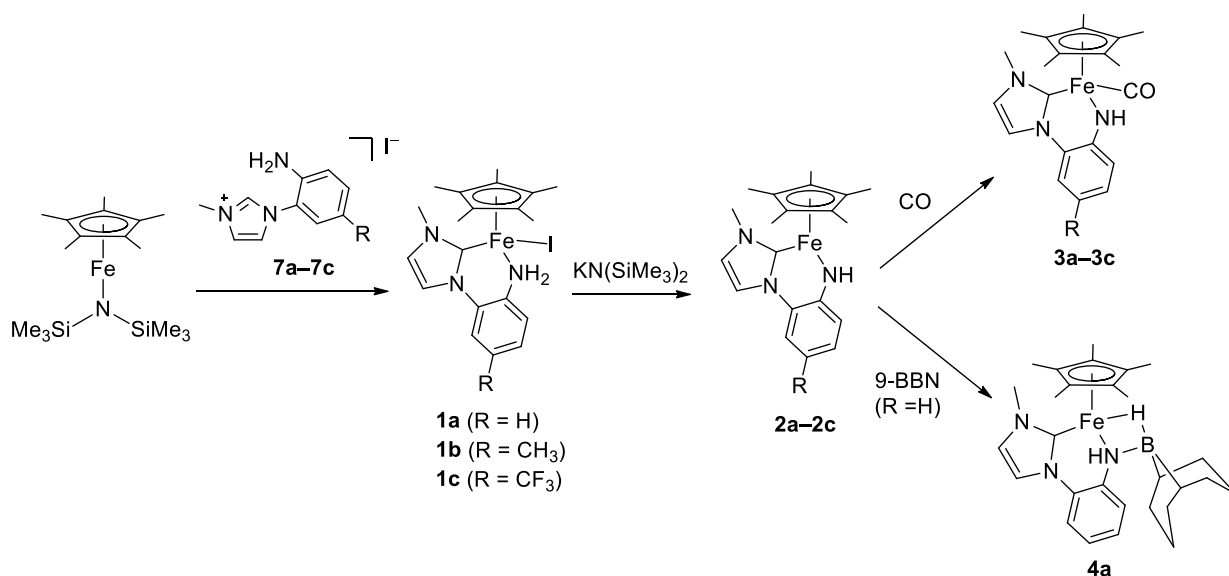


Figure 2-29. ^{11}B NMR spectrum of **4a** (128 MHz, $\text{THF-}d_8$).

2-4. Conclusion

The reactions of $\text{Cp}^*\text{FeN}(\text{SiMe}_3)_2$ with the corresponding imidazolium iodides **7a–7c** gave amino(iodido)iron complexes **1a–1c** in moderate yields. Complexes **1a–1c** were fully characterized spectroscopically and their structures were determined crystallographically. The reaction of **1a** with $\text{KN}(\text{SiMe}_3)_2$ in THF solution gave a coordinatively unsaturated (amido)iron complex **2a**, which was characterized by ^1H NMR spectroscopy and HRMS. Complex **2a** was also trapped by CO and 9-BBN to give carbonyl adduct **3a** and borane adduct **4a**, respectively. The synthesis of **3b** and **3c** were also achieved in the same way as that of **3a**. These results clearly demonstrated that the reactions of **1a–1c** with $\text{KN}(\text{SiMe}_3)_2$ generated coordinatively unsaturated complexes **2a–2c**. The formation of **3a–3c** and **4a** indicates that **2a–2c** have a vacant site on their iron center and a lone pair on their amido nitrogen. Namely, complexes **2a–2c** have a bifunctional reaction site in their structures.



Scheme 2-6. Synthesis of **1a–1c**, generation of **2a–2c**, and formation of **3a–3c** and **4a**.

2-5. References

- [1] U. Siemeling, U. Vorfeld, B. Neumann, and H.–G. Stammer, *Organometallics* **1998**, *17*, 483.
- [2] C. Savarin, J. Srogl, and L. S. Liebeskind, *Org. Lett.* **2001**, *3*, 91.
- [3] R.–T. Zhuang, W.–J. Lin, R. R. Zhuang, W.–S. Hwang, *Polyhedron* **2013**, *51*, 132.
- [4] M. C. Pirrung, Y. Liu, L. Deng, D. K. Halstead, Z. Li, J. F. May, M. Wedel, D. A. Austin, Nicholas J. G. Webster, *J. Am. Chem. Soc.* **2005**, *127*, 4609.
- [5] C.–I Lee, J. Zhou, and O. V. Ozerov, *J. Am. Chem. Soc.* **2013**, *135*, 3560.
- [6] A. A. Farahat, D. W. Boykin, *Tetrahedron Lett.* **2014**, *55*, 3049.
- [7] A. McKillop and J. A. Tarbin, *Tetrahedron* **1987**, *43*, 1753.
- [8] V. V. Ivanov, A. A. Yurchenko, A. N. Chernega, A. M. Pinchuk, and A. A. Tolmachev, *Heteroatom Chem.* **2002**, *13*, 84.
- [9] G. M. Sheldrick, *SHELXS-97, Programs for Solution of Crystal Structures*, University of Göttingen, Germany, **1997**.
- [10] G. M. Sheldrick, *SHELXL-97, Programs for Refinement of Crystal Structures*, University of Göttingen, Germany, **1997**.
- [11] K. Wakita, *Yadokari-XG, Software for Crystal Structure Analyses*, **2001**; C. Kabuto, S. Akine, T. Nemoto, E. Kwon, *Release of Software (Yadokari-XG 2009) for Crystal Structure Analyses*, *J. Cryst. Soc. Jpn.* **2009**, *51*, 218.
- [12] Gaussian 09, Revision D.01, M. J. Frisch, G. W. Trucks, H. B. Schlegel, G. E. Scuseria, M. A. Robb, J. R. Cheeseman, G. Scalmani, V. Barone, G. A. Petersson, H. Nakatsuji, X. Li, M. Caricato, A. Marenich, J. Bloino, B. G. Janesko, R. Gomperts, B. Mennucci, H. P. Hratchian, J. V. Ortiz, A. F. Izmaylov, J. L. Sonnenberg, D. Williams-Young, F. Ding, F. Lipparini, F. Egidi, J. Goings, B. Peng, A. Petrone, T. Henderson, D. Ranasinghe, V. G. Zakrzewski, J. Gao, N. Rega, G. Zheng, W. Liang, M. Hada, M. Ehara, K. Toyota, R. Fukuda, J. Hasegawa, M. Ishida, T. Nakajima, Y. Honda, O. Kitao, H. Nakai, T. Vreven, K. Throssell, J. A. Montgomery, Jr., J. E. Peralta, F. Ogliaro, M. Bearpark, J. J. Heyd, E. Brothers, K. N. Kudin, V. N. Staroverov, T. Keith, R. Kobayashi, J. Normand, K. Raghavachari, A. Rendell, J. C. Burant, S. S. Iyengar, J. Tomasi, M. Cossi, J. M. Millam, M. Klene, C. Adamo, R. Cammi, J. W. Ochterski, R. L. Martin, K. Morokuma, O. Farkas, J. B. Foresman, and D. J. Fox, Gaussian, Inc., Wallingford CT, **2016**.
- [13] The result of search on CCDC database (CSD version 5.37 updates, Feb 2016)
- [14] R. Sevinçek, H. Karabıyık, and H. Karabıyık, *J. Mol. Model.* **2013**, *19*, 5327.
- [15] J. Jusélius, and D. Sundholm, *Phys. Chem. Chem. Phys.* **1999**, *1*, 3429.
- [16] S. Heřmánek, *Chem. Rev.* **1992**, *92*, 325.

Chapter 3

Dehydrogenation of Ammonia-Borane with Bifunctional Iron Complex Having 2-Aminophenyl-Substituted *N*-Heterocyclic Carbene Ligands

3-1. Introduction

As mentioned in Chapter 1, ammonia-borane (AB) dehydrogenation using noble metal-based catalysts have been reported over a decade and a half, and these catalysts displayed good catalytic performances (Figure 3-1).

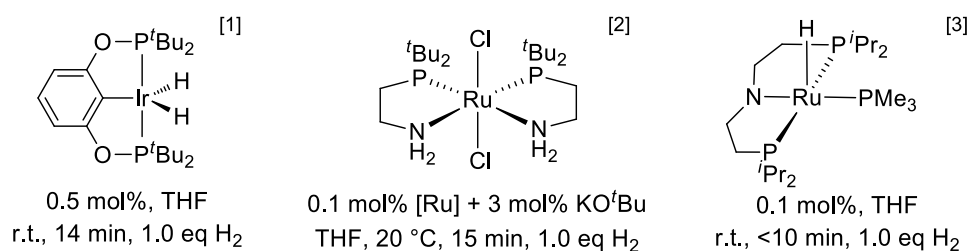
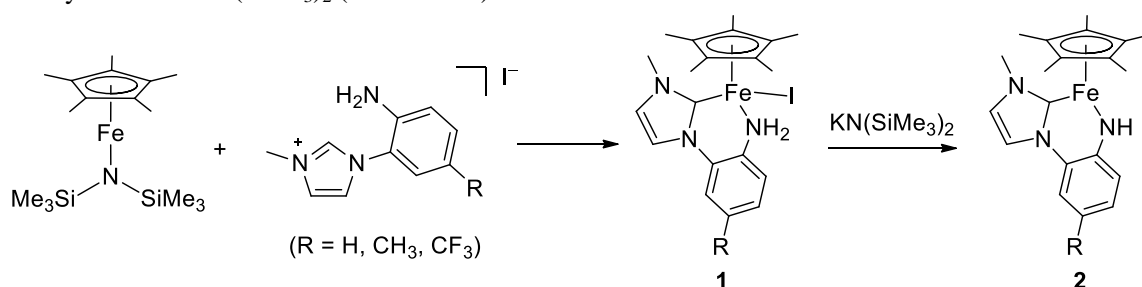


Figure 3-1. Selected examples of noble metal catalysts for dehydrogenation of AB displaying high reaction rates.

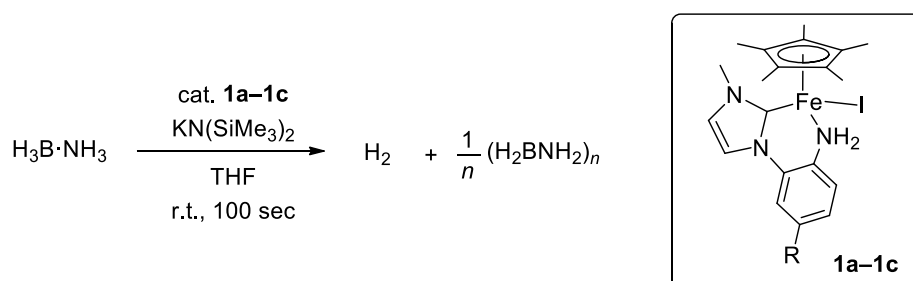
On the other hand, AB dehydrogenation using iron-based catalysts are still few in number and their reaction rates are still lower than those of the AB dehydrogenation using noble metal-based catalysts.

In Chapter 2, I described the generation of the bifunctional iron complexes **2** by the reactions of precatalysts **1** with $\text{KN}(\text{SiMe}_3)_2$ (Scheme 3-1).



Scheme 3-1. Synthesis of the bifunctional iron complexes **2**.

In this chapter, catalytic dehydrogenation of AB using the in situ-generated catalysts **2** from the precatalysts **1** and $\text{KN}(\text{SiMe}_3)_2$ will be described (Scheme 3-2). DFT calculations performed to elucidate the catalytic reaction mechanism will also be described and discussed in this chapter.



Scheme 3-2. Dehydrogenation reaction of AB catalyzed by **2** generated from **1a–1c** and $\text{KN}(\text{SiMe}_3)_2$.

3-2. Experimental Section

3-2-1. Catalytic Dehydrogenation of AB (NMR scale experiment) An NMR tube equipped with a J. Young Teflon valve was charged with **1a** (4.9 mg, 0.010 mmol) and THF-*d*₈ (ca. 0.4 mL). To this solution was added 1 equivalent of KN(SiMe₃)₂ (2.0 mg, 0.010 mmol), and then AB (6.0 mg, 0.19 mmol, 19.5 eq) was added in one portion. Rapid H₂ evolution occurred with concomitant formation of precipitation. After a few minutes, the H₂ evolution ceased. The ¹¹B NMR spectrum of the reaction mixture was recorded.

3-2-2. Catalytic Dehydrogenation of AB (Measuring the released amount of hydrogen) In a typical experiment, the volume of H₂ liberated by the dehydrogenation of AB catalyzed by **1** was measured by means of a eudiometer whose structure is illustrated in Figure 3-2. The experimental procedure was as follows: A THF solution of **1** (250 μL) was mixed with a THF solution of KN(SiMe₃)₂ (250 μL) in one of the two tubes of a forked glass vessel equipped with a J. Young Teflon valve and a stirring bar. The other tube was charged with a THF solution of AB (500 μL, 0.60 M). The glass vessel was brought out from the drybox carefully without mixing these two solutions. A thin Teflon cannula, which was purged with dry nitrogen, was attached to the side arm of the glass vessel. The opposite end of the cannula was inserted into a water-filled inverted graduated test tube. The reaction was started by mixing the two solutions and the J. Young valve was opened immediately after that. Rapid H₂ evolution with concomitant formation of precipitate occurred. The volume of liberated H₂ was measured at regular intervals (10 seconds). The equivalent (eq.) of H₂ was calculated by Eq. 3-1, where $n(X)_t$ means the molar number of X at t seconds after the beginning of the reaction.

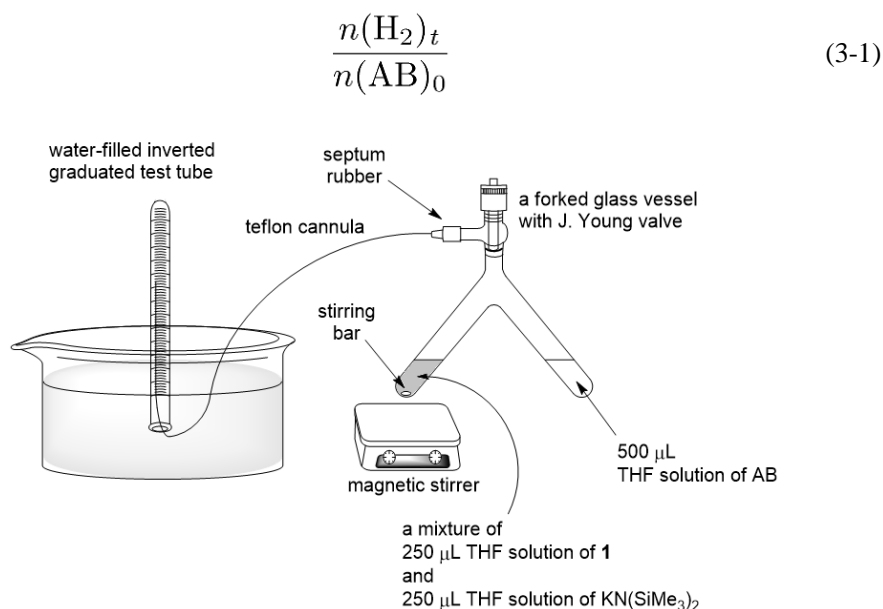


Figure 3-2. A schematic diagram of the eudiometer used for measurement of the volume of H₂.

3-2-2. Bulk Dehydrogenation of AB Catalyzed by 1a A 10 mL glass tube equipped with a J. Young Teflon valve and a stirring bar was charged with **1a** (27.1 mg, 0.0551 mmol) and THF (4 mL). To this solution was added a THF (1 mL) solution of KN(SiMe₃)₂ (11.0 mg, 0.0551 mmol). While the solution was stirred, a THF solution (1 mL) of AB (34.0 mg, 1.10 mmol, 20 eq) was added to the solution. Rapid H₂ evolution occurred immediately along with the formation of precipitate. The reaction mixture was stirred at room temperature for a week. The resulting precipitate was collected by filtration, washed with THF, and dried in vacuo to yield a pale brown powder (24.2 mg, 76%). IR (KBr pellet, cm⁻¹) 3300 (s, ν(N-H)), 3248 (s, ν(N-H)), 2391 (vs, ν(B-H)), 2316 (vs, ν(B-H)), 1560 (m, δ(N-H)), 1209 (vs, δ(B-H)), 845 (s, γ(N-H)). ¹¹B{¹H} MQMAS NMR (192.6 MHz, δ), -12.3 (br, (H₂BNH₂)_n).

3-2-3. DFT Calculations Gaussian 09 (G09) program package (revision E.01)^[4] was used for all computations. Geometry optimizations of all complexes in gas phase were performed at the B3PW91 level using 6-31G(d,p) basis sets for H, B, C, N, and F atoms and SDD basis sets for Fe and Ru atoms. Frequency analysis calculations were performed to characterize the structures to be the minima (no imaginary frequency) or transition states (one imaginary frequency) and to determine the thermal corrections that include the zero-point energy and enthalpy. Transition states were verified by intrinsic reaction coordinate (IRC) calculations. Single-point calculations on the optimized structures obtained by above calculations were performed at the M06 level in combination with 6-311+G(d,p) basis sets for H, B, C, N and F atoms and SDD basis sets for Fe and Ru atoms in order to refine the energies. The solvation effect of THF was simulated by the SMD continuum solvent model. The Gibbs free energies (298.15 K, 1 atm) were obtained by adding the thermochemistry corrections at the B3PW91 level to the energies refined at the M06 level. These functional and basis sets, and the solvation model were used as implemented in G09. This level of DFT calculation is denoted as M06-SMD(THF)/6-311+G(d,p),SDD//B3PW91/6-31G(d,p),SDD.

The optimized atomic coordinates of the structures obtained by DFT calculations are listed in Supporting Information (Tables S4–S31).

3-3. Results and Discussion

3-3-1. Catalytic Dehydrogenation of AB Using **1a** as a Precatalyst

In initial NMR scale experiment, addition of AB to a THF solution of freshly prepared **2a** caused immediate and rapid evolution of H₂ with concomitant formation of large amount of precipitate. The bubbling of H₂ ceased within a few minutes, and AB was consumed almost completely, which was confirmed by the ¹¹B NMR spectrum of the reaction mixture (Figure 3-3). The ¹¹B NMR spectrum also showed the formation of trace amount of oligomeric dehydrogenation products, such as cyclotriborazane (CTB), *B*-(cyclodiborazanyl)amine-borane (BCDB), diaminoborane (DAB), borazine (BZ), and poly(borazylene) (PBZ). The reaction was also successful on large scales. The time course profiles of the catalytic reactions are shown in Figure 3-4 and the results are summarized in Table 3-1. When 5 mol% of **1a** was used, 0.90 eq. of H₂ was emitted in 100 sec and it reached 0.94 eq. in 800 sec. The initial turnover frequency (TOF), which was estimated from the time course of the first 10 seconds, was $5.1 \times 10^3 \text{ h}^{-1}$. This result is remarkable since the highest known TOF for the dehydrogenation of AB catalyzed by homogeneous iron catalysts is 30 h^{-1} .^[5] Unfortunately, the catalyst was rapidly deactivated and further addition of AB to the system did not cause H₂ evolution. The final equivalent of H₂ was greatly changed depending on the amount of catalyst loading. When 2 mol% and 1 mol% of **1a** were used, 0.62 and 0.44 eq. of H₂ were liberated in 800 sec, respectively. In these reactions, catalyst deactivation occurred in the course of dehydrogenation reaction because unreacted AB was detected by the ¹¹B NMR spectrum of the reaction mixture (Figure 3-5).

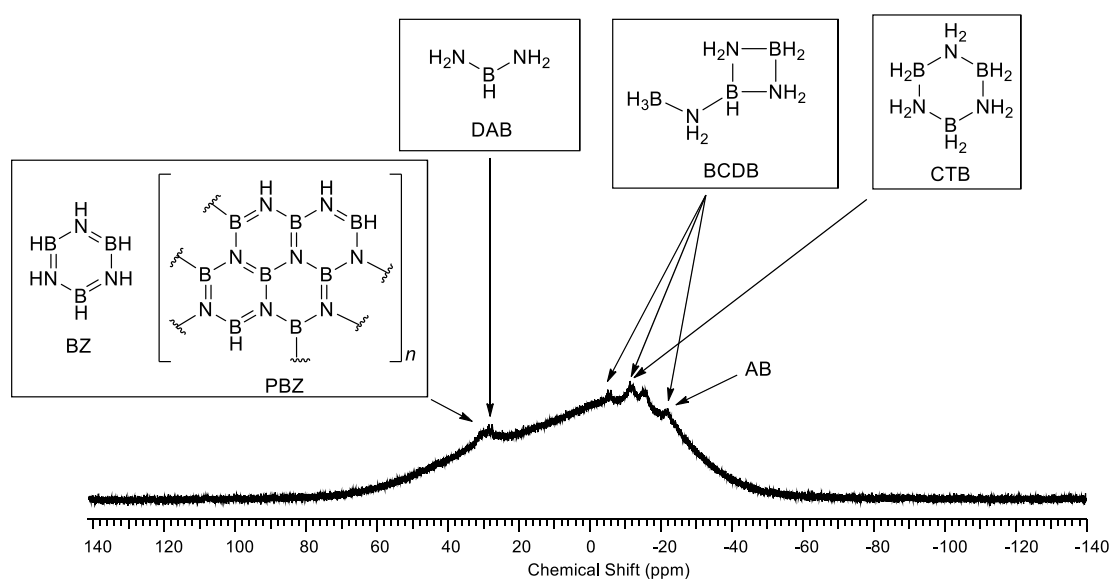


Figure 3-3. ¹¹B NMR spectrum after the catalytic reaction (5 mol% **1a**, 5 mol% KN(SiMe₃)₂, THF-*d*₈).

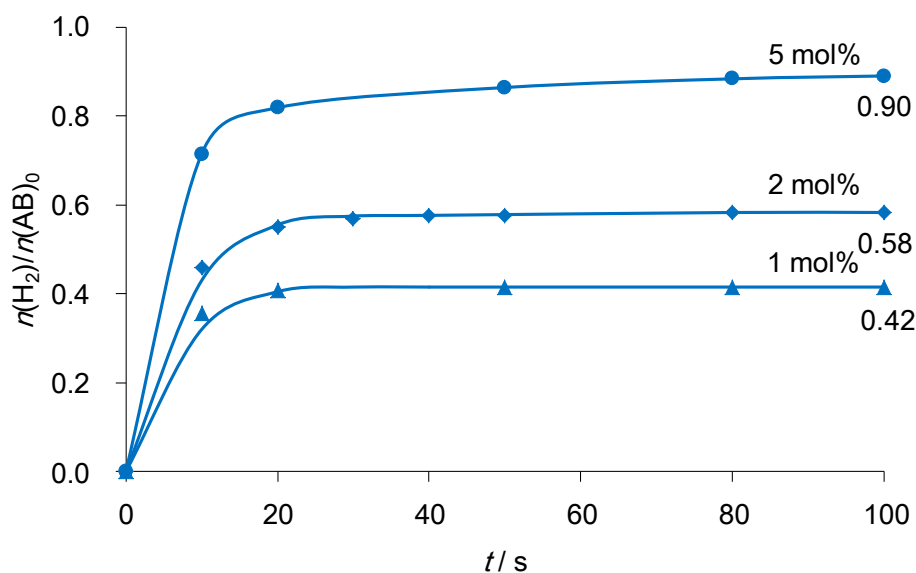
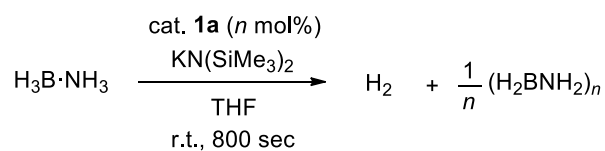


Figure 3-4. The time course profiles of catalytic dehydrogenation of AB using **1a**.

Table 3-1. Reaction conditions^a and results of the catalytic dehydrogenation of AB using **1a**



Entry	Catalyst (mol%)	H ₂ equiv. ^b	TON ^c	TOF _{10s} ^d /h ⁻¹
1	1a (5)	0.94	19	5.1 × 10 ³
2	1a (2)	0.62	32	8.3 × 10 ³
3	1a (1)	0.43	43	1.3 × 10 ⁴

^a) General reaction conditions: [AB]₀ = 0.30 M, KN(SiMe₃)₂ (1 eq. relative to the amount of catalyst), THF, r.t., 800 sec.

^b) H₂ equiv. = $n(\text{H}_2)_{800}/n(\text{AB})_0$ where $n(\text{X})$, means the amount of X at t seconds after the start of the reaction. ^c) TON = $n(\text{H}_2)_{800}/n(\text{catalyst})$, ^d) TOF_{10s} = $v/n(\text{catalyst})$, where $v = n(\text{H}_2)/10$ (average reaction rate at initial 10 seconds)

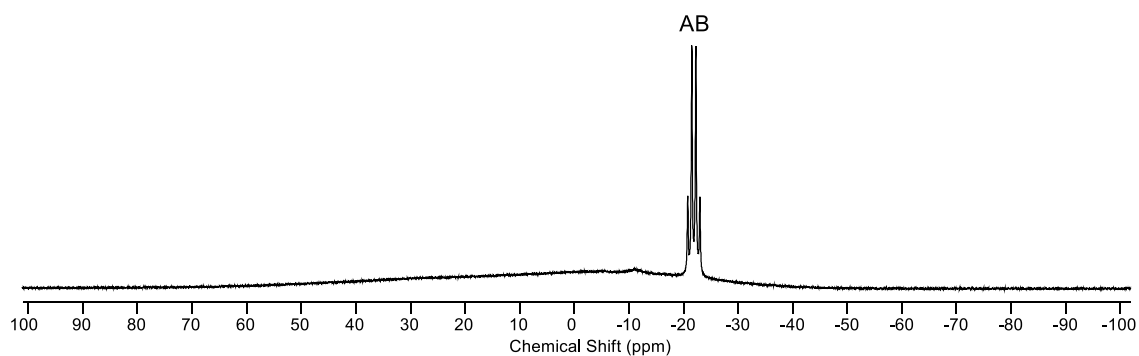


Figure 3-5. ¹¹B NMR spectrum after the catalytic reaction (2 mol% **1a**, 2 mol% KN(SiMe₃)₂, [AB]₀ = 0.30 M, THF(C₆D₆ as a lock solvent)).

3-3-2. Analysis of an Insoluble Product

The dehydrogenation reaction using **1a** as a precatalyst gave a large amount of precipitate, which was insoluble in common solvents such as hexane, toluene, diethylether, THF, acetonitrile, DMSO, and water. The IR spectrum of the insoluble precipitate showed strong absorption bands of $\nu(\text{N-H})$, $\nu(\text{B-H})$, $\delta(\text{N-H})$, $\delta(\text{B-H})$, and $\gamma(\text{N-H})$ (Figure 3-6). This spectrum is almost the same as that of poly(aminoborane) reported by other researchers.^[3] The ^{11}B MQMAS solid-state NMR spectrum of the insoluble product is shown in Figure 3-7. The most intense resonance appears at -12.3 ppm, which is comparable with the reported chemical shifts of the tetracoordinate boron atom of poly(aminoborane).^[5] A broad spreading of resonances over the range from -100 to 100 ppm was probably attributable to impurities. From these spectral data, I presume that the insoluble precipitate is poly(aminoborane).

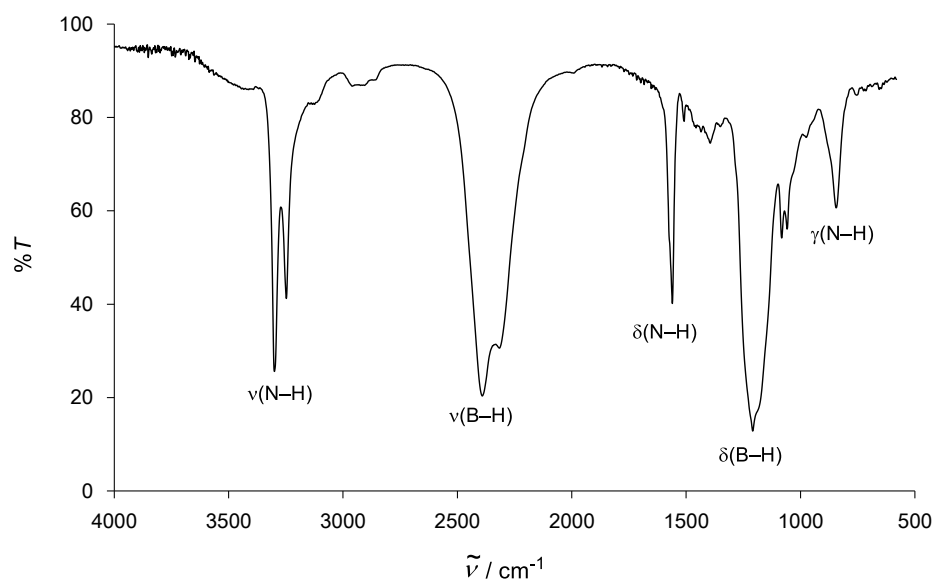


Figure 3-6. IR spectrum (KBr pellet) of the insoluble product.

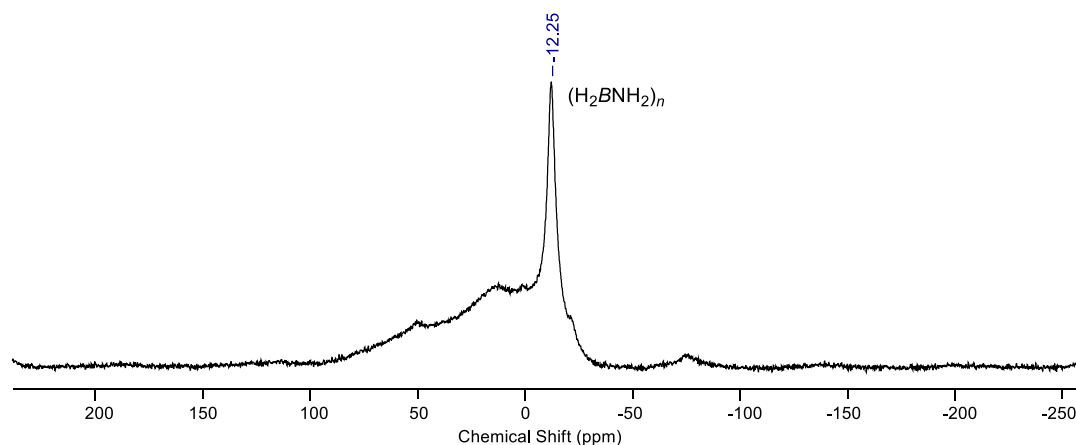


Figure 3-7. 1D $^{11}\text{B}\{^1\text{H}\}$ MQMAS NMR spectrum of the insoluble product.

3-3-3. Substituent Effect

The final equivalent of H₂ also changed depending on the substituent R on the aromatic ring of **1**. The reaction profiles are shown in Figure 3-8 and the results are summarized in Table 3-2. When 2 mol% of catalyst was used, the final equivalent of H₂ became 0.62 for **1a** (TON = 32, R = H), 0.93 for **1b** (TON = 47, R = CH₃), and 0.32 for **1c** (TON = 16, R = CF₃). TOF values also depend on the substituents: The TOF values are 8.3 × 10³ h⁻¹ for **1a**, 9.3 × 10³ h⁻¹ for **1b**, and 4.7 × 10³ h⁻¹ for **1c**. Complex **1b** exhibited the highest values in both TON and TOF among **1a–1c**. On the other hand, **1c** exhibited the lowest values among the three. These results suggest that the more electron-donating the substituent is, the more active and long-lasting the catalyst becomes, and **1b** is the most efficient catalyst among **1a–1c**.

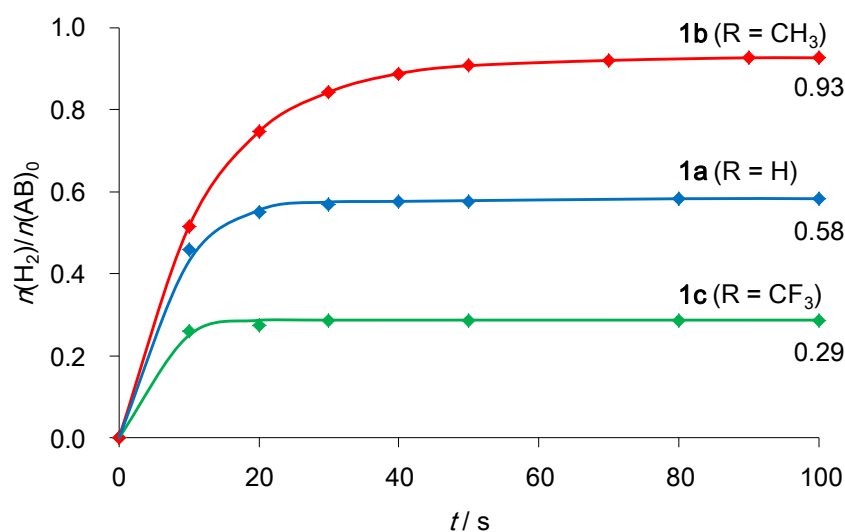
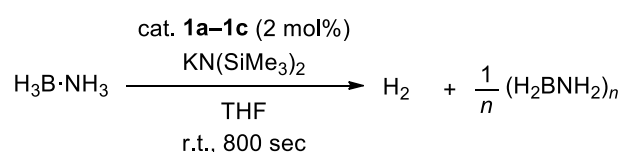


Figure 3-8. The time course profiles of catalytic dehydrogenation of AB using **1a** (blue line), **1b** (red line), and **1c** (green line).

Table 3-2. Reaction conditions^a and results of the catalytic dehydrogenation of AB using **1a–1c**



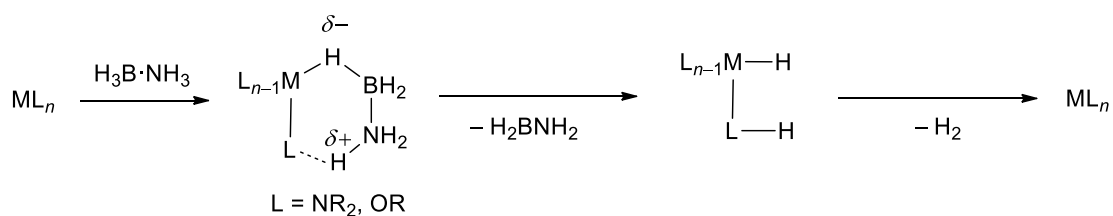
Entry	Catalyst (mol%)	H ₂ equiv. ^b	TON ^c	TOF _{10s} ^d /h ⁻¹
1	1a (2)	0.62	32	8.3 × 10 ³
2	1b (2)	0.93	47	9.3 × 10 ³
3	1c (2)	0.32	16	4.7 × 10 ³

^a) General reaction conditions: [AB]₀ = 0.30 M, KN(SiMe₃)₂ (1 eq. relative to the amount of catalyst), THF, r.t., 800 sec.

^b) H₂ equiv. = $n(\text{H}_2)_{800}/n(\text{AB})_0$ ^c) TON = $n(\text{H}_2)_{800}/n(\text{catalyst})$, ^d) TOF_{10s} = $(n(\text{H}_2)/10)/n(\text{catalyst})$

3-3-4. DFT Calculations on the Reaction Mechanisms

In order to obtain insight into the reaction mechanism, DFT calculations were performed (M06-SMD(THF)/6-311+G(d,p),SSD(Fe)//B3PW91/6-31G(d,p),SDD(Fe)). As described in Chapter 1, dehydrogenation reaction of AB generally proceeds via outer-sphere mechanisms (Scheme 3-3), which is started from coordination of a B–H of AB to the coordinatively unsaturated metal center of the catalyst ML_n .



Scheme 3-3. Schematic outer-sphere mechanisms for dehydrogenation of AB with transition metal catalysts ML_n .

On the basis of the outer-sphere mechanism, I calculated the structures and energies of intermediates and transition states. The favorable reaction pathway A is shown in Figure 3-9 and optimized and some important structures are also shown in Figure 3-10. The overall dehydrogenation reaction of AB ($AB \rightarrow H_2 + H_2BNH_2$) was calculated to be exergonic by $\Delta G^\circ = -16.4$ kJ/mol whose absolute value is only slightly smaller than previously reported results at almost same level of theory (-20.5 kJ/mol; M06/6-311+G(d,p)/SMD(THF)//M06/6-31G(d),SDD).^[6] The reaction pathway starts from interaction of the iron center of the coordinatively unsaturated complex **2a** with a H–B bond of AB to form σ -B–H complex **Aa**, which is slightly endergonic by $\Delta G^\circ = 4.0$ kJ/mol. In the structure of **Aa**, the distance of H–B bond interacting with the iron center is 1.261 \AA ($D(\text{FeH}-\text{B}) = 1.261 \text{ \AA}$), which is longer than those of other H–B bonds that have no interaction with the iron center ($D(\text{H}_{\text{terminal}}-\text{B}) = 1.208, 1.214 \text{ \AA}$) due to the formation of a 3-center 2-electron bond. At the same time, the hydrogen bonding is formed between the amido nitrogen and a H–N of AB ($D(\text{FeN}\cdots\text{HNB}) = 1.601 \text{ \AA}$, $D(\text{H}-\text{NB}) = 1.094 \text{ \AA}$). From **Aa**, intramolecular hydrogen transfer occurs to give aminoborato complex **Ba**. These two intermediates, **Aa** and **Ba**, have almost the same energy ($\Delta G^\circ = 2.6$ kJ/mol), because there is no large structural change between them except for N–H–N distances ($D(\text{FeN}-\text{H}) = 1.110 \text{ \AA}$, $D(\text{H}-\text{NB}) = 1.593 \text{ \AA}$). B–H scission accompanied by aminoborane liberation gives intermediate **Ca** with the relative free energy of $\Delta G^\circ = 7.2$ kJ/mol from the initial state (**2a** + AB). Intramolecular hydrogen transfer via **TS_{Ca-Da}** gives dihydrogen complex **Da**. In this step, the highest activation barrier has been calculated ($\Delta G^\ddagger = 58.6$ kJ/mol). However, since this value is significantly lower than the energy barrier for which the reaction occurs smoothly at room temperature ($\Delta G^\ddagger \leq 84$ kJ/mol = 20 kcal/mol), this is consistent with the experimental fact that the rapid H_2 evolution is observed. H_2 dissociates from intermediate **Da** to regenerate **2a** via **TS_{Da-2a}** with the activation barrier of $\Delta G^\ddagger = 17.4$ kJ/mol. In this catalytic cycle, no transition states could be located for each step from **2a** to **Ca**. These steps are considered to have slight activation barriers or, if any, they must be much lower than 58.6 kJ/mol because structural changes are not so large.^[5] Therefore, the rate-determining step of the cycle is considered to be H–H bond formation step (**Ca**→**Da**) in this pathway.

An alternative pathway B was also considered. Schneider et al. proposed another dehydrogenation pathway that starts from activation of N–H in the system using (PNP)Fe(CO)H (PNP = N(CH₂CH₂PⁱPr₂)₂) as a catalyst.^[5] Along this mechanism, the calculation for the reaction of **2a** and AB was performed (Figure 3-11). A large activation barrier ($\Delta G^\ddagger = 99.1$ kJ/mol) was found in the N–H bond activation process and the barrier was far larger than the highest barrier found in the pathway A ($\Delta G^\ddagger = 58.6$ kJ/mol). Therefore, the pathway B is unfavorable for this catalytic system.

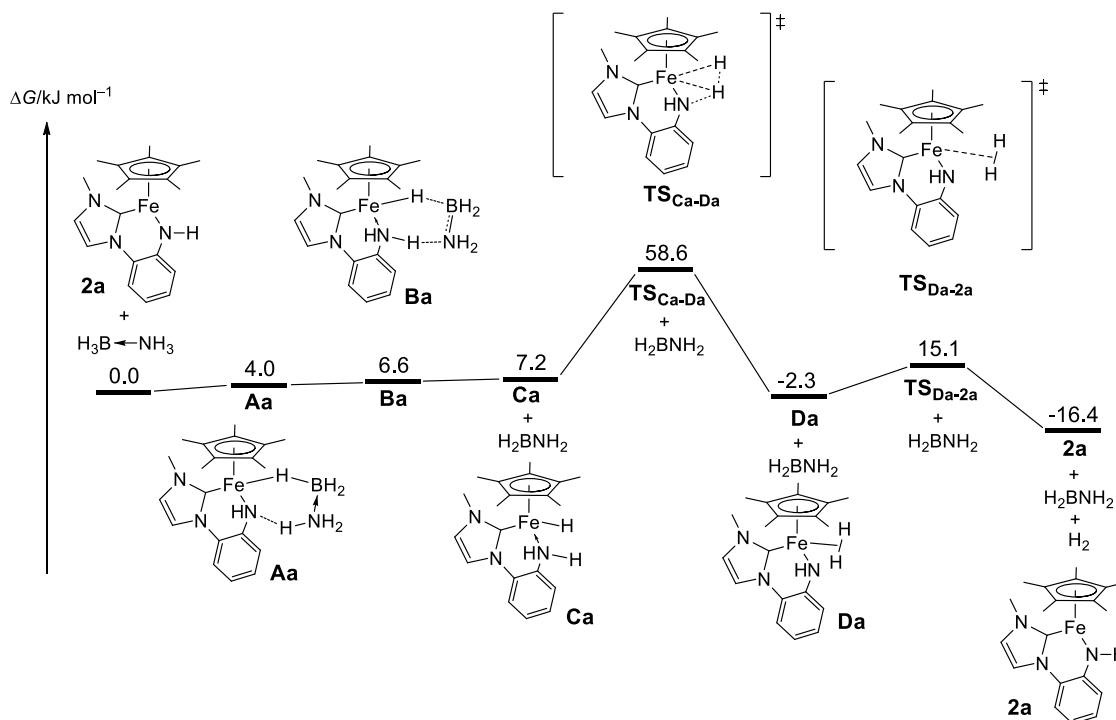


Figure 3-9. A proposed catalytic mechanism for dehydrogenation of AB using **2a** as a catalyst (pathway A).

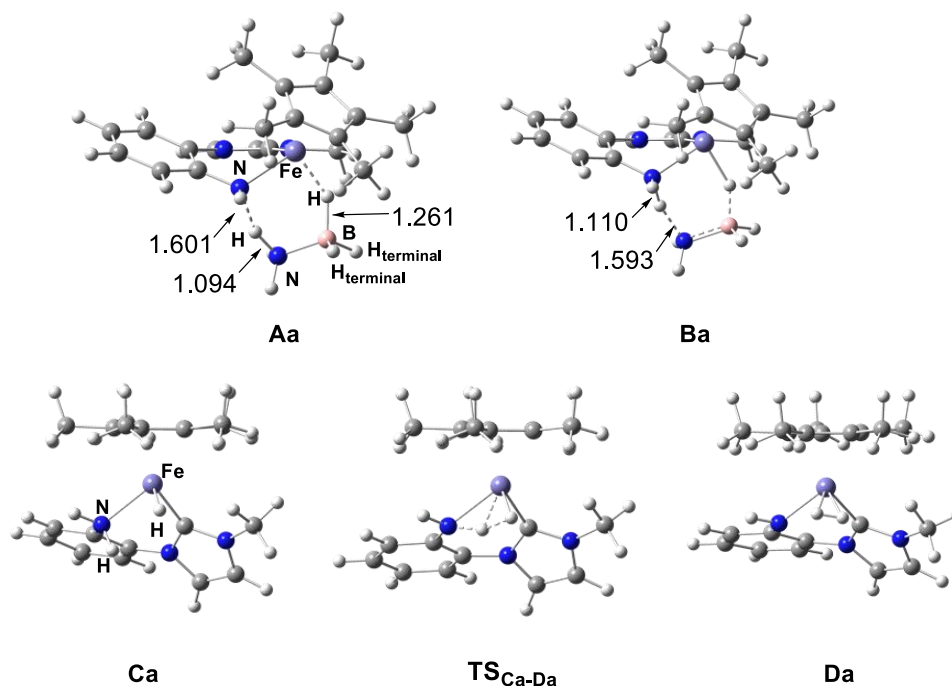


Figure 3-10. Selected optimized structures from DFT calculations.

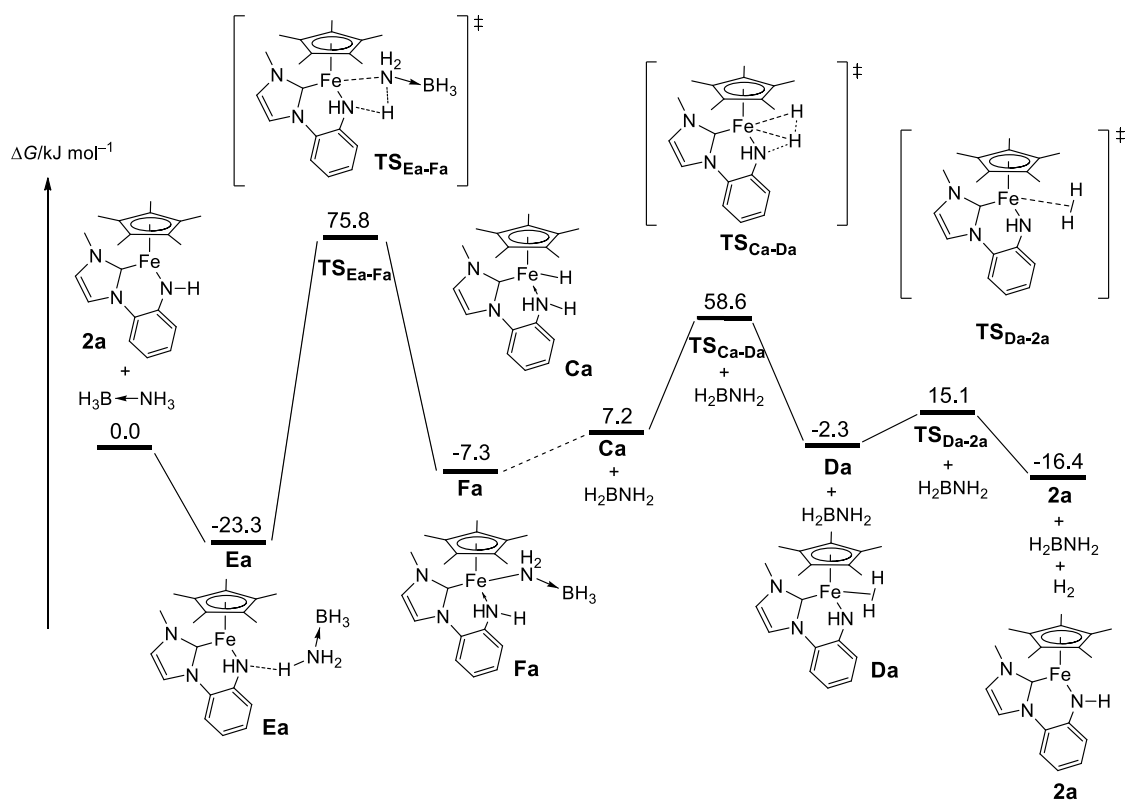


Figure 3-11. Alternative unfavorable pathway for the dehydrogenation of AB using **2a** that starts from activation of N-H (pathway B).

The effects of the substituent R on the phenyl ring were considered based on the calculations in accordance with the favorable pathway A. The results are shown in Figure 3-12. Since the rate-determining step has been found to be H–H bond formation, the pathway from **C** to **2** is discussed hereafter. The relative energies of **TS_{C-D}** vs. the initial state are 58.6 kJ/mol for R = H, 58.0 kJ/mol for R = CH₃, and 59.4 kJ/mol for R = CF₃. The differences in these energies are very small and $\Delta\Delta G^\ddagger = -0.6$ and 0.8 kJ/mol for R = CH₃ and CF₃, respectively, relative to that of R = H. The relative reaction rates (k_R/k_H) are calculated to be 1.3 for R = CH₃ and 0.7 for R = CF₃ based on Eyring equation (eq 3-2).

$$k = \frac{k_B T}{h} \exp\left(-\frac{\Delta G^\ddagger}{RT}\right) \quad (3-2)$$

These relative reaction rates are consistent with the ratio of experimentally obtained TOF values (1.1 for R = CH₃, and 0.6 for R = CF₃ relative to R = H, see Table 3-2). The reason why the energy difference in **TS_{CD}** is small is probably because the substituents R have two opposite effects on intermediates **C** and **D** (Figure 3-13). For intermediate **C**, the more electron-donating the substituent is, the lower the relative Gibbs free energy becomes. This is because electron donation of EDG through the phenyl ring increases the nucleophilicity of the amino nitrogen and, as a consequence, the Fe–N bond becomes strong. On the other hand, for intermediate **D**, the more electron-withdrawing the substituent is, the lower the relative Gibbs free energy becomes. This is because EWG decreases the negative charge on the aromatic ring that is caused by delocalization of a lone pair of the amido nitrogen. In the transition state **TS_{C-D}**, the two substituent effects cancel each other because **TS_{C-D}** has properties of both **C** and **D**. Therefore, the energy differences in **TS_{C-D}** became small. The difference of the TON value among these three systems is attributable to the relative stability of intermediates **C**. As described above, the order of the strength of the Fe–N bond can be considered as R = CF₃ < H < CH₃. If a possible deactivation process starts from dissociation of the amino ligand from the iron center of **C**, the relative stability would increase in the order of R = CF₃ < H < CH₃. As a result, the TON increases in the order of **1c** < **1a** < **1b**.

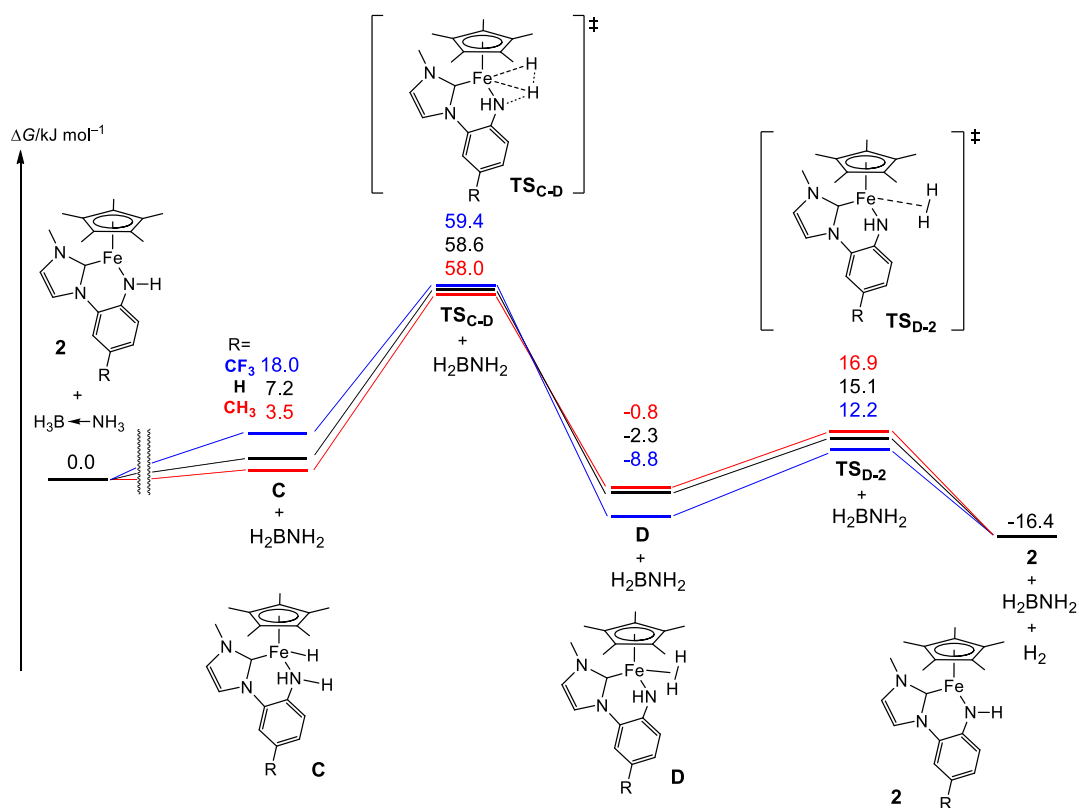


Figure 3-12. Results of DFT calculation for the proposed mechanism of dehydrogenation of AB catalyzed by **2a** (black line), **2b** (red line), and **2c** (blue line).

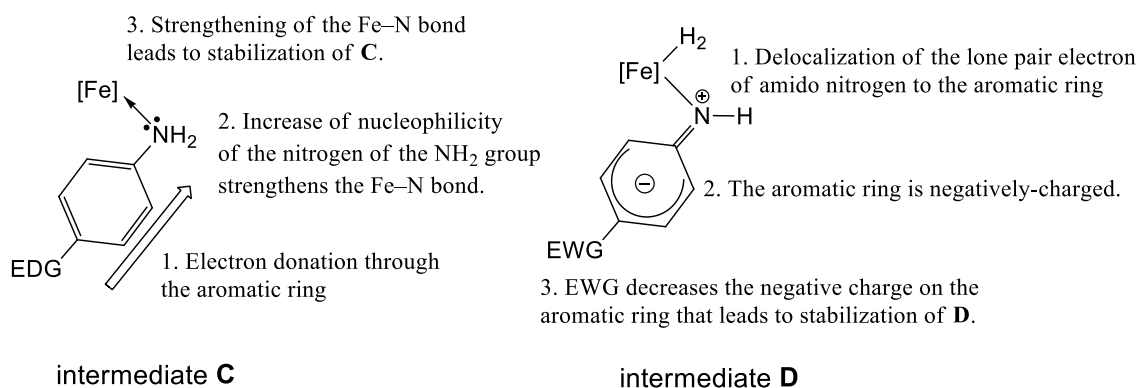


Figure 3-13. Schematic diagram of stabilization of intermediates **C** and **D** by the substituents.

The effect of the metal center was also estimated by comparing the Fe complex **2a_{Fe}** with the Ru complex having the same ligands **2a_{Ru}**. Geometry optimizations were performed based on the coordinates obtained for the Fe system. The results are shown in Scheme 3-14. The highest energy barrier can be found in the same step, i.e. the transition state for H–H bond formation. For the Ru system, the energy barrier is calculated to be $\Delta G^\ddagger(\text{Ru}, \text{TS}_{\text{Ca-Da}}) = 77.0$ kJ/mol, which is 18.4 kJ/mol higher than that of the Fe system. This difference means that the reaction rate at room temperature estimated for the Ru system is ca. 1700 times slower than that estimated for the Fe system based on Eyring equation (eq 3-2). The origin of this large kinetic barrier for the Ru system can be found in the structures of intermediate **Ca_M** and transition state **TS_{Ca-Da}**. Selected bond lengths in **Ca_M** and **TS_{Ca-Da}** were listed in Table 3-3. The M–N bond lengths ($D(\text{Fe-N}) = 2.062$, $D(\text{Ru-N}) = 2.195$ Å) and M–H bond lengths ($D(\text{Fe-H}) = 1.542$ and $D(\text{Ru-H}) = 1.634$ Å) have a relatively large differences attributable to the differences in their atomic radii. As a consequence, the length between a proton on the NH₂ and the hydrido ligand in **Ca_{Ru}** is longer than that in **Ca_{Fe}** ($D(\text{NH}\cdots\text{HM}) = 2.229$ (Fe), 2.365 (Ru) Å). This lengthening of the H \cdots H distance in **Ca_{Ru}** causes the requirement of larger deformation to reach **TS_{Ca-Da}** for the Ru system in comparison with that for the Fe system. Particularly, the N–H lengths are almost the same in both structures of **Ca_{Fe}** and **Ca_{Ru}** ($D(\text{N-H}) = 1.017$ (Fe), 1.017 (Ru) Å), but in **TS_{Ca-Da}**, the N–H length of the Ru system is longer than that of the Fe system ($D(\text{N-H}) = 1.302$ (Fe), 1.370 (Ru)). This means that, in the case of the Ru system, it is necessary to move the hydrogen farther away from the nitrogen compared with the Fe system, which indicates that the extra energy is required for this transformation.

From these results of calculation, it is assumed that the longer the H \cdots H distance is, the larger the activation energy becomes. Some calculations reported by other researchers supported this assumption. Thus, Fagnou et al. have calculated the activation barrier for the proton transfer process from intermediate **G** to **H** via **TS_{G-H}** (Figure 3-15).^[2] The H \cdots H distance in **G** is 2.591 Å and the activation barrier for proton transfer is $\Delta G^\ddagger(\text{TS}_{\text{G-H}}) = 91.6$ kJ/mol. Casey et al. have also calculated the barrier for the proton transfer process from **J** to **K** via **TS_{J-K}** (Figure 3-16).^[7] The H \cdots H distance in **J** is 3.287 Å and the activation barrier is $\Delta G^\ddagger(\text{TS}_{\text{J-K}}) = 180.7$ kJ/mol. Clearly, the longer H \cdots H distance results in the higher ΔG^\ddagger value. Since the H \cdots H distances in intermediates **Ca_{Fe}** and **Ca_{Ru}** are 2.229 and 2.365 Å, respectively, and the activation barriers for the proton transfer in **Ca_{Fe}** \rightarrow **Da_{Fe}** and **Ca_{Ru}** \rightarrow **Da_{Ru}** are 58.6 and 77.0 kJ/mol, respectively, the above relationship can be applied to the relationship between the Fe and the Ru systems.

Consequently, the advantage of using iron as the metal center originates from the shortening of the distance between the proton and the hydride and, which results in lowering of the activation energy of H–H bond formation.

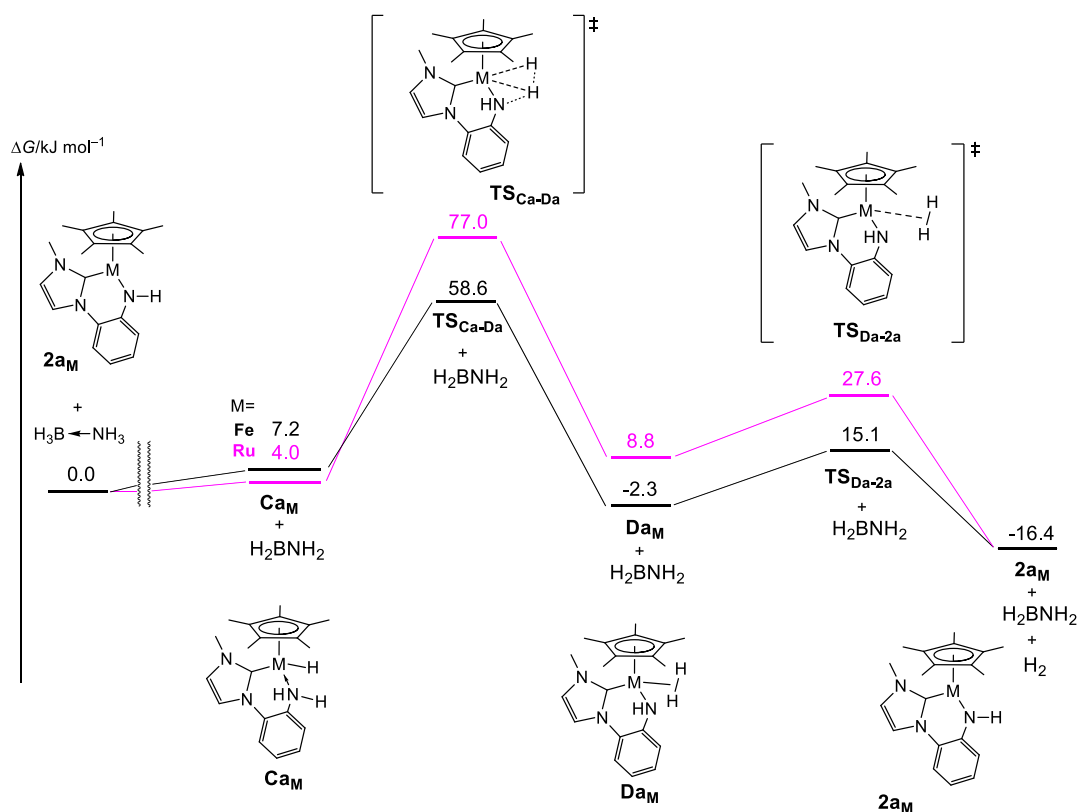


Figure 3-14. Results of DFT calculation for the proposed mechanism of dehydrogenation of AB catalyzed by iron complex $2a_{Fe}$ (black line) and ruthenium complex $2a_{Ru}$ (purple line).

Table 3-3. Selected bond lengths (Å) in Ca_M and TS_{Ca-Da}

Structure	M	M-N	M-H	N-H	NH...HM
Ca_M	Fe	2.062	1.542	1.017	2.229
	Ru	2.195	1.634	1.017	2.365
TS_{Ca-Da}	Fe	2.044	1.600	1.302	1.084
	Ru	2.194	1.709	1.370	1.074

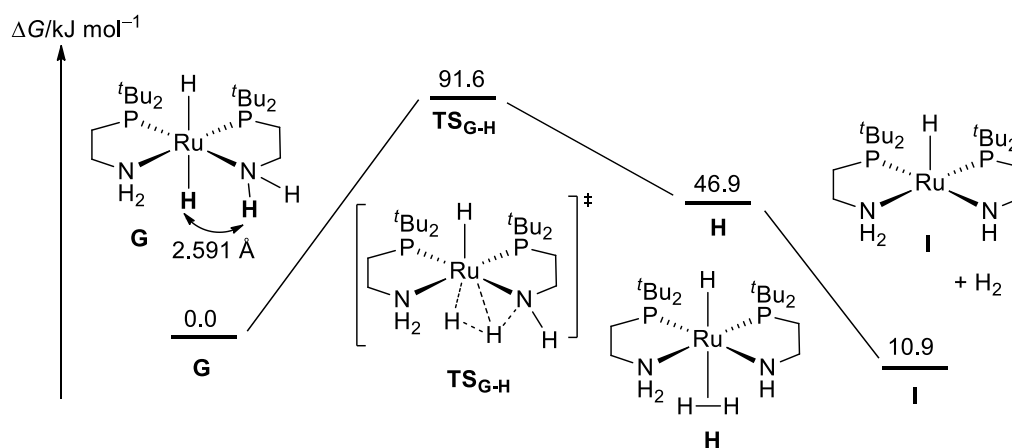


Figure 3-15. Dihydrogen elimination pathway calculated on the Ru complex **G**.

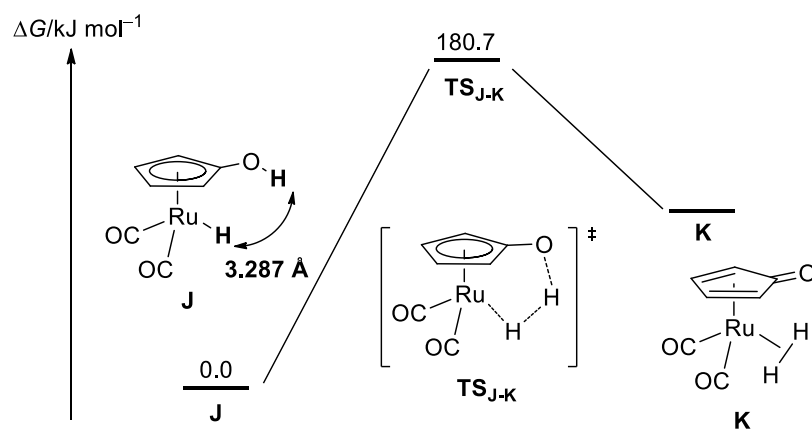
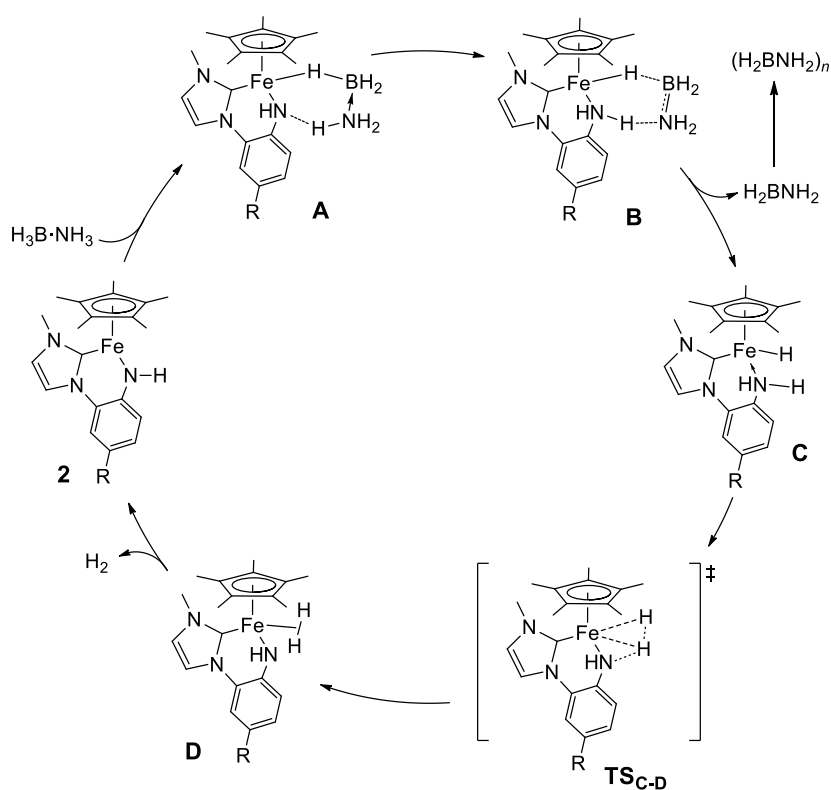


Figure 3-16. Dihydrogen elimination pathway calculated on $(\eta^5\text{-C}_5\text{H}_4\text{OH})\text{Ru}(\text{CO})_2\text{H}$ (**J**).

3-4. Conclusion

In this chapter, I described the catalytic dehydrogenation of AB using **2**, which was prepared by the reaction of **1** with $\text{KN}(\text{SiMe}_3)_2$. Addition of AB to the THF solution containing 5 mol% of **2a** resulted in rapid evolution of H_2 with concomitant formation of large amount of precipitate. The reaction almost completed within a few minutes to give 0.94 eq. of H_2 . The TOF value of this reaction was greater than $5.1 \times 10^3 \text{ h}^{-1}$ (5 mol% **1a**) and this value is the highest in the reported homogeneous iron catalyst so far. When the amount of catalyst loading was reduced, the final equivalent of H_2 decreased and unreacted AB remained. The TOF and TON values also changed depending on the substituent R on the phenyl ring of the ligands and **1b** ($\text{R} = \text{CH}_3$) was the most active and long-lasting catalyst among **1a–1c**.

I proposed a possible reaction mechanism based on DFT calculations (Scheme 3-4). The mechanism involves stepwise B–H and N–H scission and H–H bond formation, in which the last step is the rate-determining step, with the low activation barrier of $\Delta G^\ddagger = 58.6 \text{ kJ/mol}$. The substituent R on the aromatic ring of the ligand has only small effect on the energy of $\text{TS}_{\text{C-D}}$, because the substituent effects on intermediates **C** and **D** cancel each other. The energy of transition state $\text{TS}_{\text{C-D}}$ of the Fe system is lower than that of the Ru system, because two hydrogen atoms on M and N are closer to each other in the case of Fe system due to the shorter Fe–N bond compared with the Ru–N bond, which is caused by the smaller atomic radius of Fe compared with that of Ru. Therefore, deformation from **C** to $\text{TS}_{\text{C-D}}$ for the Fe system becomes smaller than that for the Ru system and, as a consequence, the energy of $\text{TS}_{\text{C-D}}$ for the Fe system becomes lower.



Scheme 3-4. A proposed catalytic cycle.

3-5. References

- [1] M. C. Denny, V. Pons, T. J. Hebden, D. M. Heineley, K. I. Goldberg, *J. Am. Chem. Soc.* **2006**, *128*, 12048.
- [2] N. Blaquiere, S. Diallo-Garcia, S. I. Gorelsky, D. A. Black, K. Fagnou, *J. Am. Chem. Soc.* **2008**, *130*, 14034.
- [3] M. Käß, A. Friedrich, M. Drees, S. Schneider, *Angew. Chem. Int. Ed.* **2009**, *48*, 905.
- [4] Gaussian 09, Revision E.01, M. J. Frisch, G. W. Trucks, H. B. Schlegel, G. E. Scuseria, M. A. Robb, J. R. Cheeseman, G. Scalmani, V. Barone, G. A. Petersson, H. Nakatsuji, X. Li, M. Caricato, A. Marenich, J. Bloino, B. G. Janesko, R. Gomperts, B. Mennucci, H. P. Hratchian, J. V. Ortiz, A. F. Izmaylov, J. L. Sonnenberg, D. Williams-Young, F. Ding, F. Lipparini, F. Egidi, J. Goings, B. Peng, A. Petrone, T. Henderson, D. Ranasinghe, V. G. Zakrzewski, J. Gao, N. Rega, G. Zheng, W. Liang, M. Hada, M. Ehara, K. Toyota, R. Fukuda, J. Hasegawa, M. Ishida, T. Nakajima, Y. Honda, O. Kitao, H. Nakai, T. Vreven, K. Throssell, J. A. Montgomery, Jr., J. E. Peralta, F. Ogliaro, M. Bearpark, J. J. Heyd, E. Brothers, K. N. Kudin, V. N. Staroverov, T. Keith, R. Kobayashi, J. Normand, K. Raghavachari, A. Rendell, J. C. Burant, S. S. Iyengar, J. Tomasi, M. Cossi, J. M. Millam, M. Klene, C. Adamo, R. Cammi, J. W. Ochterski, R. L. Martin, K. Morokuma, O. Farkas, J. B. Foresman, and D. J. Fox, Gaussian, Inc., Wallingford CT, **2016**.
- [5] A. Glüer, M. Förster, V. R. Celinski, J. S. auf der Günne, M. C. 30 Holthausen, S. Schneider, *ACS Catal.* **2015**, *5*, 7214.
- [6] Y. Zhang, Y. Zhang, Z.-H. Qi, Y. G., W. Liu, Y. Wang, *Int. J. Hydrogen Energ.* **2016**, *41*, 17208.
- [7] C. P. Casey, J. B. Johnson, S. W. Singer, Q. Cui, *J. Am. Chem. Soc.* **2005**, *127*, 3100.

Chapter 4

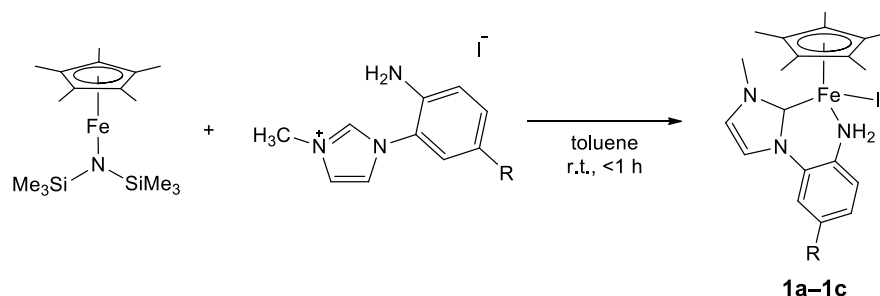
Conclusion

This thesis described the synthesis of bifunctional iron complexes having 2-aminophenyl-substituted *N*-heterocyclic carbene ligands and their application to catalytic dehydrogenation of ammonia-borane (AB).

4-1. Synthesis of Bifunctional Iron Complexes Having 2-Aminophenyl-Substituted NHC Ligands

In Chapter 2, the synthesis and structures of iron complexes having 2-aminophenyl-substituted NHC ligands **1a–1c**, generation of active species **2** from **1** by treatment with $\text{KN}(\text{SiMe}_3)_2$, and trapping of **2** with CO and 9-BBN were described.

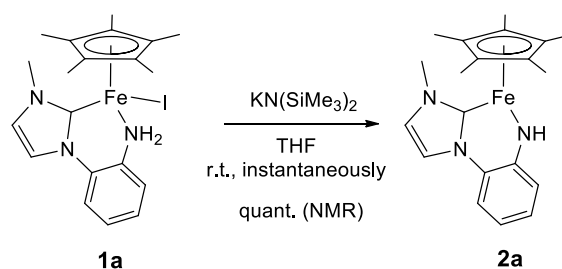
Complex **1a–1c** was synthesized by the reaction of $\text{Cp}^*\text{FeN}(\text{SiMe}_3)_2$ with the corresponding 1-(2-aminophenyl)imidazolium iodides (Scheme 4-1).



Scheme 4-1. Synthesis of **1a–1c**.

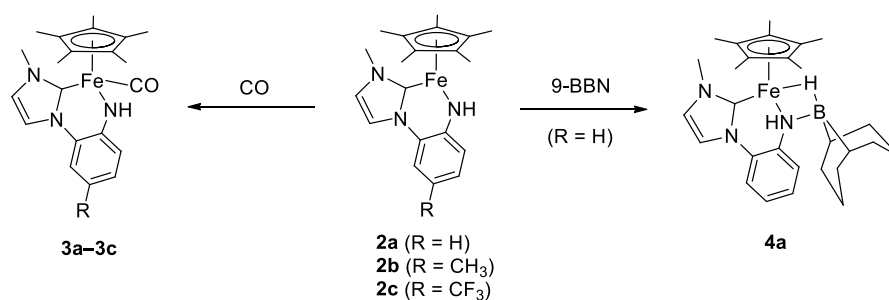
Complexes **1a–1c** adopted three-legged piano stool geometries where each of the iron centers was coordinated by a Cp^* ligand, a carbene carbon, an amino nitrogen, and an iodido ligand. The variable-temperature (VT) ^1H NMR experiments on **1a** revealed that it had a dynamic behavior of NH_2 group, which was responsible for the broadening of the signal of NH_2 protons in its ^1H NMR spectrum recorded at room temperature.

Reaction of **1a** with $\text{KN}(\text{SiMe}_3)_2$ gave coordinatively unsaturated amido complex **2a**, which was characterized by ^1H NMR and HRMS of the reaction mixture (Scheme 4-2). In this reaction, the formation of hexamethyldisilazane and the precipitate of potassium iodide were observed along with the formation of **2a**. This result suggests that **2a** is formed via abstraction of a proton from the NH_2 group of **1a** and the iodido ligand from the iron center.



Scheme 4-2. Generation of **2a** by the reaction of **1a** with $\text{KN}(\text{SiMe}_3)_2$.

Since isolation of **2a** was unsuccessful, I tried to trap freshly prepared **2a** with CO and 9-BBN, which afforded carbonyl adduct **3a** and borane adduct **4a**, respectively, in quantitative yields (Scheme 4-3). The synthesis of **3b** and **3c** were also achieved in the same way as that of **3a**. These results clearly demonstrated that the coordinatively unsaturated complexes **2a–2c** can be easily and cleanly generated by the reactions of **1a–1c** with $\text{KN}(\text{SiMe}_3)_2$.



Scheme 4-3. Trapping of **2** with CO and 9-BBN.

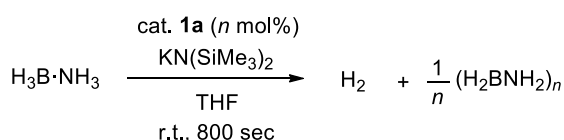
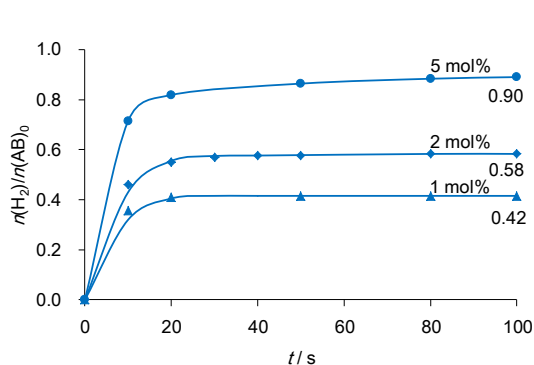
The molecular structure of **3a** was revealed by X-ray crystallography. The length of the Fe–N bond is 1.976(2) Å, which is in the range of known Fe–N(amido) lengths (1.85–2.02 Å). The sum of angles around N of **3a** is 350(4)°, which shows that the N takes a nearly planar tricoordinate geometry due to delocalization of the lone pair on the amido nitrogen over the π -system of the phenyl ring. Complex **2a** was also trapped by the reaction with 9-BBN, which afforded borane adduct **4a**. The X-ray crystal structure analysis clearly exhibited the formation of the Fe–N–B–H four-membered ring structure via coordination of the lone pair on the N to the B center of 9-BBN and the formation of a Fe–H–B 3-center 2-electron bond.

The formation of **3a–3c** and **4a** clearly shows that complexes **2a–2c** have a vacant site on the iron center and a lone pair on the amido nitrogen. In other words, complexes **2a–2c** have a bifunctional reaction site in their structures.

4-2. Dehydrogenation of Ammonia-Borane Catalyzed by Bifunctional Iron Complexes Having 2-Aminophenyl-Substituted NHC Ligands

In Chapter 3, catalytic dehydrogenation of AB by bifunctional iron complexes **2** and theoretical analysis of the reaction mechanisms were described.

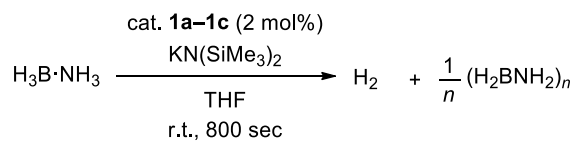
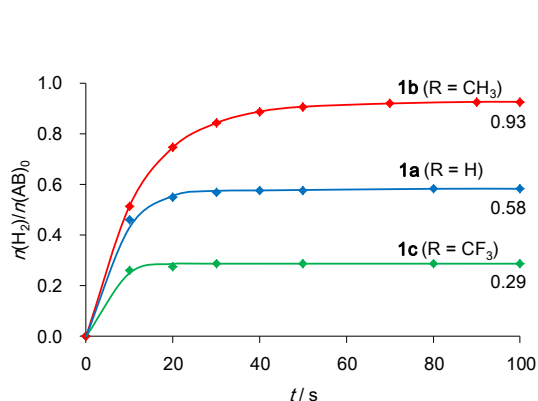
Addition of AB to a THF solution of freshly prepared **2a** caused immediate and rapid evolution of H₂ with concomitant formation of a large amount of precipitate. The bubbling of H₂ ceased within a few minutes, and AB was consumed almost completely, which was confirmed by the ¹¹B NMR spectrum of the reaction mixture. When 5 mol% of **1a** was used, 0.90 eq. of H₂ was emitted in 100 sec and it reached 0.94 eq. in 800 sec (Chart 4-1). The initial turnover frequency (TOF), which was estimated from the time course of the first 10 seconds, was 5.1 × 10³ h⁻¹. This result is remarkable since the highest known TOF for the dehydrogenation of AB catalyzed by homogeneous iron catalysts is 30 h⁻¹, which have been reported by Schneider et al. Unfortunately, the catalyst was rapidly deactivated and further addition of AB to the system did not cause H₂ evolution. The final equivalent of H₂ was greatly changed depending on the amount of catalyst loading. When 2 mol% and 1 mol% of **1a** were used, 0.62 and 0.44 eq. of H₂ were liberated in 800 sec, respectively. The precipitate formed by the catalytic reaction was analyzed by IR spectroscopy and ¹¹B MQMAS NMR spectroscopy, which revealed that the precipitate was poly(aminoborane).



Entry	Catalyst (mol%)	H ₂ eq.	TON	TOF _{10s} /h ⁻¹
1	1a (5)	0.94	19	5.1 × 10 ³
2	1a (2)	0.62	32	8.3 × 10 ³
3	1a (1)	0.43	43	1.3 × 10 ⁴

Chart 4-1. The time course profiles of catalytic dehydrogenation of AB using **1a** (left) and results of the reaction depending on the catalyst loading (right).

The final equivalent of H₂, TON, and TOF values also changed depending on the substituent R on the aromatic ring of precatalysts **1** (Chart 4-2). When 2 mol% of catalyst was used, the final equivalent of H₂ became 0.62 for **1a** (TON = 32, R = H), 0.93 for **1b** (TON = 47, R = CH₃), and 0.32 for **1c** (TON = 16, R = CF₃). The TOF values were 8.3 × 10³ h⁻¹ for **1a**, 9.3 × 10³ h⁻¹ for **1b**, and 4.7 × 10³ h⁻¹ for **1c**. Complex **1b** exhibited the highest values in both TON and TOF among **1a–1c**. On the other hand, **1c** exhibited the lowest values among the three. These results suggest that the more electron-donating the substituent is, the more active and long-lasting the catalyst becomes, and **1b** is the most efficient catalyst among **1a–1c**.



Entry	Catalyst	H ₂ eq.	TON	TOF _{10s} /h ⁻¹
1	1a	0.62	32	8.3 × 10 ³
2	1b	0.93	47	9.3 × 10 ³
3	1c	0.32	16	4.7 × 10 ⁴

Chart 4-2. The time course profiles of catalytic dehydrogenation of AB using **1a** (blue line), **1b** (red line), and **1c** (green line) (left) and results of the reaction depending on the catalyst (right).

4-3. DFT Calculations on the Reaction Mechanism

In order to obtain insight into the reaction mechanism, DFT calculations were performed (M06-SMD(THF)/6-311+G(d,p),SSD(Fe)//B3PW91/6-31G(d,p),SSD(Fe)). The overall dehydrogenation reaction of AB ($AB \rightarrow H_2 + H_2BNH_2$) was calculated to be exergonic by $\Delta G^\circ = -16.4$ kJ/mol. The catalytic reaction mechanism (Figure 4-1) involves σ -B-H complex **Aa**, aminoborato complex **Ba**, amino(hydrido) complex **Ca**, and dihydrogen complex **Da** as intermediates. Transition states were located for each step from **Ca** to **2a**. The largest activation barrier was calculated at **TS_{Ca-Da}** ($\Delta G^\ddagger = 58.6$ kJ/mol). Since this value is significantly lower than the energy barrier for which the reaction occurs smoothly at room temperature ($\Delta G^\ddagger \leq 84$ kJ/mol = 20 kcal/mol), this is consistent with the experimental fact that the rapid H_2 evolution is observed. Although no transition states could be located for each step from **2a** to **Ca**, these steps are considered to have slight activation barriers or, if any, they must be much lower than 58.6 kJ/mol because structural changes are not so large. Therefore, the rate-determining step of the catalytic cycle is considered to be H-H bond formation step (**Ca** \rightarrow **Da**) in this pathway.

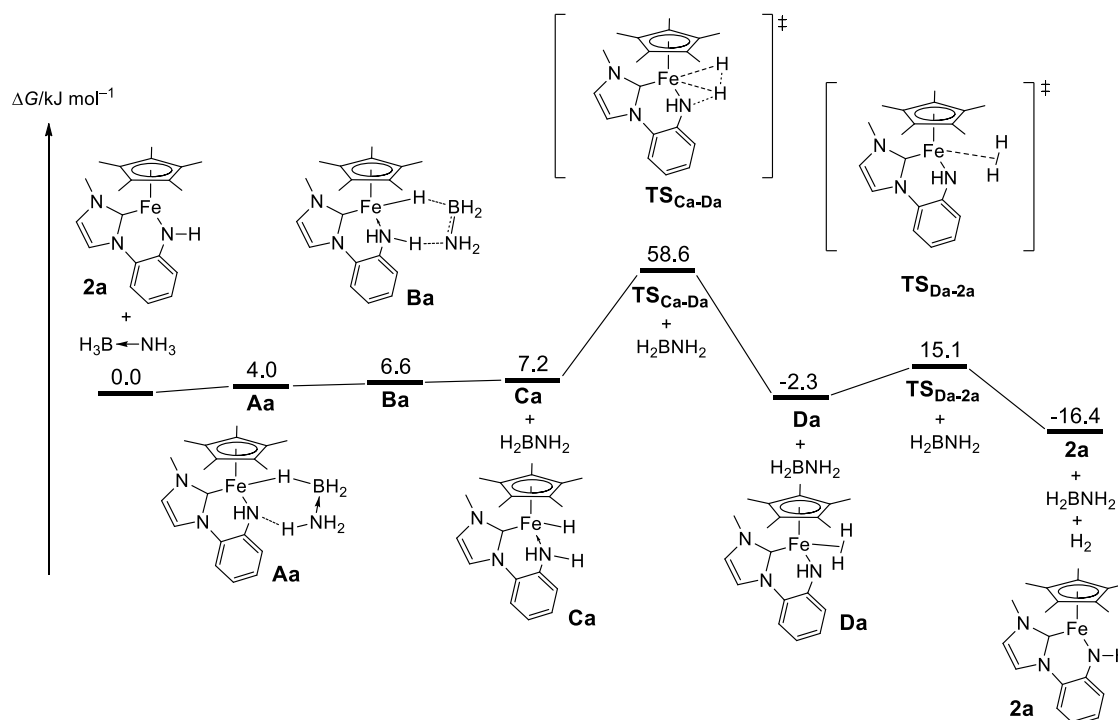


Figure 4-1. A proposed catalytic mechanism for dehydrogenation of AB using **2a** as a catalyst.

The effects of the substituent R on the phenyl ring were considered (Figure 4-2). The relative energies of the transition states $\text{TS}_{\text{C-D}}$ vs. the initial state are 58.6 kJ/mol for R = H, 58.0 kJ/mol for R = CH₃, and 59.4 kJ/mol for R = CF₃. The reason of these small differences in energies of $\text{TS}_{\text{C-D}}$ is probably that the substituent effects on intermediates **C** and **D** cancel each other. The relative reaction rates ($k_{\text{R}}/k_{\text{H}}$) are calculated to be 1.3 for R = CH₃ and 0.7 for R = CF₃ based on the Eyring equation and these values are consistent with the ratio of experimentally obtained TOF values (1.1 for R = CH₃, and 0.6 for R = CF₃ relative to the values for R = H).

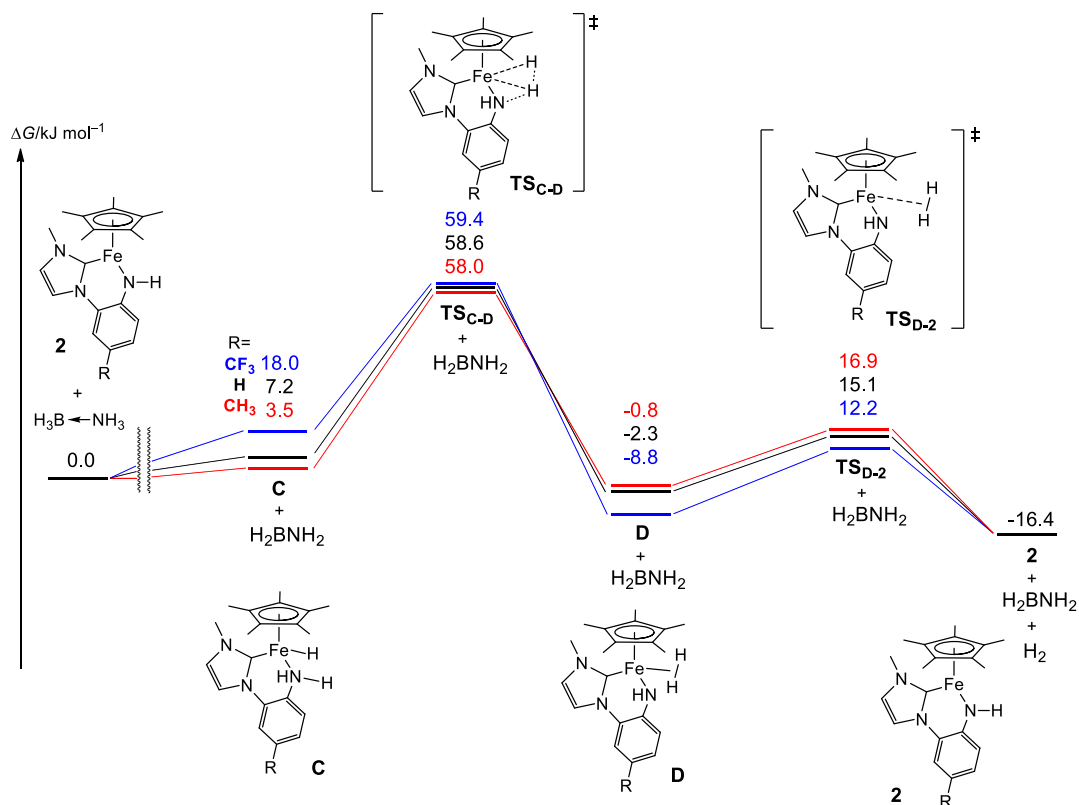


Figure 4-2. Results of DFT calculation for the proposed mechanism of dehydrogenation of AB catalyzed by **2a** (black line), **2b** (red line), and **2c** (blue line).

The effect of the metal center was also estimated by comparing the Fe complex **2a** with the hypothetical Ru complex having the same ligands **2a_{Ru}** (Figure 4-3). For the Ru system, the highest energy barrier is found in the transition state for H–H bond formation **TS_{Ca-Da}** and the energy is calculated to be $\Delta G^\ddagger(\text{Ru}, \text{TS}_{\text{Ca-Da}}) = 77.0$ kJ/mol, which is 18.4 kJ/mol higher than that of the Fe system. The origin of this large kinetic barrier for the Ru system can be found in the M–N bond lengths ($D(\text{Fe-N}) = 2.062$, $D(\text{Ru-N}) = 2.195$ Å) in **Ca_M**. It causes lengthening of the distance between a proton on the NH₂ and the hydrido ligand in **Ca_{Ru}** compared with that in **Ca_{Fe}** ($D(\text{NH}\cdots\text{HM}) = 2.229$ (Fe), 2.365 (Ru) Å). This lengthening of the H \cdots H distance in **Ca_{Ru}** induces the requirement of larger deformation to reach **TS_{Ca-Da}** for the Ru system in comparison with that for the Fe system. Namely, the extra energy is required for this transformation in the case of the Ru system. Consequently, the advantage of the use of iron as the metal center became obvious, and DFT calculation revealed that it was caused by the shortening of the distance between the proton and the hydride, which led to lowering of the activation energy of H–H bond formation.

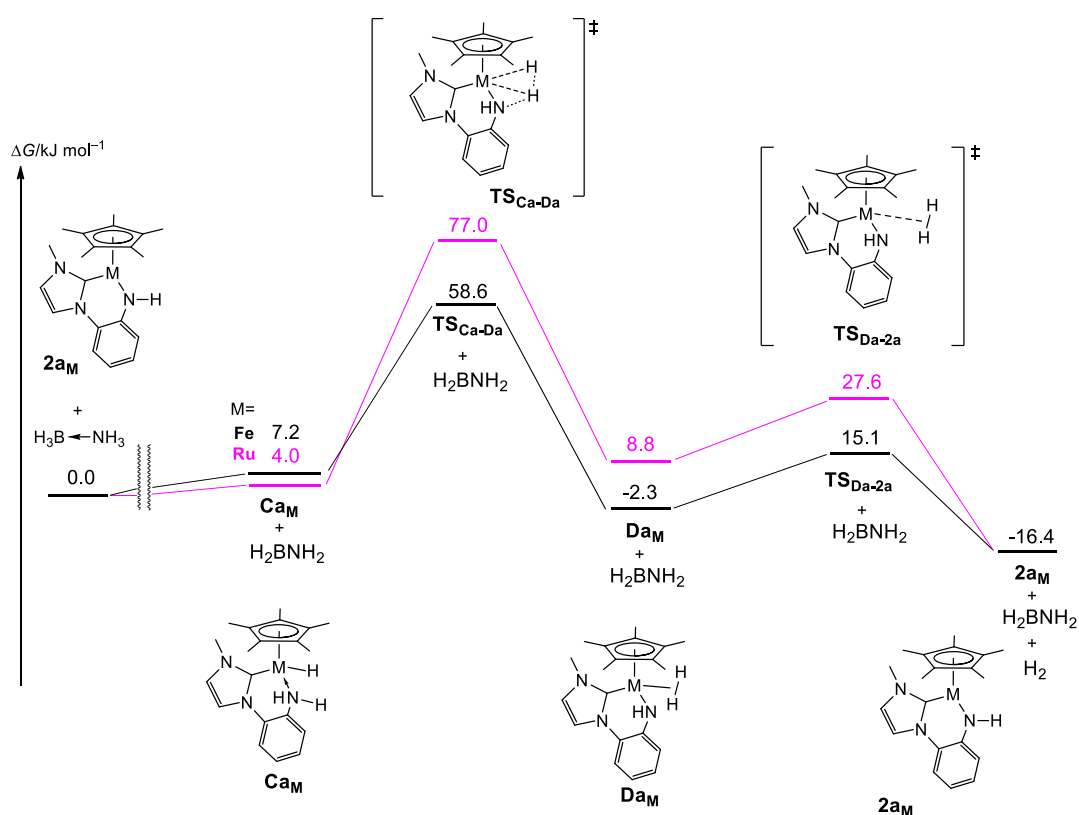


Figure 4-3. Results of DFT calculation for the proposed mechanism of dehydrogenation of AB catalyzed by iron complex **2a_{Fe}** (black line) and ruthenium complex **2a_{Ru}** (purple line).

In this research, I succeeded in the development of highly efficient iron catalysts for dehydrogenation of ammonia-borane. Moreover, I revealed that the fast dehydrogenation was attributable to (1) small structural changes during B–H and N–H bond scissions and (2) short distance between the N–H proton and the Fe–H hydride. This research will make contributions not only to organometallic and catalytic chemistry but also to the development of hydrogen storage techniques.

Supporting Information

Contents

1. NMR spectra

2. Atomic coordinates and energies for DFT optimized structures

1. NMR spectra

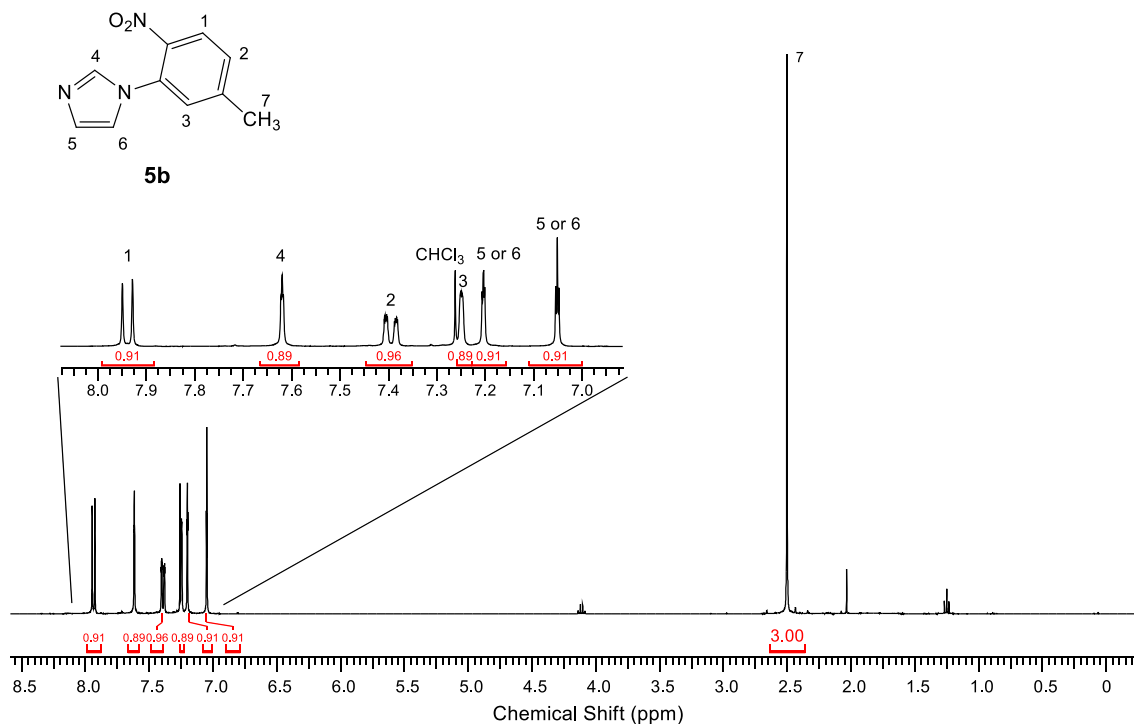


Figure S1. ¹H NMR spectrum of **5b** (400 MHz, CDCl₃).

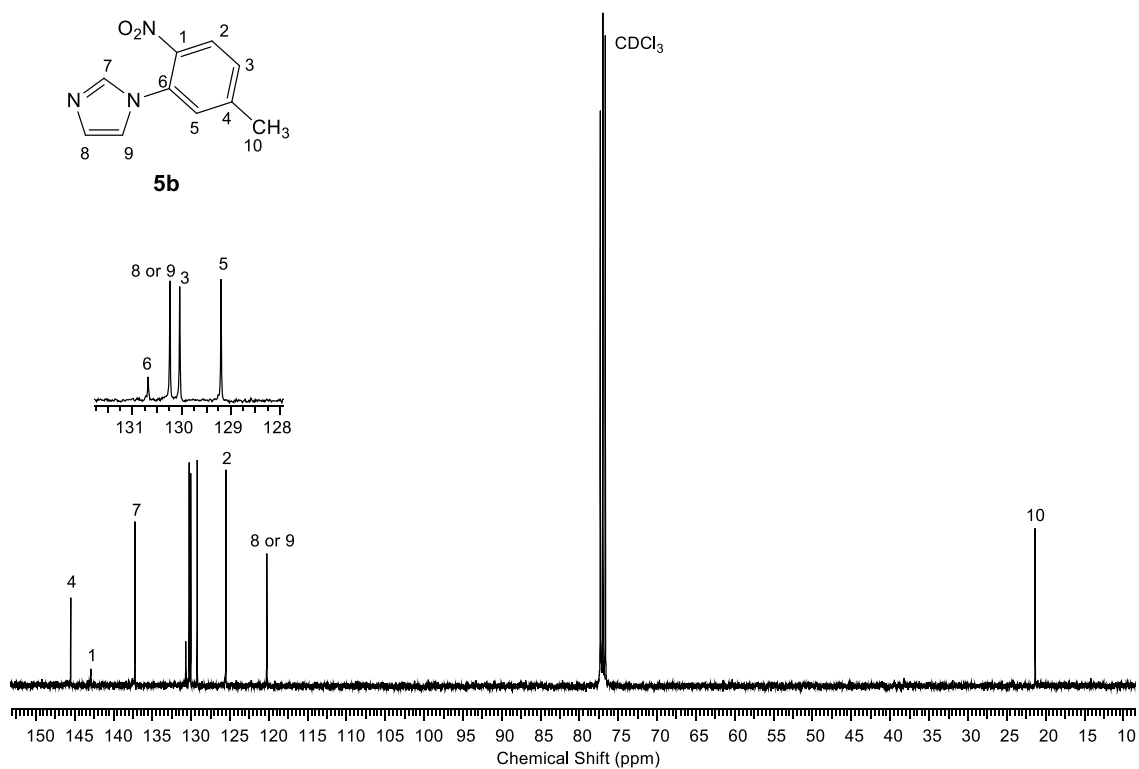


Figure S2. ¹³C{¹H} NMR spectrum of **5b** (101 MHz, CDCl₃).

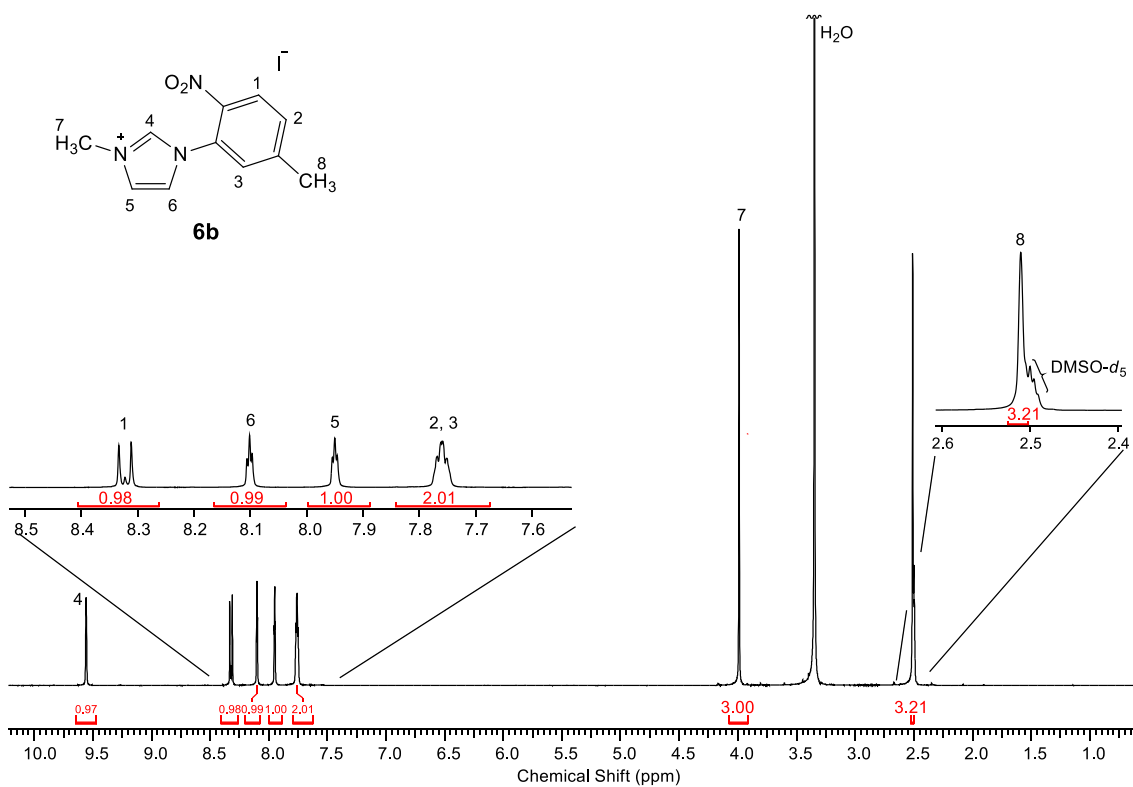


Figure S3. ^1H NMR spectrum of **6b** (400 MHz, $\text{DMSO-}d_6$).

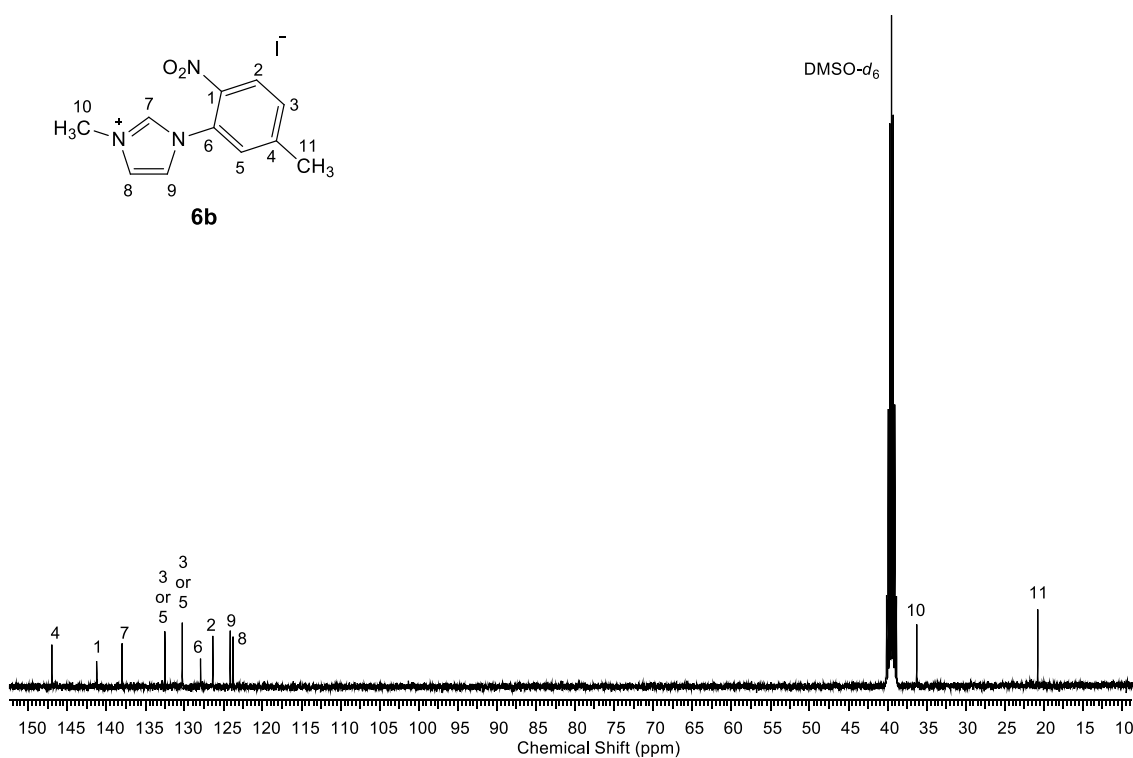


Figure S4. $^{13}\text{C}\{^1\text{H}\}$ NMR spectrum of **6b** (101 MHz, $\text{DMSO-}d_6$).

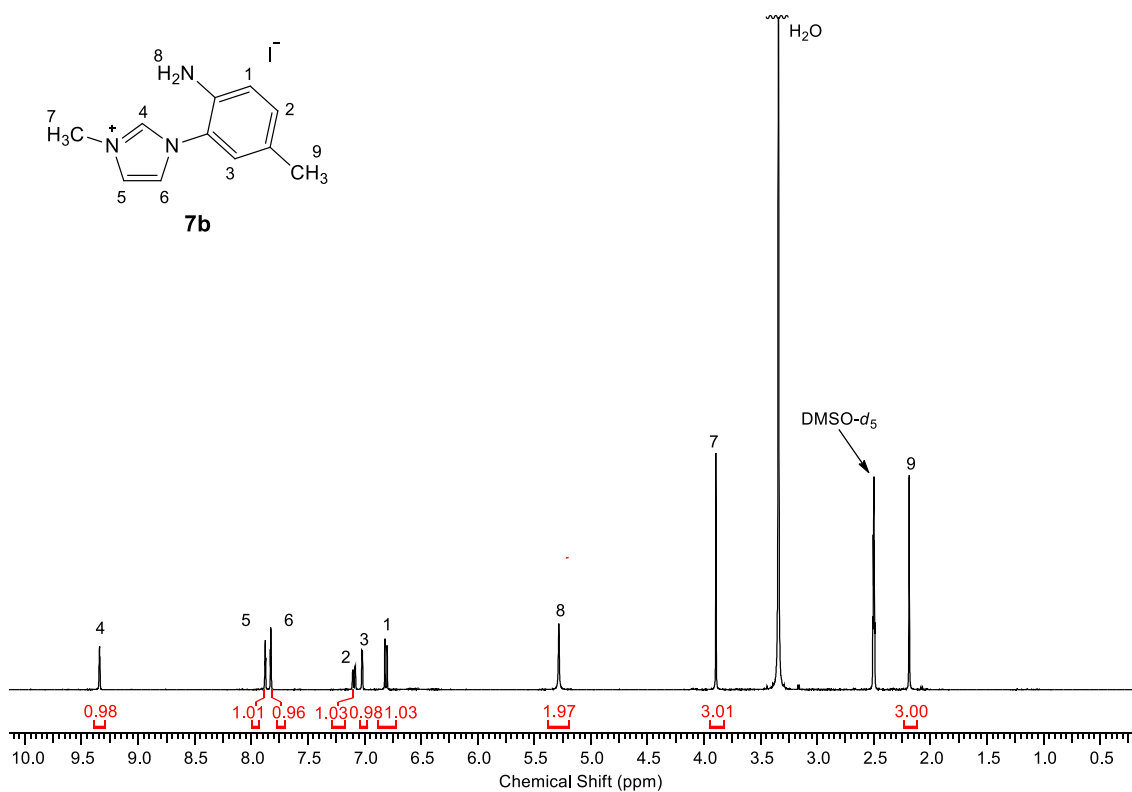


Figure S5. ^1H NMR spectrum of **7b** (400 MHz, $\text{DMSO-}d_6$).

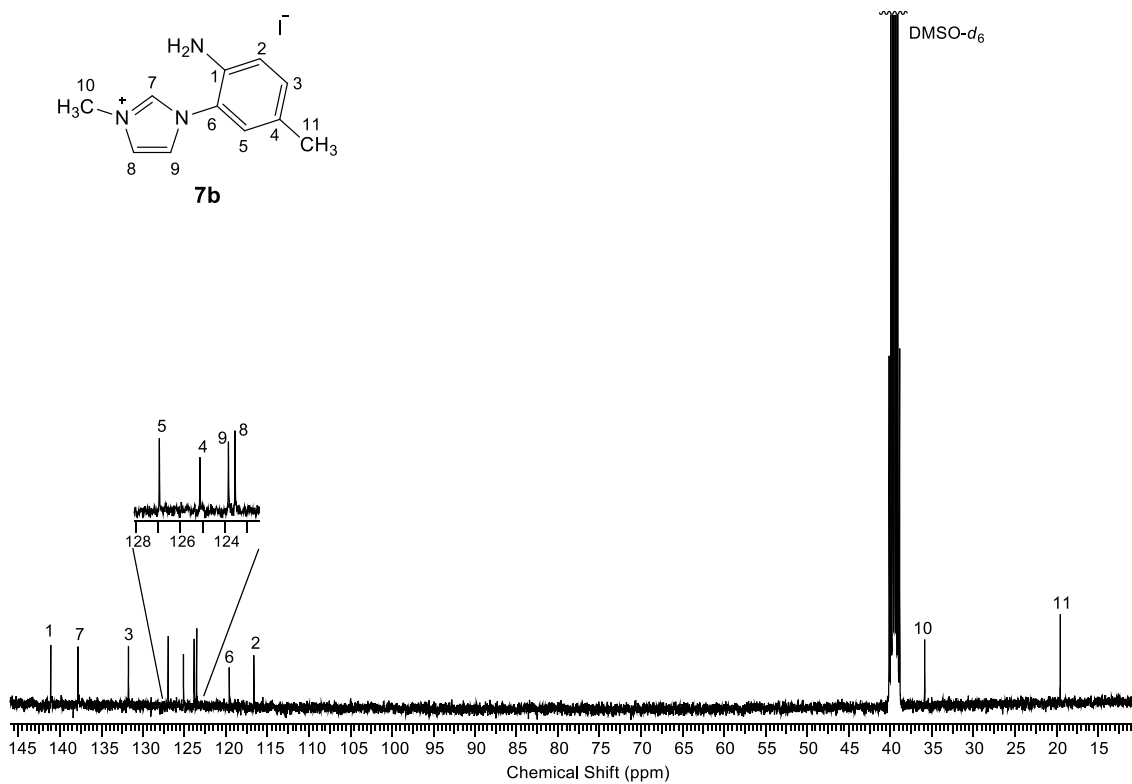
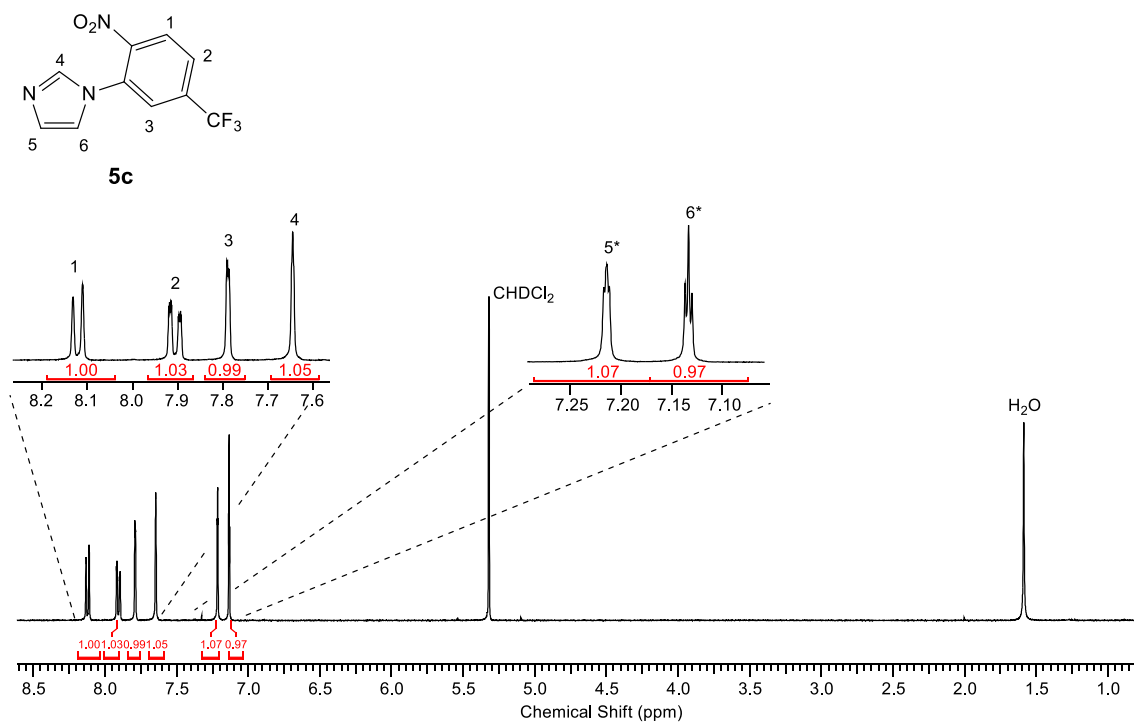
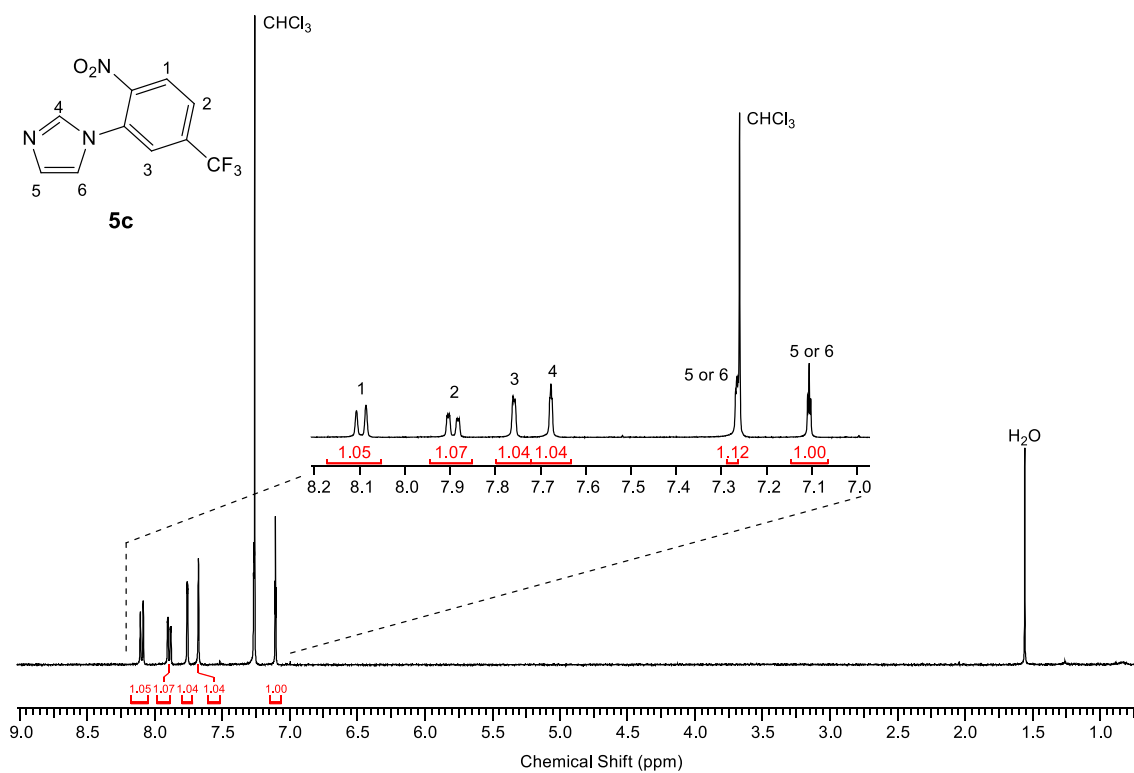


Figure S6. $^{13}\text{C}\{^1\text{H}\}$ NMR spectrum of **7b** (101 MHz, $\text{DMSO-}d_6$).



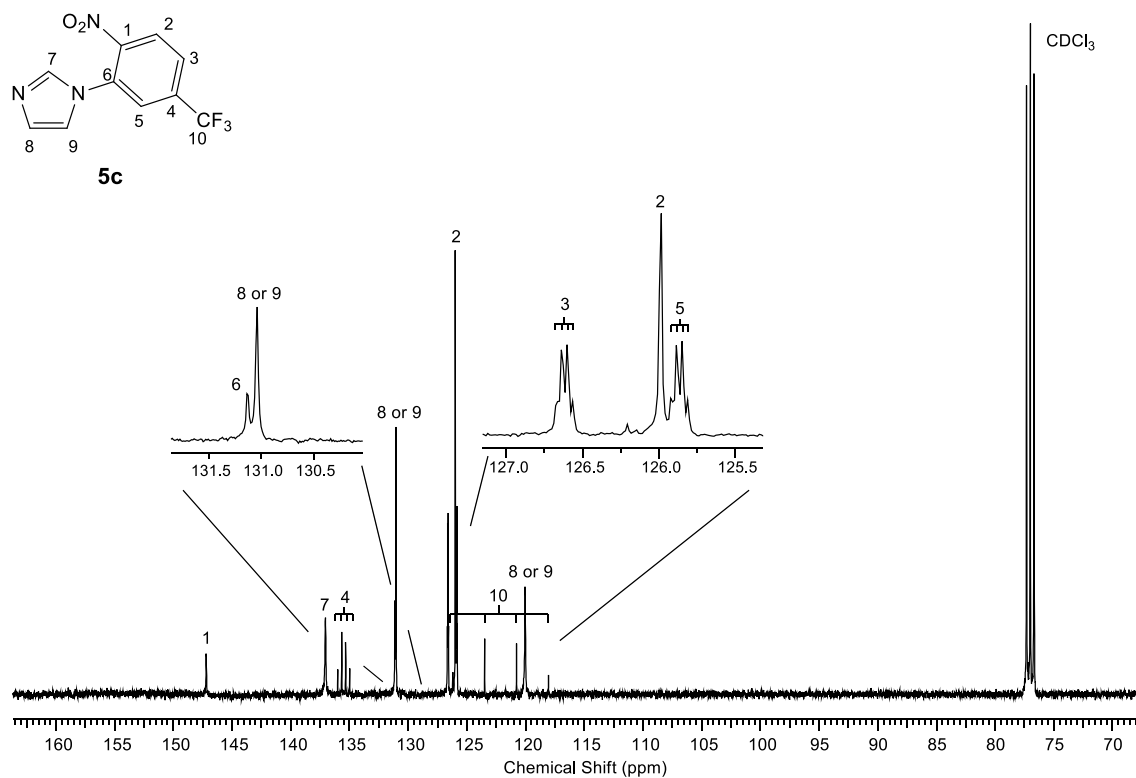


Figure S9. $^{13}\text{C}\{^1\text{H}\}$ NMR spectrum of **5c** (101 MHz, CDCl₃).

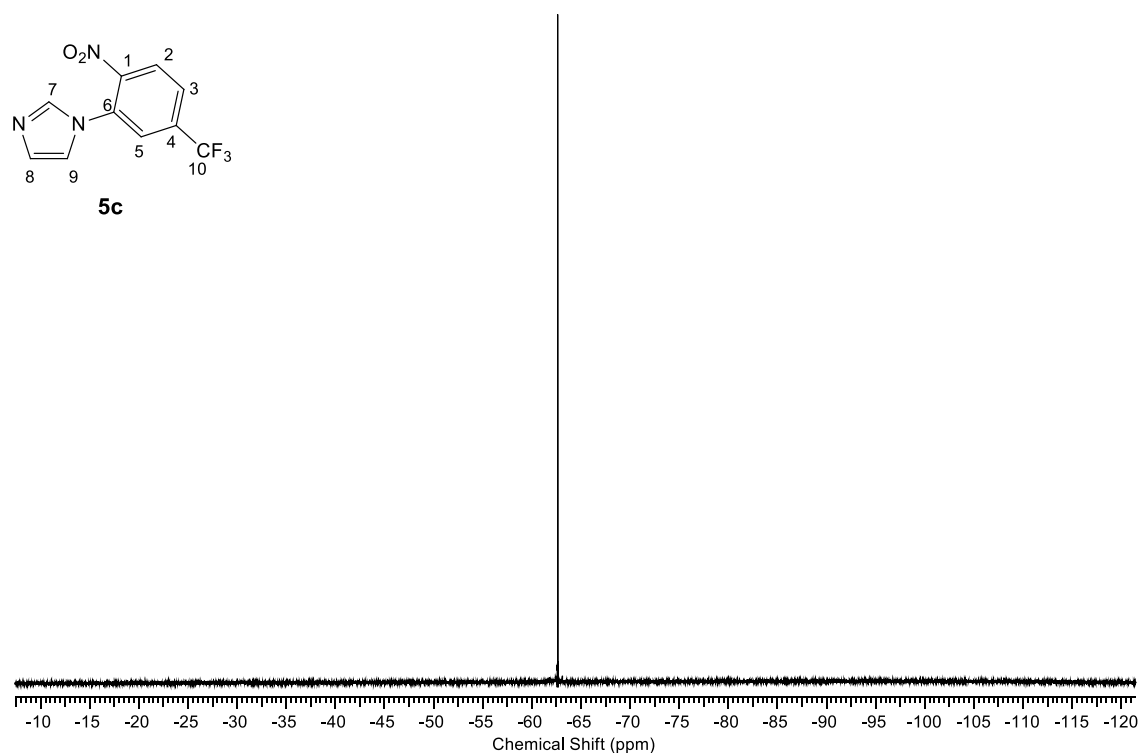


Figure S10. $^{19}\text{F}\{^1\text{H}\}$ NMR spectrum of **5c** (376 MHz, CDCl₃).

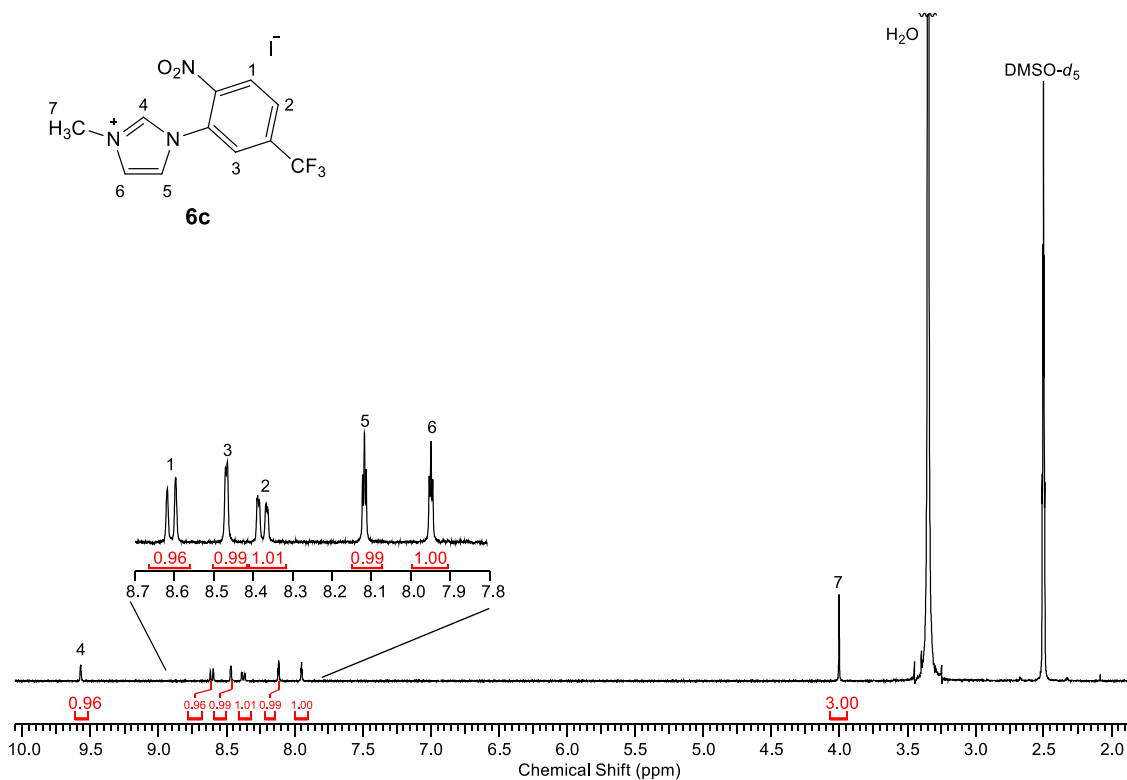


Figure S11. ¹H NMR spectrum of **6c** (400 MHz, DMSO-*d*₆).

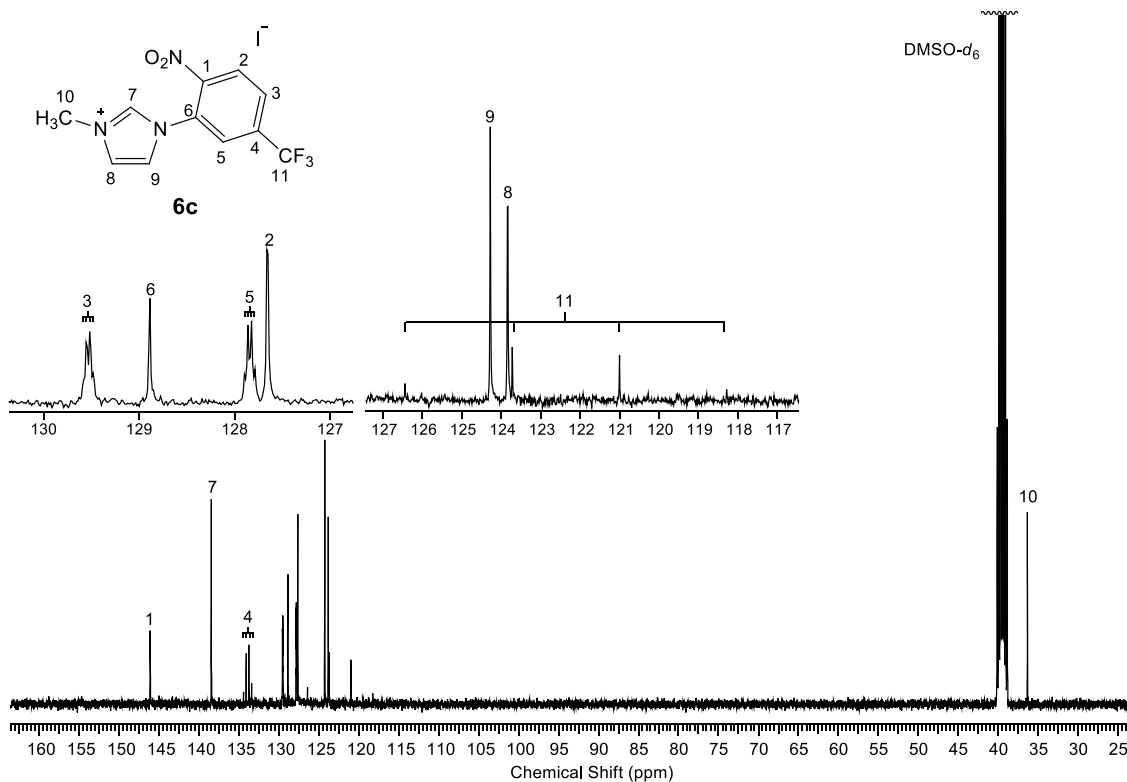


Figure S12. ¹³C{¹H} NMR spectrum of **6c** (101 MHz, DMSO-*d*₆).

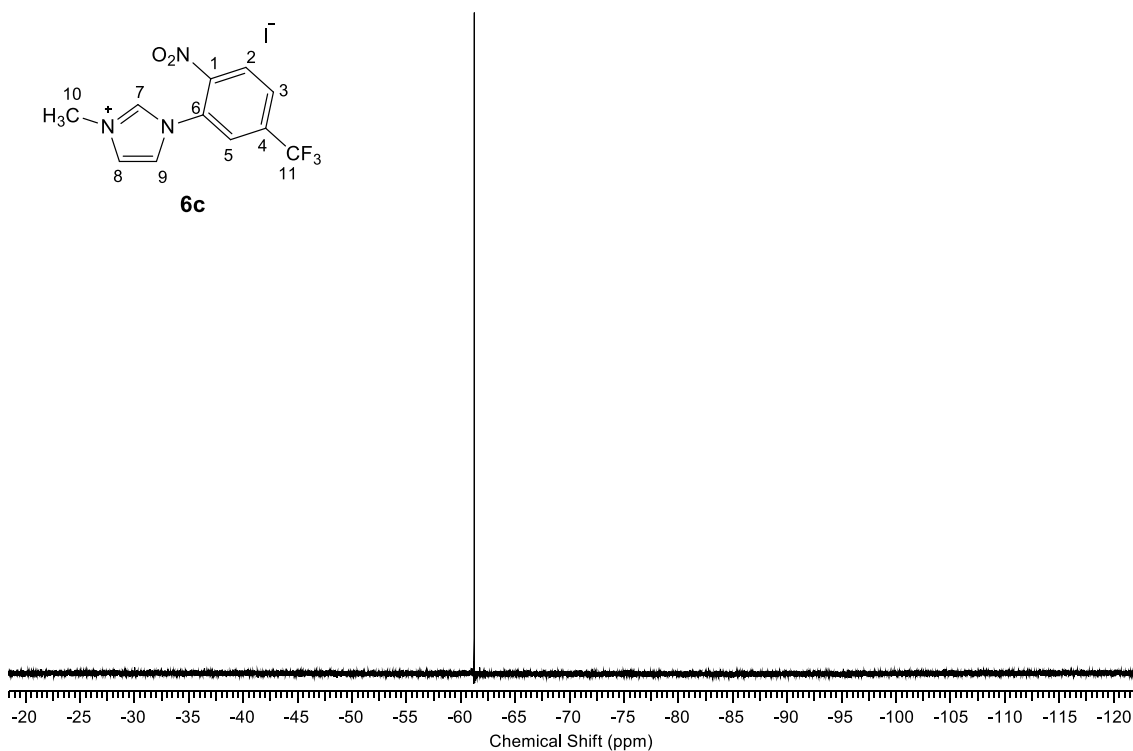


Figure S13. $^{19}\text{F}\{^1\text{H}\}$ NMR spectrum of **6c** (376 MHz, $\text{DMSO-}d_6$).

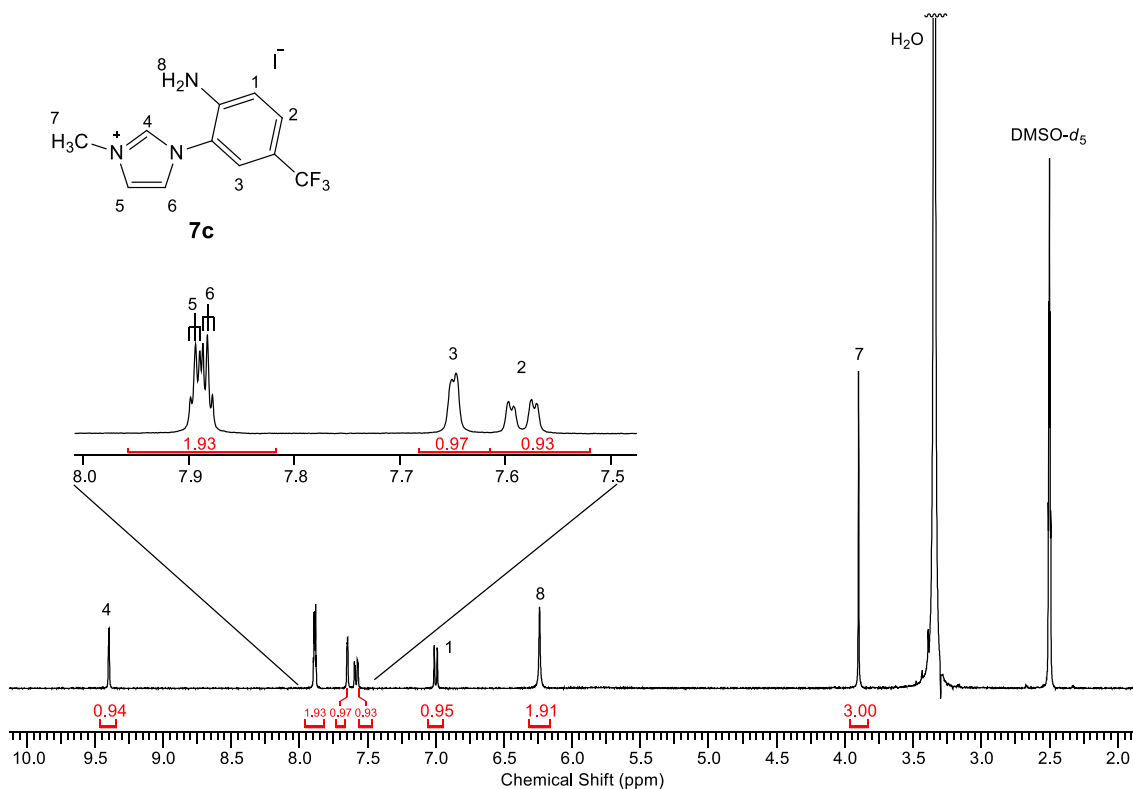


Figure S14. ^1H NMR spectrum of **7c** (400 MHz, $\text{DMSO-}d_6$).

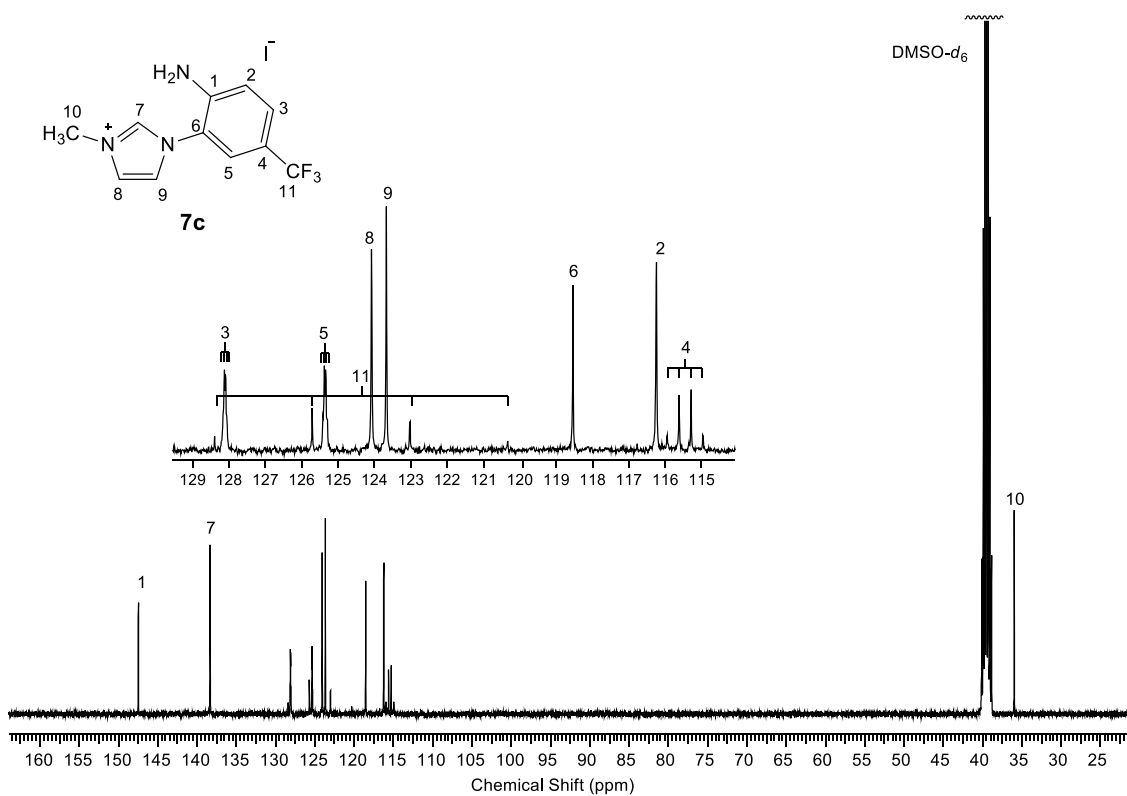


Figure S15. $^{13}\text{C}\{^1\text{H}\}$ NMR spectrum of **7c** (101 MHz, DMSO- d_6).

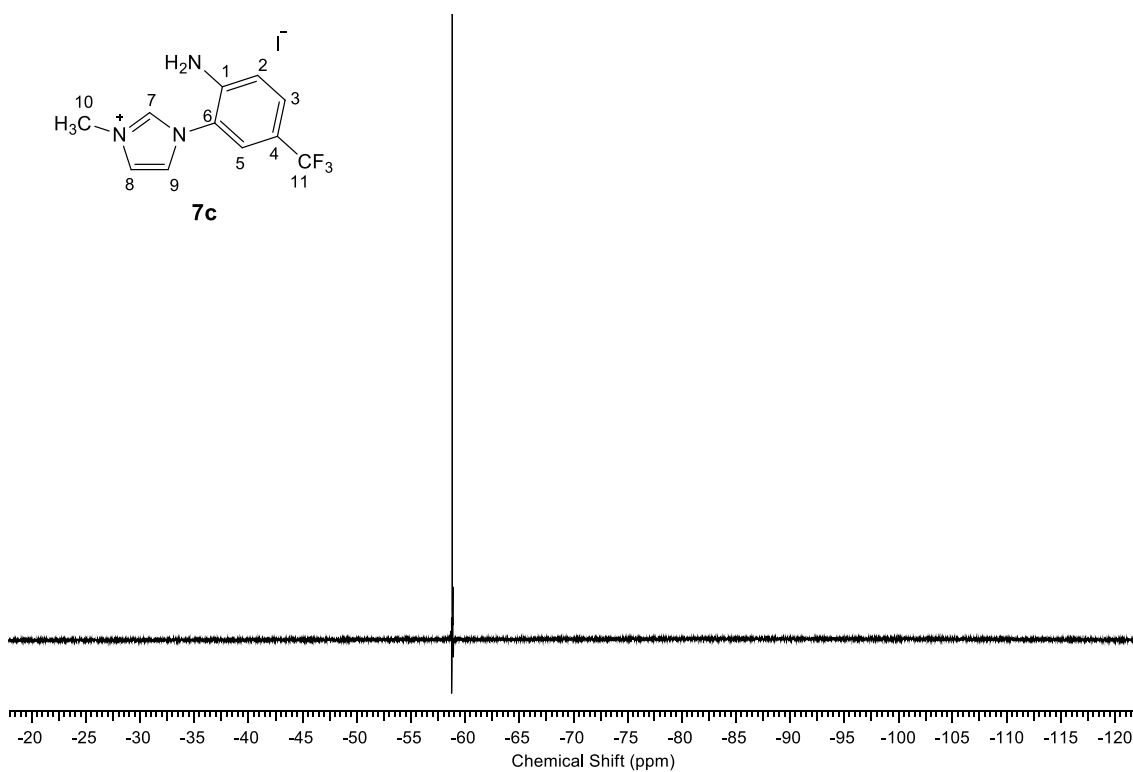


Figure S16. $^{19}\text{F}\{^1\text{H}\}$ NMR spectrum of **7c** (376 MHz, DMSO- d_6).

2. Atomic coordinates and energies for DFT optimized structures

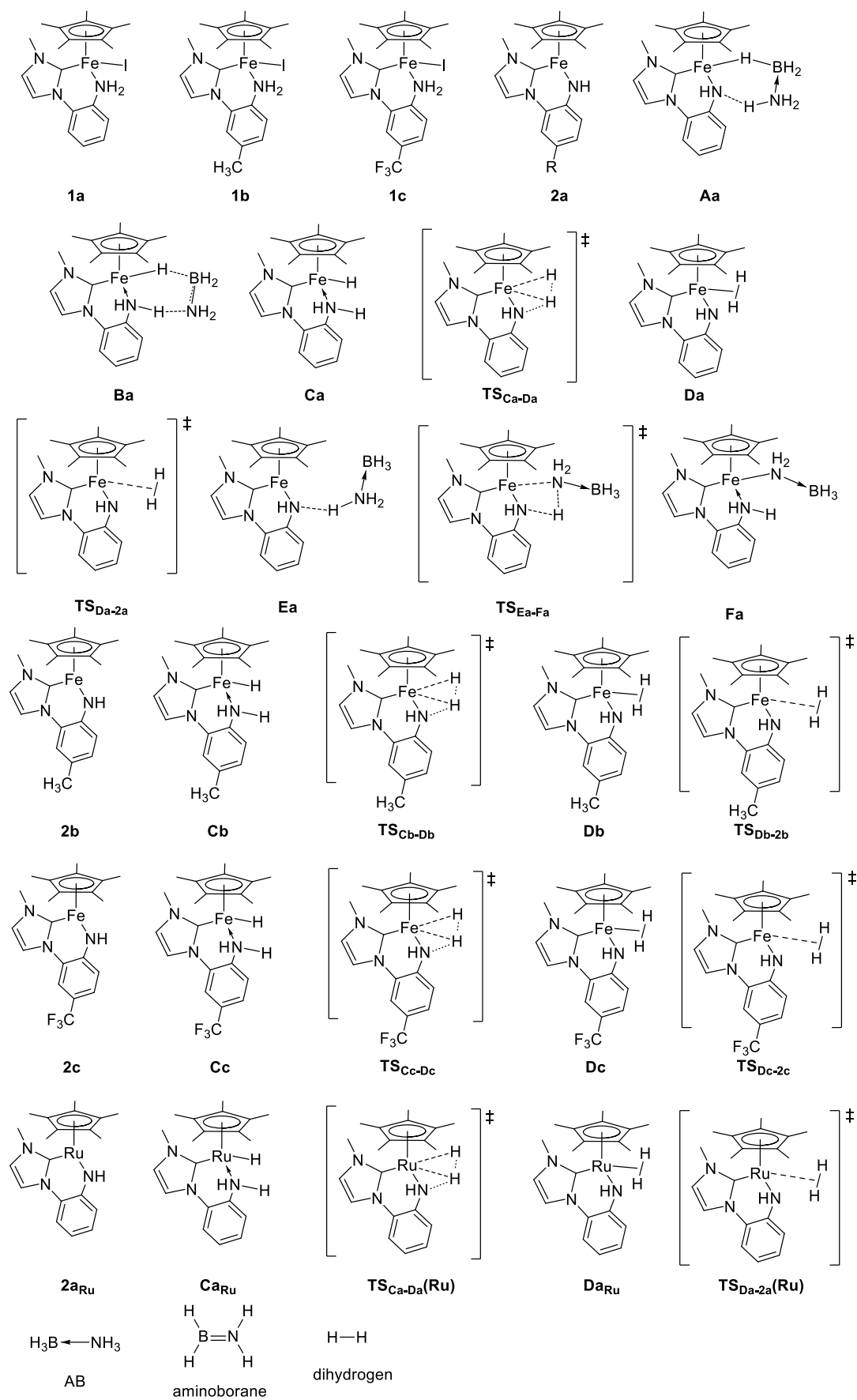


Figure S17. All DFT calculated structures.

Table S1. Atomic coordinates and energy of **1a** $E(\text{RB3PW91}) = -1076.65169859$ a.u.

Atom	Coordinates (Å)		
	<i>x</i>	<i>y</i>	<i>z</i>
H	-0.701465	-1.200184	-2.063218
H	-0.528451	0.424812	-1.987840
I	2.103195	0.884323	-1.616016
Fe	0.371995	-0.369438	0.132516
N	-0.890465	-0.388915	-1.477965
N	-1.773471	1.626535	0.251218
N	0.008158	2.445142	1.128034
C	-0.459550	1.303687	0.553001
C	-2.077675	2.931656	0.624817
H	-3.035643	3.386317	0.429569
C	-0.953241	3.439495	1.172783
H	-0.745526	4.422102	1.568734
C	1.376976	2.656136	1.558406
H	1.939991	1.750764	1.340739
H	1.404837	2.879024	2.630144
H	1.819428	3.482704	0.995760
C	-2.712177	0.724530	-0.299593
C	-2.280967	-0.279884	-1.180678
C	-3.217388	-1.159080	-1.722043
H	-2.879981	-1.925528	-2.416015
C	-4.568945	-1.054525	-1.399082
H	-5.282763	-1.748649	-1.833156
C	-4.993388	-0.057512	-0.526329
H	-6.042351	0.032180	-0.259667
C	-4.065476	0.823814	0.023611
H	-4.390341	1.577734	0.734189
C	1.596964	-2.125318	0.370828
C	0.228979	-2.480544	0.418274
C	-0.404655	-1.746223	1.480617
C	0.625540	-0.983326	2.137771
C	1.846199	-1.186901	1.442872
C	2.645420	-2.682285	-0.539712
H	2.211996	-3.101124	-1.453340
H	3.208861	-3.485345	-0.043085
H	3.353399	-1.906912	-0.846035
C	-0.453988	-3.467803	-0.477148
H	-0.428686	-4.473803	-0.037097
H	0.031561	-3.538744	-1.457253
H	-1.509284	-3.217483	-0.631594
C	-1.803639	-1.933756	1.982573
H	-1.856428	-2.736595	2.732709
H	-2.497189	-2.196463	1.177352
H	-2.187569	-1.023396	2.455087
C	0.426290	-0.197548	3.396838
H	1.248654	0.499480	3.580774
H	0.372641	-0.871329	4.262929
H	-0.504101	0.379822	3.375948
C	3.202845	-0.666046	1.804123
H	3.827475	-1.467488	2.222564
H	3.151953	0.125924	2.558070
H	3.719472	-0.262289	0.926572

Table S2. Atomic coordinates and energy of **1b** $E(\text{RB3PW91}) = -1115.95622180$ a.u.

Atom	Coordinates (Å)		
	<i>x</i>	<i>y</i>	<i>z</i>
I	2.302565	0.895974	-1.625431
Fe	0.586607	-0.368287	0.131309
N	-0.682404	-0.399537	-1.471435
H	-0.492824	-1.213399	-2.052886
C	-2.509637	0.700116	-0.283002
C	-3.011039	-1.178030	-1.699779
H	-2.679870	-1.946148	-2.395053
C	-0.256841	1.297955	0.556500
N	0.205590	2.442926	1.129055
N	-1.575889	1.609142	0.266114
C	-0.764177	3.428600	1.182814
H	-0.562067	4.412580	1.578288
C	-2.072953	-0.297508	-1.167912
C	-3.860260	0.787584	0.049248
H	-4.179427	1.538448	0.767209
C	-1.888412	2.911067	0.643365
H	-2.852123	3.357022	0.456693
C	-4.359634	-1.080616	-1.364074
H	-5.068981	-1.783207	-1.794350
C	1.575911	2.665162	1.548627
H	1.608960	2.898458	2.618021
H	2.011053	3.488270	0.975268
H	2.142096	1.760483	1.336447
C	2.072525	-1.176297	1.435469
C	-4.806814	-0.091393	-0.487071
C	0.854355	-0.979341	2.136457
C	3.427963	-0.646997	1.789045
H	3.376442	0.144272	2.543723
H	3.936714	-0.239426	0.908639
H	4.060212	-1.444603	2.203395
C	0.457631	-2.480004	0.420074
C	1.823256	-2.116690	0.365246
C	-0.224487	-3.471422	-0.471382
H	0.258679	-3.542638	-1.452645
H	-1.280951	-3.224566	-0.623605
H	-0.194838	-4.476487	-0.029444
C	-0.174653	-1.748887	1.485283
C	0.657149	-0.193160	3.395645
H	0.615649	-0.865651	4.263436
H	-0.278440	0.375968	3.380183
H	1.474517	0.511665	3.572242
C	2.870754	-2.668518	-0.549641
H	3.441610	-3.467369	-0.054651
H	3.572459	-1.889224	-0.860567
H	2.435652	-3.091441	-1.460600
C	-1.570544	-1.943085	1.993223
H	-2.265293	-2.211877	1.191033
H	-1.957901	-1.033349	2.464151
H	-1.616095	-2.743999	2.745951
C	-6.263822	0.040970	-0.129692
H	-6.749097	0.826000	-0.724270
H	-6.397251	0.303454	0.925467
H	-6.805707	-0.891606	-0.314917
H	-0.329605	0.412489	-1.990130

Table S3. Atomic coordinates and energy of **1c** $E(\text{RB3PW91}) = -1413.56741151$ a.u.

Atom	Coordinates (Å)		
	<i>x</i>	<i>y</i>	<i>z</i>
Fe	1.166504	-0.368579	0.128948
I	2.860705	0.905359	-1.635174
F	-6.290849	-1.184903	-0.165526
F	-5.831185	0.507149	1.120217
F	-6.284658	0.825078	-0.973379
N	-0.111623	-0.401481	-1.473846
H	0.237346	0.426672	-1.970413
H	0.084690	-1.201659	-2.071739
N	-0.999868	1.603770	0.264652
N	0.778235	2.441520	1.129509
C	0.321731	1.295683	0.556258
C	-1.318714	2.904179	0.645740
H	-2.284146	3.347751	0.461323
C	-0.195817	3.423441	1.185018
H	0.002752	4.407531	1.581974
C	2.148183	2.670415	1.548228
H	2.719581	1.770272	1.331442
H	2.180914	2.899449	2.618381
H	2.576530	3.498898	0.977657
C	-1.929365	0.687297	-0.270641
C	-3.275693	0.764160	0.074729
H	-3.607340	1.509002	0.789837
C	-4.195196	-0.140391	-0.454604
C	-3.769087	-1.138523	-1.326296
H	-4.479756	-1.848640	-1.735492
C	-2.423259	-1.218562	-1.669011
H	-2.086302	-1.987067	-2.360086
C	-1.493840	-0.316281	-1.153465
C	-5.652254	-0.001578	-0.114884
C	0.420353	-1.761824	1.478154
C	1.439366	-0.980853	2.130835
C	2.660238	-1.160827	1.429159
C	2.422587	-2.102372	0.357333
C	1.061914	-2.482655	0.410778
C	-0.971250	-1.976859	1.989644
H	-1.659632	-2.278735	1.193660
H	-1.379744	-1.068119	2.444315
H	-0.998584	-2.764429	2.756796
C	1.231808	-0.200100	3.391680
H	1.201992	-0.875343	4.257647
H	0.287377	0.354180	3.379090
H	2.038419	0.516749	3.568908
C	4.009595	-0.618356	1.785786
H	3.949654	0.167043	2.545786
H	4.514565	-0.200354	0.908103
H	4.649941	-1.411942	2.195038
C	3.476340	-2.641401	-0.558034
H	4.049659	-3.439822	-0.065478
H	4.174833	-1.856571	-0.861823
H	3.046924	-3.061386	-1.472939
C	0.394608	-3.480897	-0.484271
H	0.864395	-3.525314	-1.473634
H	-0.670837	-3.263407	-0.616624
H	0.459866	-4.490472	-0.056975

Table S4. Atomic coordinates and energy of **2a** $E(\text{RB3PW91}) = -1065.09616479$ a.u.

Atom	Coordinates (Å)		
	<i>x</i>	<i>y</i>	<i>z</i>
Fe	0.642347	-0.222543	-0.213992
N	-0.841237	-1.182793	-0.702754
H	-0.665744	-2.156659	-0.933229
N	-1.844078	1.379567	-0.061991
N	-0.152699	2.706289	-0.236885
C	-0.459310	1.366944	-0.150476
C	-1.275924	3.500869	-0.189578
H	-1.227471	4.576327	-0.264210
C	-2.339185	2.677819	-0.080270
H	-3.390181	2.906782	-0.068548
C	1.151878	3.250909	-0.533589
H	1.810139	2.420548	-0.768449
H	1.551809	3.811999	0.315873
H	1.087025	3.914750	-1.401387
C	-2.686633	0.247066	-0.046428
C	-4.028143	0.369957	0.331362
H	-4.397719	1.317896	0.708090
C	-4.898665	-0.707778	0.259773
C	-4.420122	-1.940104	-0.197876
H	-5.088024	-2.794116	-0.270721
C	-3.088422	-2.081045	-0.538716
H	-2.710630	-3.045931	-0.871154
C	-2.167205	-1.007804	-0.450345
C	1.682121	-0.881796	1.417345
C	1.733136	-1.891672	0.393553
C	2.348689	-1.319668	-0.749401
C	2.759866	0.022778	-0.421657
C	2.366670	0.276966	0.925083
C	1.143401	-1.053373	2.803338
H	0.803960	-0.099864	3.217530
H	1.905901	-1.457292	3.484090
H	0.291150	-1.738376	2.821464
C	1.206880	-3.286367	0.528159
H	1.937251	-3.933313	1.029875
H	0.997285	-3.743051	-0.444698
H	0.284789	-3.315593	1.116852
C	2.600930	-1.984445	-2.067825
H	1.933337	-2.834880	-2.231056
H	3.630437	-2.361011	-2.133497
H	2.453242	-1.288639	-2.899647
C	3.645415	0.855417	-1.302198
H	4.622005	0.370704	-1.431290
H	3.842410	1.844271	-0.878539
H	3.224333	0.999537	-2.303265
C	2.695833	1.470682	1.770561
H	3.357847	1.179968	2.595547
H	1.802758	1.921842	2.215431
H	3.216135	2.245909	1.203398
H	-5.934217	-0.589280	0.561856

Table S5. Atomic coordinates and energy of **Aa** $E(\text{RB3PW91}) = -1148.31294458$ a.u.

Atom	Coordinates (Å)		
	<i>x</i>	<i>y</i>	<i>z</i>
Fe	-0.782999	-0.134806	0.257326
H	-1.531919	0.673144	1.563519
N	0.792039	-0.803883	1.310816
H	0.583731	0.218647	2.525033
H	0.606729	-1.718994	1.714680
N	1.658465	1.448939	-0.110709
N	-0.048887	2.754967	-0.148937
C	0.283308	1.431848	-0.041443
C	2.144468	2.740984	-0.255749
H	3.197616	2.965425	-0.292997
C	1.068321	3.560212	-0.283972
H	1.002577	4.633485	-0.373423
C	-1.400167	3.271158	-0.070332
H	-2.057019	2.442264	0.188476
H	-1.706628	3.703860	-1.027294
H	-1.465917	4.038232	0.706852
C	2.481614	0.291156	-0.043471
C	3.716130	0.280914	-0.687327
H	4.008810	1.135666	-1.290707
C	4.566258	-0.817706	-0.589038
C	4.153670	-1.919639	0.159203
H	4.798933	-2.789490	0.250918
C	2.912391	-1.922951	0.782421
H	2.600054	-2.789730	1.361199
C	2.024226	-0.826700	0.700624
C	-0.747728	-1.189332	-1.539961
C	-1.723259	-0.133407	-1.632554
C	-2.703769	-0.338629	-0.626172
C	-2.366424	-1.554101	0.081767
C	-1.187187	-2.079371	-0.501852
C	0.387997	-1.422958	-2.488048
H	1.220751	-1.939535	-2.002995
H	0.780862	-0.480478	-2.880697
H	0.077334	-2.031361	-3.349168
C	-1.728565	0.928079	-2.689298
H	-2.079697	0.517602	-3.644778
H	-0.728526	1.338064	-2.860121
H	-2.392056	1.757923	-2.432793
C	-3.953355	0.456436	-0.395245
H	-3.916288	1.431462	-0.889652
H	-4.131724	0.630170	0.670725
H	-4.832270	-0.069256	-0.791122
C	-3.192608	-2.178791	1.163176
H	-4.016932	-2.770579	0.742343
H	-3.628009	-1.423416	1.822507
H	-2.598236	-2.847357	1.792091
C	-0.510664	-3.359751	-0.123785
H	-0.719724	-3.641916	0.912925
H	0.574360	-3.295848	-0.247521
H	-0.862158	-4.183925	-0.757469
H	5.524581	-0.813478	-1.097945
N	0.068968	0.910490	3.198076
B	-1.459862	0.694439	2.822075
H	0.265908	0.698181	4.171347
H	0.394442	1.854250	3.007829
H	-1.829783	-0.347361	3.308649
H	-2.124557	1.658798	3.140341

Table S6. Atomic coordinates and energy of **Ba** $E(\text{RB3PW91}) = -1148.31094136 \text{ a.u.}$

Atom	Coordinates (Å)		
	<i>x</i>	<i>y</i>	<i>z</i>
Fe	-0.773021	-0.136516	0.242451
H	-1.424774	0.626306	1.544580
N	0.798020	-0.728964	1.379182
H	0.721967	0.037532	2.187834
H	0.604093	-1.627050	1.814417
N	1.652472	1.463585	-0.147091
N	-0.070821	2.739944	-0.250378
C	0.272673	1.428087	-0.101773
C	2.126815	2.757867	-0.320538
H	3.177292	2.997147	-0.340822
C	1.038550	3.556688	-0.386571
H	0.958206	4.626765	-0.498228
C	-1.429175	3.242016	-0.188108
H	-2.058498	2.445181	0.204016
H	-1.777931	3.547928	-1.179096
H	-1.474725	4.097282	0.490654
C	2.476441	0.315850	-0.049572
C	3.698849	0.271222	-0.717232
H	3.996059	1.109753	-1.339550
C	4.521968	-0.847966	-0.620314
C	4.108053	-1.936606	0.141617
H	4.735935	-2.818746	0.225708
C	2.882984	-1.897273	0.802042
H	2.565306	-2.742945	1.407258
C	2.043459	-0.780015	0.722241
C	-0.761881	-1.319887	-1.482134
C	-1.703127	-0.243114	-1.644133
C	-2.688247	-0.346617	-0.624265
C	-2.384489	-1.517534	0.167947
C	-1.222368	-2.117147	-0.378534
C	0.358275	-1.658053	-2.417674
H	1.180449	-2.163392	-1.902468
H	0.775260	-0.759957	-2.883045
H	0.023625	-2.319715	-3.229119
C	-1.677656	0.746102	-2.768450
H	-2.057862	0.290035	-3.691596
H	-0.663795	1.101997	-2.974817
H	-2.302301	1.618013	-2.559281
C	-3.915894	0.494814	-0.450114
H	-3.857546	1.427862	-1.017428
H	-4.082276	0.752200	0.600694
H	-4.809141	-0.038305	-0.801621
C	-3.219017	-2.026214	1.302429
H	-4.110547	-2.552190	0.935042
H	-3.551868	-1.210794	1.950042
H	-2.663308	-2.727335	1.931238
C	-0.580287	-3.385124	0.093711
H	-0.778679	-3.575717	1.153530
H	0.503885	-3.371208	-0.055023
H	-0.968076	-4.247762	-0.462617
H	5.470018	-0.868817	-1.148269
N	0.166231	1.054541	3.213358
B	-1.316931	0.973421	2.799753
H	0.303809	0.777514	4.178886
H	0.557491	1.985332	3.113535
H	-1.898034	0.098495	3.409982
H	-1.907698	2.040618	2.784123

Table S7. Atomic coordinates and energy of **Ca** $E(\text{RB3PW91}) = -1066.27517126$ a.u.

Atom	Coordinates (Å)		
	<i>x</i>	<i>y</i>	<i>z</i>
Fe	0.781087	-0.077288	-0.499960
H	1.265111	0.471366	-1.857324
N	-0.824284	-0.828270	-1.553222
H	-0.823958	-0.156174	-2.316532
H	-0.621220	-1.744446	-1.939725
N	-1.659442	1.510689	-0.298901
N	0.059122	2.807306	-0.339173
C	-0.262793	1.474944	-0.349561
C	-2.142127	2.816429	-0.253347
H	-3.193996	3.051639	-0.250616
C	-1.059247	3.622120	-0.280627
H	-0.989564	4.698922	-0.286061
C	1.407672	3.296373	-0.522435
H	1.983887	2.476055	-0.954737
H	1.855489	3.606662	0.426779
H	1.399995	4.148829	-1.208105
C	-2.461224	0.357966	-0.192157
C	-3.651472	0.372191	0.534645
H	-3.951585	1.282718	1.043527
C	-4.429691	-0.777937	0.645626
C	-4.011821	-1.958311	0.038696
H	-4.606633	-2.862461	0.124903
C	-2.825979	-1.977256	-0.693193
H	-2.504890	-2.890411	-1.188386
C	-2.045951	-0.829261	-0.821462
C	0.884518	-1.207681	1.301769
C	1.706816	-0.036442	1.396951
C	2.698549	-0.084862	0.371333
C	2.495841	-1.303832	-0.374772
C	1.395016	-1.985980	0.207430
C	-0.182419	-1.622096	2.268681
H	-0.964857	-2.216421	1.786341
H	-0.673673	-0.754263	2.718983
H	0.223719	-2.228114	3.091887
C	1.594161	1.002770	2.470626
H	2.105789	0.679308	3.386816
H	0.550575	1.202161	2.731746
H	2.045243	1.951558	2.167934
C	3.871110	0.832703	0.204979
H	3.703000	1.803463	0.679746
H	4.096126	1.014441	-0.850882
H	4.775226	0.407047	0.662269
C	3.375549	-1.799082	-1.481493
H	4.248473	-2.341567	-1.091423
H	3.744310	-0.971635	-2.093419
H	2.841794	-2.480965	-2.150377
C	0.864303	-3.319656	-0.224289
H	1.050036	-3.510185	-1.287334
H	-0.212565	-3.407970	-0.043394
H	1.343388	-4.136625	0.330551
H	-5.350121	-0.750132	1.220456

Table S8. Atomic coordinates and energy of **TS_{Ca-Da}** $E(\text{RB3PW91}) = -1066.25919997$ a.u. (one imaginary frequency at -1204.78 cm^{-1})

Atom	Coordinates (Å)		
	x	y	z
Fe	0.773971	-0.132452	-0.476019
H	0.976281	0.308146	-2.000979
N	-0.850182	-0.988294	-1.373806
H	0.018194	-0.193092	-1.929673
H	-0.673869	-1.924919	-1.714619
N	-1.683938	1.462130	-0.199383
N	0.012617	2.768385	-0.364793
C	-0.312120	1.442925	-0.298492
C	-2.177053	2.760310	-0.205939
H	-3.230764	2.982486	-0.177839
C	-1.106896	3.579460	-0.304688
H	-1.046330	4.655436	-0.354393
C	1.344301	3.268942	-0.630033
H	1.971535	2.410056	-0.866301
H	1.747524	3.800515	0.236848
H	1.321263	3.947596	-1.487989
C	-2.507107	0.306134	-0.134527
C	-3.732535	0.367133	0.525729
H	-4.008264	1.280692	1.044321
C	-4.592877	-0.726655	0.549781
C	-4.203224	-1.901232	-0.091189
H	-4.856945	-2.769230	-0.089354
C	-2.971627	-1.976922	-0.728000
H	-2.673313	-2.899013	-1.221951
C	-2.080976	-0.884498	-0.767140
C	1.070856	-0.940961	1.446131
C	1.986938	0.146131	1.232330
C	2.803220	-0.160906	0.105460
C	2.407731	-1.461810	-0.381550
C	1.364727	-1.937136	0.460245
C	0.101642	-1.069119	2.580820
H	-0.777015	-1.655389	2.296928
H	-0.257647	-0.089884	2.910504
H	0.556556	-1.560304	3.452715
C	2.112706	1.334998	2.135309
H	2.574268	1.045444	3.087873
H	1.138567	1.776860	2.366970
H	2.740645	2.115744	1.699424
C	3.985384	0.612178	-0.396962
H	3.969123	1.654124	-0.064709
H	4.035031	0.614142	-1.490151
H	4.923803	0.176160	-0.028803
C	3.070696	-2.202630	-1.502962
H	3.967636	-2.735610	-1.159267
H	3.379504	-1.523081	-2.302645
H	2.404564	-2.946644	-1.949728
C	0.669697	-3.258549	0.346717
H	0.781329	-3.695260	-0.650579
H	-0.400097	-3.172825	0.561054
H	1.088418	-3.979612	1.059940
H	-5.543613	-0.661083	1.068525

Table S9. Atomic coordinates and energy of **Da** $E(\text{RB3PW91}) = -1066.27945209$ a.u.

Atom	Coordinates (Å)		
	<i>x</i>	<i>y</i>	<i>z</i>
Fe	0.830280	-0.125801	-0.564834
H	1.345902	0.664228	-1.874595
N	-0.781554	-0.917245	-1.383881
H	1.257106	-0.138538	-2.114208
H	-0.632451	-1.816627	-1.828596
N	-1.618259	1.456932	-0.191284
N	0.051026	2.788326	-0.448403
C	-0.263263	1.458097	-0.383511
C	-2.121452	2.748891	-0.155313
H	-3.173929	2.956390	-0.060150
C	-1.070347	3.585264	-0.310902
H	-1.025404	4.662379	-0.351288
C	1.367580	3.321449	-0.723212
H	2.065423	2.486843	-0.775008
H	1.678839	4.007131	0.070261
H	1.372577	3.855548	-1.679137
C	-2.432753	0.292822	-0.110771
C	-3.650336	0.341535	0.561099
H	-3.919740	1.239109	1.111913
C	-4.521261	-0.744780	0.547573
C	-4.145083	-1.889271	-0.161400
H	-4.811903	-2.747502	-0.199164
C	-2.919948	-1.957231	-0.805010
H	-2.639928	-2.859756	-1.344925
C	-1.991532	-0.879070	-0.789673
C	0.861259	-0.890294	1.387951
C	1.855712	0.144250	1.266289
C	2.780695	-0.239321	0.257694
C	2.379405	-1.535427	-0.241099
C	1.220930	-1.936328	0.477808
C	-0.236321	-0.941801	2.404980
H	-1.100324	-1.500370	2.037156
H	-0.588740	0.060108	2.664828
H	0.102289	-1.421808	3.333415
C	1.939420	1.353591	2.145601
H	2.355610	1.085695	3.124999
H	0.955374	1.797494	2.320142
H	2.585695	2.126346	1.721678
C	4.038180	0.476940	-0.135555
H	4.011252	1.535272	0.139259
H	4.222877	0.419259	-1.212899
H	4.911604	0.039040	0.365088
C	3.141762	-2.355125	-1.238984
H	3.927611	-2.945511	-0.749412
H	3.629584	-1.727706	-1.990868
H	2.491834	-3.055937	-1.770031
C	0.496131	-3.236251	0.330010
H	0.670001	-3.690481	-0.649791
H	-0.582581	-3.111641	0.456467
H	0.839170	-3.954271	1.085666
H	-5.466190	-0.697602	1.078411

Table S10. Atomic coordinates and energy of **TS_{Da-2a}** $E(\text{RB3PW91}) = -1066.26606392$ a.u. (one imaginary frequency at -312.63 cm^{-1})

Atom	Coordinates (Å)		
	<i>x</i>	<i>y</i>	<i>z</i>
Fe	0.731060	-0.170004	-0.399782
H	1.383514	0.576592	-2.590835
N	-0.801223	-1.057658	-1.105271
H	0.816060	0.089396	-2.668142
H	-0.632423	-2.010760	-1.412753
N	-1.743718	1.419067	-0.150675
N	-0.058729	2.744649	-0.343900
C	-0.373223	1.412252	-0.267065
C	-2.242803	2.713843	-0.156064
H	-3.296469	2.931952	-0.120147
C	-1.182111	3.543226	-0.275235
H	-1.134510	4.619228	-0.339426
C	1.260373	3.269839	-0.617753
H	1.932125	2.423836	-0.749228
H	1.613741	3.894108	0.208298
H	1.245773	3.866949	-1.535176
C	-2.568736	0.266198	-0.104616
C	-3.852735	0.350242	0.433864
H	-4.174530	1.274219	0.905675
C	-4.721341	-0.734082	0.396575
C	-4.283009	-1.924291	-0.191976
H	-4.946013	-2.784439	-0.240675
C	-2.999091	-2.026715	-0.697686
H	-2.662410	-2.963312	-1.138157
C	-2.076494	-0.947730	-0.656782
C	1.174304	-0.933166	1.436684
C	2.036549	0.194525	1.202585
C	2.817022	-0.069948	0.042687
C	2.465738	-1.390992	-0.428819
C	1.493855	-1.930557	0.449069
C	0.234505	-1.101459	2.589509
H	-0.642973	-1.690967	2.309289
H	-0.127690	-0.134448	2.949432
H	0.718877	-1.607767	3.436044
C	2.135006	1.383519	2.108512
H	2.630659	1.108133	3.047912
H	1.149177	1.783096	2.364808
H	2.718929	2.192621	1.663218
C	3.952026	0.746247	-0.501691
H	3.953062	1.767141	-0.109327
H	3.932096	0.810927	-1.595152
H	4.917942	0.301989	-0.227178
C	3.101355	-2.080815	-1.597880
H	4.050175	-2.554071	-1.312363
H	3.320992	-1.381235	-2.410127
H	2.458223	-2.864776	-2.007553
C	0.883624	-3.294937	0.377300
H	0.949988	-3.722359	-0.628127
H	-0.170915	-3.280345	0.667572
H	1.401220	-3.986226	1.054236
H	-5.715373	-0.652972	0.823831

Table S11. Atomic coordinates and energy of **Ea** $E(\text{RB3PW91}) = -1148.30156108$ a.u.

Atom	Coordinates (Å)		
	<i>x</i>	<i>y</i>	<i>z</i>
Fe	-0.681826	-0.281453	-0.010326
H	-1.408388	1.248364	3.685940
N	0.824697	-1.006203	0.817022
H	0.680643	0.349621	2.412111
H	0.662515	-1.905273	1.263738
N	1.775220	1.259620	-0.586947
N	0.077268	2.582459	-0.679614
C	0.394670	1.264917	-0.478094
C	2.263284	2.530260	-0.864168
H	3.313366	2.750470	-0.949814
C	1.193506	3.352774	-0.918025
H	1.136303	4.418600	-1.075937
C	-1.227566	3.172237	-0.463138
H	-1.886908	2.391940	-0.097893
H	-1.622229	3.596712	-1.390496
H	-1.155022	3.951221	0.300023
C	2.616605	0.145134	-0.362401
C	3.922842	0.141736	-0.858716
H	4.255144	0.955024	-1.495912
C	4.797616	-0.898798	-0.575518
C	4.354063	-1.961052	0.216255
H	5.022613	-2.784331	0.452500
C	3.052187	-1.980168	0.686730
H	2.702988	-2.821212	1.282725
C	2.130405	-0.946041	0.399803
C	-1.616738	-1.302187	-1.503940
C	-2.370929	-0.101986	-1.275554
C	-2.798386	-0.099077	0.081787
C	-2.351150	-1.331662	0.686700
C	-1.666801	-2.087982	-0.298821
C	-1.021685	-1.724618	-2.810833
H	-0.144147	-2.361429	-2.666764
H	-0.704553	-0.859850	-3.400455
H	-1.743061	-2.290764	-3.416499
C	-2.707664	0.888318	-2.348981
H	-3.339511	0.418556	-3.112710
H	-1.814105	1.267806	-2.855527
H	-3.261346	1.744929	-1.958355
C	-3.691689	0.885794	0.776415
H	-3.932870	1.743410	0.142038
H	-3.244076	1.264811	1.701283
H	-4.645784	0.413440	1.042807
C	-2.625568	-1.721310	2.106934
H	-3.655575	-2.082330	2.226021
H	-2.494689	-0.871395	2.784231
H	-1.963375	-2.523547	2.445914
C	-1.066648	-3.449373	-0.134732
H	-0.907735	-3.704332	0.917924
H	-0.103877	-3.531555	-0.648936
H	-1.727507	-4.219849	-0.550857
H	5.806246	-0.884290	-0.975307
B	-0.418547	1.945419	3.558080
N	0.820140	0.922889	3.262059
H	-0.482079	2.686310	2.595115
H	-0.130391	2.535129	4.580594
H	1.689874	1.435497	3.139037
H	0.954349	0.286128	4.043672

Table S12. Atomic coordinates and energy of $\text{TS}_{\text{Ea-Fa}}$ $E(\text{RB3PW91}) = -1148.27058919$ a.u. (one imaginary frequency at -1239.26 cm^{-1})

Atom	Coordinates (Å)		
	x	y	z
Fe	-0.752321	-0.187193	0.219213
H	0.427041	2.648586	2.433055
N	0.818671	-0.824172	1.284093
H	0.184421	0.052879	1.935682
H	0.649924	-1.711860	1.746980
N	1.711377	1.377778	-0.260956
N	0.010233	2.679216	-0.379856
C	0.341567	1.371689	-0.199184
C	2.202534	2.659554	-0.459027
H	3.255998	2.880934	-0.489531
C	1.128824	3.475929	-0.529540
H	1.064514	4.546318	-0.644349
C	-1.308719	3.234134	-0.151463
H	-2.040139	2.435061	-0.250802
H	-1.519964	4.013698	-0.887858
H	-1.358189	3.650905	0.859865
C	2.539587	0.238863	-0.085263
C	3.790755	0.191172	-0.696920
H	4.091021	1.000275	-1.355634
C	4.646111	-0.887416	-0.492979
C	4.231661	-1.933737	0.327425
H	4.883982	-2.784136	0.504003
C	2.975015	-1.899316	0.919860
H	2.655502	-2.718989	1.559523
C	2.093480	-0.821537	0.730000
C	-0.927600	-1.324701	-1.489102
C	-1.852095	-0.224232	-1.568124
C	-2.751965	-0.312093	-0.469176
C	-2.409323	-1.498317	0.285394
C	-1.317318	-2.128628	-0.362834
C	0.136236	-1.658461	-2.488541
H	0.986228	-2.161596	-2.019123
H	0.522758	-0.757840	-2.973494
H	-0.244784	-2.319607	-3.278716
C	-1.891057	0.770791	-2.686569
H	-2.351718	0.323581	-3.576271
H	-0.887944	1.102010	-2.968619
H	-2.475210	1.658624	-2.432653
C	-3.961620	0.536546	-0.210564
H	-3.948127	1.462972	-0.791194
H	-4.064353	0.808956	0.845711
H	-4.877869	0.000972	-0.490673
C	-3.151985	-1.993698	1.489082
H	-4.044016	-2.564007	1.199333
H	-3.494723	-1.169438	2.123294
H	-2.536037	-2.651706	2.108907
C	-0.657811	-3.408492	0.045444
H	-0.830655	-3.642402	1.100496
H	0.422892	-3.377746	-0.123499
H	-1.053466	-4.249036	-0.537851
H	5.617610	-0.908590	-0.975827
B	-0.188656	1.969787	3.242195
N	-0.854900	0.736055	2.409206
H	0.558153	1.474267	4.066589
H	-1.098623	2.600541	3.760986
H	-1.365703	0.119534	3.037815
H	-1.560236	1.144496	1.788410

Table S13. Atomic coordinates and energy of **Fa** $E(\text{RB3PW91}) = -1148.31179259$ a.u.

Atom	Coordinates (Å)		
	<i>x</i>	<i>y</i>	<i>z</i>
Fe	-0.762081	-0.124261	0.293713
H	0.378112	1.278446	3.114347
N	0.812631	-0.760541	1.442290
H	0.763329	-0.046185	2.198560
H	0.620677	-1.651946	1.889409
N	1.672715	1.502444	0.049181
N	-0.043666	2.781893	-0.070833
C	0.290462	1.465040	0.055340
C	2.153035	2.801312	-0.059662
H	3.203702	3.038785	-0.034030
C	1.069835	3.603388	-0.134231
H	0.993410	4.676993	-0.206776
C	-1.397079	3.296030	-0.063804
H	-2.077786	2.447904	-0.113043
H	-1.561776	3.940755	-0.931951
H	-1.585531	3.869856	0.849013
C	2.499236	0.354144	0.086198
C	3.725314	0.344653	-0.576721
H	4.029171	1.215552	-1.148868
C	4.543056	-0.782140	-0.538283
C	4.126009	-1.912057	0.158249
H	4.753311	-2.797415	0.196315
C	2.898811	-1.906240	0.817642
H	2.578144	-2.779213	1.380328
C	2.071422	-0.782492	0.792024
C	-0.609624	-1.212194	-1.522380
C	-1.561541	-0.146321	-1.672270
C	-2.614965	-0.341818	-0.735091
C	-2.331227	-1.554801	-0.004231
C	-1.114369	-2.084435	-0.501293
C	0.571479	-1.465255	-2.409082
H	1.361236	-2.015525	-1.889540
H	1.013790	-0.529711	-2.764426
H	0.293977	-2.051464	-3.296373
C	-1.488664	0.911885	-2.730655
H	-1.811558	0.509954	-3.699510
H	-0.469638	1.288935	-2.858137
H	-2.133066	1.765899	-2.506372
C	-3.880232	0.451807	-0.609143
H	-3.832412	1.390045	-1.169749
H	-4.113923	0.700324	0.432893
H	-4.738976	-0.107709	-1.001993
C	-3.230777	-2.187718	1.012833
H	-3.953203	-2.866588	0.540366
H	-3.817162	-1.443028	1.561616
H	-2.671788	-2.769906	1.751462
C	-0.478633	-3.368399	-0.064447
H	-0.719115	-3.612159	0.975685
H	0.610260	-3.337620	-0.165906
H	-0.832833	-4.206633	-0.677584
H	5.494083	-0.775152	-1.061278
B	-0.705949	0.737881	3.378097
N	-1.550968	0.606942	2.034064
H	-0.510118	-0.388210	3.826719
H	-1.296462	1.427037	4.194401
H	-2.356693	0.026790	2.254057
H	-1.951573	1.521072	1.844462

Table S14. Atomic coordinates and energy of **2b** $E(\text{RB3PW91}) = -1104.40221393$ a.u.

Atom	Coordinates (Å)		
	<i>x</i>	<i>y</i>	<i>z</i>
Fe	0.904065	-0.231443	-0.213973
N	-0.593251	-1.145333	-0.739199
H	-0.443641	-2.124959	-0.963444
N	-1.536235	1.447881	-0.127252
N	0.201660	2.720700	-0.243959
C	-0.149662	1.390763	-0.175341
C	-0.896374	3.550510	-0.223942
H	-0.811367	4.624293	-0.289795
C	-1.988283	2.761763	-0.150994
H	-3.031097	3.024844	-0.168224
C	1.530466	3.225862	-0.499441
H	2.167931	2.377526	-0.727088
H	1.925659	3.764267	0.366770
H	1.510085	3.901190	-1.360561
C	-2.413879	0.343046	-0.144538
C	-3.764970	0.509230	0.185618
H	-4.112057	1.470988	0.550644
C	-4.684999	-0.527991	0.089764
C	-4.212531	-1.774039	-0.355943
H	-4.904252	-2.607852	-0.454143
C	-2.877570	-1.962565	-0.650031
H	-2.526427	-2.941670	-0.970175
C	-1.920830	-0.924331	-0.531061
C	1.885618	-0.931642	1.437034
C	1.931890	-1.935442	0.407223
C	2.591047	-1.373679	-0.716484
C	3.033504	-0.046568	-0.368848
C	2.614735	0.210006	0.969911
C	1.309655	-1.097027	2.808757
H	0.986461	-0.137201	3.221354
H	2.044540	-1.525819	3.504560
H	0.438936	-1.758634	2.802196
C	1.362857	-3.315309	0.518694
H	2.061441	-3.986458	1.033736
H	1.164883	-3.759368	-0.462444
H	0.425741	-3.321862	1.084003
C	2.855852	-2.036728	-2.033326
H	2.167578	-2.865797	-2.219060
H	3.875154	-2.443178	-2.076936
H	2.748955	-1.331151	-2.863140
C	3.966447	0.764264	-1.220428
H	4.930802	0.250614	-1.328140
H	4.182711	1.743786	-0.784620
H	3.575959	0.927974	-2.230850
C	2.958287	1.387636	1.832168
H	3.588447	1.071391	2.672588
H	2.068223	1.864310	2.255980
H	3.517771	2.149354	1.284307
C	-6.132016	-0.330001	0.455018
H	-6.794245	-0.535060	-0.394742
H	-6.439093	-0.998949	1.267847
H	-6.325464	0.695644	0.782684

Table S15. Atomic coordinates and energy of **Cb** $E(\text{RB3PW91}) = -1105.58187311$ a.u.

Atom	Coordinates (Å)		
	<i>x</i>	<i>y</i>	<i>z</i>
Fe	1.050253	-0.100780	-0.495245
H	1.654967	0.432303	-1.810195
N	-0.516383	-0.757610	-1.660021
H	-0.428754	-0.089679	-2.422025
H	-0.337117	-1.684326	-2.033139
N	-1.310425	1.614582	-0.430318
N	0.474654	2.815413	-0.342683
C	0.082310	1.502851	-0.393276
C	-1.723626	2.944191	-0.396685
H	-2.759249	3.236579	-0.457345
C	-0.599360	3.689731	-0.343204
H	-0.471417	4.761088	-0.328134
C	1.856918	3.231024	-0.431244
H	2.414548	2.383160	-0.833886
H	2.257017	3.508783	0.548910
H	1.941371	4.087780	-1.106376
C	-2.179088	0.506098	-0.398091
C	-3.412146	0.579523	0.246826
H	-3.687151	1.502070	0.750449
C	-4.280206	-0.516178	0.298429
C	-3.870673	-1.706646	-0.303853
C	-2.641769	-1.790077	-0.955516
H	-2.345354	-2.719241	-1.436296
C	-1.786558	-0.693498	-1.016912
C	0.967359	-1.237017	1.304963
C	1.852789	-0.118763	1.458261
C	2.903776	-0.228069	0.498915
C	2.675112	-1.431729	-0.264453
C	1.498733	-2.044671	0.242773
C	-0.187037	-1.580597	2.196169
H	-0.966529	-2.132854	1.661821
H	-0.657504	-0.681205	2.605120
H	0.123403	-2.201427	3.049514
C	1.733861	0.924819	2.527092
H	2.140909	0.560826	3.479775
H	0.691233	1.206341	2.703021
H	2.282224	1.834943	2.269714
C	4.138112	0.616409	0.410441
H	3.999799	1.595861	0.876980
H	4.439383	0.784009	-0.628583
H	4.984170	0.136658	0.922082
C	3.593394	-1.979987	-1.313362
H	4.406149	-2.572422	-0.869520
H	4.048733	-1.176655	-1.898599
H	3.064722	-2.630452	-2.016759
C	0.913904	-3.341311	-0.229918
H	1.162374	-3.544982	-1.277624
H	-0.176730	-3.357779	-0.127200
H	1.297216	-4.187328	0.354979
H	-4.517961	-2.578934	-0.271429
C	-5.616649	-0.401526	0.982580
H	-6.353116	0.093246	0.337534
H	-6.016862	-1.385550	1.241242
H	-5.546923	0.185325	1.903875

Table S16. Atomic coordinates and energy of **TS_{Cb-Db}** $E(\text{RB3PW91}) = -1105.56514867$ a.u. (one imaginary frequency at -1204.76 cm^{-1})

Atom	Coordinates (Å)		
	<i>x</i>	<i>y</i>	<i>z</i>
Fe	1.041237	-0.148315	-0.472601
H	1.347895	0.295532	-1.980033
N	-0.561301	-0.929739	-1.467371
H	0.373764	-0.166843	-1.969133
H	-0.405422	-1.872149	-1.802128
N	-1.362627	1.544814	-0.314202
N	0.393846	2.779431	-0.371581
C	0.010590	1.468176	-0.338198
C	-1.799520	2.862797	-0.332903
H	-2.842883	3.129294	-0.359947
C	-0.692234	3.636741	-0.363437
H	-0.583994	4.709599	-0.397283
C	1.757450	3.225982	-0.560113
H	2.361079	2.343358	-0.768939
H	2.134253	3.735452	0.331542
H	1.809108	3.909792	-1.412750
C	-2.235692	0.423874	-0.314484
C	-3.494816	0.531963	0.273240
H	-3.756261	1.454448	0.785366
C	-4.418504	-0.513940	0.245808
C	-4.022686	-1.696934	-0.386169
H	-4.709374	-2.539500	-0.428860
C	-2.761565	-1.825028	-0.951107
H	-2.478514	-2.760440	-1.428903
C	-1.821293	-0.775864	-0.933037
C	1.202315	-0.964457	1.462758
C	2.182991	0.073708	1.293383
C	3.035912	-0.279246	0.208409
C	2.598213	-1.559494	-0.296692
C	1.492127	-1.977548	0.494097
C	0.172542	-1.037947	2.547912
H	-0.718664	-1.581624	2.221498
H	-0.153847	-0.040197	2.855736
H	0.557985	-1.546024	3.443328
C	2.327776	1.255253	2.203120
H	2.719204	0.941318	3.179094
H	1.369723	1.753302	2.382305
H	3.022834	1.997386	1.803054
C	4.276918	0.432855	-0.239218
H	4.294573	1.476802	0.086714
H	4.378962	0.424901	-1.328675
H	5.174402	-0.044964	0.176111
C	3.276210	-2.337721	-1.383260
H	4.125009	-2.917238	-0.995365
H	3.660670	-1.677686	-2.166350
H	2.594442	-3.046125	-1.863217
C	0.735415	-3.261294	0.348038
H	0.880903	-3.711805	-0.638616
H	-0.338815	-3.116820	0.499246
H	1.073548	-3.997150	1.088395
C	-5.787204	-0.363209	0.855127
H	-5.791665	0.387300	1.651700
H	-6.531038	-0.051172	0.110618
H	-6.139120	-1.306102	1.285544

Table S17. Atomic coordinates and energy of **Db** $E(\text{RB3PW91}) = -1105.58485618$ a.u.

Atom	Coordinates (Å)		
	x	y	z
Fe	1.100472	-0.146888	-0.556815
H	1.737846	0.628429	-1.821280
N	-0.493461	-0.845581	-1.488789
H	1.621222	-0.165498	-2.077405
H	-0.362731	-1.748305	-1.932512
N	-1.286872	1.552626	-0.311701
N	0.457913	2.802316	-0.451315
C	0.075877	1.488554	-0.422675
C	-1.727576	2.867403	-0.288411
H	-2.772492	3.125620	-0.253092
C	-0.629397	3.652330	-0.370169
H	-0.529590	4.726270	-0.393279
C	1.813227	3.272429	-0.638523
H	2.470845	2.404531	-0.662606
H	2.109789	3.930638	0.183344
H	1.902006	3.818542	-1.583483
C	-2.158582	0.428240	-0.296193
C	-3.412756	0.530543	0.300887
H	-3.666893	1.436908	0.846345
C	-4.349156	-0.501056	0.231663
C	-3.970992	-1.651792	-0.476378
H	-4.676298	-2.475811	-0.569832
C	-2.715056	-1.778617	-1.045059
H	-2.455388	-2.689131	-1.581869
C	-1.733172	-0.753190	-0.962422
C	0.973301	-0.919567	1.387762
C	2.031620	0.056156	1.331760
C	2.989836	-0.376744	0.375857
C	2.544102	-1.644999	-0.155485
C	1.324442	-1.980875	0.492578
C	-0.181663	-0.910560	2.340454
H	-1.050697	-1.425396	1.924060
H	-0.496197	0.109332	2.578302
H	0.078092	-1.403594	3.287332
C	2.134136	1.253990	2.224742
H	2.473043	0.956792	3.225284
H	1.169672	1.755693	2.343316
H	2.850299	1.988342	1.847328
C	4.305516	0.269089	0.058422
H	4.322241	1.326293	0.338376
H	4.546516	0.205166	-1.007378
H	5.123720	-0.219113	0.603814
C	3.314094	-2.503729	-1.113937
H	4.031922	-3.144228	-0.584473
H	3.883219	-1.902636	-1.829303
H	2.655891	-3.160139	-1.689711
C	0.536703	-3.236520	0.293224
H	0.738898	-3.693925	-0.679643
H	-0.538662	-3.051808	0.360787
H	0.796360	-3.977428	1.059996
C	-5.691157	-0.394836	0.906068
H	-5.749874	-1.016953	1.809006
H	-5.905148	0.634972	1.209310
H	-6.503034	-0.717502	0.244104

Table S18. Atomic coordinates and energy of **TS_{Db-2b}** $E(\text{RB3PW91}) = -1105.57176961$ a.u. (one imaginary frequency at -311.91 cm^{-1})

Atom	Coordinates (Å)		
	<i>x</i>	<i>y</i>	<i>z</i>
Fe	0.994810	-0.183369	-0.401379
H	1.776929	0.551784	-2.537704
N	-0.537418	-1.004354	-1.182550
H	1.200577	0.082766	-2.653937
H	-0.394558	-1.963047	-1.485743
N	-1.425229	1.501895	-0.247544
N	0.319111	2.759238	-0.353112
C	-0.052039	1.439906	-0.303280
C	-1.870599	2.816032	-0.262051
H	-2.915113	3.076640	-0.270341
C	-0.772928	3.602372	-0.326185
H	-0.679079	4.676034	-0.377498
C	1.669140	3.232168	-0.563933
H	2.311007	2.360348	-0.674958
H	2.011285	3.834157	0.283125
H	1.719076	3.837335	-1.474843
C	-2.295815	0.382437	-0.250646
C	-3.600756	0.515241	0.228517
H	-3.902128	1.450987	0.692487
C	-4.526280	-0.521993	0.153087
C	-4.091844	-1.723512	-0.429236
H	-4.785429	-2.557657	-0.516314
C	-2.793294	-1.879262	-0.876199
H	-2.481355	-2.828483	-1.307990
C	-1.826349	-0.843194	-0.788476
C	1.322665	-0.973745	1.447947
C	2.239866	0.119033	1.261525
C	3.061399	-0.170818	0.136538
C	2.678657	-1.473750	-0.360193
C	1.646237	-1.977739	0.468521
C	0.324937	-1.109862	2.555383
H	-0.563587	-1.657878	2.229501
H	-0.010982	-0.130828	2.908161
H	0.747471	-1.643768	3.417971
C	2.344948	1.297958	2.179840
H	2.780812	0.996392	3.140601
H	1.366000	1.739342	2.389820
H	2.985131	2.082762	1.769757
C	4.251930	0.601641	-0.349999
H	4.275269	1.620010	0.048221
H	4.284825	0.671893	-1.442828
H	5.185916	0.118086	-0.034396
C	3.338533	-2.183095	-1.503878
H	4.252146	-2.698169	-1.178587
H	3.625172	-1.488729	-2.299555
H	2.682505	-2.936369	-1.949177
C	0.984836	-3.315530	0.359039
H	1.078437	-3.739199	-0.645827
H	-0.080173	-3.259076	0.602182
H	1.442915	-4.031699	1.052827
C	-5.927087	-0.368834	0.683264
H	-6.099807	0.640968	1.067744
H	-6.678046	-0.557221	-0.093592
H	-6.132448	-1.069952	1.501678

Table S19. Atomic coordinates and energy of **2c** $E(\text{RB3PW91}) = -1402.01532932$ a.u.

Atom	Coordinates (Å)		
	x	y	z
Fe	1.617653	-0.237951	-0.232468
N	0.112811	-1.111371	-0.839887
H	0.248864	-2.089489	-1.078266
N	-0.778623	1.501502	-0.213166
N	0.989417	2.732921	-0.272135
C	0.605482	1.413992	-0.219736
C	-0.089604	3.588392	-0.280388
H	0.021842	4.660129	-0.338238
C	-1.201230	2.825046	-0.243970
H	-2.237013	3.112581	-0.288359
C	2.338471	3.207725	-0.480753
H	2.966769	2.344469	-0.675462
H	2.709296	3.746058	0.395966
H	2.365269	3.874732	-1.347881
C	-1.678573	0.415398	-0.262316
C	-3.023988	0.609313	0.047040
H	-3.367064	1.566310	0.421092
C	-3.948466	-0.419233	-0.084922
C	-3.518599	-1.673537	-0.539400
H	-4.231762	-2.483842	-0.652406
C	-2.184466	-1.882015	-0.812711
H	-1.846843	-2.863365	-1.138162
C	-1.206789	-0.864180	-0.658382
C	2.482348	-0.966568	1.466648
C	2.556151	-1.972604	0.440265
C	3.291305	-1.431574	-0.645188
C	3.751336	-0.116298	-0.272892
C	3.269745	0.153364	1.041109
C	1.825340	-1.113523	2.803496
H	1.511719	-0.144015	3.200353
H	2.506183	-1.566798	3.537317
H	0.935298	-1.746359	2.747226
C	1.940753	-3.334626	0.519653
H	2.588826	-4.023516	1.075343
H	1.787470	-3.775791	-0.470615
H	0.973152	-3.312689	1.030420
C	3.606649	-2.101567	-1.947209
H	2.909788	-2.914576	-2.168199
H	4.616769	-2.531922	-1.938139
H	3.560102	-1.394537	-2.781389
C	4.744076	0.671348	-1.076925
H	5.697506	0.131295	-1.141715
H	4.966437	1.643107	-0.627316
H	4.405635	0.848028	-2.103774
C	3.596696	1.323620	1.919327
H	4.171896	0.992598	2.792585
H	2.697669	1.823843	2.294044
H	4.204579	2.069121	1.401702
C	-5.395258	-0.176539	0.195530
F	-6.104984	0.066459	-0.932069
F	-5.980142	-1.240903	0.785697
F	-5.587640	0.888264	1.004673

Table S20. Atomic coordinates and energy of Cc $E(\text{RB3PW91}) = -1403.19056760$ a.u.

Atom	Coordinates (Å)		
	<i>x</i>	<i>y</i>	<i>z</i>
Fe	1.721021	-0.115440	-0.477018
H	2.471315	0.412983	-1.714183
N	0.248032	-0.672429	-1.812306
H	0.438486	0.031685	-2.520849
H	0.424784	-1.587851	-2.212737
N	-0.552341	1.707095	-0.615058
N	1.264125	2.823711	-0.315753
C	0.825033	1.531510	-0.435444
C	-0.910800	3.053712	-0.590400
H	-1.920940	3.394833	-0.749198
C	0.233535	3.744862	-0.405415
H	0.405199	4.808891	-0.353217
C	2.664530	3.181053	-0.255238
H	3.225691	2.321771	-0.626876
H	2.975449	3.415139	0.767475
H	2.849581	4.051015	-0.891984
C	-1.460810	0.636696	-0.673581
C	-2.741483	0.750970	-0.141837
H	-3.044469	1.675654	0.336310
C	-3.627165	-0.325326	-0.191463
C	-3.227526	-1.532724	-0.758528
H	-3.914765	-2.370451	-0.798671
C	-1.949748	-1.647801	-1.296023
H	-1.643105	-2.577669	-1.767411
C	-1.059299	-0.575003	-1.269265
C	1.424834	-1.299812	1.267617
C	2.324979	-0.217418	1.542279
C	3.461193	-0.334774	0.685844
C	3.270908	-1.507396	-0.134026
C	2.032324	-2.094352	0.236088
C	0.184609	-1.635642	2.038417
H	-0.558459	-2.147731	1.419024
H	-0.295898	-0.737205	2.437260
H	0.400600	-2.293410	2.892765
C	2.135661	0.798151	2.627702
H	2.454420	0.398666	3.599437
H	1.087355	1.095848	2.724520
H	2.720326	1.703622	2.444609
C	4.725580	0.466341	0.747717
H	4.574661	1.435026	1.232120
H	5.135366	0.653902	-0.249923
H	5.498830	-0.060533	1.323763
C	4.270084	-2.056678	-1.105604
H	5.014714	-2.689478	-0.602476
H	4.807071	-1.253544	-1.617049
H	3.793254	-2.668106	-1.877551
C	1.460214	-3.358514	-0.330787
H	1.788706	-3.531266	-1.361835
H	0.364938	-3.353685	-0.315800
H	1.777146	-4.233329	0.251264
C	-4.980880	-0.197857	0.444265
F	-5.457433	1.061079	0.356408
F	-5.883397	-1.014594	-0.132728
F	-4.951410	-0.511150	1.756497

Table S21. Atomic coordinates and energy of **TS_{Cc-Dc}** $E(\text{RB3PW91}) = -1403.17753277$ a.u. (one imaginary frequency at -1205.94 cm^{-1})

Atom	Coordinates (Å)		
	x	y	z
Fe	1.728393	-0.160032	-0.462104
H	2.134179	0.285325	-1.939320
N	0.164757	-0.899968	-1.562838
H	1.119015	-0.162793	-1.989446
H	0.316974	-1.840213	-1.905040
N	-0.631250	1.599067	-0.453869
N	1.157981	2.782897	-0.374106
C	0.739374	1.483241	-0.382052
C	-1.030529	2.929921	-0.487258
H	-2.061398	3.227750	-0.583265
C	0.097530	3.670444	-0.431756
H	0.237605	4.740004	-0.446190
C	2.543072	3.194138	-0.463267
H	3.134154	2.300546	-0.659872
H	2.875915	3.667800	0.464720
H	2.666270	3.899533	-1.290330
C	-1.532482	0.505890	-0.517874
C	-2.819004	0.647307	-0.013592
H	-3.099137	1.565507	0.490982
C	-3.749707	-0.385375	-0.116978
C	-3.370877	-1.581140	-0.728129
H	-4.082114	-2.396058	-0.814357
C	-2.080775	-1.735868	-1.206845
H	-1.789511	-2.674051	-1.672546
C	-1.116886	-0.709133	-1.116106
C	1.746509	-1.033301	1.455431
C	2.736649	0.005648	1.387705
C	3.666755	-0.316964	0.356721
C	3.265870	-1.580916	-0.215433
C	2.105611	-2.018966	0.479688
C	0.643357	-1.136983	2.463376
H	-0.219804	-1.677423	2.064265
H	0.290273	-0.148745	2.772145
H	0.968627	-1.665298	3.370592
C	2.814081	1.161140	2.338026
H	3.143696	0.820238	3.327547
H	1.843067	1.648515	2.469136
H	3.528516	1.917994	2.005888
C	4.943347	0.397366	0.028943
H	4.948430	1.426069	0.400107
H	5.124796	0.432744	-1.049636
H	5.802908	-0.109438	0.487545
C	4.021513	-2.329047	-1.271400
H	4.843751	-2.914393	-0.838190
H	4.456154	-1.648416	-2.009083
H	3.378860	-3.028219	-1.814338
C	1.364067	-3.298195	0.242915
H	1.560700	-3.708218	-0.752692
H	0.282782	-3.165818	0.348398
H	1.669076	-4.062712	0.968287
C	-5.148776	-0.184259	0.369300
F	-5.204780	0.680811	1.405415
F	-5.958865	0.319843	-0.591067
F	-5.712423	-1.339882	0.776384

Table S22. Atomic coordinates and energy of **Dc** $E(\text{RB3PW91}) = -1403.20089865$ a.u.

Atom	Coordinates (Å)		
	<i>x</i>	<i>y</i>	<i>z</i>
Fe	1.787444	-0.166534	-0.546394
H	2.508060	0.593856	-1.773586
N	0.227453	-0.841706	-1.546074
H	2.397452	-0.200218	-2.032927
H	0.359765	-1.738230	-2.001367
N	-0.561991	1.597003	-0.434307
N	1.221868	2.796658	-0.459539
C	0.803012	1.495111	-0.464985
C	-0.967168	2.924322	-0.424367
H	-2.004242	3.213916	-0.447081
C	0.155600	3.676719	-0.433931
H	0.286623	4.747474	-0.440990
C	2.598004	3.231970	-0.566607
H	3.234003	2.348056	-0.561123
H	2.863866	3.876732	0.275921
H	2.752613	3.782115	-1.500469
C	-1.467609	0.501579	-0.486256
C	-2.747870	0.641254	0.025403
H	-3.020420	1.542353	0.565167
C	-3.696216	-0.371104	-0.127518
C	-3.332799	-1.531548	-0.823878
H	-4.061625	-2.324360	-0.963244
C	-2.049642	-1.689275	-1.306682
H	-1.778592	-2.604007	-1.829066
C	-1.039498	-0.697731	-1.133324
C	1.531856	-0.949521	1.381718
C	2.603090	0.012587	1.398374
C	3.612804	-0.424748	0.498899
C	3.185775	-1.684790	-0.067042
C	1.925660	-2.010453	0.502949
C	0.320750	-0.932417	2.261823
H	-0.526653	-1.437499	1.792139
H	0.002480	0.089148	2.486794
H	0.517175	-1.433202	3.219473
C	2.664904	1.201875	2.306149
H	2.938029	0.890582	3.322208
H	1.701282	1.714626	2.370895
H	3.412257	1.929763	1.980907
C	4.955286	0.203534	0.271198
H	4.972232	1.256077	0.567692
H	5.260762	0.149824	-0.778461
H	5.729762	-0.306190	0.858798
C	4.003519	-2.546719	-0.982060
H	4.680000	-3.197270	-0.412350
H	4.622376	-1.948507	-1.657261
H	3.375170	-3.193283	-1.600644
C	1.137976	-3.255977	0.247443
H	1.386446	-3.705177	-0.718545
H	0.062268	-3.062553	0.262357
H	1.350334	-4.007534	1.018090
C	-5.086206	-0.184174	0.371129
F	-5.644974	-1.348071	0.771115
F	-5.141827	0.669629	1.419961
F	-5.921381	0.325861	-0.569771

Table S23. Atomic coordinates and energy of **TS_{DC-2c}** $E(\text{RB3PW91}) = -1403.18654296$ a.u. (one imaginary frequency at -288.65 cm^{-1})

Atom	Coordinates (Å)		
	<i>x</i>	<i>y</i>	<i>z</i>
Fe	1.683153	-0.198609	-0.391822
H	2.597199	0.526790	-2.563088
N	0.168138	-0.976614	-1.251356
H	1.995695	0.092783	-2.679310
H	0.299861	-1.931729	-1.570282
N	-0.684333	1.564016	-0.365084
N	1.100452	2.765737	-0.360566
C	0.687502	1.459702	-0.343034
C	-1.088588	2.891805	-0.391903
H	-2.122045	3.187058	-0.455407
C	0.034976	3.642500	-0.386965
H	0.164661	4.712990	-0.423098
C	2.474101	3.199377	-0.492564
H	3.095657	2.309895	-0.571240
H	2.783750	3.788762	0.375307
H	2.592200	3.805221	-1.396462
C	-1.588310	0.474014	-0.428839
C	-2.908083	0.648510	-0.030650
H	-3.219936	1.584198	0.419982
C	-3.849129	-0.364249	-0.195764
C	-3.444395	-1.577686	-0.768080
H	-4.169283	-2.371616	-0.918879
C	-2.128239	-1.768989	-1.132009
H	-1.821686	-2.717949	-1.566449
C	-1.131179	-0.769707	-0.953311
C	1.905081	-1.006643	1.465156
C	2.861616	0.059220	1.326827
C	3.720965	-0.248624	0.235853
C	3.323042	-1.537642	-0.285109
C	2.242407	-2.015795	0.495439
C	0.858640	-1.118266	2.529499
H	-0.021536	-1.660358	2.172978
H	0.520049	-0.131842	2.858136
H	1.237882	-1.647974	3.414215
C	2.961722	1.227973	2.258383
H	3.345630	0.905218	3.234136
H	1.988360	1.697126	2.430395
H	3.642825	1.995803	1.883937
C	4.952331	0.491307	-0.196516
H	4.996400	1.501162	0.220778
H	5.026293	0.578075	-1.286060
H	5.857003	-0.029835	0.142971
C	4.011044	-2.259161	-1.404214
H	4.894769	-2.800896	-1.042290
H	4.351278	-1.569229	-2.182289
H	3.354630	-2.992002	-1.881685
C	1.549156	-3.333779	0.349482
H	1.674018	-3.755614	-0.652709
H	0.476958	-3.250066	0.548861
H	1.957895	-4.065185	1.057731
C	-5.244320	-0.187916	0.299186
F	-5.602045	1.114977	0.365043
F	-6.144373	-0.811507	-0.492282
F	-5.426064	-0.692873	1.544021

Table S24. Atomic coordinates and energy of **2a_{Ru}** $E(\text{RB3PW91}) = -1036.14327523$ a.u.

Atom	Coordinates (Å)		
	x	y	z
Ru	0.586771	-0.192024	-0.119164
N	-0.998486	-1.305343	-0.457185
H	-0.805279	-2.291201	-0.607926
N	-2.112379	1.314454	-0.054016
N	-0.488370	2.740033	-0.123210
C	-0.721713	1.383143	-0.066376
C	-1.652221	3.467368	-0.148821
H	-1.661947	4.544312	-0.218084
C	-2.673246	2.586184	-0.108972
H	-3.731813	2.762763	-0.172280
C	0.813935	3.351150	-0.221959
H	1.509712	2.577406	-0.535509
H	1.132567	3.765806	0.739229
H	0.791538	4.150406	-0.968339
C	-2.905983	0.146713	-0.016353
C	-4.274165	0.246808	0.275868
H	-4.696515	1.204872	0.556690
C	-5.108650	-0.858474	0.248682
C	-4.572485	-2.110671	-0.073274
H	-5.210305	-2.989464	-0.109580
C	-3.221439	-2.231869	-0.323469
H	-2.795044	-3.207296	-0.549524
C	-2.334952	-1.124765	-0.280425
C	1.989617	-0.884049	1.332588
C	2.002916	-1.819957	0.226931
C	2.403324	-1.095797	-0.934827
C	2.742263	0.260838	-0.543238
C	2.510048	0.379569	0.860413
C	1.701084	-1.218707	2.762349
H	1.322872	-0.346938	3.302599
H	2.607990	-1.566128	3.277083
H	0.948506	-2.007163	2.844273
C	1.653421	-3.273112	0.304264
H	2.522420	-3.879467	0.589585
H	1.298603	-3.656289	-0.658206
H	0.869442	-3.457576	1.045635
C	2.574246	-1.644275	-2.317036
H	1.956395	-2.531061	-2.479464
H	3.619016	-1.929484	-2.500889
H	2.292885	-0.904470	-3.071709
C	3.452847	1.227391	-1.443174
H	4.474268	0.879211	-1.647912
H	3.543555	2.221386	-0.997062
H	2.946298	1.338613	-2.406888
C	2.888943	1.517195	1.759554
H	3.765475	1.251132	2.364752
H	2.080849	1.777770	2.449901
H	3.150623	2.416428	1.197419
H	-6.162135	-0.746634	0.483951

Table S25. Atomic coordinates and energy of **Ca_{Ru}** $E(\text{RB3PW91}) = -1037.33057394$ a.u.

Atom	Coordinates (Å)		
	x	y	z
Ru	0.705639	0.004767	-0.500129
H	1.071849	0.685951	-1.939620
N	-0.981324	-0.827248	-1.631452
H	-1.104690	-0.136119	-2.367108
H	-0.728088	-1.707739	-2.067093
N	-1.968992	1.398156	-0.271617
N	-0.386325	2.868524	-0.231340
C	-0.569097	1.508479	-0.308229
C	-2.578321	2.647052	-0.163799
H	-3.648677	2.774245	-0.158871
C	-1.583732	3.558651	-0.143588
H	-1.625612	4.636012	-0.098824
C	0.907197	3.503225	-0.348191
H	1.592183	2.747476	-0.737950
H	1.264811	3.863731	0.622150
H	0.846204	4.347096	-1.042284
C	-2.650054	0.171529	-0.159629
C	-3.799155	0.053520	0.622421
H	-4.168378	0.924004	1.155326
C	-4.443543	-1.173993	0.759663
C	-3.928454	-2.301994	0.126988
H	-4.416485	-3.265651	0.236328
C	-2.785963	-2.190955	-0.662174
H	-2.391791	-3.062602	-1.179391
C	-2.145031	-0.963014	-0.820670
C	1.081823	-1.311136	1.304354
C	1.669749	-0.015979	1.484946
C	2.665605	0.195572	0.460425
C	2.696185	-1.000600	-0.360680
C	1.714520	-1.899874	0.141791
C	0.126455	-2.001843	2.228210
H	-0.579212	-2.637540	1.683844
H	-0.467091	-1.282157	2.799063
H	0.650484	-2.642631	2.952856
C	1.401990	0.905828	2.636166
H	2.055336	0.673010	3.487698
H	0.367087	0.826855	2.980410
H	1.578438	1.949780	2.363559
C	3.697452	1.281707	0.436100
H	3.334468	2.197233	0.911485
H	3.991088	1.534230	-0.587237
H	4.607080	0.978666	0.974162
C	3.676297	-1.267944	-1.462106
H	4.617525	-1.674961	-1.066587
H	3.913299	-0.353411	-2.011592
H	3.284800	-1.988090	-2.185993
C	1.432560	-3.277608	-0.376656
H	1.699829	-3.374783	-1.433395
H	0.374119	-3.539278	-0.268919
H	2.004103	-4.035486	0.175204
H	-5.333230	-1.247340	1.377283

Table S26. Atomic coordinates and energy of **TS_{Ca-Da}(Ru)** $E(\text{RB3PW91}) = -1037.30571172$ a.u. (one imaginary frequency at -1228.04cm^{-1})

Atom	Coordinates (Å)		
	x	y	z
Ru	0.711587	-0.077030	-0.478806
H	0.752386	0.421884	-2.112574
N	-1.027650	-1.027674	-1.420352
H	-0.153857	-0.142905	-1.996387
H	-0.809631	-1.957234	-1.756214
N	-1.951318	1.378925	-0.183398
N	-0.353252	2.818683	-0.286643
C	-0.578414	1.469380	-0.273494
C	-2.537092	2.638104	-0.148272
H	-3.604680	2.779453	-0.123736
C	-1.532135	3.538647	-0.208386
H	-1.553585	4.617081	-0.222598
C	0.943938	3.427108	-0.484454
H	1.628982	2.629364	-0.773689
H	1.298751	3.910569	0.431474
H	0.886921	4.173217	-1.282742
C	-2.697004	0.170884	-0.100288
C	-3.895024	0.157288	0.613094
H	-4.201238	1.052513	1.146223
C	-4.688505	-0.984144	0.671411
C	-4.256834	-2.135311	0.014249
H	-4.856999	-3.040779	0.043031
C	-3.050313	-2.138619	-0.671537
H	-2.717138	-3.042684	-1.176874
C	-2.228309	-0.994773	-0.749878
C	1.186677	-1.200241	1.365451
C	1.805868	0.090024	1.436316
C	2.744858	0.214882	0.351089
C	2.719555	-1.035432	-0.384041
C	1.770875	-1.897173	0.233405
C	0.236378	-1.794851	2.358507
H	-0.502555	-2.438768	1.873055
H	-0.316296	-1.020069	2.896149
H	0.765882	-2.402950	3.105219
C	1.591779	1.095431	2.525827
H	2.265803	0.901138	3.370194
H	0.566979	1.064295	2.904594
H	1.785553	2.113914	2.179809
C	3.782657	1.283689	0.188950
H	3.469565	2.229040	0.640283
H	4.006998	1.475951	-0.864654
H	4.724146	0.993071	0.675637
C	3.624972	-1.373534	-1.528916
H	4.602727	-1.719589	-1.168106
H	3.796801	-0.504432	-2.169718
H	3.205825	-2.164720	-2.155963
C	1.463214	-3.311413	-0.150775
H	1.712622	-3.509901	-1.197061
H	0.403116	-3.543610	-0.007763
H	2.034394	-4.020068	0.462952
H	-5.618590	-0.973662	1.230127

Table S27. Atomic coordinates and energy of **Da_{Ru}** $E(\text{RB3PW91}) = -1037.32896424$ a.u.

Atom	Coordinates (Å)		
	<i>x</i>	<i>y</i>	<i>z</i>
Ru	0.789414	-0.011563	-0.589067
H	1.271279	0.947267	-1.893011
N	-0.913143	-0.900879	-1.467663
H	1.128387	0.107348	-2.238385
H	-0.707156	-1.775676	-1.935641
N	-1.873063	1.379596	-0.164892
N	-0.328995	2.869023	-0.363122
C	-0.522544	1.514741	-0.353468
C	-2.491380	2.618399	-0.088662
H	-3.558873	2.723418	0.008453
C	-1.521356	3.552758	-0.207303
H	-1.575169	4.630098	-0.209219
C	0.939925	3.530168	-0.579822
H	1.717089	2.766087	-0.576035
H	1.128953	4.256730	0.215680
H	0.946244	4.045671	-1.546027
C	-2.578031	0.144622	-0.069834
C	-3.753206	0.078385	0.671888
H	-4.064066	0.942474	1.253496
C	-4.530799	-1.077548	0.684732
C	-4.101162	-2.175155	-0.065090
H	-4.694329	-3.086436	-0.082412
C	-2.911704	-2.129783	-0.775980
H	-2.587622	-2.997125	-1.347887
C	-2.081534	-0.975851	-0.794139
C	0.894426	-0.880566	1.424345
C	1.844546	0.212138	1.341655
C	2.816326	-0.115605	0.346579
C	2.504245	-1.434449	-0.170296
C	1.338145	-1.898726	0.500082
C	-0.182667	-1.040129	2.453279
H	-1.017403	-1.632239	2.070713
H	-0.588211	-0.072011	2.758418
H	0.199403	-1.538625	3.354877
C	1.875822	1.392335	2.263911
H	2.339934	1.120654	3.220900
H	0.869362	1.760756	2.479810
H	2.452925	2.220918	1.845655
C	4.055563	0.662078	0.018970
H	3.935549	1.726622	0.237343
H	4.322726	0.569724	-1.037296
H	4.910142	0.301832	0.606859
C	3.350125	-2.209999	-1.134854
H	4.149459	-2.749831	-0.609995
H	3.825510	-1.555752	-1.870536
H	2.761380	-2.948244	-1.685161
C	0.687563	-3.234556	0.324799
H	0.929801	-3.678142	-0.644792
H	-0.400712	-3.160691	0.400319
H	1.028655	-3.932075	1.100239
H	-5.444889	-1.117707	1.267584

Table S28. Atomic coordinates and energy of **TS_{Da-2a}(Ru)** $E(\text{RB3PW91}) = -1037.31162527$ a.u. (one imaginary frequency at -349.06 cm^{-1})

Atom	Coordinates (Å)		
	x	y	z
Ru	0.678733	-0.125869	-0.386495
H	1.127263	0.735130	-2.342236
N	-0.960865	-1.161716	-1.031083
H	0.736876	0.399344	-2.902864
H	-0.758270	-2.126376	-1.273046
N	-2.009687	1.341084	-0.143853
N	-0.401178	2.775768	-0.253604
C	-0.635427	1.422667	-0.220266
C	-2.583983	2.605357	-0.143363
H	-3.649117	2.759992	-0.143245
C	-1.573863	3.500043	-0.209908
H	-1.592121	4.577800	-0.256435
C	0.893858	3.387456	-0.447785
H	1.610417	2.581282	-0.604348
H	1.183578	3.978296	0.426613
H	0.876238	4.037442	-1.328466
C	-2.778588	0.148519	-0.082213
C	-4.068458	0.193255	0.452042
H	-4.428817	1.115739	0.897168
C	-4.894529	-0.923224	0.449508
C	-4.407059	-2.115962	-0.094295
H	-5.034348	-3.003530	-0.115434
C	-3.117265	-2.183016	-0.586857
H	-2.738531	-3.120641	-0.989683
C	-2.237653	-1.066448	-0.585674
C	1.322904	-0.980610	1.422782
C	2.043593	0.271195	1.259924
C	2.846614	0.177893	0.083808
C	2.659588	-1.156198	-0.469459
C	1.771946	-1.878588	0.368289
C	0.489681	-1.365262	2.604992
H	-0.284006	-2.086917	2.330729
H	-0.014482	-0.494545	3.031879
H	1.106512	-1.816760	3.394694
C	2.028282	1.391136	2.254260
H	2.656293	1.144774	3.120209
H	1.017530	1.585744	2.623375
H	2.412934	2.320846	1.828495
C	3.891253	1.147323	-0.381320
H	3.726314	2.151247	0.019269
H	3.921919	1.226033	-1.472535
H	4.890485	0.832429	-0.050708
C	3.378112	-1.684459	-1.673064
H	4.379466	-2.045303	-1.403147
H	3.503977	-0.911815	-2.436440
H	2.840171	-2.517633	-2.132577
C	1.364612	-3.311053	0.222785
H	1.453782	-3.655470	-0.811941
H	0.328748	-3.465807	0.539194
H	1.995421	-3.963629	0.839653
H	-5.892107	-0.865524	0.872257

Table S29. Atomic coordinates and energy of ammonia-borane (AB) $E(\text{RB3PW91}) = -83.19087378$ a.u.

Atom	Coordinates (Å)		
	<i>x</i>	<i>y</i>	<i>z</i>
B	0.927740	0.000031	0.000000
N	-0.726635	0.000008	0.000000
H	1.239661	-0.584768	1.015343
H	1.239661	-0.587045	-1.014028
H	1.239781	1.171686	-0.001315
H	-1.090332	-0.949813	0.001068
H	-1.090513	0.473941	-0.823056
H	-1.090513	0.475792	0.821988

Table S30. Atomic coordinates and energy of aminoborane $E(\text{RB3PW91}) = -82.01122914$ a.u.

Atom	Coordinates (Å)		
	<i>x</i>	<i>y</i>	<i>z</i>
B	-0.778051	0.000000	0.000004
N	0.611670	0.000000	-0.000002
H	-1.359385	1.047808	0.000005
H	-1.359385	-1.047808	-0.000001
H	1.163667	-0.843499	-0.000007
H	1.163667	0.843499	-0.000002

Table S31. Atomic coordinates and energy of H₂ $E(\text{RB3PW91}) = -1.17751651$ a.u.

Atom	Coordinates (Å)		
	<i>x</i>	<i>y</i>	<i>z</i>
H	0.000000	0.000000	0.371685
H	0.000000	0.000000	-0.371685

